Fundamentals of electronic spectroscopy

The following book chapter appeared in the *Handbook of High-Resolution Spectroscopy*, Vol. 1, 176-262, Eds. M. Quack and F. Merkt, Wiley & Sons, UK, 2011, and may be found at http://dx.doi.org/10.1002/9780470749593.hrs069.

Fundamentals of electronic spectroscopy

Hans Jakob Wörner[a] *and Frédéric Merkt*[b]

[a] Steacie Institute for Molecular Sciences
National Research Council of Canada
Ottawa, Canada

[b] Laboratorium für Physikalische Chemie
ETH Zürich, CH-8093 Zurich
Switzerland

Abstract

The basic principles of electronic spectroscopy of atoms and molecules in the gas phase are presented. In the first part, the elementary concepts necessary to describe the electronic structure of atoms, diatomic molecules and polyatomic molecules are introduced in a systematic manner, with an effort to classify the different interactions (electrostatic, spin-orbit, hyperfine) and types of motions (electronic, vibrational, rotational) which determine the energy level structures. In the second part, electronic transitions are discussed, with their spin-rovibrational structures. Examples ranging from the simple band stucture of $\Sigma_u^+ \leftarrow \Sigma_g^+$ electronic transitions of homonuclear diatomic molecules to the highly complex band structure of polyatomic molecules subject to strong vibronic interactions are used to illustrate the richness of electronic spectra.

1 Introduction

Electronic spectroscopy aims at studying the structure and dynamics of atoms and molecules by observing transitions between different electronic states induced by electromagnetic radiation.

The notion of an electronic state of a molecule follows from the Born-Oppenheimer approximation, which enables one to separate the Schrödinger equation into an equation describing the motion of the electrons at fixed configurations of the much heavier nuclei, and an equation describing the motion of the nuclei on the $3N-6$- ($3N-5$-) dimensional adiabatic electronic potential energy surface of a nonlinear (linear) molecule consisting of N atoms. This separation and the very different timescales of the different types of motion in a molecule lead to the approximate description of stationary states as products of electronic $\varphi_{\mathrm{e}}(\vec{q}_i)$, vibrational $\varphi_{\mathrm{v}}^{(\mathrm{e})}(\vec{Q}_\alpha)$, rotational $\varphi_{\mathrm{r}}^{(\mathrm{ev})}(\theta,\phi,\chi)$ and nuclear spin $\phi_{\mathrm{ns}}^{(\mathrm{evr})}(m_\alpha)$ wave functions

$$\Psi = \varphi_{\mathrm{e}}(\vec{q}_i)\varphi_{\mathrm{v}}^{(\mathrm{e})}(\vec{Q})\varphi_{\mathrm{r}}^{(\mathrm{ev})}(\theta,\phi,\chi)\phi_{\mathrm{ns}}^{(\mathrm{evr})}(m_\alpha), \tag{1}$$

and sums of electronic E_{e}, vibrational E_{v}, rotational E_{r}, and hyperfine E_{ns} energies

$$E = E_{\mathrm{e}} + E_{\mathrm{v}} + E_{\mathrm{r}} + E_{\mathrm{ns}}. \tag{2}$$

In Equation (1), $\vec{q}_i$ represents the coordinates of the electrons including spin, $\vec{Q}$ stands for the $3N-6(5)$ normal coordinates used to describe the vibrations of the nuclear framework, (θ,ϕ,χ) are the Euler angles specifying the relative orientation of the space-fixed and molecule-fixed axis systems, and m_α describes the spin state of the nuclei. The spectrum of an electronic transition $\alpha' \leftarrow \alpha''$ between a lower electronic state α'' and an upper electronic state α' of a molecule never consists of a single line, but usually of a very large number of lines corresponding to all possible vibrational (v_i'), rotational $(J',\ K_a',\ K_c')$ and hyperfine levels of the upper electronic state accessible from all populated vibrational (v_i''), rotational $(J'',\ K_a'',\ K_c'')$ and hyperfine levels of the lower electronic state. An electronic spectrum thus consists of a system of vibrational bands, each of which possesses a rotational fine structure. Neglecting the hyperfine structure, the transition wave numbers can be expressed as differences of rovibronic term values

$$\tilde{\nu} = T_{\mathrm{e}}' + G'(v_1',\ v_2',\ldots) + F'(J',\ K_a',\ K_c') - T_{\mathrm{e}}'' - G''(v_1'',\ v_2'',\ldots) - F''(J'',\ K_a'',\ K_c'') \tag{3}$$

where T_{e}'' and T_{e}' represent the electronic term values (i.e., the positions of the minima of the Born-Oppenheimer potential surfaces of the corresponding electronic states), G'' and G' the vibrational term values discussed in detail in chapter hrs003 (Quack and coworkers 2010), and F'' and F' the rotational term values discussed in detail in chapter hrs002 (Bauder 2010). An electronic spectrum offers the possibility of obtaining information not only on the electronic structure of a molecule, but also on the vibrational, rotational and hyperfine structures of the relevant electronic states. The purely electronic origin of the transition is at $\tilde{\nu}_{\mathrm{e}} = T_{\mathrm{e}}' - T_{\mathrm{e}}''$, and each band of the system has its origin at $\tilde{\nu}_{\mathrm{e}} + G' - G''$, so that the origin of the band system is at $\tilde{\nu}_{00} = \tilde{\nu}_{\mathrm{e}} + G'(0,0,\ldots,0) - G''(0,0,\ldots,0)$.

The hierarchy of motion upon which Equations (1) and (2) rely implies that the energetic separation between electronic states is much larger than that between vibrational and rotational levels of a given electronic state. Consequently, the populations in the electronically excited states are negligible at room temperature, and electronic transitions, particularly those from the ground electronic state, are usually observed at shorter wavelengths than vibrational and pure rotational transitions, i.e., in the visible or the ultraviolet regions of the electromagnetic spectrum. The rovibrational levels of electronically excited states are usually located at energies where the density of rovibronic states is very large, or even above one or more dissociation and ionization limits, in which case they form resonances in the dissociation and/or ionization continua.

Interactions with neighboring electronic states and radiationless decay processes such as autoionization, predissociation, internal conversion and intersystem crossings are unavoidable and represent a breakdown of Equations (1) and (2). These interactions can cause perturbations of the spectral structures and can limit the lifetimes of the upper levels of the transitions leading to a broadening of the spectral lines and to diffuse spectra. The complex structure of electronic spectra and the frequent breakdown of the Born-Oppenheimer approximation in electronically excited states render electronic spectra more difficult to interpret than vibrational and pure rotational spectra. Their information content, however, may be larger, particularly when the spectral structures are sharp.

Despite the frequent breakdown of the Born-Oppenheimer approximation, the way electronically excited states and electronic transitions are labeled rely on the approximate description provided by Equations (1) and (2), particularly for small molecules: Vibrational and rotational levels are labeled as explained in Chapters hrs003 (Quack and coworkers 2010) and hrs002 (Bauder 2010), respectively; the electronic states are labeled with a letter, representing the "name" of the state, followed by a symmetry label or term symbol which can be derived either from the spectra themselves or from the symmetry of the occupied molecular orbitals, if these are known.

The eigenstates of a molecule with an associated Hamiltonian $\hat{H}$ remain invariant under the symmetry operations S_i of the point group. The operators $\hat{S}_i$ corresponding to the symmetry operations S_i therefore commute with $\hat{H}$ ($[\hat{H}, \hat{S}_i] = 0$). Consequently, the eigenfunctions Ψ_n of $\hat{H}$ can be chosen such that they are also eigenfunctions of $\hat{S}_i$ and can be designated with the eigenvalues of the operators $\hat{S}_i$. These eigenvalues correspond to the characters of one of the irreducible representations of the point group. The eigenfunctions Ψ_n of $\hat{H}$ thus transform as one of the irreducible representations of the corresponding symmetry group, and the irreducible representations are used to label the electronic states.

The ground electronic state is labeled by the letter X for diatomic molecules and $\tilde{\mathrm{X}}$ for polyatomic molecules. Electronically excited states are designated in order of increasing energy by the letters A, B, C, ... ($\tilde{\mathrm{A}}$, $\tilde{\mathrm{B}}$, $\tilde{\mathrm{C}}$, ... for polyatomic molecules) if they have the same total electron spin quantum number S as the ground electronic state, or by the letters a, b, c ... ($\tilde{\mathrm{a}}$, $\tilde{\mathrm{b}}$, $\tilde{\mathrm{c}}$, ... for polyatomic molecules) if they have a different spin multiplicity. The "˜" in the designation of electronic states

of polyatomic molecules is introduced to avoid confusion with the letters A and B that are used as group-theoretical labels. This labeling scheme occasionally poses problems, for instance when an electronic state thought to be the first excited state when it was first observed turns out later to be the second or third, or when several local minima of the same potential energy surface exist and lead to distinct band systems in an electronic spectrum, or because of initial misassignments. Whereas misassignments of symmetry labels are usually corrected, incorrect A, B, ... labels sometimes survive, especially when they have been accepted as names.

As the molecules become larger and/or less symmetric, this nomenclature tends to be replaced by a simpler one which uses a letter (S for singlet ($S = 0$), D for doublet ($S = 1/2$), T for triplet ($S = 1$), ...) to indicate the electron spin multiplicity, and a subscript $i = 0, 1, 2, \ldots$ to indicate the energetic ordering, 0 being reserved for the ground electronic state. For example, the lowest three electronic states of benzene are sometimes designated as $\tilde{\mathrm{X}}\ {}^1\mathrm{A}_{1g}$, $\tilde{\mathrm{a}}\ {}^3\mathrm{B}_{1u}$ and $\tilde{\mathrm{A}}\ {}^1\mathrm{B}_{2u}$ using $\mathrm{D}_{6\mathrm{h}}$-point-group symmetry labels, or as S_0, T_1, and S_1 using the second, simpler labeling scheme.

The different electronic states of a molecule can have Born-Oppenheimer potential energy surfaces of very different shapes and which reflect different binding mechanisms. Figure 1, which displays only a small subset of the adiabatic potential energy functions of molecular hydrogen illustrates this diversity and the complexity of the electronic structure of this seemingly simple molecule. In selected regions of internuclear distances, the states can be classified as

- valence states, i.e., states in which the valence electrons occupy molecular orbitals with significant amplitudes at the positions of more than one atom. Valence states can be entirely repulsive if the valence electrons occupy predominantly antibonding molecular orbitals, or attractive if they occupy predominantly bonding orbitals, in which case rigid molecular structures usually result.

- Rydberg states, i.e., states in which one of the valence electron has been excited to a diffuse orbital around a positively charged molecular ion core, resembling an excited orbital of the hydrogen atom. In such a state, the excited electron, called the Rydberg electron, is bound to the molecular ion core by the attractive Coulomb potential and can be labeled by a principal quantum number n. At sufficiently high values of n, the Rydberg electron is located, on average, at large distances from the ion core and only interacts weakly with it. The Born-Oppenheimer potential energy functions (or hypersurface in the case of polyatomic molecules) of Rydberg states thus closely resemble that of the electronic state of the molecular ion core to which the Rydberg electron is attached. Rydberg states form infinite series of states with almost identical potential energy functions (or hypersurfaces), and can also be labeled by the orbital angular momentum quantum number ℓ of the Rydberg electron. Rydberg states of H_2 can easily be identified in Figure 1 as the states with potential energy functions parallel to that of the $\mathrm{X}\ {}^2\Sigma_{\mathrm{g}}^+$ ground state of H_2^+.

- ion-pair states, i.e., states in which the molecule can be described as composed of two atoms

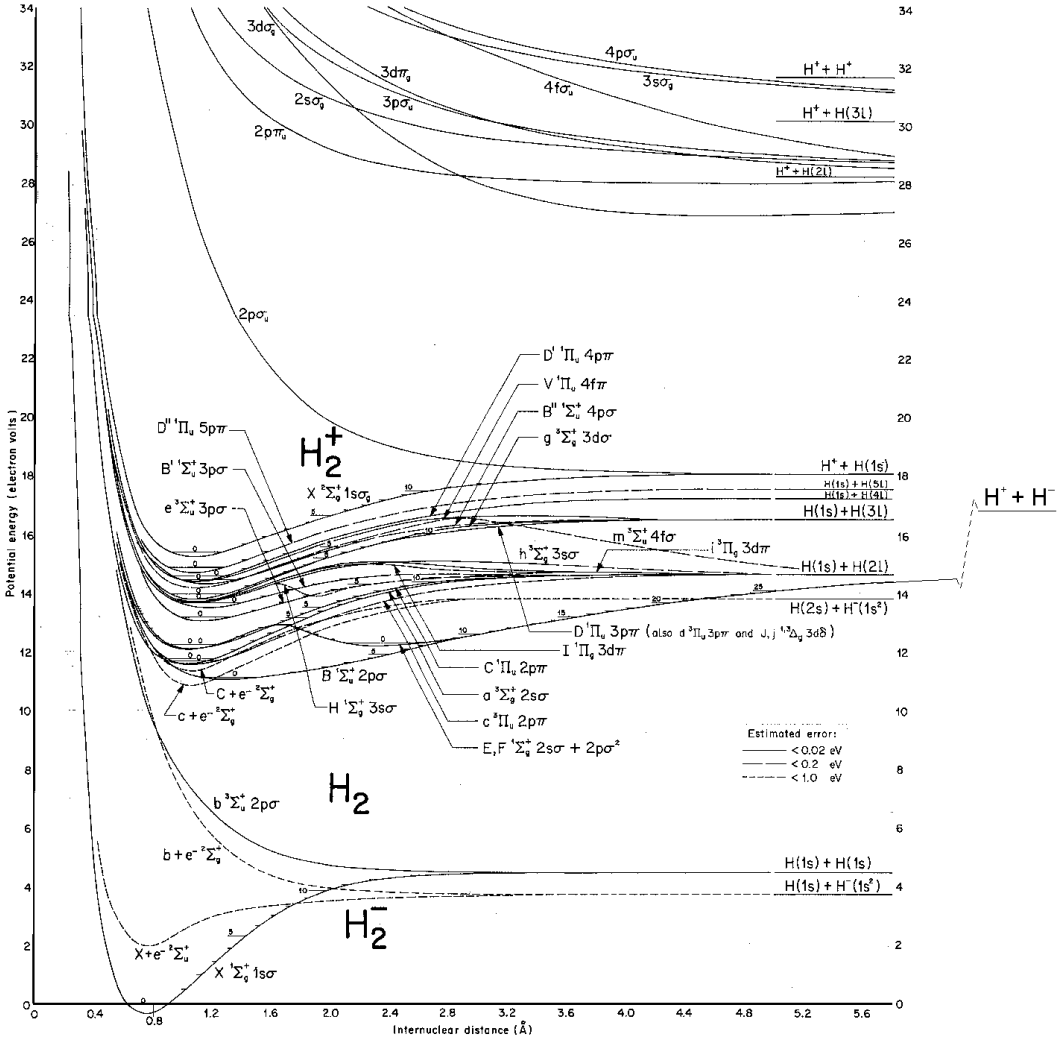

Figure 1: Potential energy functions of selected electronic states of H_2, H_2^+ and H_2^-. Adapted from Sharp (1971).

A^+ and B^- (or two groups of atoms) of opposite charge that are held together by a Coulomb potential. The potential energy of these states is proportional to $-1/R$ (R is the distance between the atoms of opposite charge) and dissociate at large distances into a cation (A^+) and an anion (B^-). At short internuclear distances, the potential energy function falls rapidly and starts overlapping with valence states with which they interact strongly, giving rise to charge transfer processes and electronic states with multiple potential wells. Ion-pair states are not only encountered in molecules such as NaCl, but also in homonuclear diatomic molecules, an example being the potential function in Figure 1 which coincides with the outer wall of the potential functions of the E,F $^1\Sigma_g^+$ and B $^1\Sigma_u^+$ states.

- states in which the atoms (or group of atoms) are held together by weak van der Waals interactions which give rise to shallow potential wells at large internuclear distances. The ground

electronic states of the rare gas dimers are prototypes of such states.

As all classifications, the classification of electronic states and binding mechanisms as valence, ion-pair, Rydberg and van der Waals represents a simplification based on idealized limiting situations. Because of configuration interactions, an electronic state that can be described as a valence state at short internuclear distances may evolve into a Rydberg state or an ion-pair state at larger distances, or even display shallow van der Waals potential wells.

The complexity of the electronic structure of even the simplest molecular systems illustrated by Figure 1 is reflected by the complexity of electronic spectra. Not only does each molecule represent a special case with its particular symmetry properties, number and arrangement of atoms, and magnetic and electric properties, but the large number and the diversity of electronic states of any given molecule, the interactions between these states, and the possibility of interactions with dissociation and ionization continua also contribute to make an exhaustive treatment of electronic spectroscopy impossible. In this chapter, we seek to present, at an introductory level, the general principles that form the basis of electronic spectroscopy, and emphasize common aspects of the electronic structure and spectra of atoms and molecules, particularly concerning the use of group theory and the classification of interactions. These aspects are best introduced using atoms, diatomic molecules and small polyatomic molecules.

More advanced material is presented in other chapters of this handbook: The determination of potential energy surfaces and rovibronic energy levels of polyatomic molecules by ab initio quantum chemical methods is the object of chapters hrs006 (Yamaguchi and Schäfer 2010), hrs007 (Tew *et al.* 2010), hrs009 (Breidung and Thiel 2010), hrs010 (Mastalerz and Reiher 2010), hrs013 (Marquardt and Quack 2010), hrs018 (Carrington 2010), and hrs019 (Tennyson 2010). The calculation of the spectral and dynamical properties of Rydberg states by ab initio quantum theory is reviewed in hrs015 (Jungen 2010b) and by multichannel quantum defect theory in hrs024 (Jungen 2010a). Experimental and theoretical investigations of the photodissociation of electronically excited states are presented in hrs092 (Ashfold *et al.* 2010) and hrs093 (Schinke 2010), respectively. The valence and inner-shell photoionization dynamics of molecules, including studies of autoionization processes in electronically excited states, are reviewed in hrs065 (Pratt 2010b) and hrs066 (Miron and Morin 2010), respectively. The use of electronic spectroscopy to study specific classes of molecular systems and electronic states is illustrated by hrs053 (Guennoun and Maier 2010), hrs056 (Schmitt and Meerts 2010), hrs054 (Pratt 2010a), hrs064 (Callegari and Ernst 2010), and hrs079 (Eikema and Ubachs 2010). The Jahn-Teller effect and nonadiabatic effects in manifolds of near-degenerate electronic states are treated in hrs060 (Köppel *et al.* 2010), the treatment of fine structure in electronically excited states using effective Hamiltonians is the object of hrs061 (Field *et al.* 2010), and studies of ultrafast electronic processes taking place on the (sub)femtosecond timescale are reviewed in hrs085 (Wörner and Corkum 2010). The use of photoelectron spectroscopy to study the electronic states of molecular cations is described by (Merkt *et al.* 2010). These chapters also provide information on the wide range of experimental

techniques and spectroscopic instruments that are employed to measure electronic spectra.

Until the second part of the 20th century, electronic spectra were almost exclusively obtained by monitoring the radiation transmitted by a given probe gas, or the radiation emitted by a sample after production of electronically excited atoms or molecules using electric or microwave discharges, flash lamps, or in flames, as a function of the wavelength. In the second half of the 20th century, the use of intense and/or highly monochromatic laser sources has greatly extended the range of applications of electronic spectroscopy, enabling studies at very high spectral resolution and unprecedented sensitivity. Multiphoton processes started to be exploited systematically to 1) study electronically excited states not accessible from the ground state by single-photon excitation, 2) reduce spectral congestion in electronic spectra by carrying out the multiphoton excitation via selected rovibrational levels of suitable intermediate electronic states, and 3) efficiently detect the resonant multiphoton transitions by monitoring the resonance-enhanced multiphoton ionization (REMPI) signal.

In combination with laser radiation, highly sensitive spectroscopic techniques, many of them enabling the background-free detection of the electronic transitions, such as laser-induced fluorescence (LIF) spectroscopy, REMPI spectroscopy, photofragment excitation spectroscopy, degenerate four-wave mixing spectroscopy, cavity-ring-down spectroscopy, and a wide range of modulation techniques have revolutionized the field of high-resolution electronic spectroscopy, revealing for the first time the finest details of the energy level structure of atoms and molecules, and allowing systematic studies of the electronic spectra and structure of unstable and/or highly reactive species such as weakly-bound molecular complexes, free radicals and molecular ions.

The different techniques currently in use in high-resolution electronic spectroscopy are presented in the articles of this handbook mentioned above and will not be described in this introductory chapter. Instead, we provide the elementary knowledge and introduce the most important concepts that are necessary to access and optimally use the scientific literature related to electronic spectra of atoms and molecules. The chapter consists of two main parts, one devoted to the electronic structure of atoms and molecules, the other to their electronic spectra. Because the spectra of atoms are not complicated by the vibrational and rotational fine structures, they reveal most aspects of the electronic structure and dynamics more purely and clearly than molecular spectra and are ideally suited to introduce many important concepts. We have therefore chosen to begin the sections on electronic structure and electronic spectra by a treatment of the electronic structure and spectra of atoms. This choice enables the subsequent presentation of the electronic structure and spectra of molecules in a more compact manner.

2 Electronic structure

The electronic structure of atoms and molecules is characterized by the electronic wave function that corresponds to the solution of the electronic Schrödinger equation. When the effects of electron

correlation are not dominant, the electronic wave function can be approximated by a single electronic configuration, i.e., a product of single-electron wave functions or orbitals, reflecting the occupancy of these orbitals.

A given electronic configuration gives rise to several states, or terms, corresponding to the different relative orientations of the electronic orbital and spin angular momentum vectors. To distinguish the different terms of a given configuration, term symbols are used which indicate the electronic symmetry and the relative orientation of the orbital and spin angular momentum vectors. The symmetry properties of the orbitals and of the electronic wave functions are conveniently described in the point group of the molecule of interest.

When electron correlation is important, the electronic wave function must be described by a sum of contributions corresponding to electronic configurations differing in the occupation of one, two or more orbitals. The configurations contributing to a given electronic state have the same electronic symmetry, which is therefore an essential element of the electronic structure. The symmetry properties of the electronic states also determine whether a transition between two electronic states can be induced by electromagnetic radiation or not.

The general principles that enable one to classify the electronic structure in terms of symmetry properties and to exploit these properties in the analysis of electronic spectra are the same for atoms and molecules. However, whereas nonlinear polyatomic molecules belong to point groups with a finite number of symmetry elements, and thus a finite number of irreducible representations, atoms and linear molecules belong to point groups with an infinite number of symmetry elements and irreducible representations. This difference justifies the treatment of the electronic structure of atoms, linear, and nonlinear molecules in separate subsections.

2.1 Atoms

Atoms belong to the point group K_h, the character and direct-product tables of which are presented in Tables 1 and 2. The symmetry operations of the point group K_h consist of the identity (E), the inversion (i), all rotation (∞C_∞^φ), rotation-reflection (∞S_∞^φ) symmetry operations of a sphere, and of the operations that can be obtained by combining them. The quantum states of an atom can therefore be designated by the symmetry labels S, P, D, F, ..., which reflect the symmetry of the wave functions with respect to rotation and rotation-reflection operations, and a label g/u (from the german words "gerade"(=even)/"ungerade"(=odd)), which gives the symmetry with respect to inversion through the symmetry center (i). This widely used group-theoretical nomenclature actually originates from observations of the spectral characteristics of the electronic spectra of the alkali metal atoms: s=sharp series, p=principal series, d=diffuse series, f=fundamental series. The states of u symmetry are often labeled with a superscript "o" for "odd".

Neglecting the motion of the heavy nucleus, the Hamiltonian operator of a N-electron atom can

Table 1: Character table of the point group K_h appropriate to label the electronic states of atoms.

K_h	E	∞C_∞^φ	∞S_∞^φ	i		
$\mathrm{S_g}$	1	1	1	1		$x^2+y^2+z^2$
$\mathrm{P_g}$	3	$1+2\cos\varphi$	$1-2\cos\varphi$	3	R_x, R_y, R_z	
$\mathrm{D_g}$	5	$1+2\cos\varphi+2\cos 2\varphi$	$1-2\cos\varphi+2\cos 2\varphi$	5		$x^2+y^2-2z^2$, x^2-y^2, xy, xz, yz
$\mathrm{F_g}$	7	$1+2\cos\varphi+2\cos 2\varphi+2\cos 3\varphi$	$1-2\cos\varphi+2\cos 2\varphi-2\cos 3\varphi$	7		
...	...	...	...	...		
$\mathrm{S_u}$	1	1	-1	-1		
$\mathrm{P_u}$	3	$1+2\cos\varphi$	$-1+2\cos\varphi$	-3	x, y, z	
$\mathrm{D_u}$	5	$1+2\cos\varphi+2\cos 2\varphi$	$-1+2\cos\varphi-2\cos 2\varphi$	-5		
$\mathrm{F_u}$	7	$1+2\cos\varphi+2\cos 2\varphi+2\cos 3\varphi$	$-1+2\cos\varphi-2\cos 2\varphi+2\cos 3\varphi$	-7		
...	...	...	...	...		

Table 2: Direct product table of the point group K_h. In addition, the rules $g \otimes g = u \otimes u = g$ and $g \otimes u = u \otimes g = u$ are obeyed.

$\otimes$	S	P	D	F	...
S	S	P	D	F	...
P	P	S, P, D	P, D, F	D, F, G	...
D	D	P, D, F	S, P, D, F, G	P, D, F, G, H	...
F	F	D, F, G	P, D, F, G, H	S, P, D, F, G, H, I	...
...	...	...	...	...	...

be written as

$$\hat{H} = \sum_{i=1}^{N} \underbrace{\left(\frac{\hat{p}_i^2}{2m_e} - \frac{Ze^2}{4\pi\epsilon_0 r_i} \right)}_{\hat{h}_i} + \underbrace{\sum_{i=1}^{N} \sum_{j>i}^{N} \frac{e^2}{4\pi\epsilon_0 r_{ij}}}_{\hat{H}'} + \hat{H}'' \ , \tag{4}$$

where $\sum_i \hat{h}_i$ represents a sum of one-electron operators each containing a kinetic energy term and a potential energy term representing the interaction with the nucleus. $\hat{H}'$ represents the repulsion between the electrons, and $\hat{H}''$ all the very small contributions to $\hat{H}$ that can be neglected in first approximation (e.g., hyperfine interactions, see below).

2.1.1 The hydrogen atom and one-electron atoms

In one-electron atoms such as H, He^+, Li^{2+}, ..., $\hat{H}' = 0$ in Equation (4). If $\hat{H}''$ is neglected, the Schrödinger equation can be solved analytically, as demonstrated in most quantum mechanics textbooks. The eigenvalues $E_{n\ell m_\ell}$ and eigenfunctions $\Psi_{n\ell m_\ell}$ are then described by Equations (5) and (6), respectively

$$E_{n\ell m_\ell} = -hcZ^2 R_M / n^2 \tag{5}$$

$$\Psi_{n\ell m_\ell}(r, \theta, \phi) = R_{n\ell}(r) Y_{\ell m_\ell}(\theta, \phi). \tag{6}$$

In Equation (5), Z is the nuclear charge, R_M is the mass-corrected Rydberg constant for a nucleus of mass M

$$R_M = \frac{\mu}{m_\mathrm{e}} R_\infty, \tag{7}$$

where $R_\infty = m_\mathrm{e} e^4/(8h^3\epsilon_0^2 c) = 109737.31568527(73)\ \mathrm{cm}^{-1}$ (Mohr *et al.* (2008)) represents the Rydberg constant for a hypothetical infinitely heavy nucleus and $\mu = m_\mathrm{e} M/(m_\mathrm{e} + M)$ is the reduced mass of the electron-nucleus system. The principal quantum number n can take integer values from 1 to ∞, the orbital angular momentum quantum number ℓ integer values from 0 to $n-1$, and the magnetic quantum number m_ℓ integer values from $-\ell$ to ℓ. In Equation (6), r, θ,and ϕ are the polar coordinates. $R_{n\ell}(r)$ and $Y_{\ell m_\ell}(\theta, \phi)$ are radial wave functions and spherical harmonics, respectively. Table 3 lists the possible sets of quantum numbers for the first values of n, the corresponding expressions for $R_{n\ell}(r)$ and $Y_{\ell m_\ell}(\theta, \phi)$, and the symmetry designation $n\ell m_\ell$ of the orbitals.

The energy eigenvalues given by Equation (6) do not depend on the quantum numbers ℓ and m_ℓ and have therefore a degeneracy factor of n^2. They form an infinite series which converges at $n = \infty$ to a value of 0. Positive energies thus correspond to situations where the electron is no longer bound to the nucleus, i.e., to an ionization continuum. Expressing the energy relative to the lowest ($n = 1$) level

$$E_{n\ell m_\ell} = hcZ^2 R_M \left(1 - \frac{1}{n^2}\right) = hcT_n, \tag{8}$$

one recognizes that the ionization energy of the 1s level is $hcZ^2 R_M$, or, expressed as a term value in the wave-number unit of cm^{-1}, $T_{n=\infty} = R_M$.

The functions $\Psi_{n\ell m_\ell}(r, \theta, \phi)$ represent orbitals and describe the bound states of one-electron atoms; their norm $\Psi^*_{n\ell m_\ell} \Psi_{n\ell m_\ell}$ represent the probability densities of finding the electron at the position

Table 3: Quantum numbers, wave functions and symmetry designation of the lowest eigenstates of the hydrogen atom. Linear combinations of the complex-valued $R_{n\ell}(r)Y_{\ell m_\ell}(\theta,\phi)$ can be formed that are real and correspond to the orbitals actually used by chemists with designations given in parentheses in the last column. $a = a_0\frac{m_e}{\mu}$ and $\rho = \frac{2Z}{na}r$.

n	ℓ	m_ℓ	$R_{n\ell}(r)$	$Y_{\ell m_\ell}(\theta,\phi)$	orbital designation
1	0	0	$2\left(\frac{Z}{a}\right)^{3/2}\mathrm{e}^{-\rho/2}$	$\sqrt{\frac{1}{4\pi}}$	1s
2	0	0	$2^{-3/2}\left(\frac{Z}{a}\right)^{3/2}\mathrm{e}^{-\rho/2}(2-\rho)$	$\sqrt{\frac{1}{4\pi}}$	2s
2	1	0	$\frac{1}{2\sqrt{6}}\left(\frac{Z}{a}\right)^{3/2}\rho\mathrm{e}^{-\rho/2}$	$\sqrt{\frac{3}{4\pi}}\cos\theta$	$2\mathrm{p}_0$ (or $2\mathrm{p}_z$)
2	1	±1	$\frac{1}{2\sqrt{6}}\left(\frac{Z}{a}\right)^{3/2}\rho\mathrm{e}^{-\rho/2}$	$-\sqrt{\frac{3}{8\pi}}\sin\theta\mathrm{e}^{\pm\mathrm{i}\phi}$	$2\mathrm{p}_{\pm1}$ (or $2\mathrm{p}_{x,y}$)
3	0	0	$3^{-5/2}\left(\frac{Z}{a}\right)^{3/2}\mathrm{e}^{-\rho/2}(6-6\rho+\rho^2)$	$\sqrt{\frac{1}{4\pi}}$	3s
3	1	0	$\frac{1}{9\sqrt{6}}\left(\frac{Z}{a}\right)^{3/2}\rho\mathrm{e}^{-\rho/2}(4-\rho)$	$\sqrt{\frac{3}{4\pi}}\cos\theta$	$3\mathrm{p}_0$ (or $3\mathrm{p}_z$)
3	1	±1	$\frac{1}{9\sqrt{6}}\left(\frac{Z}{a}\right)^{3/2}\rho\mathrm{e}^{-\rho/2}(4-\rho)$	$-\sqrt{\frac{3}{8\pi}}\sin\theta\mathrm{e}^{\pm\mathrm{i}\phi}$	$3\mathrm{p}_{\pm1}$ (or $3\mathrm{p}_{x,y}$)
3	2	0	$\frac{1}{9\sqrt{30}}\left(\frac{Z}{a}\right)^{3/2}\rho^2\mathrm{e}^{-\rho/2}$	$\sqrt{\frac{5}{16\pi}}(3\cos^2\theta-1)$	$3\mathrm{d}_0$ (or $3\mathrm{d}_{z^2}$)
3	2	±1	$\frac{1}{9\sqrt{30}}\left(\frac{Z}{a}\right)^{3/2}\rho^2\mathrm{e}^{-\rho/2}$	$-\sqrt{\frac{15}{8\pi}}\sin\theta\cos\theta\mathrm{e}^{\pm\mathrm{i}\phi}$	$3\mathrm{d}_{\pm1}$ (or $3\mathrm{d}_{xz,yz}$)
3	2	±2	$\frac{1}{9\sqrt{30}}\left(\frac{Z}{a}\right)^{3/2}\rho^2\mathrm{e}^{-\rho/2}$	$\sqrt{\frac{15}{32\pi}}\sin^2\theta\mathrm{e}^{\pm\mathrm{i}2\phi}$	$3\mathrm{d}_{\pm2}$ (or $3\mathrm{d}_{xy,x^2-y^2}$)

(r,θ,ϕ) and imply the following general behavior, which is also important to understand the properties of polyelectronic atoms and of molecular Rydberg states:

- The average distance between the electron and the nucleus is proportional to n^2, in accordance with Bohr's model (Bohr 1914) of the hydrogen atom, which predicts that the classical radius of the electron orbit should grow with n as a_0n^2, $a_0 = 0.52917720859(36)$ Å being the Bohr radius. This implies that, in polyelectronic atoms and in molecules, very similar electronically excited states also exist as soon as n is large enough for the excited electron to be located mainly outside the positively charged atomic or molecular ion core consisting of the nuclei and the other electrons. These states are called Rydberg states. They have already been mentioned in the introduction and will be discussed further in Subsection 2.1.6.

- The probability of finding the electron in the immediate vicinity of the nucleus, i.e., within a sphere of radius on the order of a_0, decreases with n^{-3}. This implies that all physical properties which depend on this probability, such as the excitation probability from the ground state, the radiative decay rate to the ground state, or relativistic effects such as the spin-orbit coupling or hyperfine interactions involving the excited electron should also scale with n^{-3}.

- The same probability decreases exponentially, and rapidly becomes negligible with increasing value of ℓ because the centrifugal barrier in the electron-ion interaction potential increases with ℓ^2, effectively suppressing the tunneling probability of the excited electron into the region close to

the nucleus, or close to the atomic/molecular core in the case of Rydberg states of polyelectronic atoms and molecules. Low-ℓ states are thus called penetrating Rydberg states, and high-ℓ states nonpenetrating. In polyelectronic atoms and molecules, the latter behave almost exactly as in the hydrogen atom.

The orbital angular momentum quantum number ℓ, which comes naturally in the solution of the Schrödinger equation of the hydrogen atom, is also a symmetry label of the corresponding quantum states. Indeed the $2\ell+1$ functions $\Psi_{n\ell m_\ell}(r,\theta,\phi)$ with $m_\ell = -\ell, -\ell+1, \ldots, \ell$ transform as the $2\ell+1$ components of the irreducible representations of the K_h point group listed in Table 1. These irreducible representations are designated by letters as s ($\ell=0$), p ($\ell=1$), d ($\ell=2$), f ($\ell=3$), g ($\ell=4$), with subsequent labels in alphabetical order, i. e., h, i, k, l, etc. for $\ell = 5$, 6, 7, 8, etc. The reason for using small letters to label orbitals, instead of using the capital letters designating the irreducible representations of the K_h point group, is that capital letters are reserved to label electronic states. The distinction between electronic orbitals and electronic states is useful in polyelectronic atoms.

The nodal structure of the s, p, d, f, ... spherical harmonics also implies that s, d, g, ... orbitals with even values of ℓ have g symmetry, and that p, f, h, ... orbitals with odd values of ℓ have u symmetry. Orbitals with $\ell = 2k+1$ (k being an integer number) of g symmetry and orbitals with $\ell = 2k$ of u symmetry do not occur.

The operators $\hat{\vec{\ell}}^2$ and $\hat{\ell}_z$ describing the squared norm of the orbital angular momentum vector and its projection along the z axis commute with $\hat{H}$ and with each other. The spherical harmonics $Y_{\ell m_\ell}(\theta,\phi)$ are thus also eigenfunctions of $\hat{\vec{\ell}}^2$ and $\hat{\ell}_z$ with eigenvalues given by the eigenvalue equations

$$\hat{\vec{\ell}}^2 Y_{\ell m_\ell}(\theta,\phi) = \hbar^2 \ell(\ell+1) Y_{\ell m_\ell}(\theta,\phi) \tag{9}$$

and

$$\hat{\ell}_z Y_{\ell m_\ell}(\theta,\phi) = \hbar m_\ell Y_{\ell m_\ell}(\theta,\phi). \tag{10}$$

2.1.2 Polyelectronic atoms

The Schrödinger equation for atoms with more than one electron cannot be solved analytically. If $\hat{H}'$ in Equation (4) is neglected, $\hat{H}$ becomes separable in N one-electron operators $\hat{h}_i(\hat{p}_i,\hat{q}_i)$ [$\hat{h}_i(\hat{p}_i,\hat{q}_i)\phi_i(q_i) = \epsilon_i\phi_i(q_i)$] (To simplify the notation, we use here and in the following the notation q_i instead of $\vec{q}_i$ to designate all spatial x_i, y_i, z_i and spin m_{s_i} coordinates of the polyelectron wave function):

$$\hat{H}_0 = \sum_{i=1}^{N} \hat{h}_i(\hat{\vec{p}}_i, \hat{\vec{q}}_i) \tag{11}$$

with eigenfunction

$$\Psi_k(q_1,\ldots,q_N) = \phi_1^{(k)}(q_1)\phi_2^{(k)}(q_2)\ldots\phi_N^{(k)}(q_N) \tag{12}$$

and eigenvalues

$$E_k = \epsilon_1 + \epsilon_2 + ... + \epsilon_N, \tag{13}$$

where $\phi_i^{(k)}(q_i) = R_{n\ell}(r_i)Y_{\ell m_\ell}(\theta_i, \phi_i)\phi_{m_s}$ represents a spin orbital with ϕ_{m_s} being the spin part of the orbital, either α for $m_s = 1/2$ or β for $m_s = -1/2$.

The electron wave function [Equation (12)] gives the occupation of the atomic orbitals and represents a given electron configuration [e.g., Li: $\Psi_1(q_1, q_2, q_3) = 1s\alpha(q_1), 1s\beta(q_2), 2s\alpha(q_3)$]. Neglecting the electron-repulsion term in Equation (4) is a very crude approximation, and $\hat{H}'$ needs to be considered to get a realistic estimation of the eigenfunctions and eigenvalues of $\hat{H}$. A way to consider $\hat{H}'$ without affecting the product form of Equation (12) is to introduce, for each electron, a potential energy term describing the interaction with the mean field of all other electrons. Iteratively solving one-electron problems and modifying the mean-field potential term leads to the so-called "Hartree-Fock Self-Consistent Field" (HF-SCF) wave functions, which still have the form (Equation (12)) of a single electronic configuration but now incorporate most effects of the electron-electron repulsion except their instantaneous correlation. Because polyelectronic atoms, like hydrogen, belong to the K_h point group, the angular part of the improved orbitals can also be described by spherical harmonics $Y_{\ell m_\ell}(\theta_i, \phi_i)$. However, the radial functions $R_{n\ell}(r)$ and the orbital energies (ϵ_i in Equation (14)) differ from the hydrogenic case because of the electron-electron repulsion term $\hat{H}'$.

An empirical sequence of orbital energies can be determined that can be used to predict the ground-state configuration of most atoms in the periodic system using Pauli's Aufbau-principle:

$$\begin{array}{lllllllllllll} \epsilon_{1\mathrm{s}} & \leq & \epsilon_{2\mathrm{s}} & \leq & \epsilon_{2\mathrm{p}} & \leq & \epsilon_{3\mathrm{s}} & \leq & \epsilon_{3\mathrm{p}} & \leq & \epsilon_{4\mathrm{s}} & \leq & \epsilon_{3\mathrm{d}} & \leq & \epsilon_{4\mathrm{p}} & \leq \\ \epsilon_{5\mathrm{s}} & \leq & \epsilon_{4\mathrm{d}} & \leq & \epsilon_{5\mathrm{p}} & \leq & \epsilon_{6\mathrm{s}} & \leq & \epsilon_{4\mathrm{f}} & \leq & \epsilon_{5\mathrm{d}} & \leq & \epsilon_{6\mathrm{p}} & \leq & \epsilon_{7\mathrm{s}} & \leq \\ \epsilon_{5\mathrm{f}} & \leq & \epsilon_{6\mathrm{d}}. & & & & & & & & & & & & & \end{array} \tag{14}$$

This sequence of orbital energies can be qualitatively explained by considering the shielding of the nuclear charge by electrons in inner shells and the decrease, with increasing value of ℓ, of the penetrating character of the orbitals.

When instantaneous correlation effects in the electronic motion are also considered, the wave functions depart from a simple product form of the type of Equation (12) and must be represented by a sum of configurations. One therefore says that electron correlation leads to configuration mixing.

For most purposes and in many atoms, single-configuration wave functions represent an adequate description, or at least a useful starting point in the discussion of electronic structure and spectra. Equation (12) is, however, not compatible with the generalized Pauli principle. Indeed, electrons have a half-integer spin quantum number ($s = 1/2$) and polyelectronic wave functions must be antisymmetric with respect to the exchange (permutation) of the coordinates of any pair of electrons. Equation (12) must therefore be antisymmetrized with respect to such an exchange of coordinates. This is achieved by writing the wave functions as determinants of the type:

$$\Psi(q_1,\ldots,q_N)=\frac{1}{\sqrt{N!}}\det\begin{vmatrix}\phi_1(q_1) & \phi_1(q_2) & \ldots & \phi_1(q_N)\\ \phi_2(q_1) & \phi_2(q_2) & \ldots & \\ . & & & \\ . & & & \\ . & & & \\ \phi_N(q_1) & \ldots & \ldots & \phi_N(q_N)\end{vmatrix} \tag{15}$$

in which all ϕ_i are different spin orbitals. Such determinants are called Slater determinants and represent suitable N-electron wave functions which automatically fulfill the Pauli principle for fermions. Indeed, exchanging two columns in a determinant, i.e., permuting the coordinates of two electrons, automatically changes the sign of the determinant. The determinant of a matrix with two identical rows is zero so that Equation (15) is also in accord with Pauli's exclusion principle, namely that any configuration with two electrons in the same spin orbital is forbidden. This is not surprising given that Pauli's exclusion principle can be regarded as a consequence of the generalized Pauli principle for fermions. The ground-state configuration of an atom can thus be obtained by filling the orbitals in order of increasing energy (see Equation (14)) with two electrons, one with $m_s = 1/2$, the other with $m_s = -1/2$, a procedure known as Pauli's Aufbau-principle.

2.1.3 States of different spin multiplicities with the example of singlet and triplet states

The generalized Pauli principle for fermions also restricts the number of possible wave functions associated with a given configuration, as illustrated with the ground electronic configuration of the carbon atom in the following example.

Example: C $(1s)^2(2s)^2(2p)^2$

Because the full $(1s)^2$ shell and the full $(2s)^2$ subshell are totally symmetric, only the $(2p)^2$ open subshell need be considered. There are six spin orbitals and therefore 36(=6^2) possible configurations $(2pm_lm_s)(2pm_l'm_s')$ with $m_l, m_l' = 0, \pm1$ and $m_s, m_s = \pm1/2$:

Electron 1

Electron 2	ϕ_{2p1_α}	ϕ_{2p1_β}	ϕ_{2p0_α}	ϕ_{2p0_β}	ϕ_{2p-1_α}	ϕ_{2p-1_β}
ϕ_{2p1_α}	×		*			
ϕ_{2p1_β}		×				
ϕ_{2p0_α}	*		×			
ϕ_{2p0_β}				×		
ϕ_{2p-1_α}					×	
ϕ_{2p-1_β}						×

corresponding to the 36 entries of the table. Diagonal elements of the table (designated by a cross) are forbidden by the Pauli principle because both electrons are in the same spin orbital. According to Equation (15), each pair of symmetric entries with respect to the diagonal can be used to make one antisymmetric wave function. For example,

the entries of the table marked by an asterisk lead to the wave function

$$\Psi(q_1, q_2) = (\phi_{2\mathrm{p}0\alpha}(q_1)\phi_{2\mathrm{p}1\alpha}(q_2) - \phi_{2\mathrm{p}1\alpha}(q_1)\phi_{2\mathrm{p}0\alpha}(q_2))/\sqrt{2}, \tag{16}$$

which is antisymmetric with respect to permutation of q_1 and q_2 and thus fulfills the generalized Pauli principle for fermions, and to one symmetric wave function

$$\Psi(q_1, q_2) = (\phi_{2\mathrm{p}0\alpha}(q_1)\phi_{2\mathrm{p}1\alpha}(q_2) + \phi_{2\mathrm{p}1\alpha}(q_1)\phi_{2\mathrm{p}0\alpha}(q_2))/\sqrt{2} \tag{17}$$

which is forbidden by the Pauli principle. In total there are 15 wave functions for the $(2\mathrm{p})^2$ configuration that fulfill the Pauli principle. Not all of these 15 wave functions correspond to states of the same energy.

For an excited configuration with two unpaired electrons such as He $(1\mathrm{s})^1(2\mathrm{s})^1$, the Pauli principle does not impose any restriction, because the two electons are in different orbitals. However, the electrostatic repulsion between the two electrons leads to an energetic splitting of the possible states. In this configuration, four spin orbitals ($1\mathrm{s}\alpha$, $1\mathrm{s}\beta$, $2\mathrm{s}\alpha$, and $2\mathrm{s}\beta$) need to be considered, because each electron can be either in the 1s or the 2s orbital with either $m_s = 1/2$ or $m_s = -1/2$. Four antisymmetrized functions fulfilling the Pauli principle result, which can be represented as products of a symmetric/antisymmetric spatial part depending on the x_i, y_i and z_i coordinates of the two electrons ($i = 1, 2$) and an antisymmetric/symmetric spin part:

$$(1/\sqrt{2})\,[1\mathrm{s}(1)2\mathrm{s}(2) - 1\mathrm{s}(2)2\mathrm{s}(1)]\,\alpha(1)\alpha(2) = \Psi_{\mathrm{T},M_S=1} \tag{18}$$

$$(1/\sqrt{2})\,[1\mathrm{s}(1)2\mathrm{s}(2) - 1\mathrm{s}(2)2\mathrm{s}(1)]\,\beta(1)\beta(2) = \Psi_{\mathrm{T},M_S=-1} \tag{19}$$

$$(1/\sqrt{2})\,[1\mathrm{s}(1)2\mathrm{s}(2) - 1\mathrm{s}(2)2\mathrm{s}(1)]\,(1/\sqrt{2})\,[\alpha(1)\beta(2) + \alpha(2)\beta(1)] = \Psi_{\mathrm{T},M_S=0} \tag{20}$$

$$(1/\sqrt{2})\,[1\mathrm{s}(1)2\mathrm{s}(2) + 1\mathrm{s}(2)2\mathrm{s}(1)]\,(1/\sqrt{2})\,[\alpha(1)\beta(2) - \alpha(2)\beta(1)] = \Psi_{\mathrm{S},M_S=0}, \tag{21}$$

where the notation $1\mathrm{s}(i)\alpha(i)$ has been used to designate electron i being in the 1s orbital with spin projection quantum number $m_s = 1/2$.

The first three functions (Equations (18), (19) and (20)), with $M_S = m_{s_1} + m_{s_2} = \pm 1, 0$, have an antisymmetric spatial part and a symmetric electron-spin part with respect to the permutation of the two electrons. These three functions represent the three components of a triplet ($S = 1$) state. The fourth function has a symmetric spatial and an antisymmetric electron-spin part with $M_S = 0$ and represents a singlet ($S = 0$) state. These results are summarized in Tables 4 and 5, where the spin part of the wave functions are designated with an superscript "S" and the spatial parts with a superscript "R". The subscripts "a" and "s" indicate whether the functions are symmetric or antisymmetric with respect to the permutation of the coordinates of the two electrons.

The contribution to the energy of the electron-repulsion term $\hat{H}' = e^2/(4\pi\epsilon_0 r_{12})$ in Equation (4)

Table 4: Permutationally symmetric and antisymmetric two-electron spin functions

$\Psi^{\mathrm{S}}_{(\mathrm{s})}(m_1, m_2)$	$\alpha(1)\alpha(2)$	$M_S = 1$	$S = 1$(triplet)
	$\frac{1}{\sqrt{2}}(\alpha(1)\beta(2) + \alpha(2)\beta(1))$	$M_S = 0$	
	$\beta(1)\beta(2)$	$M_S = -1$	
$\Psi^{\mathrm{S}}_{(\mathrm{a})}(m_1, m_2)$	$\frac{1}{\sqrt{2}}(\alpha(1)\beta(2) - \alpha(2)\beta(1))$	$M_S = 0$	$S = 0$(singlet)

Table 5: Permutationally symmetric and antisymmetric two-electron spatial functions

$\Psi^{\mathrm{R}}_{(\mathrm{s})}(q_1, q_2)$	$\frac{1}{\sqrt{2}}(\phi_1(1)\phi_2(2) + \phi_1(2)\phi_2(1))$	(singlet)
$\Psi^{\mathrm{R}}_{(\mathrm{a})}(q_1, q_2)$	$\frac{1}{\sqrt{2}}(\phi_1(1)\phi_2(2) - \phi_1(2)\phi_2(1))$	(triplet)

can be evaluated in the first order of perturbation theory as:

$$\begin{aligned}
\frac{e^2}{(8\pi\epsilon_0)}\langle 1s(1)2s(2) - 1s(2)2s(1)|\frac{1}{r_{12}}|1s(1)2s(2) - 1s(2)2s(1)\rangle &= \frac{e^2}{(8\pi\epsilon_0)}[\langle 1s(1)2s(2)|\frac{1}{r_{12}}|1s(1)2s(2)\rangle \\
&+ \langle 1s(2)2s(1)|\frac{1}{r_{12}}|1s(2)2s(1)\rangle \\
&- \langle 1s(1)2s(2)|\frac{1}{r_{12}}|1s(2)2s(1)\rangle \\
&- \langle 1s(2)2s(1)|\frac{1}{r_{12}}|1s(1)2s(2)\rangle] \\
&= [J_{12} + J_{21} - K_{12} - K_{21}]/2 \\
&= J_{12} - K_{12} \qquad (22)
\end{aligned}$$

for the triplet state, and as

$$\frac{e^2}{(8\pi\epsilon_0)}\langle 1s(1)2s(2) + 1s(2)2s(1)|\frac{1}{r_{12}}|1s(1)2s(2) + 1s(2)2s(1)\rangle = J_{12} + K_{12} \qquad (23)$$

for the singlet state. In Equations (22) and (23), the integral $J_{12} = J_{21}$ and $K_{12} = K_{21}$ represent so-called Coulomb and exchange integrals, respectively. The Coulomb integral can be interpreted as the energy arising from the repulsion between the electron clouds of the 1s and 2s electrons. The exchange integral is more difficult to interpret and results from the repulsion between the two electron having "exchanged" their orbitals.

Because J_{12} and K_{12} are both positive in this case, the triplet state lies lower in energy than the singlet state by twice the exchange integral. The energy splitting between the singlet and triplet states can therefore be formally viewed as resulting from an electrostatic (including exchange) coupling of the motion of the two electrons with spin vectors $\vec{s}_1$ and $\vec{s}_2$, resulting in states of total spin angular momentum $\vec{S} = \vec{s}_1 + \vec{s}_2$ with $S = 1$ for the triplet state, and $S = 0$ for the singlet state.

These considerations can easily be generalized to situations with more than two unpaired electrons. In atoms with configurations with three unpaired electrons, such as, for instance, N ($(1s)^2(2s)^2(2p)^3$, quartett ($S = 3/2$) and doublet ($S = 1/2$) states result.

2.1.4 Terms and term symbols in atoms: LS and jj coupling

For all atoms extensive lists of term values are tabulated (see, e.g., Moore (1949, 1952, 1958)). To understand how the different terms arise and derive the term symbols used to label them, it is necessary to understand how the different orbital and spin angular momenta in an atom are coupled by electromagnetic interactions and in which sequence the angular momentum vectors are added to form the total angular momentum vector $\vec{J}$. This can be achieved by ordering the different interactions according to their relative strengths and by adding the angular momentum vectors that are most strongly coupled first.

Each angular momentum vector can be described quantum mechanically by eigenvalue equations of the type of Equations (9) and (10), e.g.,

$$\hat{\vec{S}}^2|SM_S\rangle = \hbar^2 S(S+1)|SM_S\rangle, \tag{24}$$

$$\hat{S}_z|SM_S\rangle = \hbar M_S|SM_S\rangle, \tag{25}$$

$$\hat{\vec{L}}^2|LM_L\rangle = \hbar^2 L(L+1)|LM_L\rangle, \tag{26}$$

$$\hat{L}_z|LM_L\rangle = \hbar M_L|LM_L\rangle, \tag{27}$$

$$\hat{\vec{J}}^2|JM_J\rangle = \hbar^2 J(J+1)|JM_J\rangle, \tag{28}$$

$$\hat{J}_z|JM_J\rangle = \hbar M_J|JM_J\rangle. \tag{29}$$

In the absence of coupling between the different angular momenta, all quantum numbers arising from eigenvalue equation of this type are good quantum numbers. In the presence of couplings between the different angular momenta, however, only a subset of these quantum numbers remain good quantum numbers, and the actual subset of good quantum numbers depends on the hierarchy of coupling strengths (see Zare (1988)).

Two limiting cases of angular momentum coupling hierarchy are used to label the terms of atoms: the LS coupling hierarchy, which adequatly describes the ground state of almost all atoms except the heaviest ones and is also widely used to label the electronically excited states of the lighter atoms, and the jj coupling hierarchy, which is less frequently encountered and becomes important in the description of the heaviest atoms and of electronically excited states.

a) The LS coupling hierarchy:

$\vec{L}$	$=\sum_{i=1}^{N} \vec{\ell}_i$	strong coupling of orbital angular momenta resulting from electrostatic interactions
$\vec{S}$	$=\sum_{i=1}^{N} \vec{s}_i$	strong coupling of spins resulting from exchange terms in the electrostatic interaction (see Equations (22) and (23))
$\vec{J}$	$=\vec{L}+\vec{S}$	weaker coupling between $\vec{S}$ and $\vec{L}$ resulting from the spin-orbit interaction, a relativistic effect.

In LS coupling, one obtains the possible terms by first adding vectorially the orbital angular momenta $\vec{\ell}_i$ of the electrons to form a resultant total orbital angular momentum $\vec{L}$. Then, the total electron spin $\vec{S}$ is determined by vectorial addition of the spins $\vec{s}_i$ of all electrons. Finally, the total angular momentum $\vec{J}$ is determined by adding vectorially $\vec{S}$ and $\vec{L}$ (see Figure 5a below). For a two-electron system, one obtains:

$$\vec{L} = \vec{\ell}_1 + \vec{\ell}_2; \quad L = \ell_1 + \ell_2, \ell_1 + \ell_2 - 1, \ldots, |\ell_1 - \ell_2| \tag{30}$$

$$M_L = m_{\ell_1} + m_{\ell_2} = -L, -L+1, \ldots, L \tag{31}$$

$$\vec{S} = \vec{s}_1 + \vec{s}_2; \quad S = 1, 0 \tag{32}$$

$$M_S = m_{s_1} + m_{s_2} = -S, -S+1, \ldots, S \tag{33}$$

$$\vec{J} = \vec{L} + \vec{S}; \quad J = L + S, L + S - 1, \ldots, |L - S| \tag{34}$$

$$M_J = M_S + M_L = -J, -J+1, \ldots, J. \tag{35}$$

The angular momentum quantum numbers L, S and J that arise in Equations (30), (32), and (34) from the addition of the pairs of coupled vectors $(\vec{\ell}_1, \vec{\ell}_2)$, $(\vec{s}_1, \vec{s}_2)$ and $(\vec{L}, \vec{S})$, respectively, can be derived from angular momentum algebra as explained in most quantum mechanics textbooks. For the addition of the angular momentum vectors, the values of L resulting from the addition of $\vec{\ell}_1$ and $\vec{\ell}_2$ can be obtained from the direct products of the corresponding representations of the K_h point group (see Table 2). For instance, if $\ell_1 = 1$ (irreducible representation P) and $\ell_2 = 3$ (irreducible representation F), the direct product $\mathrm{P} \otimes \mathrm{F} = \mathrm{D} \oplus \mathrm{F} \oplus \mathrm{G}$ yields $L = 2, 3$ and 4, a result that can be generalized to Equations (30), (32) and (34).

The different terms (L, S, J) that are obtained for the possible values of L, S and J in Equations (30), (32), and (34) are written in compact form as term symbols

$$(L, S, J) = {}^{2S+1}L_J. \tag{36}$$

However, not all terms that are predicted by Equations (30), (32), and (34) are allowed by the Pauli principle. This is best explained by deriving the possible terms of the C $(1s)^2(2s)^2(2p)^2$ configuration in the following example.

Example: C $(1s)^2(2s)^2(2p)^2$. Only the partially filled 2p subshell needs to be considered. In this case $l_1 = 1$, $l_2 = 1$ and $s_1 = s_2 = 1/2$. From Eqs. (30), (32), and (34) one obtains, neglecting the Pauli principle:

$$L = 0(\mathrm{S}), 1(\mathrm{P}), 2(\mathrm{D})$$

$$S = 0(\text{singlet}), 1(\text{triplet})$$

$$J = 3, 2, 1, 0,$$

which leads to the following terms:

Term	^{1}S$_0$	^{3}S$_1$	^{1}P$_1$	^{3}P$_0$	^{3}P$_1$	^{3}P$_2$	^{1}D$_2$	^{3}D$_1$	^{3}D$_2$	^{3}D$_3$.
Degeneracy factor ($g_J = 2J + 1$)	1	3	3	1	3	5	5	3	5	7

Taking the $(2J+1)$ degeneracy factor of each term (which corresponds to all possible values of M_J), a total of 36 states result. As discussed above, only 15 states are allowed by the Pauli principle for the configuration $(1s)^2(2s)^2(2p)^2$. The terms allowed by the Pauli principle can be determined by first finding the M_L, M_S and M_J values resulting from all 15 possible occupations of the six $2p$ spin-orbitals with the two electrons in *different* spin orbitals, as explained in the following table:

El. 1	El. 2	M_L	M_S	M_J
$\phi_{2p1\alpha}$	$\phi_{2p1\beta}$	2	0	2
	$\phi_{2p0\alpha}$	1	1	2
	$\phi_{2p0\beta}$	1	0	1
	$\phi_{2p-1\alpha}$	0	1	1
	$\phi_{2p-1\beta}$	0	0	0
$\phi_{2p1\beta}$	$\phi_{2p0\alpha}$	1	0	1
	$\phi_{2p0\beta}$	1	-1	0
	$\phi_{2p-1\alpha}$	0	0	0
	$\phi_{2p-1\beta}$	0	-1	-1
$\phi_{2p0\alpha}$	$\phi_{2p0\beta}$	0	0	0
	$\phi_{2p-1\alpha}$	-1	1	0
	$\phi_{2p-1\beta}$	-1	0	-1
$\phi_{2p0\beta}$	$\phi_{2p-1\alpha}$	-1	0	-1
	$\phi_{2p-1\beta}$	-1	-1	-2
$\phi_{2p-1\alpha}$	$\phi_{2p-1\beta}$	-2	0	-2

The maximum value of M_L is 2 and occurs only in combination with $M_S = 0$. This implies a ^{1}D term with five M_J components corresponding to $(M_L\ M_S) = (2\ 0)$, (1 0), (0 0), (-1 0) and (-2 0). Eliminating these entries from the table, the remaining entry with the highest M_L value has $M_L = 1$ and comes in combination with a maximal M_S value of 1. We can conclude that the corresponding term is ^{3}P (consisting of $^3P_0$, $^3P_1$ and $^3P_2$). There are 9 components corresponding to $(M_L\ M_S) = (1\ 1)$, (1 0), (1 -1), (0 1), (0 0), (0 -1), (-1 1), (-1 0) and (-1 -1). Eliminating these entries from the table, only one component remains, (0 0), which corresponds to a $^1S_0$ state. The terms corresponding to the $(2p)^2$ configuration allowed by the Pauli principle are therefore $^1D_2$, $^3P_2$, $^3P_1$, $^3P_0$ and $^1S_0$. As in the case of the He $(1s)^1(2s)^1$ configuration discussed above, the electrostatic exchange interaction favors the triplet state over the singlet states.

The lowest energy term of the ground electronic configuration of almost all atoms can be predicted using three empirical rules, know as Hund's rules in honor of the physicist Friedrich Hund. These rules state that

1. The lowest term is that with the highest value of the total spin angular momentum quantum number S.

2. If several terms have the same value of S, the term with the highest value of the total angular momentum quantum number L lies lowest in energy.

3. If the lowest term is such that both L and S are nonzero, the ground state is the term component with $J = |L - S|$ if the partially filled subshell is less than half full, and the term component with $J = L + S$ if the partially filled subshell is more than half full.

According to Hund's rules, the ground state of C is the term component $^3P_0$, and the ground state of F is the term component $^2P_{3/2}$, in agreement with experimental results. Hund's rules do not reliably predict the energetic ordering of electronically excited states.

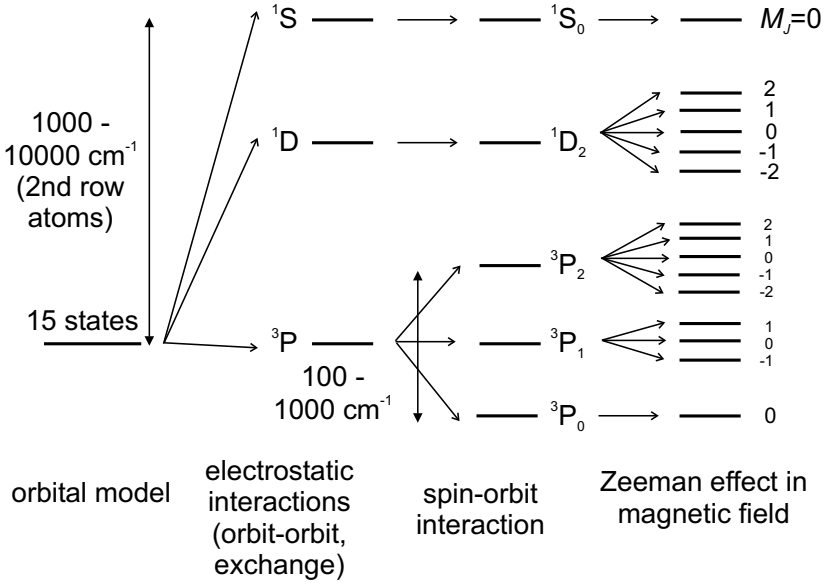

Figure 2: Schematic energy level structure of the $(2p)^2$ configuration in LS coupling.

The energy level splittings of the components of a term ^{2S+1}L can be described by considering the effect of the effective spin-orbit operator

$$\hat{H}_{\mathrm{SO}} = \frac{hcA}{\hbar^2}\hat{\vec{L}} \cdot \hat{\vec{S}} \tag{37}$$

on the basis functions $|LSJ\rangle$ ($\hat{\vec{J}} = \hat{\vec{L}} + \hat{\vec{S}}$). In Equation (37), the spin-orbit coupling constant A is expressed in cm^{-1}. From $\hat{\vec{J}}^2 = \hat{\vec{L}}^2 + \hat{\vec{S}}^2 + 2\hat{\vec{L}} \cdot \hat{\vec{S}}$ one finds

$$\hat{\vec{L}} \cdot \hat{\vec{S}} = \frac{1}{2}\left[\hat{\vec{J}}^2 - \hat{\vec{L}}^2 - \hat{\vec{S}}^2\right]. \tag{38}$$

The diagonal matrix elements of $\hat{H}_{\mathrm{SO}}$, which represent the first-order corrections to the energies in a perturbation theory treatment, are

$$\langle LSJ|\hat{H}_{\mathrm{SO}}|LSJ\rangle = \frac{1}{2}hcA[J(J+1) - L(L+1) - S(S+1)], \tag{39}$$

from which one sees that two components of a term with J and $J+1$ are separated in energy by $hcA(J+1)$. However, one should bear in mind that first-order perturbation theory breaks down when the energetic spacing between different terms is of the same order of magnitude as the spin-orbit splittings calculated with Equation (39). Hund's third rule implies that the spin-orbit coupling constant A is positive in ground terms arising from less than half-full subshells and negative in ground terms arising from more than half-full subshells.

To illustrate the main conclusions of this subsection, Figure 2 shows schematically by which interactions the 15 states of the ground-state configuration of C can be split. The strong electrostatic

interactions (including exchange) lead to a splitting into three terms ^{3}P, ^{1}D and ^{1}S. The weaker spin-orbit interaction splits the ground ^3P term into three components $^3\mathrm{P}_0$, $^3\mathrm{P}_1$ and $^3\mathrm{P}_2$. Each term component can be further split into $(2J+1)$ M_J levels by an external magnetic field, an effect known as the Zeeman effect, which is discussed in more detail in Subsection 2.1.7.

b) The jj coupling hierarchy:

$$\begin{array}{ll} \vec{l}_i + \vec{s}_i & = \vec{j}_i \quad \text{strong spin-orbit coupling} \\ \sum \vec{j}_i & = \vec{J} \quad \text{weaker electrostatic coupling.} \end{array}$$

In heavy atoms, relativistic effects become so large that the spin-orbit interaction can become comparable in strength, or even larger, than the electrostatic (including exchange) interactions that are dominant in the lighter atoms. In jj coupling, the dominant interaction is the spin-orbit coupling between $\vec{l}_i$ and $\vec{s}_i$. The possible terms are obtained by first adding vectorially the orbital angular momentum vector $\vec{l}_i$ and the electron spin vector $\vec{s}_i$ of each electron (index i) to form a resultant electronic angular momentum $\vec{j}_i$. The total electronic angular momentum $\vec{J}$ results from the vectorial addition of all $\vec{j}_i$.

For a two electron system, one obtains, using the same angular momentum addition rules that led to Equations (30), (32), and (34):

$$\vec{j}_1 = \vec{l}_1 + \vec{s}_1; \qquad j_1 = l_1 + \frac{1}{2},\ |l_1 - \frac{1}{2}| \tag{40}$$

$$m_{j_1} = m_{l_1} + m_{s_1} = -j_1, -j_1 + 1, \ldots, j_1 \tag{41}$$

$$\vec{j}_2 = \vec{l}_2 + \vec{s}_2; \qquad j_2 = l_2 + \frac{1}{2},\ |l_2 - \frac{1}{2}| \tag{42}$$

$$m_{j_2} = m_{l_2} + m_{s_2} = -j_2, -j_2 + 1, \ldots, j_2 \tag{43}$$

$$\vec{J} = \vec{j}_1 + \vec{j}_2; \qquad J = j_1 + j_2, j_1 + j_2 - 1, \ldots, |j_1 - j_2| \tag{44}$$

$$M_J = m_{j_1} + m_{j_2} = -J, -J + 1, \ldots, J. \tag{45}$$

The total orbital and spin angular momentum quantum numbers L and S are no longer defined in jj coupling. Instead, the terms are now specified by a different set of angular momentum quantum numbers: the total angular momentum j_i of all electrons (index i) in partially filled subshells and the total angular momentum quantum number J of the atom. A convenient way to label the terms is $(j_1, j_2, \ldots, j_N)_J$. Alternatively, the jj-coupling basis states may be written as

$$(j_1, j_2, \ldots, j_N)_J = \Pi_{i=1}^{N} |j_i, m_{j_i}\rangle. \tag{46}$$

Example: The $(n\mathrm{p})^1((n+1)\mathrm{s})^1$ excited configuration:

LS coupling: $S = 0, 1$; $L = 1$. Termsymbols: $^1\mathrm{P}_1$, $^3\mathrm{P}_{0,1,2}$, which give rise to 12 states.

jj coupling: $l_1 = 1, s_1 = \frac{1}{2}, j_1 = \frac{1}{2}, \frac{3}{2}$ and $l_2 = 0, s_2 = \frac{1}{2}, j_2 = \frac{1}{2}$. Termsymbols: $[(j_1, j_2)_J]$: $(\frac{1}{2}, \frac{1}{2})_0; (\frac{1}{2}, \frac{1}{2})_1; (\frac{3}{2}, \frac{1}{2})_1; (\frac{3}{2}, \frac{1}{2})_2$,

which also gives rise to 12 states.

The evolution from LS coupling to jj coupling can be observed by looking at the evolution of the energy level structure associated with a given configuration as one moves down a column in the periodic table. Figure 3 illustrates schematically how the energy levels arising from the $(np)^1((n+1)s)^1$ excited configuration are grouped according to LS coupling for $n = 2$ and 3 (C and Si) and according to jj coupling for $n = 6$ (Pb). The main splitting between the $(1/2, 1/2)_{0,1}$ and the $(3/2, 1/2)_{1,2}$ states of

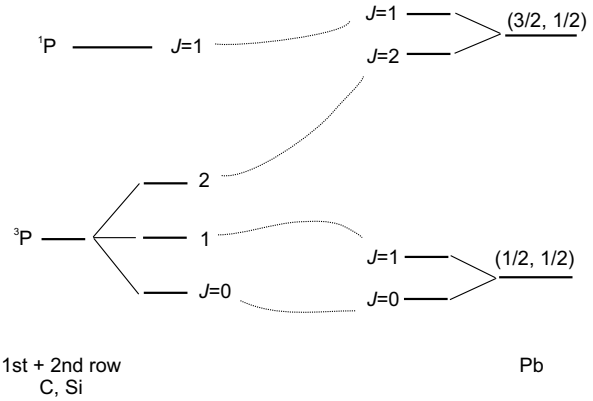

Figure 3: Correlation diagram depicting schematically, and not to scale, how the term values for the $(np)((n + 1)s)$ configuration evolve from C, for which the LS coupling limit represents a good description, and Pb, the level structure of which is more adequately described by the jj coupling limit.

Pb is actually much larger than the splitting between the ^{3}P and ^{1}P terms. Figure 3 is a so-called correlation diagram, which represents how the energy level structure of a given system (here the states of the $(np)^1((n+1)s)^1$ configuration) evolves as a function of one or more system parameters (here the magnitude of the spin-orbit and electrostatic interactions). States with the same values of all good quantum numbers (here J) are usually connected by lines and do not cross in a correlation diagram.

The actual evolution of the energy level structure in the series C, Si, Ge, Sn and Pb, drawn to scale in Figure 4 using reference data on atomic term values (Moore 1958), enables one to see quantitatively the effects of the gradual increase of the spin-orbit coupling. For the comparison, the zero point of the energy scale was placed at the center of gravity of the energy level structure. In C, the spin-orbit interaction is weaker than the electrostatic interactions, and the spin-orbit splittings of the ^{3}P state are hardly recognizable on the scale of the figure. In Pb, it is stronger than the electrostatic interactions and determines the main splitting of the energy level structure.

2.1.5 Hyperfine coupling

Magnetic moments arise in systems of charged particles with nonzero angular momenta to which they are proportional. In the case of the orbital angular momentum of an electron, the origin of the magnetic moment can be understood by considering the similarity between the orbital motion of an

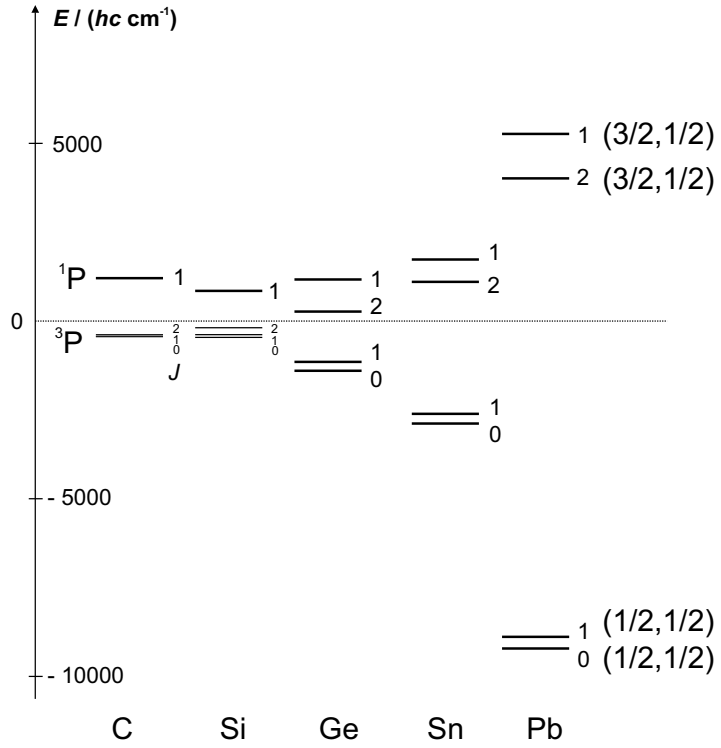

Figure 4: Evolution from LS coupling to jj coupling with the example of the term values of the $(n\mathrm{p})^1((n+1)\mathrm{s})^1$ configuration of C, Si, Ge, Sn and Pb. The terms symbols are indicated without the value of J on the left-hand side for the LS coupling limit and on the right-hand side for the jj coupling limit. The values of J are indicated next to the horizontal bars corresponding to the positions of the energy levels.

electron in an atom and a "classical" current generated by an electron moving with velocity v in a circular loop or radius r. The magnetic moment is equal to

$$\vec{\mu} = -\frac{e}{2m_\mathrm{e}}\vec{r} \times m_\mathrm{e}\vec{v} = -\frac{e}{2m_\mathrm{e}}\vec{\ell} = \gamma\vec{\ell}. \tag{47}$$

For the orbital motion of an electron in an atom, Equation (47) can be written using the correspondence principle as

$$\hat{\vec{\mu}} = \gamma\hat{\vec{\ell}} = -\frac{\mu_\mathrm{B}}{\hbar}\hat{\vec{\ell}}, \tag{48}$$

where $\gamma = -e/(2m_\mathrm{e})$ represents the magnetogyric ratio of the orbital motion and $\mu_\mathrm{B} = e\hbar/(2m_\mathrm{e}) = 9.27400915(23) \cdot 10^{-24}$ JT^{-1} is the Bohr magneton. By analogy, similar equations can be derived for all other momenta. The electron spin $\vec{s}$ and the nuclear spin $\vec{I}$, for instance, give rise to the magnetic moments

$$\hat{\vec{\mu}}_s = -g_\mathrm{e}\gamma\hat{\vec{s}} = g_\mathrm{e}\frac{\mu_\mathrm{B}}{\hbar}\hat{\vec{s}}, \tag{49}$$

and

$$\hat{\vec{\mu}}_I = \gamma_I\hat{\vec{I}} = g_I\frac{\mu_\mathrm{N}}{\hbar}\hat{\vec{I}}, \tag{50}$$

respectively, where g_e is the so-called g value of the electron ($g_\mathrm{e} = -2.0023193043622(15)$), γ_I is the magnetogyric ratio of the nucleus, $\mu_\mathrm{N} = e\hbar/(2m_\mathrm{p}) = 5.05078324(13) \cdot 10^{-27}$ JT^{-1} is the nuclear magneton (m_p is the mass of the proton), and g_I is the nuclear g factor ($g_\mathrm{p} = 5.585$ for the proton). Because $\mu_\mathrm{N}/\mu_\mathrm{B} = m_\mathrm{e}/m_\mathrm{p}$, the magnetic moments resulting from the electronic orbital and spin motions are typically 2 to 3 orders of magnitude larger than the magnetic dipole moments (and higher moments) of nuclear spins.

The hyperfine structure results from the interaction between the magnetic moments of nuclear spins, electron spins and orbital angular momenta. The interaction between two angular momentum vectors (such as $\hat{\vec{L}}$ or $\hat{\vec{S}}$ to form a resulting angular momentum vector $\hat{\vec{J}}$ (see subsection 2.1.4)) can be interpreted in the realm of a vector model (Zare 1988), based on a classical treatment and illustrated schematically in Figures 5a and b. This vector model is used here to discuss the hyperfine coupling.

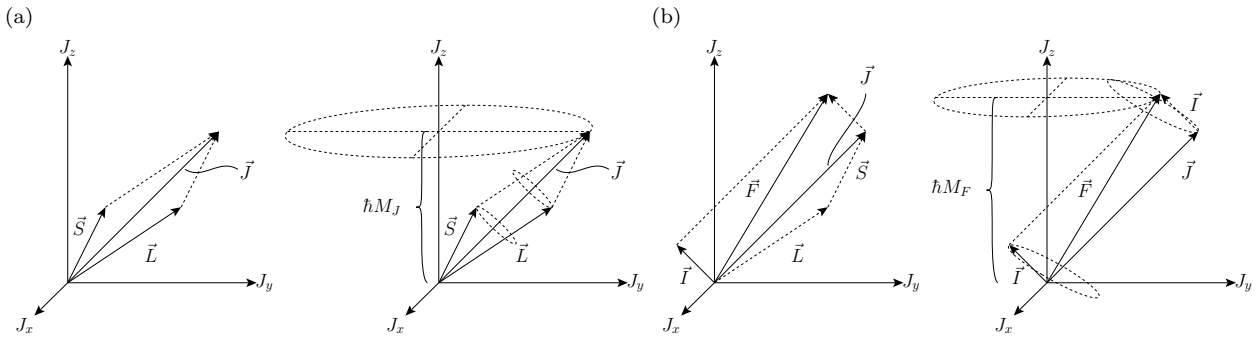

Figure 5: a) Schematic illustration of the vector model for the addition of two interacting angular momentum vectors with the example of the LS coupling. The interacting vectors $\vec{L}$ and $\vec{S}$ precess around the axis defined by the resultant vector $\vec{J}$, which has a well-defined projection $\hbar M_J$ along the space-fixed z axis. b) In the presence of a nuclear spin, the hyperfine interaction, which is typically much weaker than the spin-orbit interaction can be described as an interaction between $\vec{J}$ and $\vec{I}$.

The interaction between the two angular momentum vectors leads to a precession of both vectors around the axis defined by the resulting vector ($\vec{J}$ in the case of the interaction of $\vec{S}$ and $\vec{L}$) which is a constant of motion (see left-hand side of Figure 5a). Quantum mechanically, this implies constant norms $|\vec{L}|^2 = \hbar^2 L(L+1)$, $|\vec{S}|^2 = \hbar^2 S(S+1)$, and $|\vec{J}|^2 = \hbar^2 J(J+1)$ for $\vec{L}$, $\vec{S}$, and $\vec{J}$, respectively, and a constant component $J_z = \hbar M_J$ along a quantization axis usually chosen as the z axis. The projections of $\vec{L}$ and $\vec{S}$ along the z axis are not longer defined, nor is the direction of $\vec{J}$, except that the tip of the vector must lie on the dashed circle on the right-hand side of Figure 5a), which corresponds to a specific value of M_J. The possible values of the quantum number J and M_J that result from the addition of $\vec{L}$ and $\vec{S}$ are given by Equations (34) and (35). The larger the interaction, the faster the precession of $\vec{L}$ and $\vec{S}$ around $\vec{J}$.

The spin-orbit interaction is in general much stronger than the interactions involving nuclear spins. On the timescale of the slow precession of nuclear spin vectors, the fast precession of $\vec{L}$ and $\vec{S}$ thus

appears averaged out. The hyperfine interaction can therefore be described as an interaction between $\vec{I}$, with magnetic moment $(g_I \mu_N/\hbar)\hat{\vec{I}}$, and $\vec{J}$, with magnetic moment

$$\hat{\vec{\mu}}_J = g_J \gamma \hat{\vec{J}}, \tag{51}$$

rather than as two separate interactions of $\vec{I}$ with $\vec{L}$ and $\vec{S}$ (see Figure 5b). In Equation (51), g_J is the g factor of the LS-coupled state, also called Landé g factor, and is given in good approximation by

$$g_J = 1 + \frac{J(J+1) + S(S+1) - L(L+1)}{2J(J+1)}. \tag{52}$$

The hyperfine interaction results in a total angular momentum vector $\vec{F}$ of norm $|\vec{F}|^2 = \hbar^2(F(F+1))$ and z-axis projection $\hbar M_F$. The possible values of the quantum numbers F and M_F can be determined using the usual angular momentum addition rules:

$$F = |J-I|,\ |J-I|+1, \ldots, J+I, \tag{53}$$

and

$$M_F = -F,\ -F+1, \ldots, F. \tag{54}$$

The hyperfine contribution to $\hat{H}$ arising from the interaction of $\hat{\vec{\mu}}_J$ and $\hat{\vec{\mu}}_I$ is one of the terms included in $\hat{H}''$ in Equation (4) and is proportional to $\hat{\vec{\mu}}_I \cdot \hat{\vec{\mu}}_J$, and thus to $\hat{\vec{I}} \cdot \hat{\vec{J}}$. Following the same argument as that used to derive Equation (39), one obtains

$$\hat{\vec{I}} \cdot \hat{\vec{J}} = \frac{1}{2}\left[\hat{\vec{F}}^2 - \hat{\vec{I}}^2 - \hat{\vec{J}}^2\right] \tag{55}$$

with $\hat{\vec{F}} = \hat{\vec{I}} + \hat{\vec{J}}$ and $\hat{\vec{F}}^2 = \hat{\vec{I}}^2 + \hat{\vec{J}}^2 + 2\hat{\vec{I}} \cdot \hat{\vec{J}}$. The hyperfine energy shift of state $|IJF\rangle$ is therefore

$$\langle IJF| \frac{ha}{\hbar^2} \hat{\vec{I}} \cdot \hat{\vec{J}} |IJF\rangle = \frac{ha}{2}\left[F(F+1) - I(I+1) - J(J+1)\right] \tag{56}$$

as can be derived from Equation (55) and the eigenvalues of $\hat{\vec{F}}^2$, $\hat{\vec{I}}^2$ and $\hat{\vec{J}}^2$. In Equation (56), a is the hyperfine coupling constant in Hz. Note that choosing to express A in cm^{-1} and a in Hz is the reason for the additional factor of c in Equation (37). As examples, we now briefly discuss the hyperfine structures of H ($I = 1/2$) and $^{83}\mathrm{Kr}^+$($I = 9/2$).

For the H atom in the $(1s)^1\ ^2S_{1/2}$ ground state, $\ell = 0$ and $\hat{\vec{\mu}}_J = \hat{\vec{\mu}}_S$. The hyperfine interaction goes through direct contact of the electron and the nucleus, and is proportional to the electron probability density at the position of the nucleus ($r = 0$), $|\Psi(0)|^2 = \frac{1}{\pi\, a_0^3}$. This interaction is known as Fermi-contact interaction and the value of the hyperfine coupling constant is a=1420.4057517667(16) MHz (Essen *et al.* 1971). The hyperfine structure of the ground state of H is depicted in Figure 6a. The absolute ground state is therefore the $F = 0,\ M_F = 0$ component of the hyperfine doublet and is separated by only 1420 MHz (= 0.0475 cm^{-1}) from the upper $F = 1,\ M_F = 0, \pm 1$, levels which are degenerate in the absence of external fields. This three-fold degeneracy of the upper hyperfine component is lifted in the presence of a magnetic field, as will be explained in the next subsection.

Because the electron density in the immediate vicinity of the nucleus scales as n^{-3}, the hyperfine splitting of excited members of the s Rydberg series can be obtained directly from that of the ground state by dividing by n^3, and rapidly becomes negligible. The hyperfine coupling constant in the

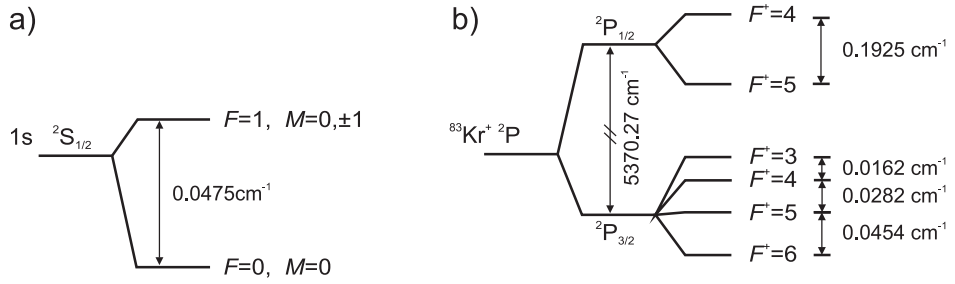

Figure 6: a) Hyperfine structure of (a) the 1 $^2S_{1/2}$ ground state of H and b) the two spin-orbit components of the ^2P_J ground term of Kr with $J = 1/2, 3/2$ (Schäfer and Merkt 2006; Paul *et al.* 2009)

ground state of atomic hydrogen is almost the same as in the ground state of ortho H_2^+, because the $1\sigma_g$ orbital has the form $(\frac{1s_a+1s_b}{\sqrt{2}})$ and the electron density at each nucleus is to a good approximation half that of the H atom (see also Subsection 2.2.1).

The $\ldots(4p)^5$ ground-state configuration of $^{83}Kr^+$ leads to two spin-orbit components $^2P_{3/2}$ and $^2P_{1/2}$ separated by 5370.27 cm^{-1} (Paul *et al.* 2009). The hyperfine structure is well represented by Equation (57)

$$\tilde{\nu}(J,F) = \tilde{\nu}_J + \frac{A_J C}{2} + B_J \frac{\frac{3}{4}C(C+1) - I(I+1)J(J+1)}{2I(2I-1)J(2J-1)}, \tag{57}$$

in which $\tilde{\nu}_J$ is the position of the barycenter of the hyperfine structure of the spin-orbit component with total angular momentum quantum number J, and $C = F(F+1) - I(I+1) - J(J+1)$. The second term on the right-hand side of the equation represents the splitting arising from the magnetic-dipole interaction and is proportional to the magnetic-dipole hyperfine coupling constant A_J. The third term is the next hyperfine coupling term in $\hat{H}''$ in Equation (4) and describes the electric quadrupole hyperfine interaction (Kopfermann 1958), which is proportional to the electric quadrupole hyperfine coupling constant B_J. B_J is zero for the upper spin-orbit component with $J = 1/2$. Indeed dipole, quadrupole, octupole, ... moments are nonzero only in systems with angular momentum quantum numbers $J \geq 1/2,\ 1,\ 3/2,\ \ldots$, respectively (Zare 1988). The octupole coupling in the $^2P_{3/2}$ state is negligible. The values of the hyperfine coupling constants of the $^2P_{3/2}$ and $^2P_{1/2}$ components of the ground state of Kr^+ are $A_{1/2} = -0.0385(5)$ cm^{-1}, $A_{3/2} = -0.00661(3)$ cm^{-1} and $B_{1/2} = -0.0154(7)$ cm^{-1} (Schäfer and Merkt 2006; Paul *et al.* 2009).

2.1.6 Rydberg states

Rydberg states are electronic states in which one of the electrons (called Rydberg electron) has been excited to an hydrogen-like orbital having a principal quantum number n larger than the quantum

number of the valence shell. The properties of these states can therefore be understood from the properties of the electronic states of the hydrogen atom described in Subsection 2.1.1. The expectation value of the distance between the electron and the proton in the hydrogen atom increases as n^2, and the amplitude of the Rydberg electron wave function in the immediate vicinity of the proton decreases as $n^{-3/2}$ so that, in a polyelectronic atom, the electron density in the region of the positively charged core, where the Rydberg electron interacts with the other electrons, decreases as n^{-3}. The electron density in the core region also decreases rapidly with the orbital angular momentum quantum number ℓ because of the centrifugal barrier in the electron-ion-core interaction potential, which is proportional to $\ell(\ell+1)$.

Electronic states with a given value of ℓ but different values of n ($n > \ell$) form infinite series of electronic states known as Rydberg series. The energetic positions of the different members of a given Rydberg series can be described in good approximation by Rydberg formula

$$E_{n\ell m_\ell} = E_{\mathrm{I}}(\alpha^+) - \frac{hcR_M}{(n-\delta_\ell)^2}, \tag{58}$$

where $E_{\mathrm{I}}(\alpha^+)$ represents the energy of a given quantum state α^+ of the ionized atom (or molecule) and δ_ℓ is the so-called quantum defect which is to a good approximation constant in a given series. δ_ℓ only appreciably differs from zero in s, p and d Rydberg states and rapidly decreases with increasing ℓ value.

Figure 7 depicts the energy level structure characteristic of Rydberg states of the hydrogen atom (panel (a)), polyelectronic atoms (panel (b)), and molecules (panel (c)) at high n values. In polyelectronic atoms, the energy level structure resembles closely that of the hydrogen atom with the only exception that the low-ℓ states are displaced to lower energies because the Rydberg electron is exposed to an increasing nuclear charge when in penetrates through the inner electron shells (their quantum defect is positive). In molecules, the situation is additionally complicated by the fact that series of core-penetrating and core-nonpenetrating Rydberg series converge on every rotational (denoted by N^+ in Figure 7), vibrational (denoted by v^+) and electronic states of the molecular cation. Because the potential that binds the Rydberg electron to the positively charged ion core can be well approximated by a Coulomb potential, the Rydberg electron wave functions in polyelectronic atoms and molecules are hydrogen-like and can be labeled by the same quantum numbers.

Most properties of Rydberg states scale as integer powers of the principal quantum number, as summarized by Table 6, so that Rydberg states of high principal quantum number behave very differently from other electronic states. The scaling laws in Table 6 can be derived from the well-known properties of the eigenstates of the hydrogen atom (see Gallagher (1994); Bethe and Salpeter (1957)).

Properties of particular relevance for electronic spectroscopy are (i) the very long lifetimes of high Rydberg states (the lifetimes scale as n^3), which result in very narrow spectral lines, (ii) the absorption cross sections from the ground or a low-lying electronic state, which decrease very rapidly with n (as n^{-3}) and make high Rydberg states difficult to observe in single-photon absorption spectra

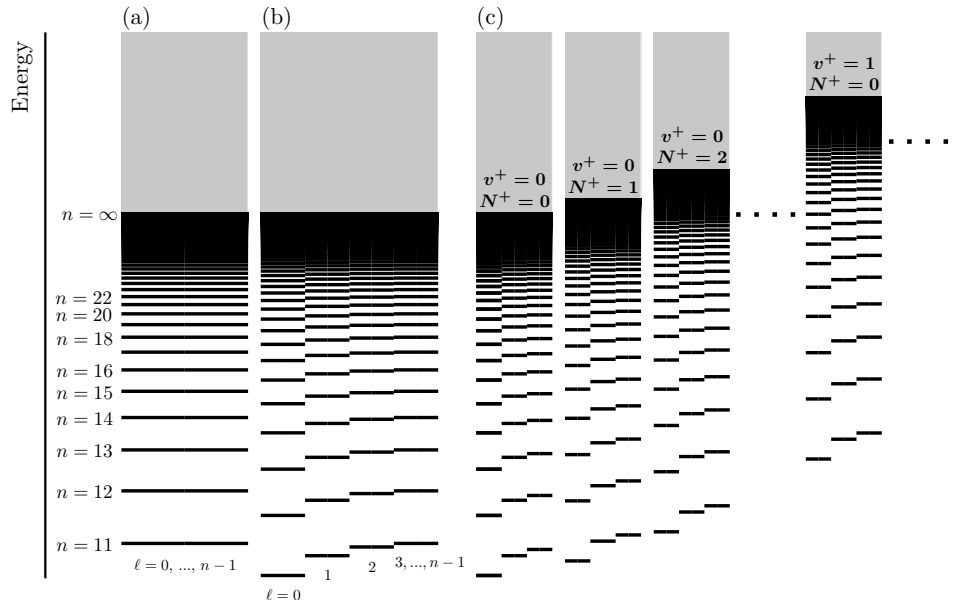

Figure 7: a) Energy level structure of the Rydberg states of a) the hydrogen atom, b) polyelectronic atoms, and c) molecules.

Table 6: Properties of Rydberg atoms [a]

Property	n dependence	Na(10d) [b]	H(100d)
Binding energy	n^{-2}	1100 cm^{-1}	11 cm^{-1}
Energy between adjacent n states	n^{-3}	190 cm^{-1}	0.22 cm^{-1}
Threshold ionization field	n^{-4}	33 $\mathrm{kV\,cm}^{-1}$	3.3 $\mathrm{V\,cm}^{-1}$
Orbital radius	n^2	147 a_0	1.50×10^4 a_0
Geometric cross section	n^4	6.8×10^4 a_0^2	7.1×10^8 a_0^2
Dipole moment $\langle n\ell \vert er \vert n(\ell+1)\rangle$	n^2	143 ea_0	1.50×10^4 ea_0
Polarizability	n^7	0.21 $\mathrm{MHz\,cm}^2\,\mathrm{V}^{-2}$	2×10^6 $\mathrm{MHz\,cm}^2\,\mathrm{V}^{-2}$
Radiative lifetime	n^3 [c]	1.0 μs	0.53 ms [d]

[a] Atomic units: Bohr radius $a_0 = 0.5292 \times 10^{-10}$ m; dipole moment $ea_0 = 8.478 \times 10^{-30}$ C m = 2.542 D.

[b] From Gallagher (1988).

[c] In the presence of electric fields the lifetimes scale as n^4 and if the electric fields are inhomogeneous even as n^5 (Merkt 1997).

[d] Extrapolated from the values given by Lindgård and Nielsen (1977).

from the ground state, (iii) the fine-structure (e.g., from the spin-orbit interaction) and hyperfine-structure (e.g., from the Fermi contact interaction) splittings involving the Rydberg electron, which are proportional to the Rydberg electron density in the core region, i.e., to n^{-3}, and become negligible at high n values, (iv) the spacings between neighboring Rydberg states of a given series, which also

decrease as n^{-3} and make it difficult to spectrally resolve adjacent members of a Rydberg series at high n values, (v) the very high sensitivity to electric and magnetic fields (the polarizability scales as n^7), and (vi) the binding energies, which decrease as n^{-2} and vanish at $n = \infty$ and make it possible to derive precise ionization energies and ionic energy levels by extrapolation of the Rydberg series. Chapters hrs024 (Ch. Jungen, 2010) and hrs015 (M. Jungen, 2010) of this handbook are specifically devoted to Rydberg states, and Chapter hrs071 (Merkt et al., 2010) illustrates the use of high Rydberg state in high-resolution photoelectron spectroscopy.

2.1.7 Atoms in magnetic fields

In the presence of a magnetic field, an additional term,

$$-\hat{\vec{\mu}}_{\mathrm{m}} \cdot \vec{B}, \tag{59}$$

arises in the Hamiltonian of a system having a magnetic moment $\vec{\mu}_{\mathrm{m}}$. In the case of a homogeneous magnetic field $\vec{B} = (0, 0, B)$ applied along the z axis of the laboratory frame, this term simplifies to $-\hat{\mu}_z B$ and induces energy shifts and/or lifts the degeneracy of the magnetic sublevels. The effect of a magnetic field on the spectrum of an atom or a molecule is called the Zeeman effect, the physicist P. Zeeman being the first to observe it as a broadening of the sodium D lines. This subsection summarizes the main aspects of the Zeeman effect on the energy levels of atoms.

The normal Zeeman effect

The simplest situation is that of an atom with $S = 0$, for which the effect of the magnetic field is referred to as the normal Zeeman effect for historical reasons. In this case, $J = L$ and $M_J = M_L$, and the magnetic moment originates from the orbital motion of the electrons (see Equation (48)):

$$\hat{\mu}_{\mathrm{m},z} = -\frac{\mu_{\mathrm{B}}}{\hbar}\hat{L}_z. \tag{60}$$

In first-order perturbation theory, the energy shift caused by the magnetic field is, according to Equations (59) and (60), given by

$$\Delta E = -\mu_{\mathrm{m},z} B = \mu_{\mathrm{B}} B M_L. \tag{61}$$

A given term with $L = J$ thus splits into $2L + 1$ magnetic sublevels corresponding to the possible M_L values. The energy separation of two sublevels differing in M_L by 1 is simply $\mu_{\mathrm{B}}B$, grows linearly with B, and does not depend on the atom nor on the state of the atom under consideration. The normal Zeeman effect on the energy level structure of ^{1}S, ^{1}P, and ^{1}D terms is illustrated in Figure 8. Particularly simple spectra result, as will be discussed in Subsection 3.2.3. The normal Zeeman effect is primarily used to unambiguously distinguish $S = 0$ from $S \neq 0$ terms and can also be used to measure magnetic field strengths, the value of the Bohr magneton being known with high precision (see above).

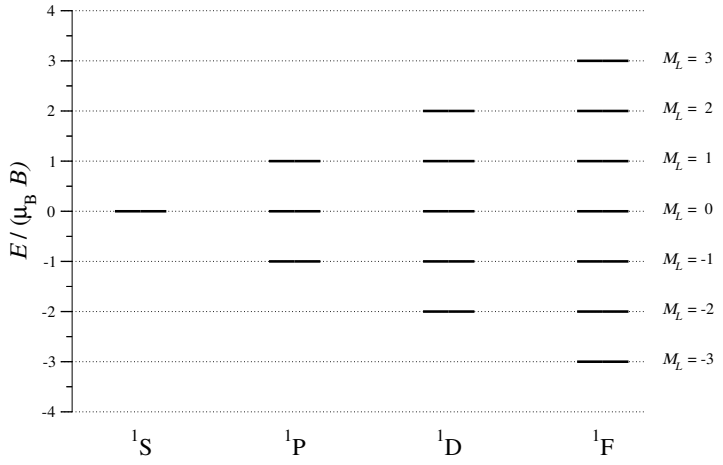

Figure 8: The normal Zeeman effect on the energy level structure of a) ^{1}S, b) ^{1}P, c) ^{1}D and d) ^{1}F terms

The anomalous Zeeman effect

When $S \neq 0$, the component of the magnetic moment along the field axis (taken here as the z axis) is given by

$$\hat{\mu}_{\mathrm{m},z} = -g_J \frac{\mu_\mathrm{B}}{\hbar} \hat{J}_z, \tag{62}$$

and the energy levels are shifted by

$$\Delta E = g_J \mu_\mathrm{B} B M_J. \tag{63}$$

The shifts and splittings of the energy levels now depend on the state under investigation through the dependence of g_J on S, L and J (see Equation (52)). The anomalous Zeeman effect thus leads to more complex spectra than the normal Zeeman effect (see Subsection 3.2.3), and the observed splittings permit the unambiguous determination of the term symbols. In the early part of the 20th century, the interpretation of the anomalous Zeeman effect represented a real puzzle and played an important role in the discovery of the electron spin (Enz 2002). Today the distinction between normal and anomalous Zeeman effect seems artificial because the normal Zeeman effect is merely a special case of Equation (63) for $S = 0$ and $g_J = 1$.

The Paschen-Back effect

In the limit of very high magnetic field strength, the interaction of the magnetic moments $\hat{\vec{\mu}}_S$ and $\hat{\vec{\mu}}_L$ of a state subject to LS coupling at zero magnetic field strength with the magnetic field becomes stronger than the spin-orbit interaction. This situation is know as the Paschen-Back effect. In terms of the vector model discussed in the context of Figure 5, this limit implies that the precession of $\vec{L}$ and $\vec{S}$ around the axis determined by the magnetic field vector (i.e., the z axis of the laboratory frame) is faster than that of $\vec{L}$ and $\vec{S}$ around the axis determined by the direction of $\vec{J}$ in the absence of magnetic field. Consequently, the spin-orbit interaction can be described as taking place between the "averaged" spin and orbital angular momentum vectors, i.e., their z components, as is illustrated by

Figure 9a. The corresponding operator (see Equation (37)) can be approximated by $(2\pi c/\hbar)A\hat{L}_z\hat{S}_z$. In this high-field limit, the Zeeman level shifts ΔE can be described by

$$\Delta E = \mu_\mathrm{B} B(M_L - g_\mathrm{e} M_S) + hcAM_L M_S. \tag{64}$$

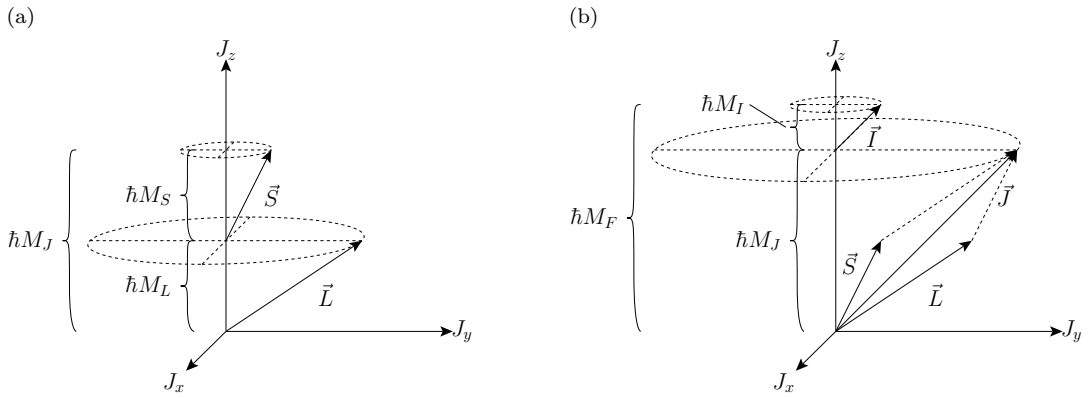

Figure 9: Vector model illustration of (a) the Paschen-Back effect and (b) the nuclear Paschen-Back effect

The Paschen-Back effect is only observable in atoms subject to a particularly weak spin-orbit interaction and/or at extremely large magnetic field strengths. Below 1 T, the anomalous Zeeman effect discussed above is typically observed. The anomalous Zeeman and Paschen-Back effects can thus be recognized as low- and high-field limits of the interaction between LS coupled states and magnetic fields. The treatment of intermediate cases leads to more complicated energy level patterns than predicted by Equations (63) and (64). An effect similar to the Paschen-Back effect can also be observed in electric fields and, indeed, the electronic angular momentum coupling scheme for diatomic molecules discussed as case (a) in Subsection 2.2.5 can be regarded as a Paschen-Back effect induced by the electric field along the internuclear axis of a diatomic molecule.

The nuclear Paschen-Back effect

The hyperfine interaction being much weaker than the spin-orbit interaction, even moderate magnetic fields lead to precessions of $\vec{J}$ and $\vec{I}$ around the axis determined by the field vector that are faster than that of $\vec{J}$ and $\vec{I}$ around $\vec{F}$ (see Figure 9b). In this case, referred to as the nuclear Paschen-Back effect, the effect of the magnetic field on the hyperfine structure can be described as

$$\Delta E = B(\mu_\mathrm{B} g_J M_J - \mu_\mathrm{N} g_I M_I) + haM_J M_I. \tag{65}$$

The nuclear Paschen-Back effect is usually encountered at field strengths large enough to resolve the nuclear Zeeman effect in electronic spectra. As a simple illustration, Figure 10 shows the evolution of the hyperfine structure of the H atom with the magnetic field. At field strengths beyond $\approx$ 1 T, the energy level pattern reveals a main splitting arising from the first term of Equation (65) with

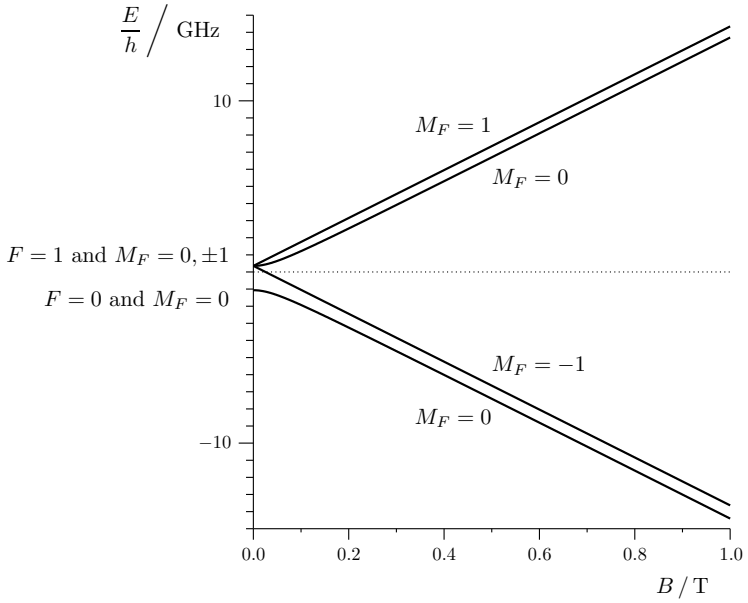

Figure 10: The hyperfine structure of the H atom in its $^2S_{1/2}$ ground state and its dependence on the magnetic field.

$M_J = M_S = m_s$ and $g_J = -g_e \approx 2$. Each of the two groups of m_s levels are further split by the other two terms. After Figure 3, which illustrated the evolution from LS to jj coupling, Figure (10) is a second example of a correlation diagram and shows how the energy level structure of the $(1s)^1\ ^2S_{1/2}$ ground state of H evolves from the situation described by Equation (56) and depicted in Figure 6a at $B = 0$ to that described by Equation (65) at $B = 1$ T. In the presence of a homogeneous magnetic field, the anisotropy of free space is broken, and even F ceases to be a good quantum number. The only good quantum number that can be used as a label for the states through the entire diagram is M_F.

2.1.8 Atoms in electric fields

Atomic energy levels are also affected by electric fields and the resulting energy shifts and splittings are referred to as the Stark effect. The effect of the electric fields is particularly pronounced in Rydberg states which are highly polarizable (the polarizability scales as n^7, see Table 6). The primary effect of an electric field is to couple energy levels from configurations differing by one spin-orbital only, with the additional restriction that the coupled spin-orbitals should only differ by one unit of the orbital angular momentum quantum number ℓ. The hydrogen atom represents a very special case because all orbitals of the same principal quantum number n are degenerate. If the field is applied along the z axis ($\vec{E} = (0, 0, E)$), the term $eEz = eEr\cos\theta$ has to be added to the Hamiltonian operator which becomes:

$$\hat{H} = -\frac{\hbar^2}{2m_e}\nabla_e^2 - \frac{e^2}{4\pi\epsilon_0 r} + eEr\cos\theta = \hat{H}_o + \hat{H}', \tag{66}$$

At low field strength, the effect of the electric field can be treated adequately with first-order perturbation theory for degenerated states. The matrix elements of $\hat{H}'$ in the $|n\ell m\rangle$ basis (we use m instead of m_ℓ to simplify the notation) can be written as $\langle n'\ell'm'|Er\cos\theta|n\ell m\rangle$. These elements can be expressed as products of radial and angular matrix elements $E\langle n'\ell'|r|n\ell\rangle\langle\ell'm'|\cos\theta|\ell m\rangle$ and imply the perturbation selection rules:

$$\Delta m = m' - m = 0, \quad \Delta\ell = \ell' - l = \pm 1, \quad \Delta n = 0, \pm 1, \pm 2, \ldots. \tag{67}$$

The $\Delta\ell$ selection rule can be derived using Tables 1 and 2 if one uses the fact that $z = r\cos\theta$ transforms as the irreducible represention $\mathrm{P_u}$ of the K_h point group. The selection rule of the magnetic quantum number can be rationalized by the fact that m remains a good quantum number in cylindrical symmetry. Because of the degenerate nature of all $|n\ell m\rangle$ states having the same n value in the hydrogen atom at zero fields, the perturbation leads to a linear splitting of the degenerate energy levels (the linear Stark effect) represented in Figure 11a for $n = 5$. The electric field breaks the central symmetry, so that the orbital angular momentum quantum number ℓ ceases to be a good quantum number. Instead, states of different angular momentum quantum number ℓ but the same values of m are mixed by the electric field. The atoms are polarized by the electric field, as illustrated in Figure 11b, in which the electron density in a plane containing the z axis is displayed for the five $m = 0$ levels. The energy levels are more easily expressed as a function of the so-called parabolic quantum numbers n_1 and n_2 that arise from the solution of Schrödinger equation of the H atom in parabolic coordinates (Gallagher 1994) than as a function of ℓ, because the $|nn_1n_2m\rangle$ basis functions are adapted to the cylindrical symmetry of the problem. The quantum numbers n_1 and n_2 can each take the values between 0 and $n - 1$. In atomic units, the energy levels are given to first order of perturbation theory by

$$E_{nn_1n_2m} = -\frac{1}{2n^2} + \frac{3}{2}(n_1 - n_2)nE \tag{68}$$

and depend linearly on the field strength. One thus speaks of the linear Stark effect. To label the states, it is useful to use the difference k between n_1 and n_2. For given values of n and $|m|$, k takes values ranging from $-(n - |m| - 1)$ to $(n - |m| - 1)$ in steps of 2 (see Figure 11a). The plots of the electron density represented in Figure 11b enable one to see that all states except the $k = 0$ states have electric dipole moments and to understand why the states with a positive value of k are shifted to higher energies by the field, whereas those with a negative value of k are shifted to lower energies. Equation (68) can be converted to SI units using the fact that the ratio between the atomic unit of energy and the atomic unit of electric field is ea_0 with $e = 1.602176487(40) \cdot 10^{-19}$ C and $a_0 = 5.2917720859(36) \cdot 10^{-11}$ m:

$$E_{nn_1n_2m} = -\frac{hcR_\mathrm{H}}{n^2} + \frac{3}{2}ea_0(n_1 - n_2)nE. \tag{69}$$

Expressing the positions in the spectroscopic unit of cm^{-1}, one obtains:

$$\tilde{\nu}_{nn_1n_2m}/\mathrm{cm}^{-1} = -\frac{R_\mathrm{H}/\mathrm{cm}^{-1}}{n^2} + 6.40215 \cdot 10^{-5}(n_1 - n_2)n(E/(\mathrm{V/cm})). \tag{70}$$

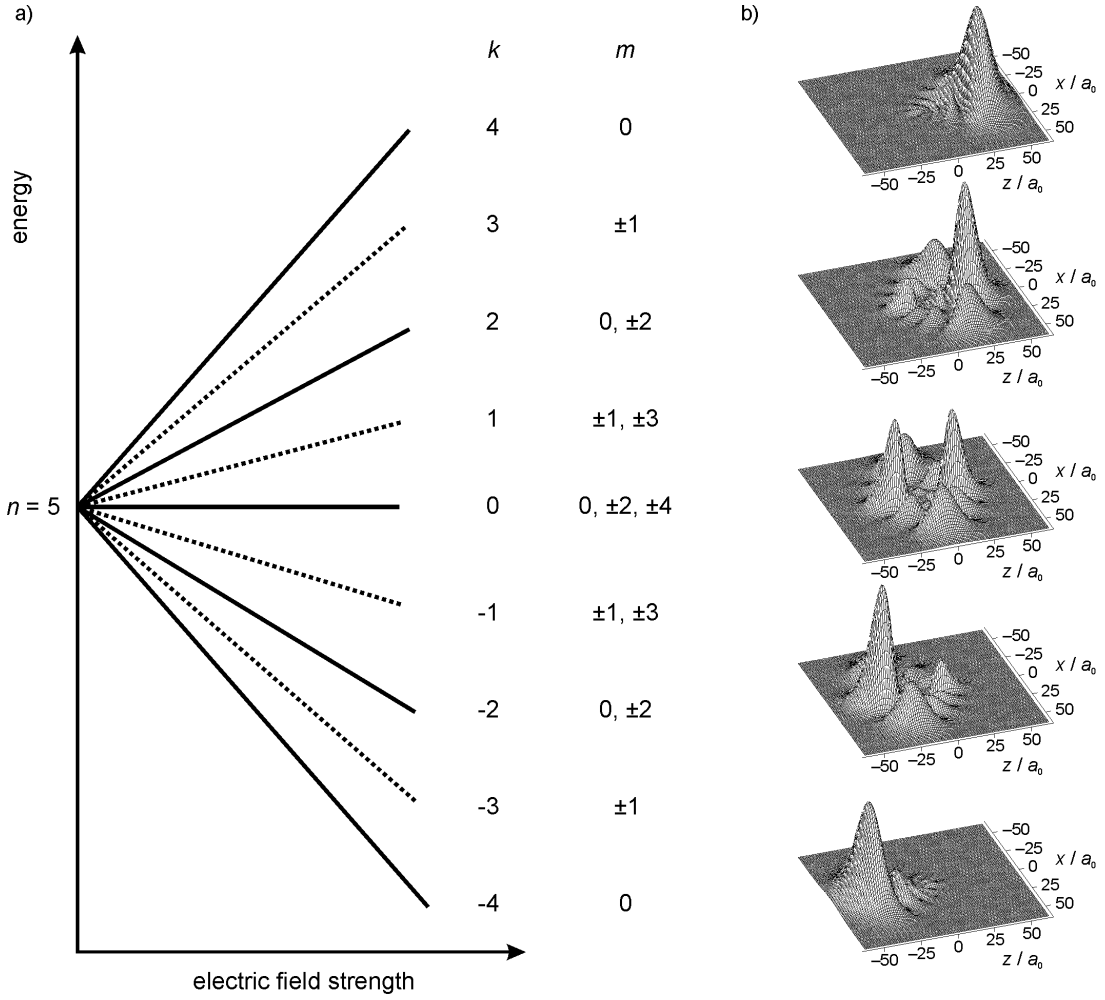

Figure 11: The linear Stark effect in the $n = 5$ state of atomic hydrogen. (a) Energy level diagram; (b) Electron density in the xz plane of the $m = 0$ states. The position of the nucleus is at the origin of the coordinate system. k represents the difference $n_1 - n_2$.

In polyelectronic atoms, the levels that can be coupled by the electric field are nondegenerate and the Stark effect is quadratic, i.e., the energies depend quadratically on E, as is expected from second-order perturbation theory. However, nonpenetrating Rydberg states, which are degenerate at zero-field (see Figure 7), represent an exception to this behavior, and behave very similarly in an electric field to the states of the hydrogen atom. Stark spectra of Ar Rydberg states are discussed in Subsection 3.2.3 (see Figure 43).

2.2 Diatomic molecules

Homonuclear diatomic molecules (H_2, N_2,...) and heteronuclear diatomic molecules (NO, HCl,...) belong to the $D_{\infty h}$ and $C_{\infty v}$ point groups, respectively. The character tables of these point groups are given in Tables 7 and 8, and the corresponding product table is presented in Table 9.

Table 7: Character table of the $C_{\infty v}$ point group.

$C_{\infty v}$	E	$2C_\infty^\varphi$	...	$\infty\sigma_v$		
$\Sigma^+(=A_1)$	1	1	...	1	z	x^2+y^2, z^2
$\Sigma^-(=A_2)$	1	1	...	-1	R_z	
$\Pi(=E_1)$	2	$2\cos\varphi$	...	0	$x, y; R_x, R_y$	xz, yz
$\Delta(=E_2)$	2	$2\cos 2\varphi$	...	0		x^2-y^2, xy
$\Phi(=E_3)$	2	$2\cos 3\varphi$	...	0		
...	...	...	...	...		

Table 8: Character table of the $D_{\infty h}$ point group.

$D_{\infty h}$	E	$2C_\infty^\varphi$	...	$\infty\sigma_v$	i	$2S_\infty^\varphi$	...	∞C_2		
Σ_g^+	1	1	...	1	1	1	...	1		x^2+y^2, z^2
Σ_g^-	1	1	...	-1	1	1	...	-1	R_z	
Π_g	2	$2\cos\varphi$	...	0	2	$-2\cos\varphi$	...	0	R_x, R_y	xz, yz
Δ_g	2	$2\cos 2\varphi$	...	0	2	$2\cos 2\varphi$	...	0		x^2-y^2, xy
...	...	...	...	...	...	...	...	...		
Σ_u^+	1	1	...	1	-1	-1	...	-1	z	
Σ_u^-	1	1	...	-1	-1	-1	...	1		
Π_u	2	$2\cos\varphi$	...	0	-2	$2\cos\varphi$	...	0	x, y	
Δ_u	2	$2\cos 2\varphi$	...	0	-2	$-2\cos 2\varphi$	...	0		
...	...	...	...	...	...	...	...	...		

Table 9: Direct product table of the point groups $C_{\infty v}$ and $D_{\infty h}$. For $D_{\infty h}$: $g \times g = u \times u = g$ und $g \times u = u \times g = u$.

$\times$	Σ^+	Σ^-	Π	Δ	Φ	...
Σ^+	Σ^+	Σ^-	Π	Δ	Φ	...
Σ^-		Σ^+	Π	Δ	Φ	...
Π			$\Sigma^+, \Sigma^-, \Delta$	Π, Φ	Δ, Γ	...
Δ				$\Sigma^+, \Sigma^-, \Gamma$	Π, H	...
Φ					$\Sigma^+, \Sigma^-, \mathrm{I}$	...
...	...	...	...	...	...	...

The orbitals and electronic states of molecules are labeled σ^+, π, δ,... and Σ^+, Σ^-, Π, Δ, ..., respectively, according to the irreducible representations of the corresponding point groups. Nondegenerate orbitals (or states) belong to one-dimensional irreducible representations (σ (Σ)), whereas doubly-degenerate orbitals (or states) belong to two-dimensional irreducible representations (π (Π), δ (Δ), ϕ (Φ),...).

The symmetry labels of molecular orbitals and electronic states of diatomic molecules are determined using the same procedure as for atoms: Molecular orbitals are designated by lower-case Greek letters ($\sigma^+, \pi, \delta, \ldots$ for heteronuclear diatomic molecules and $\sigma_g^+, \sigma_u, \pi_g, \pi_u, \ldots$ for homonuclear diatomic molecules). Electronic states are designated by capital Greek letters ($\Sigma^+, \Sigma^-, \Pi, \Delta, \ldots$ for heteronuclear diatomic molecules and $\Sigma_g^+, \Sigma_g^-, \Sigma_u^+, \Sigma_u^-, \Pi_g, \Pi_u, \ldots$ for homonuclear diatomic molecules). As in atoms, the symmetry labels also contain information on the electronic angular momentum. In the absence of spin-orbit coupling, the orbital angular momentum is a conserved quantity in a spherically symmetric potential. L and ℓ are therefore good quantum numbers in atoms (see Section 2.1). In diatomic molecules, the symmetry of the potential is reduced to cylindrical symmetry, so that only the projection of the total orbital angular momentum onto the internuclear axis is conserved as long as spin-orbit coupling can be neglected. The irreducible representations $\sigma, \pi, \delta, \ldots$ correspond to orbitals with values of 0, 1, 2, ... of the orbital angular momentum projection quantum number λ on the internuclear axis. Similarly, $\Sigma, \Pi, \Delta, \ldots$ are used to label electronic states with total orbital angular momentum projection quantum number $\Lambda = 0,\ 1,\ 2, \ldots$ on the internuclear axis, respectively. Orbitals of σ^- symmetry do not exist because no σ molecular orbital can be formed that has a nodal plane containing the internuclear axis, but electronic states of Σ^- result from configurations in which at least two orbitals of symmetry π, or δ, or ϕ, ... are singly occupied (See Tables 7, 8, and 9, and also Table 10 below).

How the quantum number λ arises in a linear molecule can also be understood by writing the

Schrödinger equation for a single electron in an axially symmetric potential in cylindrical coordinates:

$$\frac{\partial^2\Psi}{\partial z^2}+\frac{\partial^2\Psi}{\partial \rho^2}+\frac{1}{\rho}\frac{\partial\Psi}{\partial\rho}+\frac{1}{\rho^2}\frac{\partial^2\Psi}{\partial\varphi^2}+\frac{8\pi^2 m}{h}(E-V)\Psi=0, \tag{71}$$

where z is the coordinate of the electron along the symmetry axis, ρ its distance from the axis and φ the azimuthal angle.

Inserting the ansatz

$$\Psi(z,\rho,\varphi)=\chi(z,\rho)f(\varphi) \tag{72}$$

in Eq. (71) and multiplying the equation with ρ^2/Ψ gives

$$\frac{\rho^2}{\chi}\frac{\partial^2\chi}{\partial z^2}+\frac{\rho^2}{\chi}\frac{\partial^2\chi}{\partial\rho^2}+\frac{\rho}{\chi}\frac{\partial\chi}{\partial\rho}+\frac{8\pi^2 m\rho^2}{h}(E-V(z,\rho))=-\frac{1}{f}\frac{\partial^2 f}{\partial\varphi^2}. \tag{73}$$

Equating both sides to a constant λ^2, one obtains the differential equation in φ

$$\frac{\partial^2 f(\varphi)}{\partial\varphi^2}+\lambda^2 f(\varphi)=0, \tag{74}$$

which has the solutions

$$f_\pm(\varphi)=\mathrm{e}^{\pm\mathrm{i}\lambda\varphi}. \tag{75}$$

Because $f(\varphi)=f(\varphi+2\pi)$, λ must be an integer number. The general solution of Equation (71) is therefore

$$\Psi_\pm(z,\rho,\varphi)=\chi(z,\rho)\mathrm{e}^{\pm\mathrm{i}\lambda\varphi}. \tag{76}$$

Since the $\Psi_\pm$ are energetically degenerate (the $\pm\lambda$ solutions have identical eigenvalues), an arbitrary linear combination is also a solution. The $\Psi_\pm$ have a well-defined value of λ, but their linear combination does not. The labels σ, π, δ,... give the absolute value of λ.

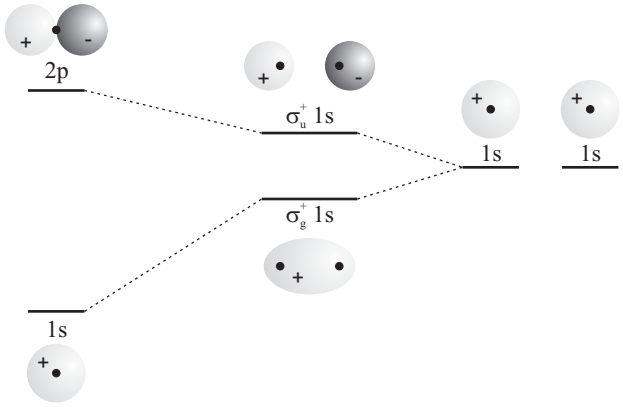

Figure 12: Correlation diagram from the two 1s atomic orbitals of two identical separated atoms to the 1s and $2p_z$ orbitals of the corresponding united atom through the σ_u^+ and σ_g^+ molecular orbitals

2.2.1 Molecular orbitals

In the qualitative representation of molecular orbitals, it is helpful to discuss two extreme situations: the united-atom limit and the separated-atom limit. In the united-atom limit, the atoms that form the molecule are considered to have coalesced into a single atom. The united atom limit of $^{16}O_2$ and H_2 are ^{32}S and ^{2}He, respectively. The molecular structure is determined by progressively separating the atomic components of the molecule towards the equilibrium internuclear separation. In the limit of the separated atoms, the atoms forming the molecule are considered at an infinite internuclear separation. Molecular states are formed by progressively approaching the atoms towards the equilibrium internuclear separation. The expected form and energetical order of the molecular orbitals can be predicted by linking the two limiting cases in a correlation diagram by making sure that curves of the same symmetry do not cross. Figure 12 shows how the two 1s atomic orbitals of the two separated H atoms correlate through the σ_u^+ and σ_g^+ molecular orbitals with the 1s and $2p_z$ orbitals of the united atoms. By convention the z axis is chosen to be the internuclear axis. Figures 13 and 14 display the correlation diagrams connecting the energy levels of the separated atoms with those of the united atoms in the case of homonuclear and heteronuclear diatomic molecules, respectively. Different molecules with their specific internuclear separation occupy different positions along the horizontal axis of these figures.

The determination of molecular orbitals often relies on the LCAO (linear combination of atomic orbitals) method. Molecular orbitals ϕ_j are formed from symmetry-adapted linear combinations of atomic orbitals φ_i following

$$\phi_j = \sum_i c_{ji}\varphi_i. \tag{77}$$

Several conditions must be fulfilled to form molecular orbitals that are distinct from the original atomic orbitals:

- The energies of the atomic orbitals that are combined must be similar.
- The atomic orbitals must overlap at the equilibrium internuclear separation.
- The atomic orbitals must be symmetry compatible.

Figure 15a shows the structure of molecular orbitals of homonuclear diatomic molecules consisting of atoms of the second row of the periodic system. For Li_2^+, Li_2, Li_2^-, B_2^+, B_2, B_2^-, C_2^+, C_2, C_2^-, N_2^+ and N_2, the energetic ordering of the orbitals is

$$1\sigma_g(1s) < 1\sigma_u^*(1s) < 2\sigma_g(2s) < 2\sigma_u^*(2s) < 1\pi_u(2p) < 3\sigma_g(2p) < 1\pi_g^*(2p) < 3\sigma_u^*(2p). \tag{78}$$

In the case of O_2^+, O_2, O_2^-, F_2^+, F_2, F_2^- and Ne_2^+, it is

$$1\sigma_g(1s) < 1\sigma_u^*(1s) < 2\sigma_g(2s) < 2\sigma_u^*(2s) < 3\sigma_g(2p) < 1\pi_u(2p) < 1\pi_g^*(2p) < 3\sigma_u^*(2p). \tag{79}$$

These two cases are depicted schematically in Figure 15b and c, respectively.

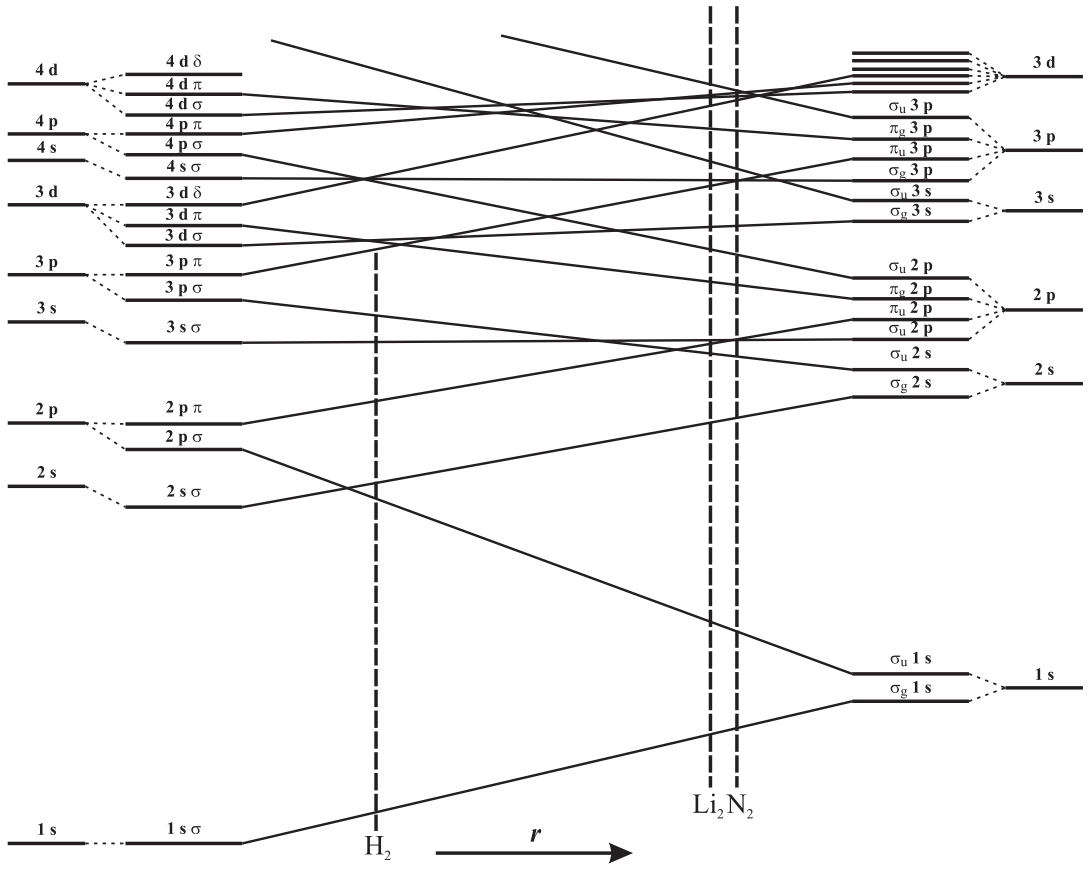

Figure 13: Correlation diagram illustrating the evolution of molecular orbitals between the separated atoms limit (right) and the united atoms limit (left) for homonuclear diatomic molecules (Adapted from Herzberg (1989)).

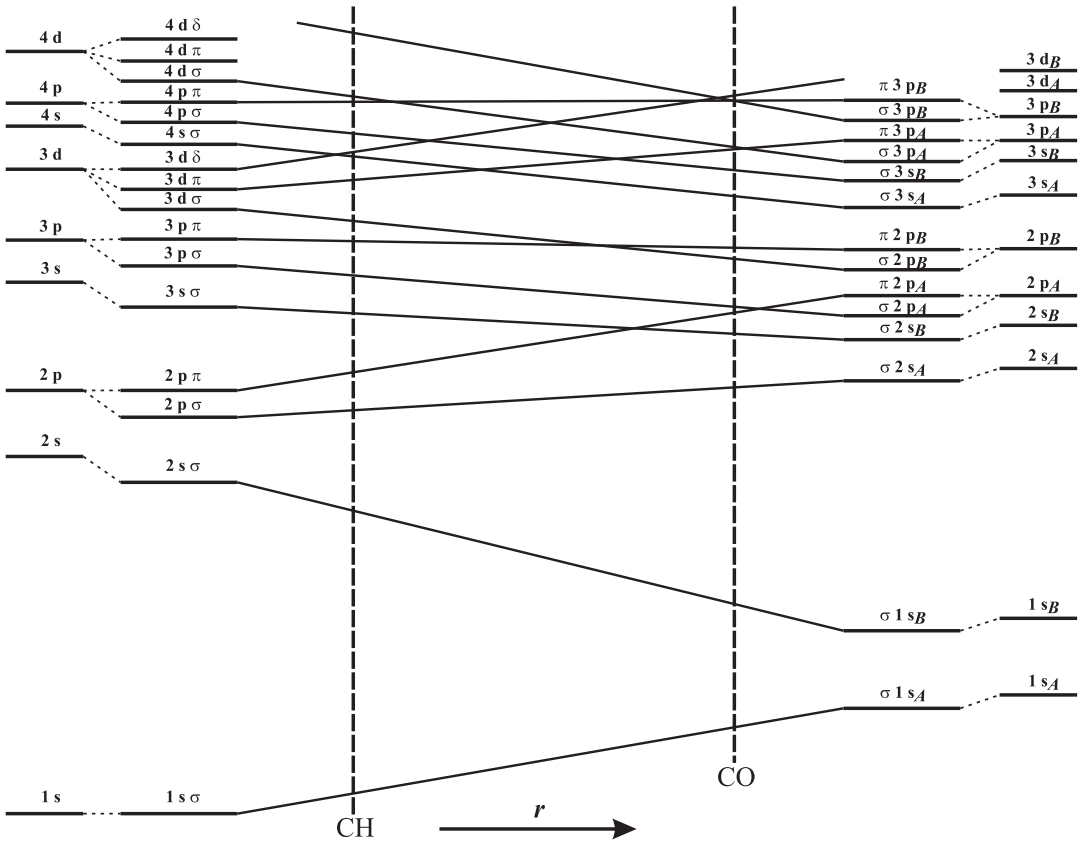

Figure 14: Correlation diagram between separated atoms (right) and united atoms (left) for heteronuclear diatomic molecules. (Adapted from Herzberg (1989)).

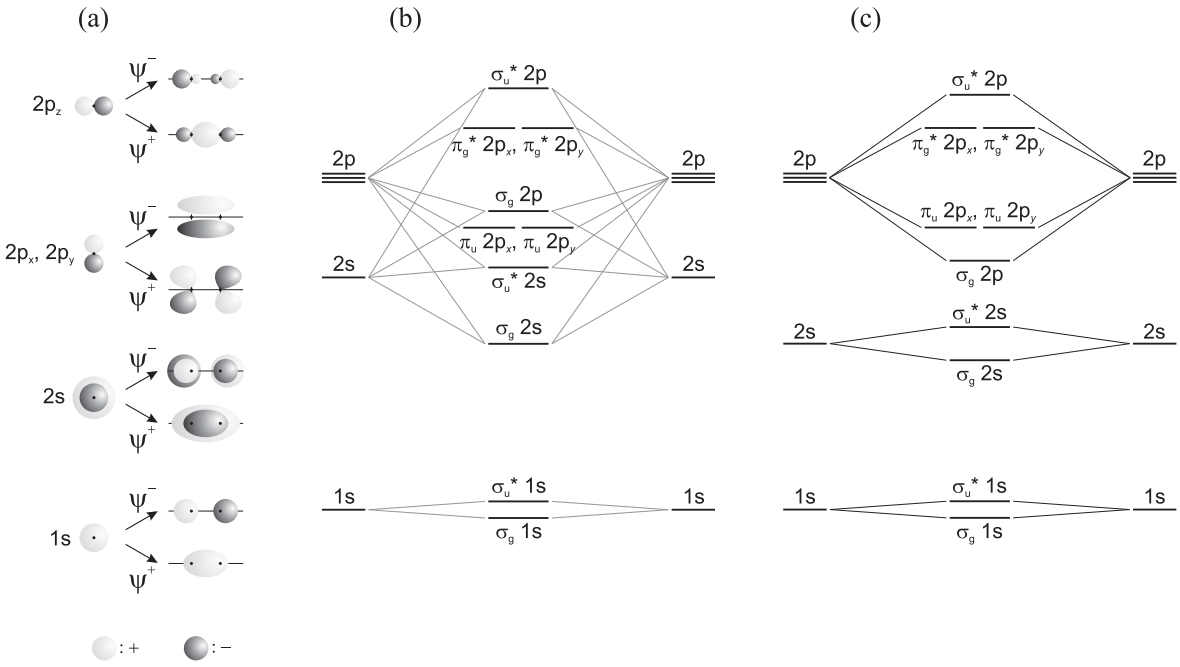

Figure 15: (a) Schematic representation of molecular orbitals in homonuclear diatomic molecules made from 1s, 2s and 2p atomic orbitals. Molecular orbital energy diagram for homonuclear diatomic molecules formed from the lighter (b) and the heavier (c) atoms from the second row of the periodic system of elements.

2.2.2 Electronic configurations

Electronic configurations are obtained by filling the spatial orbitals according to the Pauli principle with no more than two electrons. The ground-state configuration of N_2, e.g., is

$$(1\sigma_g)^2(1\sigma_u^*)^2(2\sigma_g)^2(2\sigma_u^*)^2(1\pi_u)^4(3\sigma_g)^2 \tag{80}$$

and the first two excited configurations are

$$(1\sigma_g)^2(1\sigma_u^*)^2(2\sigma_g)^2(2\sigma_u^*)^2(1\pi_u)^4(3\sigma_g)^1(1\pi_g^*)^1 \tag{81}$$

and

$$(1\sigma_g)^2(1\sigma_u^*)^2(2\sigma_g)^2(2\sigma_u^*)^2(1\pi_u)^3(3\sigma_g)^2(1\pi_g^*)^1. \tag{82}$$

The ground-state configuration of O_2 is

$$(1\sigma_g)^2(1\sigma_u^*)^2(2\sigma_g)^2(2\sigma_u^*)^2(3\sigma_g)^2(1\pi_u)^4(1\pi_g^*)^2. \tag{83}$$

If two electrons are located in the same spatial orbital, they must have opposite spins. As in the case of atoms, an electronic configuration leads in general to several electronic terms and several electronic states.

2.2.3 Electronic wave functions and electronic terms

As explained in Subsection 2.1.2, N-electron wave functions $\Psi(q_1, q_2, \ldots, q_N)$ of molecules must obey the generalized Pauli principle. Consequently, they must be antisymmetric under the pairwise permutation of electrons, which is automatically fulfilled by Slater determinants of the general form given by Equation (15). The spatial part of the one-electron functions ϕ_i corresponds to a molecular orbital of the form (76) and (77). To determine the possible electronic terms, only shells and subshells with partially filled orbitals need be considered, because full shells and subshells are totally symmetric ($^1\Sigma_g^+$ and $^1\Sigma^+$ for homonuclear and heteronuclear diatomic molecules, respectively.). The character Γ of the spatial part of the electronic term is determined from the direct product (see Table 9) of the irreducible representations

$$\Gamma = \Gamma(f(q_i)) \otimes \Gamma(f(q_j)) \otimes \ldots \tag{84}$$

of the molecular orbitals, where the product extends over all electrons in partially filled molecular orbitals.

Applying Eq. (84) to the configurations (80)-(83), one can draw the following conclusions:

1. Since all orbitals of the configuration (80) are fully occupied, the totally-symmetric representation Σ_g^+ results. Moreover, because all electrons are paired, a unique singlet term of symmetry $^1\Sigma_g^+$ is obtained. Consequently, the ground electronic state of N_2 is designated as X $^1\Sigma_g^+$.

2. The $(3\sigma_g)^1(1\pi_g^*)^1$ part of configuration (81) leads to a Π_g term. The corresponding spin multiplicities are derived below in Subsection 2.2.4.

3. Because $(1\pi_u)^3$ can be considered as a $(1\pi_u)^1$ electron hole, the $(1\pi_u)^3(1\pi_g^*)^1$ part of the configuration (82) can be treated as the configuration $1(\pi_u)^1(1\pi_g^*)^1$, which leads to the terms Σ_u^+, Σ_u^- and Δ_u. Their energetic order and multiplicities are derived in the next subsection.

2.2.4 Spin multiplicity

As explained in Subsection 2.1.3, polyelectron wave functions can be written as a product of a spatial part ($\Psi^R(q_i)$) and a spin part ($\Psi^S(m_i)$).

$$\Psi(q_1, m_1, q_2, m_2, \ldots) = \Psi^R(q_1, q_2, \ldots) \times \Psi^S(m_1, m_2, \ldots). \tag{85}$$

For simplicity, we consider here only two-electron wave functions and can therefore use the results presented in Tables 4 and 5. The extension to more complicated situations is straightforward. Because a two-electron wave function must be antisymmetric under permutation of the coordinates of the electrons, it must have either a symmetric spatial part ($\Psi^R_{(s)}(q_i)$) and an antisymmetric spin part ($\Psi^S_{(a)}(m_i)$) or vice versa ($\Psi^R_{(a)}(q_i)$ and $\Psi^S_{(s)}(m_i)$).

In the determination of the multiplicity of an electronic term in accordance to Tables 4 and 5, three cases have to be distinguished:

- **case 1:**

  The two electrons are located in different molecular-orbital shells, as in the configuration (81) ($(3\sigma_g)^1(1\pi_g^*)^1$). Both the symmetric and the antisymmetric spatial parts are nonzero. Consequently, both singlet and triplet states are allowed, and configuration (81) leads to the two terms $^1\Pi_g$ and $^3\Pi_g$.

- **case 2:**

  The two electrons are located in the same molecular-orbital shell and in the same spatial orbital ($\phi_1 = \phi_2$), so that $\Psi^R_{(a)}(q_1, q_2) = 0$. The triplet state thus does not exist. This situation arises in the $(1\pi_g)^2$ configuration of O_2, when both electrons are located in either the $\lambda = 1$ or the $\lambda = -1$ orbital. In this case, Λ is equal to ± 2 and the corresponding term is $^1\Delta_g$.

- **case 3:**

  The two electrons are located in the same MO-shell but in different orbitals. This situation also arises in the $(2\pi_g)^2$ configuration of O_2, when each of the two $\lambda = \pm 1$ orbitals is occupied by one electron ($\Lambda = 0$). The spatial part may be either symmteric ($\Psi^R_{(s)}(q_1, q_2) = (\pi_+(1)\pi_-(2) + \pi_+(2)\pi_-(1))/\sqrt{2}$), which results in a $^1\Sigma_g$ term, or antisymmetric ($\Psi^R_{(a)}(q_1, q_2) = (\pi_+(1)\pi_-(2) - \pi_+(2)\pi_-(1))/\sqrt{2}$), which corresponds to a $^3\Sigma_g$ term. To determine whether these $^1\Sigma_g$ and $^3\Sigma_g$ terms are Σ_g^- or Σ_g^+, one has to determine their symmetry with respect to the operation σ_v (see Table 8), which represents the reflection through an arbitrary plane containing the internuclear axis. Using the ansatz (76) for the π_+ and π_- functions, we obtain

$$\begin{aligned}
\Psi^R_{(a)}(q_1, q_2) &= \frac{1}{\sqrt{2}}\left[\chi(z_1, \rho_1)e^{i\varphi_1}\chi(z_2, \rho_2)e^{-i\varphi_2} - \chi(z_2, \rho_2)e^{i\varphi_2}\chi(z_1, \rho_1)e^{-i\varphi_1}\right] \\
&= \frac{1}{\sqrt{2}}\chi(z_1, \rho_1)\chi(z_2, \rho_2)\left(e^{i(\varphi_1-\varphi_2)} - e^{-i(\varphi_1-\varphi_2)}\right) \\
&= \sqrt{2}i\chi(z_1, \rho_1)\chi(z_2, \rho_2)\sin(\varphi_1 - \varphi_2). \qquad (86)
\end{aligned}$$

  for the $^3\Sigma$ term, and

$$\Psi^R_{(s)}(q_1, q_2) = \sqrt{2}\chi(z_1, \rho_1)\chi(z_2, \rho_2)\cos(\varphi_1 - \varphi_2) \qquad (87)$$

  for the $^1\Sigma$ term.

  A σ_v reflection inverts the sign of $(\varphi_1 - \varphi_2)$. Because of the relations $\sin(-x) = -\sin(x)$ and $\cos(-x) = \cos(x)$, $\Psi^R_{(s)}(q_1, q_2)$ corresponds to the $^1\Sigma_g^+$ term and $\Psi^R_{(a)}(q_1, q_2)$ to the $^3\Sigma_g^-$ term.

  Consequently, the $(1\pi_g)^2$ configuration of O_2 possesses the three terms $^3\Sigma_g^-$, $^1\Sigma_g^+$ und $^1\Delta_g$. The energetically favorable exchange interaction in the triplet term causes the X $^3\Sigma_g^-$ state to be the ground state of O_2.

This procedure can be applied to arbitrary configurations. Table 10 summarizes the terms resulting from the most common electronic configurations of diatomic molecules.

Table 10: Terms belonging to the most frequent electronic configurations of diatomic molecules. The index i designates inverted term multiplets. The g and u labels relevant for homonuclear diatomic molecules can determined from the number N of electrons in MO orbitals of u symmetry, When N is gerade, the terms are g, otherwise they are u.

config.	terms	config.	terms
σ^2	$^1\Sigma^+$	$\pi^2\sigma\delta$	$^1\Sigma^+,^1\Sigma^-,^1\Delta(2),^1\Gamma,^3\Sigma^+,^3\Sigma^-,^3\Delta(3),$ $^3\Gamma,^5\Delta$
π^2	$^1\Sigma^+,^3\Sigma^-,^1\Delta$	$\pi^2\pi\pi$	$^1\Sigma^+(3),^1\Sigma^-(3),^1\Delta(4),^1\Gamma,^3\Sigma^+(4),$ $^3\Sigma^-(4),^3\Delta(5),^3\Gamma,^5\Sigma^+,^5\Sigma^-,^5\Delta$
π^3	$^2\Pi_i$	$\pi^2\pi^2$	$^1\Sigma^+(3),^1\Sigma^-,^1\Delta(2),^1\Gamma,^3\Sigma^+(2)$ $^3\Sigma^-(2),^3\Delta(2),^5\Sigma^+$
π^4	$^1\Sigma^+$	$\pi^3\sigma$	$^1\Pi,^3\Pi_i$
δ^2	$^1\Sigma^+,^3\Sigma^-,^1\Gamma$	$\pi^3\pi$	$^1\Sigma^+,^1\Sigma^-,^1\Delta,^3\Sigma^+,^3\Sigma^-,^3\Delta$
δ^3	$^2\Delta_i$	$\pi^3\delta(\pi^3\delta^3)$	$^1\Pi,^1\Phi,^3\Pi,^3\Phi$
δ^4	$^1\Sigma^+$	$\pi^3\sigma\sigma$	$^2\Pi(2),^4\Pi$
$\pi^2\sigma$	$^2\Sigma^+,^2\Sigma^-,^2\Delta,^4\Sigma^-$	$\pi^3\pi^2$	$^2\Pi_i,^2\Pi(2),^2\Phi_i,^4\Pi_i$
$\pi^2\pi$	$^2\Pi,^2\Pi_i(2),^2\Phi,^4\Pi$	$\pi^3\pi^3$	$^1\Sigma^+,^1\Sigma^-,^1\Delta,^3\Sigma^+,^3\Sigma^-,^3\Delta_i$
$\pi^2\delta$	$^2\Sigma^+,^2\Sigma^-,^2\Delta,^2\Delta_i,^2\Gamma,^4\Delta$	$\pi^3\pi^2\sigma$	$^1\Pi(3),^1\Phi,^3\Pi_i(2),^3\Pi(2),^3\Phi_i,^5\Pi_i$
$\pi^2\sigma\sigma$	$^1\Sigma^+,^1\Sigma^-,^1\Delta,^3\Sigma^+,^3\Sigma^-(2),^3\Delta,^5\Sigma^-$	$\pi^3\pi^3\sigma$	$^2\Sigma^+(2),^2\Sigma^-(2),^2\Delta,^2\Delta_i,^4\Sigma^+,^4\Sigma^-,^4\Delta_i$
$\pi^2\sigma\pi$	$^1\Pi(3),^1\Phi,^3\Pi(2),^3\Pi_i(2),^3\Phi,^5\Pi$		

The classification of terms presented in this subsection relies on the assumption that electrostatic (including exchange) interactions are dominant and the effects of spin-orbit coupling can be disregarded. This assumption is justified as long as the $^{2S+1}\Lambda$ terms are separated in energy by an amount larger than the spin-orbit interaction. This tends to be case in molecules made of light atoms, for which spin-orbit inteactions are genuinely weak, and at short internuclear distances, where the atomic orbitals significantly overlap, the electronic motion is strongly coupled to the internuclear axis, and the exchange interaction is substantial. Consideration of the spin-orbit interaction makes it necessary to extend the classification of electronic terms.

2.2.5 Spin-Orbit Coupling

To assess the effects of the spin-orbit coupling on the electronic structure of diatomic molecules, one needs to establish the relative strength of the interactions that couple the different electronic angular momenta. The treatment is similar to that discussed for atoms in Subsection 2.1.4, with the important difference that only the projections $\hbar\lambda_i$ ($\hbar\Lambda; \Lambda = \sum_i \lambda_i$) of the (total) orbital angular momentum vectors $\vec{\ell}_i$ ($\vec{L}$) along the internuclear axis, rather than the vectors $\vec{\ell}_i$ and $\vec{L}$ themselves, are constants of motion in the absence of spin-orbit coupling.

The strength of the spin-orbit coupling depends on the molecule, the electronic configuration and the internuclear separation. It is convenient to classify and label the electronic states according to idealized limiting cases, presented as cases (a)-(d) below, which form the starting point of the widely used classification of angular momentum coupling in rotating molecules originally introduced by F. Hund (Hund 1926b,a, 1927a,c,b,d, 1928, 1930, 1933) and extended by Mulliken (Mulliken 1930a,b,c; Mulliken and Christy 1931; Mulliken 1931). If the rotational motion is neglected, the relevant interactions are:

1. The interactions of the orbital motion of the electrons with the cylindrically symmetric electrostatic field of the nuclei. This interaction causes a precession of the orbital angular momentum vectors around the internuclear axis. Whereas neither $\vec{\ell_i}$ nor $\vec{L}$ are constants of motion in cylindrical symmetry (compare Table 1 with Tables 7 and 8), λ_i and Λ are good quantum numbers in the absence of spin-orbit coupling. When the electrostatic interactions between electrons and nuclei are strong, the terms resulting from the different configurations are widely spaced in energy, and even the different terms of a given configuration are energetically well separated.

2. The electrostatic exchange interaction. This interaction gives rise to an energetic splitting between states of different total electron spin quantum number S, as discussed in the previous subsection.

3. The spin-orbit interaction. The spin-orbit interaction can be regarded as an interaction between the magnetic moments resulting from the spin and orbital angular momentum vectors. This interaction can be described as inducing a precession of $\vec{S}$ (or $\vec{s_i}$) and $\vec{L}$ (or $\vec{\ell_i}$) around the resultant vectors $\vec{J}$ (or $\vec{j_i}$) (see Subsection 2.1.4). When the spin-orbit interaction becomes larger than the exchange interaction, S ceases to be a good quantum number.

Angular momentum coupling cases of the "LS-coupling" type

When interactions 1 and 2 above are larger than interaction 3, situations analogous to LS coupling in atoms result that can be described by two limiting cases, called cases (a) and (b) below. In both cases, S and Λ are good quantum numbers.

Case (a):

In this first case, the electrostatic coupling of the orbital motion to the internuclear axis induces a fast precession of $\vec{L}$ around the internuclear axis. On the longer time scale of the weaker spin-orbit interaction, the precession of the orbital anular momentum vector is effectively averaged out and is perceived as a vector of length $\hbar\Lambda$ pointing along the internuclear axis, with magnetic moment $-\gamma_e\Lambda\hbar$. The orbital motion leads to a magnetic field pointing along the internuclear axis which then becomes the quantization axis for the electron spin vector $\vec{S}$. $\vec{S}$ precesses with projection quantum number Σ around the internuclear axis as a result of the spin-orbit interaction (see Figure 16a). Next to S, the projection quantum numbers Λ and Σ and their sum Ω are good quantum numbers. Because of the spin-orbit coupling, the total energy depends on the relative sign of Σ and Λ, so that usually only the

absolute values of Λ and Ω are used to designate the terms. The nomenclature $^{2S+1}\Lambda_\Omega$ is used, and the $2S+1$ components of the spin multiplet are split according to their spin-orbit interaction energies which can be well approximated by

$$E_{\mathrm{SO}} = hcA\Lambda\Sigma, \tag{88}$$

where A (in cm^{-1}) represents an effective spin-orbit coupling constant (compare with Equations (37)). The spin-orbit splittings usually depend on the internuclear distance and thus on the vibrational level so that the spin-orbit coupling constant of a given vibrational level is further labeled with the subscript "v" as A_v. A and A_v can be negative, in which case one speaks of inverted multiplets. Equation (88) can be regarded as a Paschen-Back effect induced by the electrostatic field of the nuclei (see last term on the right-hand side of Equation (64)).

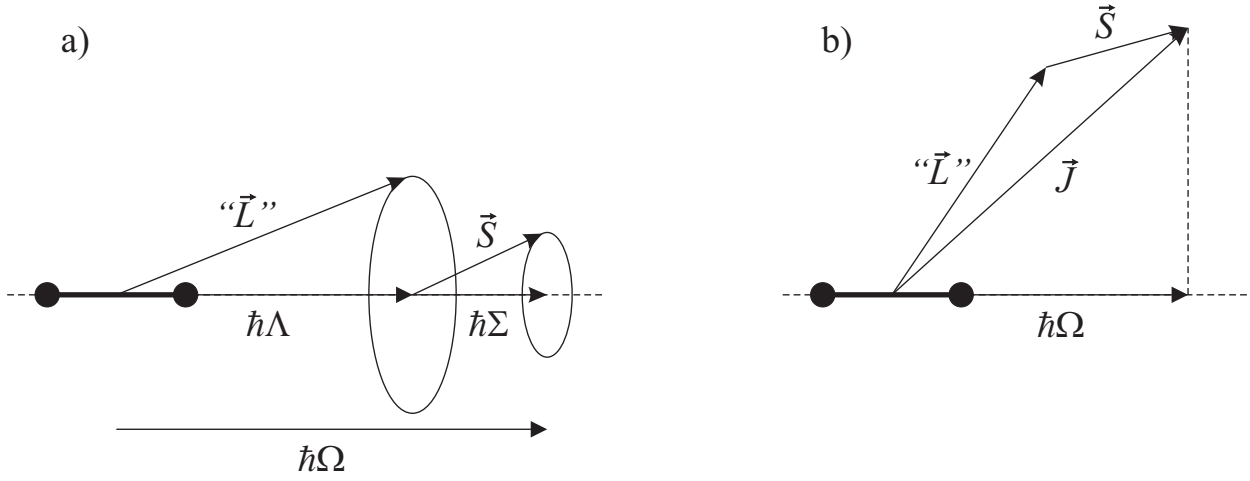

Figure 16: Electronic angular momentum coupling in the limit of (a) weak spin-orbit interaction (Case (a)) and (b) strong spin-orbit interaction (case (c)). "$\vec{L}$" is used instead of $\vec{L}$ to stress that L is usually not a good quantum number in molecules.

Example: The $[\ldots][\sigma(2\mathrm{p})]^2[\pi(2\mathrm{p})]^4[\pi^*(2\mathrm{p})]^1$ X $^2\Pi$ ground electronic state of NO is separated from the first electronically excited state by $\approx$ 44000 cm^{-1}. The two spin-orbit components with $\Omega = 1/2$, 3/2 are only separated by $\approx$ 120 cm^{-1}, and the ground state is X $^2\Pi_{1/2}$. A weak coupling between the vibrational and the electronic motion causes a dependence of the spin-orbit constant (A in Equation (88)) on the vibrational state ($A_v/(\mathrm{cm}^{-1}) = 123.26 - 0.1906(v+1/2) - 0.018(v+1/2)^2$) (Huber and Herzberg 1979).

Case (b):

In this second case, the spin-orbit interaction is negligible and $\vec{S}$ is not quantized along the internuclear axis. Consequently Σ is not defined and the $2S+1$ components of the spin multiplet remain degenerate in the nonrotating molecule. This case is characteristic of $\Lambda = 0$ states. The good electronic angular momentum quantum numbers in this case are Λ and S.

Example: The $[\ldots][\pi_u(2p)]^4[\sigma_g(2p)]^1$ X $^2\Sigma_g^+$ ground electronic state of N_2^+ is separated from the first electronically excited state by about 9000 cm^{-1} (Huber and Herzberg 1979). Except for the twofold spin degeneracy, the situation is similar to that in a $^1\Sigma_g^+$ state.

Angular momentum coupling cases of the "jj-coupling" type

When the spin-orbit interaction is stronger than the electrostatic interactions, $\vec{S}$ is not a constant of motion, nor are the projections $\hbar\Lambda$ and $\hbar\Sigma$ of the orbital and spin angular momentum vectors. This situation can arise either when the spin-orbit interaction is particularly large, for instance in molecules containing heavy atoms (see case (c) below), or when the electrostatic coupling of the electronic angular momenta to the internuclear axis is particularly weak, for instance in weakly bound molecules or in Rydberg states (see case (d) below).

Case (c):

In this case, the strong spin-orbit interaction couples the spin ($\vec{s}_i$ or $\vec{S}$) and orbital ($\vec{\ell}_i$ or $\vec{L}$) angular momentum vectors, which can be viewed as precessing around the resultant vectors ($\vec{j}_i$ or $\vec{J}_a$). The weaker electrostatic coupling of the orbital motion to the internuclear axis leads to a slower precession of the resultant vectors around the internuclear axis with projection $\hbar\Omega$. The only good quantum number of the nonrotating molecule is Ω (see Figure 16b).

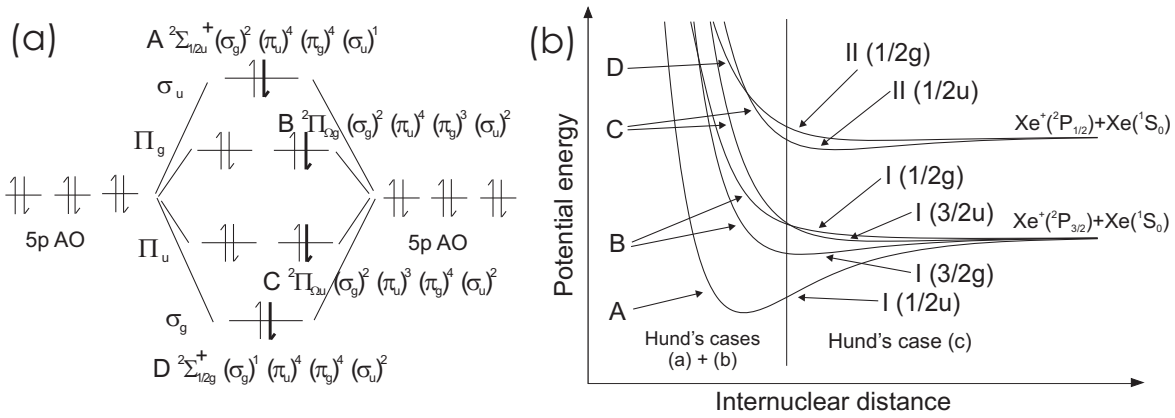

Figure 17: a) Lowest four electronic configurations of Xe_2^+ in the notation introduced by Mulliken (1970). The bold arrows indicate the electrons that are missing in the respective configurations. b) Potential energy functions of the six corresponding low-lying electronic states which can be described by cases (a) and (b) at short internuclear distances and by case (c) at large internuclear distances.

Example: The low-lying electronic states of Xe_2^+ (see Mulliken (1970); Zehnder and Merkt (2008)). Neglecting the spin-orbit interaction, the electronic configurations $A = [\ldots][\sigma_g(5p)]^2[\pi_u(5p)]^4[\pi_g^*(5p)]^4[\sigma_u{}^*(5p)]^1$,

Table 11: Spin-orbit interaction matrix describing the coupling between the states of $^2\Sigma^+$ and $^2\Pi$ symmetry in the homonuclear rare gas dimer ions.

	$^2\Sigma^+_{1/2}$	$^2\Pi_{1/2}$	$^2\Pi_{3/2}$
$^2\Sigma^+_{1/2}$	$V_\Sigma(R)$	$-\frac{a}{\sqrt{2}}$	0
$^2\Pi_{1/2}$	$-\frac{a}{\sqrt{2}}$	$V_\Pi(R)+\frac{a}{2}$	0
$^2\Pi_{3/2}$	0	0	$V_\Pi(R)-\frac{a}{2}$

$B = [\ldots][\sigma_g(5p)]^2[\pi_u(5p)]^4[\pi_g^*(5p)]^3[\sigma_u{}^*(5p)]^2$, $C = [\ldots][\sigma_g(5p)]^2[\pi_u(5p)]^3[\pi_g^*(5p)]^4[\sigma_u{}^*(5p)]^2$, and $D = [\ldots][\sigma_g(5p)]^1[\pi_u(5p)]^4[\pi_g^*(5p)]^4[\sigma_u{}^*(5p)]^2$ give rise to four electronic states A $^2\Sigma_u^+$, B $^2\Pi_g$, C $^2\Pi_u$ and D $^2\sigma_g$ (see Figure 17a). At short internuclear distances, the electrostatic interactions lead to splittings that are larger than those resulting from the spin-orbit interaction. Consequently, the two $^2\Sigma^+$ and the two $^2\Pi$ states can be approximately described by the cases (b) and (a) presented above, respectively, and six states result: A $^2\Sigma_u^+$, B $^2\Pi_{3/2g}$, B $^2\Pi_{1/2g}$, C $^2\Pi_{3/2u}$ C $^2\Pi_{1/2u}$ and D $^2\Sigma_g^+$ (see left-hand side of Figure 17b). As the internuclear distance increases, the electrostatic coupling to the internuclear axis weakens, and the spin-orbit interaction starts dominating. As the internuclear distance goes towards infinity, two dissociation limits result, the lower one being Xe $^1S_0$ + Xe$^+$ $^2P_{3/2}$, and the upper one Xe $^1S_0$ + Xe$^+$ $^2P_{1/2}$. The energetic splitting between these two limits corresponds to the spin-orbit splitting of the Xe$^+$ ion (see right-hand side of Figure 17b). The lower limit has $J_a = 3/2$, and thus four states, two $\Omega = 3/2$ and two $\Omega = 1/2$ states, designated by "I", dissociate to this limit, whereas only two $\Omega = 1/2$ states, designated by "II", dissociate to the upper limit which has $J_a = 1/2$. The $\Omega = 1/2$ states of g (u) symmetry become equal mixtures of the B $^2\Pi_{1/2g}$ and D $^2\Sigma_g^+$ states (A $^2\Sigma_u^+$ and C $^2\Pi_{1/2u}$ states) at large internuclear distances, and the Λ label becomes inadequate. The evolution from the coupling cases (a) and (b) at short distances to case (c) at large distances can be described semi-quantitatively by considering the spin-orbit coupling matrix in Table 11 (Cohen and Schneider 1974). The matrix, in the derivation of which the spin-orbit coupling constant is assumed to be independent of the internuclear separation, clearly shows that the spin-orbit interaction does not only split the $^2\Pi$ state into two components with $\Omega = 3/2$ and $1/2$ but also mixes the two $\Omega = 1/2$ states.

Case (d):

This case arises when the electrostatic coupling of the electron orbital motion to the internuclear axis becomes negligible. This case is encountered in Rydberg states at large values of the principal quantum number of the Rydberg electron. In these states, the Rydberg electron density in the region of the diatomic molecular ion core, and thus the coupling of the electron to the internuclear axis, are very small, so that λ and Λ are not defined. Usually, the Rydberg electron spin is not coupled to the internuclear axis either, and the spin-orbit interaction of the Rydberg electron is negligible. A J^+, j-type coupling scheme $[^{(2S^+ + 1)}\Lambda^+_{\Omega^+}]|n\ell(sj)\rangle$ similar to that described for atoms by Equation (46), and

which represents the state as a product of the electronic functions of the ion core and of the Rydberg electron, is adequate.

Example: N_2: $|[N_2^+]\ldots(1\pi_u)^4(1\sigma_g)^1\ {}^2\Sigma_g^+\rangle|20p\rangle$.

2.2.6 Vibronic Structure

Diatomic molecules only possess one vibrational degree of freedom, and thus one vibrational mode that corresponds to a totally-symmetric representation ($^1\Sigma_g^+$ in $D_{\infty h}$ and $^1\Sigma^+$ in $C_{\infty v}$). The vibronic symmetry is thus the same as the electronic symmetry. The energetic position of the vibrational energy levels relative to the minimum T_e^α of the potential curve of the α^{th} electronic state is given by

$$E_v^\alpha = T_e^\alpha + \omega_e^\alpha(v+1/2) - \omega_e x_e^\alpha(v+1/2)^2 + \omega_e y_e^\alpha(v+1/2)^3 - \ldots, \tag{89}$$

where the second and subsequent terms are a consequence of the anharmonicity of the potential curve.

2.2.7 Rovibronic Structure

The treatment of the rotational structure of diatomic molecules is sometimes reduced to the well-known formula

$$E_{\text{ROT}} = B_v J(J+1) - D_v(J(J+1))^2, \tag{90}$$

which includes centrifugal distortion effects and also the variation of the rotational and centrifugal distortion constants that results from the anharmonicity of the vibrational motion. Equation (90) is adequate to describe the rotational structure of states of $^1\Sigma^+$ symmetry, but it does not account for the details of the rotational energy structure of states of other electronic symmetry, for which the coupling of rotational, orbital and spin angular momenta must be considered. To present a complete treatment would extend beyond the scope of this introductory chapter. We limit ourselves here to qualitative considerations and a presentation of the rotational structures of the simplest situations. The interested readers are referred to the original articles of F. Hund and R. S. Mulliken (Hund 1926a, 1927c,d, 1928, 1930, 1933; Mulliken 1930b,c; Mulliken and Christy 1931) and to the excellent overviews by Herzberg (Herzberg 1989), Hougen (Hougen *et al.* 1970), Zare (Zare 1988), Watson (Watson 1999b), Lefebvre-Brion and Field (Lefebvre-Brion and Field 2004) and Brown and Carrington (Brown and Carrington 2003) for more detailed treatments.

Since diatomic molecules have a vanishing moment of inertia along the internuclear axis, the angular momentum vector $\vec{R}$ describing the rotation of the nuclei lies perpendicular to the internuclear axis. The total angular momentum (without nuclear spins) $\vec{J}$ of a rotating molecule is equal to

$$\vec{J} = \vec{S} + \vec{L} + \vec{R} = \vec{S} + \vec{N}, \tag{91}$$

where $\vec{N}$ represents the total angular momentum without electron spins. The quantum number R associated with $\vec{R}$ is only a good quantum number in molecules without electronic angular momentum, i.e., in $^1\Sigma$ states ($\vec{J} = \vec{N} = \vec{R}$), and this is why Equation (90) can only be used for such states. In all other cases, the coupling between the spin, orbital and rotational motions must be considered explicitly. The spin-orbit and rotational motions can be described by the effective Hamiltonian

$$\hat{H} = \hat{H}_{\mathrm{el}} + T_{\mathrm{N}}(Q) + \hat{H}_{\mathrm{ROT}} + \hat{H}_{\mathrm{SO}}, \tag{92}$$

where the kinetic energy of the nuclei has been divided into rotational motion $\hat{H}_{\mathrm{ROT}}$ and vibrational motion $T_N(Q)$. The spin-orbit coupling is described by

$$\hat{H}_{\mathrm{SO}} = A\vec{\hat{L}} \cdot \vec{\hat{S}} = A(\hat{L}_x\hat{S}_x + \hat{L}_y\hat{S}_y + \hat{L}_z\hat{S}_z), \tag{93}$$

which is adequate as long as the spin-orbit interaction can be treated in an "LS"-like coupling manner, and the rotational motion by

$$\hat{H}_{\mathrm{ROT}} = \frac{1}{2\mu R^2}\vec{\hat{R}}^2 = B(r)[\vec{\hat{J}} - \vec{\hat{L}} - \vec{\hat{S}}]^2. \tag{94}$$

The classification in the cases (a)-(d) made in Subsection 2.2.5 can be generalized to rotating molecules, as was first done by F. Hund (Hund 1927c, 1930, 1933). The angular momentum coupling schemes can be described by the vector models depicted in Figures 18(a)-(d) (Zare 1988). The basis for the classification is a hierarchical ordering of the interactions similar to that introduced above for the nonrotating molecules, but which now includes the interaction between the rotational and electronic motion. The rotation of the molecule, with its inhomogeneous charge distribution, leads to a magnetic moment along $\vec{R}$ which couples the rotational motion to the electronic orbital and spin motions.

Hund's angular momentum coupling case (a)

This case arises when the energy splittings resulting from the spin-orbit interaction (Equation (88)) are significantly larger than the separation $\approx 2BJ$ of two neighboring rotational states. In this case, the hierarchy of interactions of the angular momenta is:

$$\begin{aligned}\text{electrostatic coupling of } L \text{ to internuclear axis} &\gg \text{spin} - \text{orbit coupling} \\ &\gg \text{coupling between rotational and electronic motion.}\end{aligned} \tag{95}$$

The total angular momentum $\vec{J}$ results from the vectorial addition of $\vec{R}$ and the components $\hbar\Omega = \hbar(\Lambda + \Sigma)$ of the electronic angular momentum along the internuclear axis (see Figure 18a). J, Ω, Λ, S and Σ are good quantum numbers in this case. The rotational motion can be described as a rotation (nutation) of $\vec{R}$ and $\hbar\Omega$ around $\vec{J}$.

The coupling between the rotational motion and the electronic motion increases with the degree of rotational excitation. As J increases to large values, the coupling of the electron spin (and ultimately also of the orbital) motion with the rotational motion becomes larger than the spin-orbit coupling

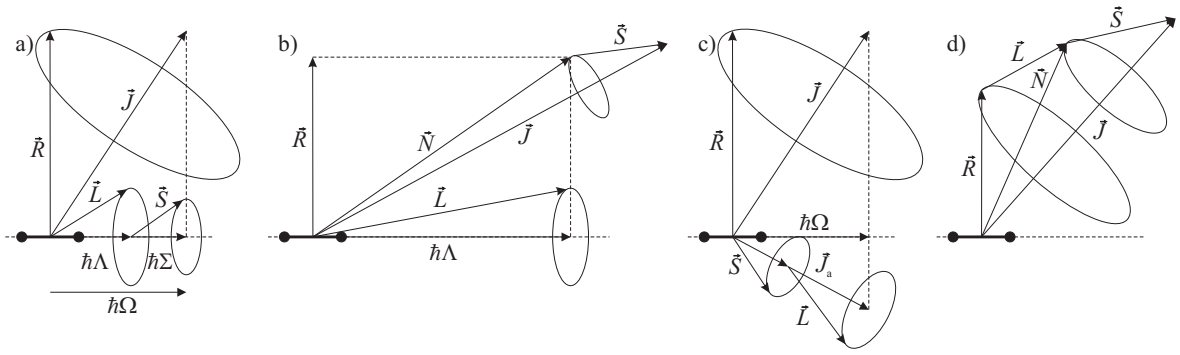

Figure 18: (a) Coupling scheme of angular momenta in Hund's case (a)-(d)

(and ultimately also larger than the electrostatic coupling of the orbital angular momentum to the internuclear axis), so that this coupling case evolves first toward Hund's case (b) and than toward Hund's case (d) as R increases and $\vec{S}$ and $\vec{L}$ get decoupled from the internuclear axis. These phenomena are referred to as S and L uncoupling, respectively, and will be described in more detail below.

Hund's angular momentum coupling case (b)

In Hund's case (b), the spin-orbit coupling is negligible and $\vec{S}$ is not coupled to the orbital motion of the electrons. The hierarchy of angular momentum coupling is

$$\begin{aligned} \text{coupling of } \vec{L} \text{ to internuclear axis} &\gg \text{interaction between rotational and electronic motion} \\ &\gg \text{spin} - \text{orbit coupling} \end{aligned} \tag{96}$$

The total angular momentum $\vec{J}$ results from (1) the vectorial addition of $\vec{R}$ with the component $\hbar\Lambda$ to form a total angular momentum without spin $\vec{N}$, and (2) the addition of $\vec{N}$ and $\vec{S}$ (see Figure 18b). The good quantum numbers in Hund's case (b) are Λ, N, S und J.

Hund's angular momentum coupling case (c)

In Hund's case (c), the hierarchy of angular momentum coupling is

$$\text{spin} - \text{orbit interaction} \gg \text{coupling of } \tilde{\text{L}} \text{ to internuclear axis} \tag{97}$$

$$\gg \text{coupling of rotational and electronic motion.} \tag{98}$$

$\vec{S}$ and $\vec{L}$ couple to form an electronic angular momentum J_a, with component $\hbar\Omega$ along the internuclear axis. $\vec{J}$ represents the vectorial sum of $\vec{R}$ and $\hbar\Omega$ (siehe Figure 18c). The good quantum numbers in this case are Ω und J.

Hund's angular momentum coupling case (d)

In Hund's case (d), all angular momentum couplings are weak. Neither $\vec{L}$ nor $\vec{S}$ are coupled to the internuclear axis. $\vec{J}$ is formed from (1) the vector addition of $\vec{R}$ and $\vec{L}$ to $\vec{N}$, and (2) the vector addition of $\vec{N}$ and $\vec{S}$ to $\vec{J}$. The good quantum numbers are R, S, L und J.

Example: NO $(1\sigma)^2(1\sigma^*)^2(2\sigma)^2(2\sigma^*)^2(3\sigma)^2(1\pi)^4(n\text{p})^1$. The electronic state can be represented by a closed-shell

ground-state X $^1\Sigma^+$ NO^+ cationic core surrounded by a weakly bound electron in a diffuse Rydberg orbital of principal quantum number n and orbital angular momentum quantum number $\ell = 1$. Consequently, $L = 1$ and $S = 1/2$. The rotational quantum number R is equal to that of the ionic core. The weak interaction between $\vec{L}$ and $\vec{R}$ splits each rotational level into three levels with $N = R,\ R \pm 1$ which are each further split into doublets with $J = N \pm 1/2$ by the still weaker interaction with the Rydberg electron spin.

Angular momentum coupling case (e):

The treatment of Rydberg states with $\Lambda > 0, S^+ > 0$ open-shell ion cores and of the rotational motion of weakly bound open-shell molecules such as $KrHe^+$ makes it necessary to introduce an additional angular momentum coupling case, case (e), which exists in several variants as discussed in more detail by Carrington *et al.* (1996); Watson (1999b); Brown and Carrington (2003); Lefebvre-Brion and Field (2004).

The situations described above as Hund's cases (a)-(e) represent idealized limiting cases. The sets of good quantum numbers in these limiting cases are helpful in defining the basis functions with which the Hamiltonian matrix describing the rotational motion is most conveniently expressed. Convenience can either mean that one would like to have a Hamiltonian matrix that is as close as possible to a diagonal matrix, in which case one chooses the basis provided by the coupling case which describes the molecular system under study most closely. This approach has the advantage that the eigenvalues of the rotational matrix can be determined more easily, an advantage that was important in earlier days, when computers were not available. Alternatively, convenience can mean that one would like to set up the Hamiltonian matrix using the basis providing the largest number of quantum numbers, i.e., the basis corresponding to Hund's case (a), regardless of which coupling case best describes the system under study. This procedure, advocated by Hougen *et al.* (1970), has the advantage that the treatment of the rotational structure can be made in a universal and straightforward manner. Although the Hamiltonian matrix has more off-diagonal elements in this case, the determination of the eigenvalues does not pose significant problems to present-day computers.

The reasons why Hund's angular momentum coupling cases still need to be introduced today are twofold: First, the hierarchy of interactions upon which the classification is based is reflected by distinct spectral patterns. Second, the electronic states are labeled by their good quantum numbers, and the nomenclature thus depend on the Hund's coupling case that best describe them: For instance, the ground electronic state of NO is labeled as X $^2\Pi_{3/2}$, as appropriate for a system that can be approximately described by Hund's case (a). The ground state of Xe_2^+, on the other hand, is labeled X $1/2_u$, or I(1/2u), as appropriate for a system that can be approximately described by Hund's case (c).

In the treatment of the rotational structure of diatomic molecules, $\hat{H}_{\rm ROT} + \hat{H}_{\rm SO}$ is set up in matrix form using standard relations of angular momentum algebra

$$\hat{J}_\pm = \hat{J}_x \pm \mathrm{i}\hat{J}_y, \tag{99}$$

$$\hat{J}^2 = \hat{J}_x^2 + \hat{J}_y^2 + \hat{J}_z^2 = \frac{\hat{J}_+\hat{J}_- + \hat{J}_-\hat{J}_+}{2} + \hat{J}_z^2 \tag{100}$$

$$\hat{\vec{J}}_1 \cdot \hat{\vec{J}}_2 = \hat{J}_{1x}\hat{J}_{2x} + \hat{J}_{1y}\hat{J}_{2y} + \hat{J}_{1z}\hat{J}_{2z} = \frac{\hat{J}_{1+}\hat{J}_{2-} + \hat{J}_{1-}\hat{J}_{2+}}{2} + \hat{J}_{1z}\hat{J}_{2z}, \tag{101}$$

where $\hat{\vec{J}}$, $\hat{\vec{J}}_1$ and $\hat{\vec{J}}_2$ represent arbitrary angular momentum vectors and could also stand for $\hat{\vec{S}}$ and $\hat{\vec{L}}$. Using these expressions, Equation (94) can be rewritten as

$$\begin{aligned} \hat{H}_{\rm ROT} + \hat{H}_{\rm SO} &= AL_zS_z + B(\hat{J}^2 + \hat{S}^2 - L_z^2 - 2J_zS_z) \\ &- B(J_+S_- + J_-S_+) \\ &- B(J_+L_- + J_-L_+) \\ &+ (A/2 + B)(L_+S_- + L_-S_+) \\ &+ (B/2)(L_+L_- + L_-L_+). \end{aligned} \tag{102}$$

The matrix elements arising from the different terms can be determined from standard results of angular momentum algebra, e.g., using the Hund's case (a) basis $|J\Omega, \Lambda, S\Sigma\rangle$

$$\langle J\Omega, \Lambda, S\Sigma|\hat{J}^2|J\Omega, \Lambda, S\Sigma\rangle = \hbar^2 J(J+1) \tag{103}$$

$$\langle J\Omega, \Lambda, S\Sigma|\hat{J}_z|J\Omega, \Lambda, S\Sigma\rangle = \hbar\Omega \tag{104}$$

$$\langle J\Omega \mp 1|\hat{J}_\pm|J\Omega\rangle = \hbar\sqrt{J(J+1) - \Omega(\Omega \mp 1)} \tag{105}$$

$$\langle J\Omega, \Lambda, S\Sigma|\hat{S}^2|J\Omega, \Lambda, S\Sigma\rangle = \hbar^2 S(S+1) \tag{106}$$

$$\langle J\Omega, \Lambda, S\Sigma|\hat{S}_z|J\Omega, \Lambda, S\Sigma\rangle = \hbar\Sigma \tag{107}$$

$$\langle S\Sigma \pm 1|\hat{S}_\pm|S\Sigma\rangle = \hbar\sqrt{S(S+1) - \Sigma(\Sigma \pm 1)} \tag{108}$$

$$\langle J\Omega, \Lambda, S\Sigma|\hat{L}_z|J\Omega, \Lambda, S\Sigma\rangle = \hbar\Lambda. \tag{109}$$

Instead of setting up the Hamiltonian matrix (102) using the Hund's case (a) basis functions $|J\Omega, \Lambda, S\Sigma\rangle$, which do not have a well-defined parity, it is more convenient to use as basis functions the linear combinations

$$|J\Omega, \Lambda, S\Sigma\pm\rangle = |J\Omega, \Lambda, S\Sigma\rangle \pm (-1)^{J-S+s}|J-\Omega, -\Lambda, S-\Sigma\rangle \tag{110}$$

which have a well-defined parity ($\pm$). s in Equation (110) is 1 for Σ^- states and 0 otherwise.

If the rotational and spin-orbit Hamiltonian matrix is expressed in Hund's coupling case (a) basis set, the first line of Equation (102) only gives rise to diagonal elements, with value $A\Lambda\Sigma + B(J(J+1) + S(S+1) - \Lambda^2 - 2\Omega\Sigma)$. The second line leads to off-diagonal elements of the rotational matrix. Its effect is to mix states with values of Σ and Ω differing by ± 1, i.e., it mixes different components of a spin-orbit multiplet. The mixing becomes significant when the value of the off-diagonal element ($\approx BJ$) becomes comparable to, or larger than, the energy separation ($\approx A$) between neighboring spin-orbit components. This term thus (1) decouples S from the internuclear axis (corresponding to

the S uncoupling towards Hund's case (b) mentioned above) and causes a splitting of the otherwise doubly degenerate rotational levels, with basis functions $|J\Omega, \Lambda, S\Sigma\pm\rangle$, of each spin-orbit component.

The term in the third line of Equation (102) couples electronic states with Λ and Ω values differing by ± 1, e.g., Σ states with Π states. When such states are energetically well separated, this term does not play a significant role, but it can lead to noticeable perturbations of the rotational structure if the separations between Σ and Π states are accidentally small at certain J values. At very high values of J, this term starts to efficiently mix states of different Λ values and to decouple $\vec{L}$ from the internuclear axis (corresponding to the L uncoupling towards case (d) mentioned above).

The term in the fourth line of Equation (102) couples states of the same Ω value but differing in their Λ and Σ values by ± 1 and ∓ 1, respectively. In cases where the spin-orbit constant A becomes comparable or larger than the spacing between, for instance, a $^2\Sigma_{1/2}$ state and a $^2\Pi_{1/2}$ state, efficient mixing of these states results, but the other spin-orbit component of the Π state ($^2\Pi_{3/2}$) remains unaffected. This situation has already been encountered in the example discussed in the previous section (see Table 11) and leads to Hund's case (c).

The term in the fifth line of Equation (102) does not directly affect the rotational and spin-orbit structures but can shift the origin of a given electronic state. Chapter hrs004 (Western 2010) in this handbook discusses the rotational energy level structure of several molecules. Here, we limit ourselves to the treatment of the simplest cases of $^1\Sigma^+$, $^1\Pi$, $^2\Sigma^+$, and $^2\Pi$ states. These examples can be generalized to more complex cases. However, when studying a specific case, it is advisable to first consult the extensive literature on diatomic molecules, in particular the textbooks by Herzberg (1989); Lefebvre-Brion and Field (2004); Brown and Carrington (2003). The rotational energy level structures (with symmetry labels) of the most commonly encountered electronic states of diatomic molecules are depicted schematically in Figure 19.

Examples:

$^1\Sigma^+$ states:

The rotational energy level structure of a diatomic molecule in a $^1\Sigma^+$ state can be described to a good approximation by Equation (90). The parity of the rotational functions is determined in this case by the even/odd nature of the angular momentum quantum number J (J=R in a $^1\Sigma^+$ state).

$^1\Pi$ states:

Only the first, third and fifth lines of Equation (102) need be considered in this case, because $S = 0$. The term in the fifth line does not lead to any J dependence, and its effects are incorporated into the purely electronic term value. The term in the third line can couple the $^1\Pi$ state with neighboring $^1\Sigma^+$ and $^1\Sigma^-$ states. In the absence of such perturbations, the rotational levels of a $^1\Pi$ state are given by

$$E(^1\Pi, J, \pm)/(hc) = B[J(J+1) - 1], \tag{111}$$

and each rotational level is doubly degenerate and has one component of positive and one of negative parity. Because $|\Lambda| = |\Omega| = 1$, the lowest rotational level has $J = 1$. Perturbations caused by the term in the third line of

Equation (102) may cause a J-dependent splitting of the two components of each rotational level, an effect known as Λ doubling.

$^2\Sigma^+$ states:

The rotational energy level structure of a $^2\Sigma^+$ state is very similar to that of a $^1\Sigma^+$ state, with the difference that each rotational level is now split into a doublet because of the magnetic interaction between the rotational and electron spin motions. The energy level structure can be described phenomelogically by the following expressions (the $\pm$ signs in the parentheses label the parity)

$$E(^2\Sigma^+, N, +)/(hc) = BN(N+1) + \frac{\gamma N}{2} \tag{112}$$

$$E(^2\Sigma^+, N, -)/(hc) = BN(N+1) - \frac{\gamma(N+1)}{2}, \tag{113}$$

where γ represents the spin-rotation coupling constant and N the quantum number associated with the total angular momentum excluding spin. This situation is characteristic of Hund's case (b).

$^2\Pi$ states:

The rotational energy level structure of a molecule in a $^2\Pi$ state can be obtained from the matrix $\hat{H}_{\rm ROT} + \hat{H}_{\rm SO}$ as described above. Because both the total angular momentum quantum number J and the parity ($p = \pm$) are good quantum numbers, the matrix has a block-diagonal form. Each block can be characterized by its parity and J value and be represented by a (2 x 2) matrix

$$\begin{array}{lcc} & ^2\Pi_{3/2},\, J,p & ^2\Pi_{1/2},\, J,p \\ ^2\Pi_{3/2},\, J,p & B(J(J+1)-7/4)+A/2 & -B\sqrt{J(J+1)-3/4} \\ ^2\Pi_{1/2},\, J,p & -B\sqrt{J(J+1)-3/4} & B(J(J+1)+1/4)-A/2. \end{array} \tag{114}$$

The diagonal elements ($A\Lambda\Sigma + B(J(J+1) + S(S+1) - \Lambda^2 - 2\Omega\Sigma$) correspond to the first line of Equation (102) and the off-diagonal elements to its second line. The matrix (114) has the eigenvalues

$$E(^2\Pi, J, p)/(hc) = B[(J-1/2)(J+3/2) \pm \sqrt{(J-1/2)(J+3/2) + \left(\frac{A}{2B} - 1\right)^2}]. \tag{115}$$

The eigenfunctions have mixed $^2\Pi_{3/2}$ and $^2\Pi_{1/2}$ character, the mixing being caused by the off-diagonal elements which are approximately equal to BJ. When BJ is much less than the energy difference ($\approx A$) between the diagonal elements, the mixing becomes negligible and the rotational levels retain their $^2\Pi_{3/2}$ or $^2\Pi_{1/2}$ character. This situation corresponds to a pure Hund's case (a). When BJ is much larger than A, the splitting between the two levels is primarily given by the value of the off-diagonal elements, and the $\Omega = 1/2$ and 3/2 characters are fully mixed. This situation corresponds to Hund's case (b). This example serves to show how the "S-uncoupling" term in the second line of Equation (102) decouples S from the internuclear axis and recouples it to the rotational motion. It also shows that it is the relative magnitude of BJ and A which determines whether the angular momentum coupling scheme is better described by Hund's case (a) or (b). Each energy level described by Equation (115) corresponds to two rotational states of opposite parity.

Coupled $^2\Sigma^+$ and $^2\Pi$ states:

When there is a strong mixing between neighboring $^2\Sigma^+$ and $^2\Pi$ states, induced by the term in the fourth line of Equation (102), as in the case of Xe_2^+ discussed in the previous subsection (see Table 11), a Hund's case (c) situation arises. The rotational energy levels can in this case also be derived in a Hund's case (c) formalism (Veseth

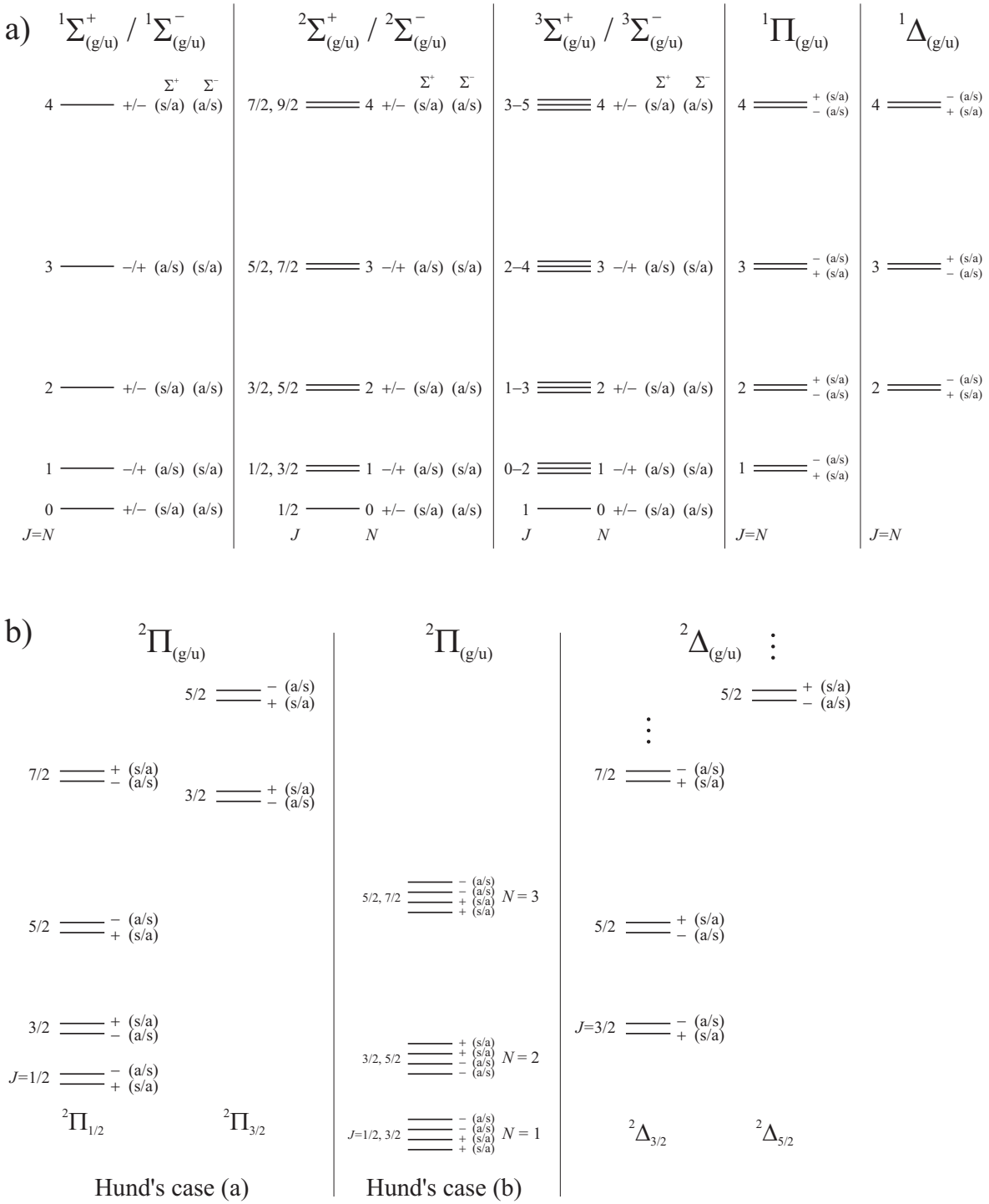

Figure 19: Rotational energy level structures of $^1\Sigma^+$, $^1\Sigma^-$, $^2\Sigma^+$, $^2\Sigma^-$, $^3\Sigma^+$, $^3\Sigma^-$, $^1\Pi$, $^1\Delta$, $^2\Pi$, and $^2\Delta$ states. The $\pm$ labels next to the rotational levels indicate the parity of the rotational levels. The a/s label is only appropriate for homonuclear diatomic molecules and designates the symmetry of the rovibronic wave functions with respect to permutation of the coordinates of the identical nuclei (see Subsection 3.3.4 for more details). The g/u labels are also only relevant in homonuclear diatomic molecules and describe the symmetry of the electronic function with repect to inversion through the center of symmetry.

1973; Carrington *et al.* 1999)

$$E(\Omega = 1/2,\, J) = T_{3/2} + B_{1/2}\left[J(J+1) - \frac{1}{2}\right] + (-1)^{(J-\frac{1}{2}+q)} P\left(J + \frac{1}{2}\right) \tag{116}$$

$$E(\Omega = 3/2,\, J) = T_{3/2} + B_{3/2}\left[J(J+1) - \frac{9}{2}\right]. \tag{117}$$

In Equations (116) and (117) T_Ω, B_Ω, and P represent the vibronic term energies, the rotational constants, and the Ω-doubling constant, respectively. The phase factor $(-1)^q$ in Equation (116) (with $q = 0$ and 1 for electronic states of u and g symmetry, respectively), which is not present in the equation for heteronuclear diatomic molecules or molecules with nuclei $I \neq 0$, was introduced in order to treat both sets of states in $^{40}Ar_2^+$ with the same formula (Rupper and Merkt 2002).

2.2.8 Hyperfine Structure

As in the case of atoms, the hyperfine structure in molecules results from the interaction of the magnetic dipole and/or electric quadrupole moments of the nuclei having a nonzero nuclear spin $\vec{I}$ ($|\vec{I}|^2 = \hbar^2 I(I+1)$) with the electric and magnetic field distributions arising from other motions. In addition to the electron orbital and spin motions, the rotational motion of the molecular framework must be considered in the treatment of the hyperfine structure of molecules. A systematic classification of the possible angular momentum coupling cases can be made following the same general principles as used in the discussion of Hund's angular momentum coupling cases in the previous subsection. However, the necessity to include the hyperfine interactions in the hierarchical ordering of angular momentum couplings leads to an explosion of the number of limiting cases, particularly if Rydberg states are considered.

The following nomenclature, introduced by Frosch and Foley (1952) (see also Dunn (1972)), is used to label the limiting cases of the angular momentum coupling: The letters (a)-(e) are used to describe the angular momentum coupling scheme without nuclear spins. A right subscript (α or β) is added to indicate whether the nuclear spin motion is coupled to the internuclear axis or not. In the former case (subscript α) the projection $\hbar I_z$ of the nuclear spin vector on the internuclear axis is well defined. In the latter case (subscript β), the nuclear spin vector is coupled to another angular momentum vector, i.e., $\vec{R}$, $\vec{N}$, $\vec{S}$ or $\vec{J}$, which is added in the subscript next to β. For example, "a_α" implies a Hund's case (a) coupling situation (see Figure 18a) in which the nuclear spin $\vec{I}$ is coupled to the internuclear axis. "$b_{\beta S}$" refers to a Hund's case (b) coupling situation (see Figure 18b) in which the nuclear spin is coupled to the electron spin vector $\vec{S}$, in which case the total spin vector $\vec{G} = \vec{S} + \vec{I}$ results. "$c_{\beta J}$" describes a Hund's case (c) situation (see Figure 18f) in which the nuclear spin is coupled to $\vec{J}$.

In general, the hyperfine interactions are much weaker than the electrostatic (including exchange) and spin-orbit interactions. Moreover, the Fermi-contact hyperfine interaction, which is only of appreciable strength in electronic states with a significant electron-spin density at the nuclei, is weak in $\Lambda \neq 0$ states because the nuclei are located in the nodal plane of the partially filled molecular orbitals.

Consequently "α-type" coupling cases, which can only arise as a_α and c_α cases, are rather unusual and more probable in Hund's case (c) situations because the electronic wave functions often contain significant Σ contributions, even when $\Omega \neq 0$.

Figure 20 illustrates schematically the vector models corresponding to several of the angular momentum coupling schemes mentioned above. The hyperfine structure of the ground state (X $^2\Sigma_g^+$ ($v^+ = 0, N^+ = 1$) of ortho H_2^+ and of para D_2^+ depicted in Figure 27 of hrs071 (Merkt *et al.* 2010) represents an example of case $b_{\beta S}$.

An exhaustive discussion of the hyperfine structure of diatomic molecules, which would go beyond the scope of this introductory chapter, would need to include cases in which both nuclei have a (different) nuclear spin and would need to describe the many coupling cases arising in Rydberg states with their specific coupling cases (d) and (e). We refer here to the "Further reading list" at the end of this chapter for more extensive treatments.

2.3 Polyatomic molecules

The electronic structure of polyatomic molecules can be described using the same principles as those introduced for diatomic molecules in the previous subsection. However, the same polyatomic molecule can have different geometries and belong to different point groups depending on its electronic state. The variety of possible electronic states and molecular structures is so large that it is impossible to give a complete overview in this chapter. We therefore restrict the discussion to only a few representative molecular systems: Molecules of the form HAH as prototypical small molecules, the cyclopentadienyl cation and benzene as typical highly symmetrical molecules and adenine as example of a nonsymmetrical large molecule. The principles that we describe are easily generalized to arbitrary molecules.

2.3.1 Molecular orbitals, electronic configurations, and electronic states

a) Small polyatomic molecules with the example of HAH molecules. Molecules possessing the chemical formula HAH (A designates an atom, e.g., Be, B, C, N, O, etc.) are either linear and belong to the $D_{\infty h}$ point group, or bent and belong to the C_{2v} point group, the character table of which is given in Table 12. Molecular orbitals are therefore classified either in the $D_{\infty h}$ (see Table 8 in Section 2.2) or the C_{2v} point group. For simplicity we consider here only valence states of HAH molecules with A being an atom from the second or third row of the perodic table, so that $\ell \geq 2$ atomic orbital can be ignored in the discussion of the electronic structure.

The determination of the molecular orbitals may proceed along the following scheme:
(a) Identification of all atomic orbitals participating in the formation of molecular orbitals. Symmetry restricts the number of these orbitals. In the case of HAH molecules, the required orbitals are the two 1s orbitals of the hydrogen atoms and the ns and np valence orbitals of the central atom A, where $n \geq 2$ represents the row of the periodic system of elements to which A belongs. Orbitals belonging

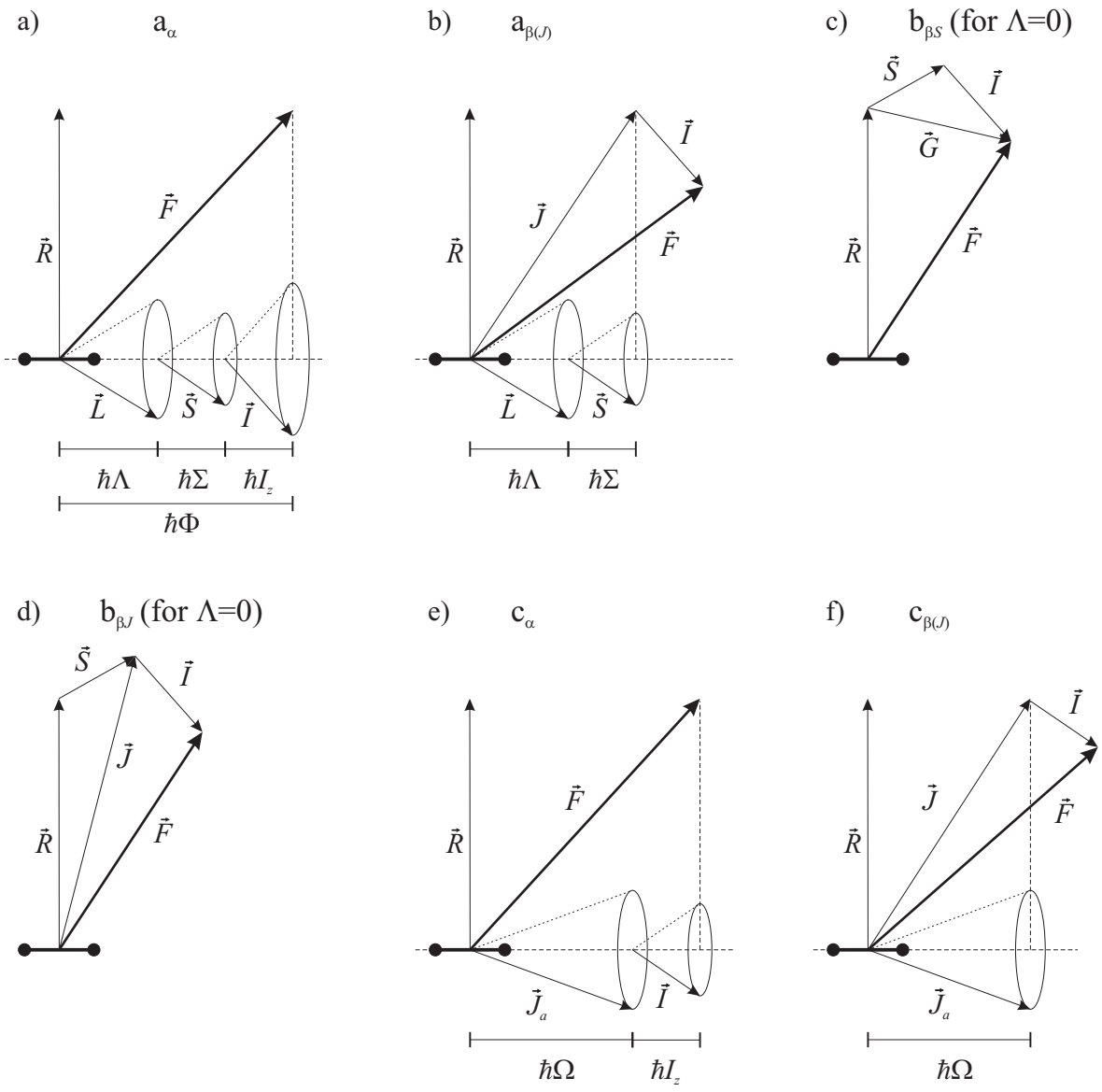

Figure 20: Selected illustrative angular momentum coupling schemes in diatomic molecules, including nuclear spins. a) case a_α; b) case $a_{\beta(J)}$; c) case $b_{\beta S}$; d) $b_{\beta J}$; e) c_α; f) $c_{\beta(J)}$. The nomenclature used to label these schemes is explained in the text. More complex situations arise when two nuclear spins ($\vec{I}_1$ and $\vec{I}_2$) are considered or in the treatment of the hyperfine structure of Rydberg states.

Table 12: Character table of the C_{2v} point group.

C_{2v}	I	C_2	$\sigma_v(xz)$	$\sigma'_v(yz)$		
A_1	1	1	1	1	T_z	$\alpha_{xx}, \alpha_{yy}, \alpha_{zz}$
A_2	1	1	−1	−1	R_z	α_{xy}
B_1	1	−1	1	−1	T_x, R_y	α_{xz}
B_2	1	−1	−1	1	T_y, R_x	α_{yz}

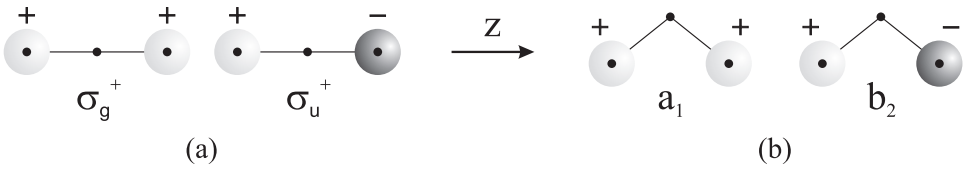

Figure 21: Symmetry adapted linear combinations of 1s orbitals that participate in the construction of molecular orbitals of (a) linear and (b) bent HAH molecules.

to inner shells of the central atom usually lie so deep in energy and are so strongly localized on the nucleus that they hardly contribute to molecular bonds.

(b) Formation of i symmetry-adapted molecular orbitals from the set of i atomic orbitals determined under (a) ($i = 6$ in the case of HAH molecules). Symmetry-adapted molecular orbitals transform as irreducible representations of the corresponding point group. In molecules such as HAH in which two or more atoms are equivalent, it is convenient to first build symmetry-adapted linear combinations of the orbitals of these equivalent atoms, i.e., of the H 1s orbitals in the case of HAH molecules (see Figure 21). These orbitals are then used to form molecular orbitals with the orbitals of the central atom A (or of other atoms in the case of other molecules) having the corresponding symmetry, as shown in Figure 22 for the point group $D_{\infty h}$.

The ns (σ_g) and np$_z$ (σ_u) orbitals of the central atom can be combined with the symmetry-adapted orbitals of the H atoms in two ways each, resulting in four molecular orbitals of σ symmetry. The energetic ordering of these molecular orbitals can be derived from the number of nodal planes of the wave functions. The $2\sigma_g$ (zero nodal plane) and $1\sigma_u$ (one nodal plane) orbitals in Figure 22 are bonding, whereas the $3\sigma_g$ (two nodal planes) and $2\sigma_u$ (three nodal planes) orbitals are antibonding. For symmetry reasons, the 2p$_x$ and 2p$_y$ orbitals of the central atom (both of π_u symmetry) cannot combine with the 1s orbitals of the H atoms and are therefore nonbonding orbitals.

The energetic ordering of these molecular orbitals is given on the right-hand side of Figure 23 which also shows how the energies of the molecular orbitals change as the molecule is progressively bent from the linear $D_{\infty h}$ structure ($\angle$(HAH)= 180°) toward the C_{2v} structure with $\angle$(HAH)= 90°. The orbitals of the bent molecules displayed on the left-hand side of Figure 23 are given symmetry labels of the C_{2v} point group according to their transformation properties (see Table 12). The two

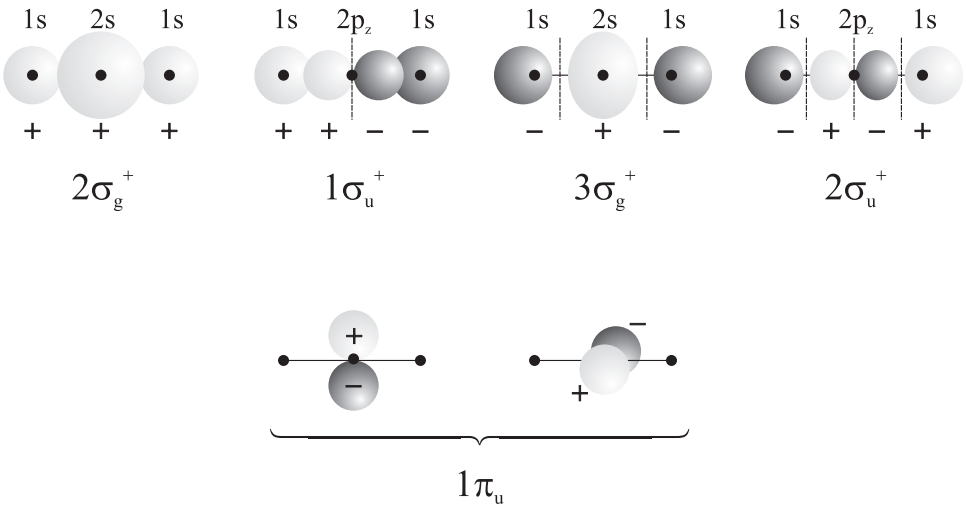

Figure 22: Linear combinations of atomic orbitals in linear HAH molecules

lowest-lying orbitals are invariant under rotations around the C_2 (z) axis, and also under reflection in both the σ_{xz} and σ_{yz} planes, and are therefore totally symmetric (a_1). The next higher-lying orbital is antisymmetric under C_2 rotation and under σ_{xz} reflection, but symmetric under σ_{yz} reflection, and is thus of b_2 symmetry. As in the linear geometry, the energetic ordering essentially follows the number of nodal planes.

The degeneracy of the two nonbonding π_u orbitals is lifted as the molecule bends. The molecular orbital corresponding to the p orbital in the molecular plane becomes bonding and correlates with the $3a_1$ molecular orbital of the bent molecule. The other molecular orbital, which is perpendicular to the molecular plane, remains a nonbonding orbital and correlates with the $1b_1$ orbital of the bent molecule. The angle dependence of the $1\pi_u - 3a_1$ orbital energy is of particular importance, because this orbital is the only one that becomes significantly more stable in the nonlinear geometry. All other molecular orbitals are destabilized when the HAH angle is decreased. The occupation of this orbital with one or two electrons can result in a bent equilibrium structure of the molecule. Correlation diagrams as the one shown in Figure 23 are known as Walsh diagrams.

As in the case of atoms and diatomic molecules, the electronic configurations of polyatomic molecules are obtained by filling the molecular orbitals with a maximum of two electrons. Whether a molecule of the form HAH is linear or bent depends on the occupation of the orbitals, especially of the $3a_1$ orbital, as discussed above. The symmetries of the electronic states that result from a given configuration are obtained from the direct product of the irreducible representations of the occupied molecular orbitals (see Equation (84)). Finally, the multiplicities $(2S+1)$ are derived following exactly the same procedure as discussed for atoms and diatomic molecules in the previous subsections (see also subsection 2.3.2 below).

Examples:

BeH_2: $\ldots(2\sigma_g)^2(1\sigma_u)^2$

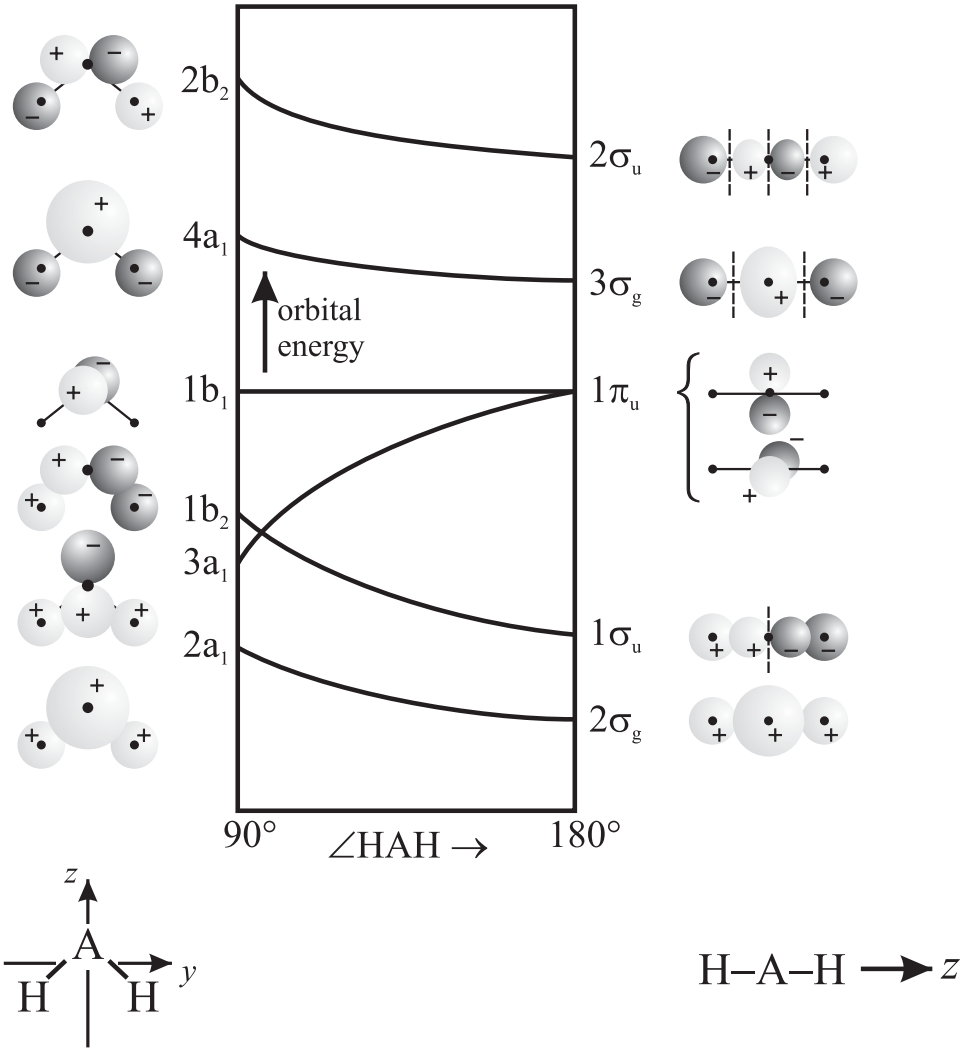

Figure 23: Walsh diagram for HAH molecules. The symmetry labels on the left-hand side correspond to C_{2v} point-group symmetry, those on the right-hand side to $D_{\infty h}$ symmetry.

The dependence of the energies of the occupied orbitals favors a linear structure (see Figure 23) and the ground electronic state is therefore the $\tilde{\mathrm{X}}\ ^1\Sigma_\mathrm{g}^+$ state.

BeH_2: $\ldots(2a_1)^2(1b_2)^1(3a_1)^1$

The first excited configuration leads to a bent structure because the $3a_1 - 1\pi_u$ orbital is occupied. The electronic configuration is thus given using C_{2v} symmetry labels. The two electronic states resulting from this configuration are of $^3B_2$ and $^1B_2$ symmetry.

H_2O: $\ldots(2a_1)^2(1b_2)^2(3a_1)^2(1b_1)^2$

Because the $3a_1$ orbital in H_2O is doubly occupied, the electronic ground state is also bent. The ground electronic state is thus the $\tilde{\mathrm{X}}\ ^1A_1$ state.

H_2O^+: $\ldots(2a_1)^2(1b_2)^1(3a_1)^2(1b_1)^1$ $\tilde{\mathrm{X}}^+\ ^2B_1$.

Walsh diagrams such as that displayed in Figure 23 are also useful in the discussion of vibronic interactions because they enable one to see how the degeneracy of π orbitals and of the $\Pi, \Delta, \Phi, \ldots$ electronic states are lifted, and how the electronic character changes, when the molecules bend out of their linear structures. The coupling of electronic motion and bending vibrations can significantly perturb the energy level structure and gives rise to the Renner-Teller effect that will be discussed further in Section 2.3.6.

b) Larger symmetric molecules. To determine the molecular orbitals of larger polyatomic molecules that have a high symmetry, it is useful to introduce a systematic approach. The symmetrized linear combination of atomic orbitals (LCAO) are determined using projection operators $\hat{p}_\gamma$ that are applied onto one of the atomic orbitals of the set of identical atoms. The projectors are defined as

$$\hat{p}_\gamma = \frac{1}{h}\sum_R \chi^\gamma(R)^* \cdot \hat{R} \quad \text{“Projection formula”}, \tag{118}$$

where $\hat{R}$ are the geometrical operations of the point group, $\chi^\gamma(R)$ is the character of the irreducible representation γ under the operation $\hat{R}$ and h is the order of the point group.

To illustrate the application of the projection formula (Equation (118)), we use it to derive the system of π molecular orbitals of benzene in the D_{6h} point group by building symmetry-adapted linear combinations

$$\varphi_\gamma^{(s)} = \sum_{i=1}^{6} c_{\gamma,i}\varphi_i \tag{119}$$

of the carbon $2p_z$ orbitals φ_i $(i = 1 - 6)$. From the six $2p_z$ atomic orbitals involved in the π orbital system, which form a six-dimensional reducible representation of the D_{6h} point group, a total of 6 orthogonal molecular orbitals can be formed. The reducible representation Γ of the carbon $2p_z$ orbitals can be constructed using the character table of the D_{6h} point group presented in Table 13.

Under the group operations of D_{6h}, the $2p_z$ orbitals φ_i have the same symmetry properties as the components z_i of the nuclear displacement vectors of the carbon atoms. The $2p_z$ orbitals are mapped onto each other by the symmetry operations of the group. From the properties of the representation matrices, it can be easily established that

Table 13: Character table of the D_{6h} point group.

D_{6h}	E	$2C_6$	$2C_3$	C_2	$3C_2'$	$3C_2''$	i	$2S_3$	$2S_6$	σ_h	$3\sigma_d$	$3\sigma_v$	
A_{1g}	1	1	1	1	1	1	1	1	1	1	1	1	
A_{2g}	1	1	1	1	-1	-1	1	1	1	1	-1	-1	R_z
B_{1g}	1	-1	1	-1	1	-1	1	-1	1	-1	1	-1	
B_{2g}	1	-1	1	-1	-1	1	1	-1	1	-1	-1	1	
E_{1g}	2	1	-1	-2	0	0	2	1	-1	-2	0	0	R_x, R_y
E_{2g}	2	-1	-1	2	0	0	2	-1	-1	2	0	0	
A_{1u}	1	1	1	1	1	1	-1	-1	-1	-1	-1	-1	
A_{2u}	1	1	1	1	-1	-1	-1	-1	-1	-1	1	1	z
B_{1u}	1	-1	1	-1	1	-1	-1	1	-1	1	-1	1	
B_{2u}	1	-1	1	-1	-1	1	-1	1	-1	1	1	-1	
E_{1u}	2	1	-1	-2	0	0	-2	-1	1	2	0	0	x, y
E_{2u}	2	-1	-1	2	0	0	-2	1	1	-2	0	0	

- each orbital that is left unchanged by a symmetry operation $\hat{R}$ adds 1 to the character $\chi(R)$,
- each orbital that is inverted adds -1 to the character,
- each orbital that is mapped onto another orbital gives no contribution to the character.

Thus, the characters of the reducible representation Γ of the six $2p_z$ orbitals under the different classes of symmetry operations $\hat{R}$ are:

c:	E	$2C_6$	$2C_3$	C_2	$3C_2'$	$3C_2''$	i	$2S_3$	$2S_6$	σ_h	$3\sigma_d$	$3\sigma_v$
$\chi(c)$:	6	0	0	0	-2	0	0	0	0	-6	0	2

This representation must now be transformed into a sum of irreducible representations using the reduction formula

$$a_\gamma = \frac{1}{h} \sum_R n(R) \chi^\Gamma(R) \chi^\gamma(R), \tag{120}$$

where a_γ is the number of times the irreducible representation γ is contained in the reducible representation Γ, h (= 24) is the order of the group, $n(R)$ is the number of operations of a particular class of operations, $\chi^\Gamma(R)$ is the character of the reducible representation corresponding to the class of the operation $\hat{R}$, and $\chi^\gamma(R)$ is the corresponding character of the irreducible representation γ.

Reducing Γ using Equation (120) yields the symmetries of the six π molecular orbitals:

$$\Gamma = b_{2g} \oplus a_{2u} \oplus e_{1g} \oplus e_{2u}, \tag{121}$$

each of the two e irreducible representations being two-dimensional. The orthonormal set of symmetry-adapted basis functions $\{\varphi_i^{(s)}\}$ is constructed by projecting the φ_i on their irreducible components using Equation (118) and Table 13:

1. $\mathbf{a_{2u}}$:
$$\varphi^{(\mathrm{s})}_{\mathrm{a_{2u}}} = \frac{1}{N}\hat{p}_{\mathrm{a_{2u}}}\varphi_1 = \frac{1}{\sqrt{6}}\big(\varphi_1 + \varphi_2 + \varphi_3 + \varphi_4 + \varphi_5 + \varphi_6\big), \tag{122}$$
where N is a normalization constant. The same result is obtained by applying the projector to any other $\varphi_i,\ i \neq 1$.

2. $\mathbf{b_{2g}}$:
$$\varphi^{(\mathrm{s})}_{\mathrm{b_{2g}}} = \frac{1}{N}\hat{p}_{\mathrm{b_{2g}}}\varphi_1 = \frac{1}{\sqrt{6}}\big(\varphi_1 - \varphi_2 + \varphi_3 - \varphi_4 + \varphi_5 - \varphi_6\big). \tag{123}$$

3. $\mathbf{e_{1g}}$: For multi-dimensional subspaces, the projection technique usually yields nonorthogonal linear combinations of the original basis vectors. To construct the symmetry-adapted basis, it is sufficient to determine d_i linearly independent vectors and then choose suitable orthogonal linear combinations of them:
$$\varphi^{(\mathrm{s})}_{\mathrm{e_{1g},1}} = \frac{1}{N}\hat{p}_{\mathrm{e_{1g}}}\varphi_1 = \frac{1}{\sqrt{12}}\big(2\varphi_1 + \varphi_2 - \varphi_3 - 2\varphi_4 - \varphi_5 + \varphi_6\big), \tag{124}$$
$$\varphi^{(\mathrm{s})}_{\mathrm{e_{1g},2}} = \frac{1}{N}\hat{p}_{\mathrm{e_{1g}}}\varphi_2 = \frac{1}{\sqrt{12}}\big(\varphi_1 + 2\varphi_2 + \varphi_3 - \varphi_4 - 2\varphi_5 - \varphi_6\big). \tag{125}$$
The set of vectors $\{\varphi^{(\mathrm{s})}_{\mathrm{e_{1g},1}}, \varphi^{(\mathrm{s})}_{\mathrm{e_{1g},2}}\}$ is linearly independent, but not orthogonal. A set of orthogonal basis vectors can be obtained by using the Schmidt orthogonalization algorithm: if ϕ_1, ϕ_2 are nonorthogonal, normalized basis vectors, then a basis vector $\phi_2^{\perp}$ which is orthogonal to ϕ_1 can be constructed using Equation (126)
$$\phi_2^{\perp} = \phi_2 - \big\langle \phi_2 \big| \phi_1 \big\rangle \phi_1, \tag{126}$$
where $\langle .|. \rangle$ denotes the scalar product. Thus:
$$\begin{aligned}\varphi^{(\mathrm{s}),\perp}_{\mathrm{e_{1g},2}} &= \varphi^{(\mathrm{s})}_{\mathrm{e_{1g},2}} - \big\langle \varphi^{(\mathrm{s})}_{\mathrm{e_{1g},2}} \big| \varphi^{(\mathrm{s})}_{\mathrm{e_{1g},1}} \big\rangle \varphi^{(\mathrm{s})}_{\mathrm{e_{1g},1}} \\ &= \varphi^{(\mathrm{s})}_{\mathrm{e_{1g},2}} - \frac{1}{2}\varphi^{(\mathrm{s})}_{\mathrm{e_{1g},1}}.\end{aligned} \tag{127}$$
After normalization, one obtains
$$\varphi^{(\mathrm{s}),\perp}_{\mathrm{e_{1g},2}} = \frac{1}{2}\big(\varphi_2 + \varphi_3 - \varphi_5 - \varphi_6\big). \tag{128}$$
The set of symmetry-adapted basis vectors $\{\varphi^{(\mathrm{s})}_{\mathrm{e_{1g},a}}, \varphi^{(\mathrm{s})}_{\mathrm{e_{1g},b}}\} = \{\varphi^{(\mathrm{s})}_{\mathrm{e_{1g},1}}, \varphi^{(\mathrm{s}),\perp}_{\mathrm{e_{1g},2}}\}$ for the $\mathrm{e_{1g}}$ subspace is thus:
$$\varphi^{(\mathrm{s})}_{\mathrm{e_{1g},a}} = \frac{1}{\sqrt{12}}\big(2\varphi_1 + \varphi_2 - \varphi_3 - 2\varphi_4 - \varphi_5 + \varphi_6\big), \tag{129}$$
$$\varphi^{(\mathrm{s})}_{\mathrm{e_{1g},b}} = \frac{1}{2}\big(\varphi_2 + \varphi_3 - \varphi_5 - \varphi_6\big). \tag{130}$$

4. $\mathbf{e_{2u}}$: Similarly, one obtains an orthonormal set of symmetry-adapted basis vectors for the $\mathrm{e_{2u}}$ subspace:
$$\varphi^{(\mathrm{s})}_{\mathrm{e_{2u},a}} = \frac{1}{\sqrt{12}}\big(2\varphi_1 - \varphi_2 - \varphi_3 + 2\varphi_4 - \varphi_5 - \varphi_6\big), \tag{131}$$
$$\varphi^{(\mathrm{s})}_{\mathrm{e_{2u},b}} = \frac{1}{2}\big(\varphi_2 - \varphi_3 + \varphi_5 - \varphi_6\big). \tag{132}$$

These molecular orbitals are depicted in Figure 24. Their energetic ordering can be determined from the number of nodal planes. The a_{2u} orbital must be the most stable because it possesses a single nodal plane (the plane containing the carbon atoms). The e_{1g} orbital possesses two nodal planes and has therefore the second lowest energy. The e_{2u} and b_{2g} orbitals possess three and four nodal planes and are thus the orbitals of second highest and highest energy, respectively.

A more quantitative estimate of the relative energies of the molecular orbitals can be achieved using the Hückel moleclar orbital (HMO) model. The HMO model represents a simple semi-empirical method to calculate the electronic energy level structure of molecules that exhibit conjugated π molecular orbitals such as polyenes and aromatic molecules. The model is useful to gain a semi-quantitative description of the π molecular orbitals and their relative energies and is widely used in physical-organic chemistry. Within the framework of the HMO model, the π molecular orbitals are constructed by linear combinations of orthogonal $2p_z$ atomic orbitals centered on the carbon atoms. The energies E_k of the π molecular orbitals are obtained by solving the secular determinant

$$\det\big|H_{ij} - E_k S_{ij}\big| = 0, \tag{133}$$

where H_{ij} are the matrix elements of a formal Hamiltonian operator $\mathbf{H}$ describing the π electron system (the "Hückel operator") and S_{ij} denotes the overlap integral between the p_z orbitals of atoms i and j. The expansion coefficients $c_i^{(k)}$ of the molecular orbital Φ_k in the basis of the atomic $2p_z$ orbitals $\{\varphi_i\}$ are obtained by solving the set of secular equations

$$\sum_i c_i^{(k)}\big(H_{ij} - E_k S_{ij}\big) = 0. \tag{134}$$

The following approximations are introduced:

- All overlap integrals vanish ($S_{ij} = 0$) unless $i = j$, in which case $S_{ii} = 1$.
- All diagonal elements of $\mathbf{H}$ are the same: $H_{ii} = \alpha$.
- All off-diagonal elements of $\mathbf{H}$ are set to zero, except those between neighboring atoms, which are $H_{ij} = \beta$. β is usually negative ($\beta < 0$).

α and β are treated as effective parameters that can in principle be estimated from calorimetric data.

The matrix representation of the Hückel operator $\mathbf{H}$ describing the π molecular orbital system can be derived in the basis of the carbon $2p_z$ atomic orbitals $\{\varphi_i\}$, and is

$$\big[H_{ij}\big] = \begin{bmatrix} \alpha & \beta & 0 & 0 & 0 & \beta \\ \beta & \alpha & \beta & 0 & 0 & 0 \\ 0 & \beta & \alpha & \beta & 0 & 0 \\ 0 & 0 & \beta & \alpha & \beta & 0 \\ 0 & 0 & 0 & \beta & \alpha & \beta \\ \beta & 0 & 0 & 0 & \beta & \alpha \end{bmatrix}. \tag{135}$$

The eigenvectors and eigenvalues of the matrix (135) represent the molecular orbitals and their energies, respectively. Alternatively, the Hückel operator can be expressed in the basis of symmetry-adapted basis function $\{\varphi_i^{(s)}\}$ by evaluating the matrix elements according to

$$H_{ij}^{(s)} = \langle \varphi_i^{(s)} | \mathbf{H} | \varphi_j^{(s)} \rangle \tag{136}$$

using the basis functions given in Equations (122, 123, 129, 130, 131, 132). For the $\varphi_{a_{2u}}^{(s)}$ orbital (Equation (122)), one finds, for instance:

$$\begin{aligned} \langle \varphi_{a_{2u}}^{(s)} | \mathbf{H} | \varphi_{a_{2u}}^{(s)} \rangle &= \frac{1}{6} \langle \varphi_1 + \varphi_2 + \varphi_3 + \varphi_4 + \varphi_5 + \varphi_6 | \mathbf{H} | \varphi_1 + \varphi_2 + \varphi_3 + \varphi_4 + \varphi_5 + \varphi_6 \rangle \\ &= \alpha + 2\beta. \end{aligned} \tag{137}$$

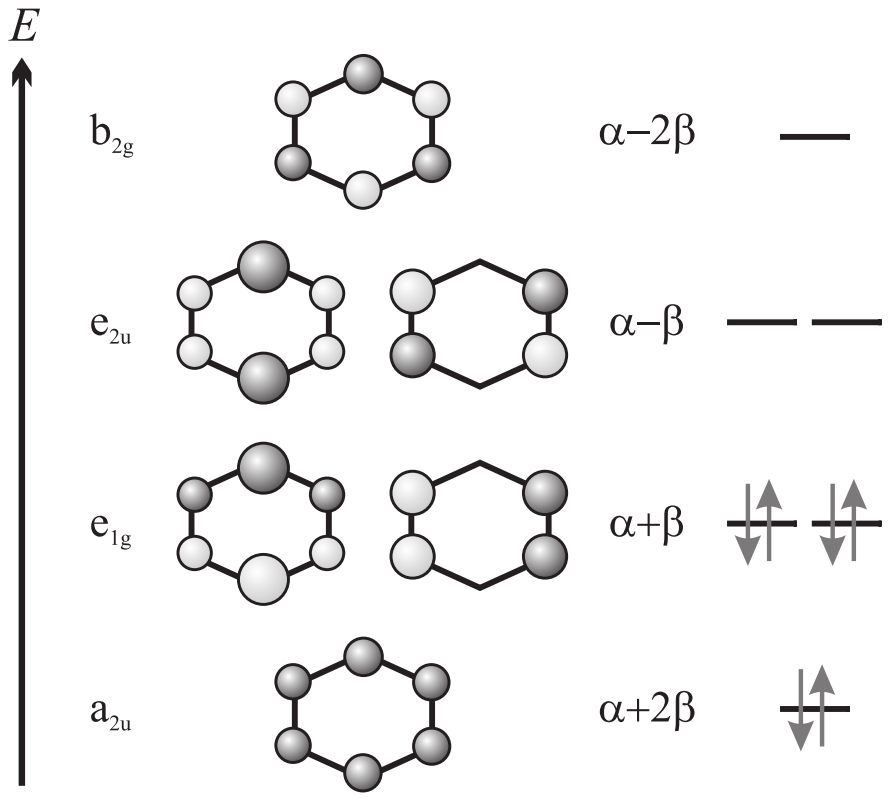

Figure 24: Energy level diagram and schematic representation of the π molecular orbitals of benzene. The size of the circles represents the weight of the atomic orbital in the molecular orbital wave function. The two grey tones of the shading indicate the relative sign of the $2p_z$ orbitals which form the molecular orbital. The energies of the molecular orbitals increase with the number of nodal planes and are expressed, on the right-hand side of the figure, as a function of the Hückel parameters α and β. The arrows represent schematically the occupation of the molecular orbitals in the ground-state configuration of benzene.

Matrix elements between functions of different symmetry and matrix elements between orthogonal basis functions within the e_{1g} and e_{2u} subspaces are zero because **H** is totally symmetric, so that one obtains the following Hückel matrix

$$\left[H_{ij}^{(s)}\right] = \begin{bmatrix} \alpha+2\beta & 0 & 0 & 0 & 0 & 0 \\ 0 & \alpha-2\beta & 0 & 0 & 0 & 0 \\ 0 & 0 & \alpha+\beta & 0 & 0 & 0 \\ 0 & 0 & 0 & \alpha+\beta & 0 & 0 \\ 0 & 0 & 0 & 0 & \alpha-\beta & 0 \\ 0 & 0 & 0 & 0 & 0 & \alpha-\beta \end{bmatrix}, \tag{138}$$

which is already in diagonal form. The symmetry-adapted orthonormal basis functions $\{\varphi_i^{(s)}\}$ are thus the eigenvectors of the Hückel operator and represent the π molecular orbitals $\{\Phi_i\}$ of benzene depicted in Figure 24. One should note that a group theoretical treatment normally only divides the Hamiltonian matrix in as many diagonal blocks as there are irreducible representations, i.e., in the present case, in two 1×1 diagonal blocks corresponding to A_{2u} and A_{2g} and two 2×2 diagonal blocks corresponding to E_{1g} and E_{2u}. The fact that the Hamiltonian matrix is fully diagonal in Equation (138) is a consequence of the particular choice made during the Schmidt orthogonalization procedure.

The lowest energy configuration of π electrons in benzene can thus be written $(a_{2u})^2(e_{1g})^4$, giving rise to a single electronic state of symmetry $^1A_{1g}$. The first excited electronic configuration of benzene is $(a_{2u})^2(e_{1g})^3(e_{2u})^1$. This configuration gives rise to several electronic states as will be discussed in Section 2.3.2. The direct product of the partially occupied orbitals is $e_{1g} \otimes e_{2u} = b_{1u} \oplus b_{2u} \oplus e_{1u}$. Since two different spatial orbitals are partially occupied, there is no restriction on the total electron spin imposed by the generalized Pauli principle (see Section 2.2.4), and all electronic states contained in the direct product can exist as either singlet or triplet states. The configuration $(a_{2u})^2(e_{1g})^3(e_{2u})^1$ thus gives rise to the electronic states $^3B_{1u}$, $^1B_{1u}$, $^3B_{2u}$, $^1B_{2u}$, $^3E_{1u}$ and $^1E_{1u}$.

To illustrate the case where each orbital of a degenerate pair of orbitals is singly occupied, we now present the group theoretical and HMO treatments of the electronic structure of the cyclopentadienyl cation $C_5H_5^+$ using the D_{5h} point group, the character table of which is presented in Table 14.

The matrix representation of the Hückel operator can be determined in analogy to benzene and takes the form

$$\left[H_{ij}\right] = \begin{bmatrix} \alpha & \beta & 0 & 0 & \beta \\ \beta & \alpha & \beta & 0 & 0 \\ 0 & \beta & \alpha & \beta & 0 \\ 0 & 0 & \beta & \alpha & \beta \\ \beta & 0 & 0 & \beta & \alpha \end{bmatrix}. \tag{139}$$

Diagonalization of this matrix gives rise to the five eigenvalues $\alpha+2\beta$, $\alpha+\omega_1\beta$ and $\alpha+\omega_2\beta$, where ω_1 and ω_2 are defined in Table 14. The application of the reduction formula (Equation (120)) to the five-dimensional reducible representation of the five p_z orbitals and of the projection operators gives rise to five eigenvectors of symmetries a_2'', e_1'' and e_2''. The energetic ordering of the corresponding

Table 14: Character table of the D_{5h} point group.

D_{5h}	E	$2C_5$	$2C_5^2$	$5C_2$	σ_h	$2S_5$	$2S_5^2$	$5\sigma_d$	
A_1'	1	1	1	1	1	1	1	1	
A_2'	1	1	1	-1	1	1	1	-1	R_z
E_1'	2	ω_2	ω_1	0	2	ω_2	ω_1	0	x, y
E_2'	2	ω_1	ω_2	0	2	ω_1	ω_2	0	
A_1''	1	1	1	1	-1	-1	-1	-1	
A_2''	1	1	1	-1	-1	-1	-1	1	z
E_1''	2	ω_2	ω_1	0	-2	$-\omega_2$	$-\omega_1$	0	R_x, R_y
E_2''	2	ω_1	ω_2	0	-2	$-\omega_1$	$-\omega_2$	0	

where $\omega_1 = 2\cos(4\pi/5)$ and $\omega_2 = 2\cos(2\pi/5)$

orbitals is depicted in Figure 25a in the form of a so-called Frost-Musulin diagram. A Frost-Musulin diagram is derived by drawing a regular polygone representing the cyclic polyene into a circle, placing one vertex on the lowest point of the circle. The vertices of the polygone then provide the energies of the π orbitals of the polyene. Such diagrams provide an elegant graphical method to determine the sequence and degeneracy of the HMO of cyclic polyenes. Looking back at Figure 24, it becomes apparent that a Frost-Musulin diagram indeed adequately describes the HMOs of benzene.

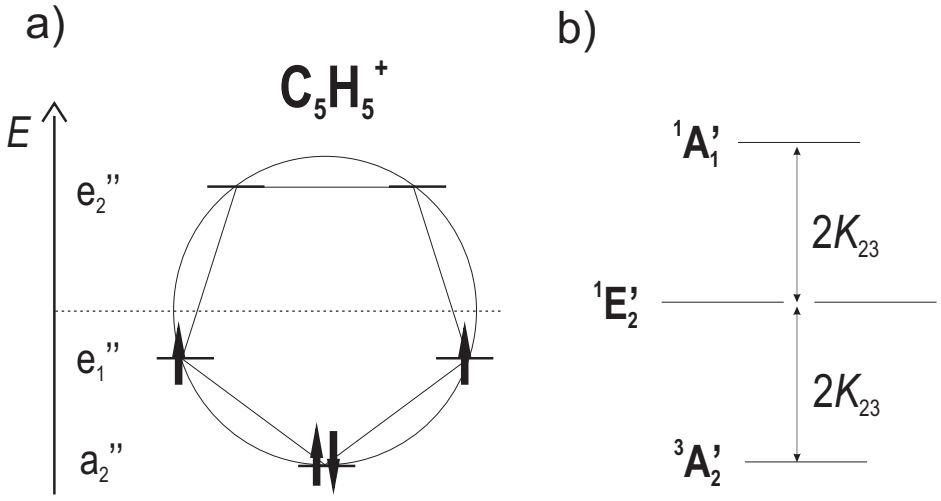

Figure 25: a) Frost-Musulin diagram of the π molecular orbitals of the cyclopentadienyl cation. The arrows indicate the occupation corresponding to the lowest-lying electronic configuration. b) Energetic ordering of the corresponding electronic states in D_{5h} symmetry (right-hand side). K_{23} represents the exchange integral (see text; adapted from Wörner and Merkt (2007))

The most stable electronic configuration of $C_5H_5^+$ is $((a_2'')^2(e_1'')^2)$, as depicted in Figure 25a. The direct product of the irreducible representations of the partially occupied orbitals is $e_1'' \otimes e_1'' = a_2' \oplus$

$e'_2 \oplus a'_1$. In this case, the two components of a degenerate orbital may both be singly occupied. The total electronic wave function must be antisymmetric under the exchange of the two electrons in the e''_1 orbitals, which restricts the number of possible states, as will be discussed in general terms in Section 2.3.2. The electronic symmetry of the singlet states, which have an antisymmetric (with respect to permutation of the electrons) electron spin function, must be determined from the *symmetric* (rather than the *direct*) product of the irreducible representations $[e''_1 \otimes e''_1] = e'_2 \oplus a'_1$, resulting in a $^1E'_2$ and a $^1A'_1$ state. Correspondingly, the electronic symmetry of the triplet state is obtained from the antisymmetric product $\{e''_1 \otimes e''_1\} = a'_2$, resulting in a single $^3A'_2$ state (Compare with the analogous discussion of the electronic structure of O_2 in Subsection 2.2.4). The energetic ordering of the three states $^3A'_2$, $^1E'_2$ and $^1A'_1$ is given in Figure 25b. The Hartree-Fock energies of these three states are $2h + J_{23} - K_{23}$, $2h + J_{23} + K_{23}$ and $2h + J_{22} + K_{23}$, respectively, where h, J_{ij} and K_{ij} represent the one-electron orbital energy, the Coulomb and the exchange integrals, respectively, and the indices designate the π molecular orbitals in order of increasing energy (Borden 1982; by symmetry, $J_{22} - J_{23} = 2K_{23}$). Using the Hückel molecular orbital approach, one can determine the one-electron energy to be $h = \alpha + \omega_1\beta$.

c) Large polyatomic molecules

Unlike small polyatomic molecules, most large molecules have a low symmetry, and the classification of electronic states by their irreducible representations loses its relevance. When the molecule possesses no symmetry elements, all electronic transitions involving nominally a single electron are allowed by symmetry. Consequently, a different nomenclature is used to label both the electronic states and the electronic transitions of large molecules, as already mentioned in the introduction.

The electronic states are designated by a capital letter representing their spin multipicity: S for singlets, D for doublets, T for triplets etc. A numerical subscript is used to indicate the ground state (e.g. S_0) and the higher-lying excited states of the same multiplicity (S_1, S_2 etc...). States of another multiplicity of the same molecule are also labeled in order of increasing energies but starting with the subscript "1" rather than "0" (e.g. T_1, T_2 etc.).

Electronic transitions in polyatomic molecules are often labeled according to the type of molecular orbitals involved. One distinguishes between bonding orbitals of σ or π type, the corresponding anti-bonding orbitals (σ^* or π^*) and nonbonding orbitals (n). This nomenclature has the advantage that it highlights the nature of the electronic transition, from which qualitative predictions of their intensities can be made: Transitions involving the excitation of an electron from a bonding to the corresponding antibonding orbital ($\sigma \rightarrow \sigma^*$ or $\pi \rightarrow \pi^*$) are usually associated with a large oscillator strength, whereas transitions from nonbonding to anti-bonding orbitals ($n \rightarrow \sigma^*$ or $n \rightarrow \pi^*$) are weak.

The nomenclature outlined above is often used in the discussion of the photochemistry and photophysics of larger molecules, like the DNA bases. Although the isolated DNA bases absorb strongly in the ultraviolet (200-300 nm), they hardly show any fragmentation, unlike many other molecules.

This property may be of importance in preserving the genetic information (Sobolewski and Domcke 2002) and arises from the ability of the molecules to convert the energy of the photon to vibrational energy, as will be discussed in Section 3.5.3.

Adenine also represents a good example illustrating the difficulty associated with all nomenclature systems for large molecules. The sequence of singlet states consists of the S_0 ground state with the configuration $\ldots(\pi)^2(n)^2(\pi^*)^0$, followed by two electronic states of dominant configurations, $\ldots(\pi)^2(n)^1(\pi^*)^1$ and $\ldots(\pi)^1(n)^2(\pi^*)^1$, respectively. One can only indicate the dominant configurations for these two electronic states because they lie energetically very close, and configuration interaction between them is important. Since the energetic ordering of these states has been debated in the literature (see Sobolewski and Domcke (2002), and references therein), it is difficult to apply the usual labels S_1 and S_2 to these electronic states. To avoid this difficulty, the recent literature uses the designation $^1n\pi^*$ and $^1\pi\pi^*$ for these two states, the ^{1} superscript designating the spin multiplicity. Figure 26 shows a resonant two-photon ionization spectrum of adenine in a supersonic expansion and a diagram of the electronic energy levels as derived from this spectrum (Kim *et al.* 2000). The band labeled "A" was assigned to the origin of the $^1n\pi^*$ state, whereas band "D" was assigned to the origin of the $^1\pi\pi^*$ state. The wave number scale on top of Figure 26 is given with respect to band "A". The energy-integrated absorption of the $^1\pi\pi^*$ state is strong, and the band turns into a broad absorption band above 36230 cm^{-1}.

2.3.2 Spin multiplicity

As in the treatment of diatomic molecules in Subsection 2.2.4, we will only consider two-electron wave functions. Because of the Pauli principle, the two-electron wave function must either have a symmetric spatial part ($\Psi^{\mathrm{R}}_{(\mathrm{s})}(q_i)$) and an antisymmetric spin part ($\Psi^{\mathrm{S}}_{(\mathrm{a})}(m_i)$) or vice versa ($\Psi^{\mathrm{R}}_{(\mathrm{a})}(q_i)$) and ($\Psi^{\mathrm{S}}_{(\mathrm{a})}(m_i)$), see Tables 4 and 5.

The situation is slightly different from the case of diatomic molecules, because the components of degenerate orbitals can no longer be classified according to a good quantum number (λ in the case of diatomic molecules). However, group theory provides a simple approach to determining the existing multiplicities. Two cases can be distinguished:

1. The two electrons are located in different MO-shells. Both the symmetric and the antisymmetric spatial parts of the wave functions are nonzero in this case. No restrictions result from the Pauli principle: The electronic states are given by the direct product of the representations of the partially occupied orbitals, and all terms contained in the direct product exist as both singlet and triplet states. This situation arises in the first excited states of BeH_2 arising from the configuration $\ldots(2a_1)^2(1b_2)^1(3a_1)^1$. Since $b_2 \otimes a_1 = b_2$, the two electronic states $^3B_2$ and $^1B_2$ are obtained. The same applies to the $(a_{2u})^2(e_{1g})^3(e_{2u})^1$ configuration of benzene discussed in Section 2.3.1b, giving rise to the electronic states $^3B_{1u}$, $^1B_{1u}$, $^3B_{2u}$, $^1B_{2u}$, $^3E_{1u}$ and $^1E_{1u}$.

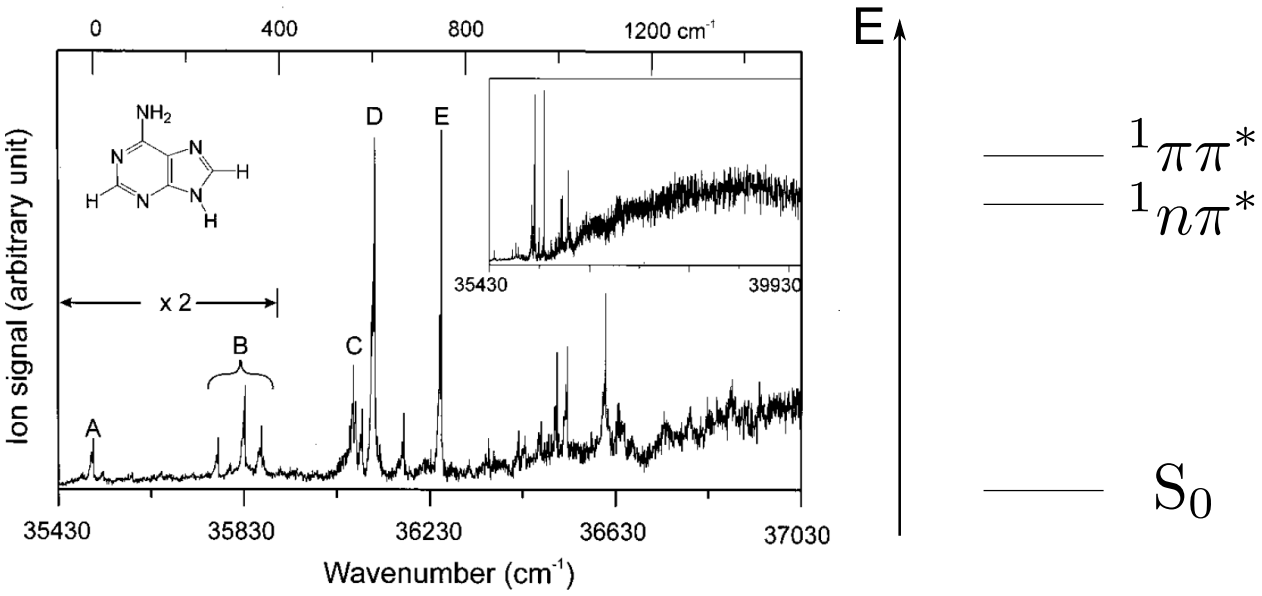

Figure 26: Resonance-enhanced two-photon ionization spectrum of adenine in the gas phase (adapted from Kim *et al.* (2000)). The bands A and D are assigned to the origins of the $n \rightarrow \pi^*$ and $\pi \rightarrow \pi^*$ excitations, respectively. The bands B, C and E are vibronic levels of mixed electronic character. The right-hand side of the figure shows an energy level diagram of the three lowest electronic singlet states of adenine.

2. The two electrons are located in the same MO-shell. If the MO-shell is nondegenerate, the spatial part of the wave function is necessarily symmetric. The spin part must therefore be antisymmetric, resulting in a totally symmetric (A_1') singlet state. If the MO-shell is degenerate, the spatial part has both symmetric and anti-symmetric components. The symmetry properties of these components is determined by the symmetric and antisymmetric parts, respectively, of the direct product of the orbital symmetry with itself. This situation arises in the $(a_2'')^2(e_1'')^2$ configuration of $C_5H_5^+$ discussed in Section 2.3.1b. The symmetric spatial part of the wave function is given by $[e_1'' \otimes e_1''] = e_2' \oplus a_1'$, resulting in a $^1E_2'$ and a $^1A_1'$ state. Correspondingly, the triplet state is obtained from the antisymmetric product $\{e_1'' \otimes e_1''\} = a_2'$, resulting in a single $^3A_2'$ state.

2.3.3 Spin-orbit coupling

Spin-orbit coupling in polyatomic molecules can lead to very complex spectral patterns and dynamical behaviors (e.g., intersystem crossings, see Section 3.5.3). In order to keep the discussion simple, we only discuss here the limiting cases where the spin-orbit coupling is small compared to the energy intervals between neighboring rotational energy levels, and the opposite case, where the spin-orbit coupling is

Table 15: Character table of the spin double group C_{2v}^2. The first five rows and columns correspond to the C_{2v} point group (see Table 12).

C_{2v}	I	C_2	$\sigma_v(xz)$	$\sigma_v'(yz)$	R	
A_1	1	1	1	1	1	T_z
A_2	1	1	−1	−1	1	R_z
B_1	1	−1	1	−1	1	T_x, R_y
B_2	1	−1	−1	1	1	T_y, R_x
$E_{1/2}$	2	0	0	0	−2	

Table 16: Character table of the spin double group C_{3v}^2. The first four rows and columns correspond to the C_{3v} point group

C_{3v}	I	$2C_3$	σ_v	R	$2C_3^2$	
A_1	1	1	1	1	1	T_z
A_2	1	1	−1	1	1	R_z
E	2	−1	0	2	−1	$T_{x,y}, R_{x,y}$
$E_{1/2}$	2	1	0	−2	−1	
$E_{3/2}$	2	−2	0	−2	2	

very large, even larger than the splitting between electronic states of different multiplicities caused by the exchange interaction. The first case is related to the Hund's case (b), the second case to the Hund's case (c) describing the angular momentum coupling in diatomic molecules (see Subsection 2.2.5).

The description of spin-orbit coupling in polyatomic molecules requires the use of the spin double groups already introduced in the discussion of intercombination transitions in diatomic molecules (see Subsection 3.3.2). The character table of the spin double group for C_{2v} and C_{3v} molecules are presented in Tables 15 and 16, respectively, and Table 17 shows how the spin functions with $S = 0, 1/2, 1, 3/2, \ldots$ transform in these spin double groups.

We first consider the case where spin-orbit coupling is small compared to the rotational intervals of the molecule. Spin-orbit interaction splits a rotational state of total angular momentum (without spin) N into $(2S+1)$ nearly degenerate states. As an example we consider a C_{2v} molecule in its $^2B_1$

Table 17: Transformation properties of the spin functions in the spin double groups C_{2v} and C_{3v}.

S	0	1/2	1	3/2	2	5/2
$\Gamma(C_{2v})$	A_1	$E_{1/2}$	$A_2 + B_1 + B_2$	$2E_{1/2}$	$2A_1 + A_2 + B_1 + B_2$	$3E_{1/2}$
$\Gamma(C_{3v})$	A_1	$E_{1/2}$	$A_2 + E$	$E_{1/2} + E_{3/2}$	$A_1 + 2E$	$2E_{1/2} + E_{3/2}$

electronic ground state. The ground rovibronic state has the symmetry $\Gamma_{\rm rve} = \mathrm{B}_1$. The spin-rovibronic symmetries of this level are thus $\Gamma_{\rm srve} = \Gamma_{\rm rve} \otimes \Gamma_{S=1/2} = \mathrm{B}_1 \otimes \mathrm{E}_{1/2} = \mathrm{E}_{1/2}$, showing that the spin-rovibronic ground state is doubly degenerate. The same holds true for all other rovibronic levels of this electronic state. However, the degeneracy may be lifted in the rovibronic levels of a $C_{2\mathrm{v}}$ molecule in a $^3\mathrm{B}_2$ electronic state. In this case, the rovibronic ground state gives rise to spin-rovibronic levels of symmetries $\Gamma_{\rm srve} = \Gamma_{\rm rve} \otimes \Gamma_{S=1} = \mathrm{B}_1 \otimes (\mathrm{A}_2 + \mathrm{B}_1 + \mathrm{B}_2) = \mathrm{B}_2 \oplus \mathrm{A}_1 \oplus \mathrm{A}_2$.

A more interesting case occurs in molecules of the $C_{3\mathrm{v}}$ point group, as, e.g., the methyl halides CH_3X (X=halogen atom) and their cations. The cations CH_3X^+ have ^{2}E ground electronic states. Neglecting vibronic interactions (see Section 2.3.6), spin-orbit coupling splits their ground electronic state into two components of symmetry $\mathrm{E} \otimes \mathrm{E}_{1/2} = \mathrm{E}_{1/2} \oplus \mathrm{E}_{3/2}$. In CH_3I^+, these two components are separated by ≈ 0.5 eV, corresponding to a case where spin-orbit coupling gives rise to much larger splittings than the vibronic interactions. We note that, in this case, the vibronic interactions (the Jahn-Teller effect) are suppressed (see chapter hrs060 for details).

We now illustrate the transition between the limiting cases of weak and strong spin-orbit coupling with the example of the $(\tilde{\mathrm{X}}\ ^2\mathrm{E})(n\mathrm{s})$ Rydberg states of CH_3X (X=halogen), which have the electronic configuration $\ldots(\mathrm{e})^3(\mathrm{a}_1)^1$. In low Rydberg states, the exchange interaction between the Rydberg electron and the ionic core is larger than the spin-orbit coupling, resulting in a ^{3}E state and a ^{1}E state, as illustrated in Figure 27. Spin-orbit coupling splits the ^{3}E state into $\mathrm{E} \otimes (\mathrm{E} \oplus \mathrm{A}_2) = \mathrm{A}_1 \oplus \mathrm{A}_2 \oplus \mathrm{E} \oplus \mathrm{E}$ states. The ^{1}E state remains unaffected in the weak-coupling limit. In high Rydberg states, the spin-orbit interaction in the CH_3X^+ ion is much larger than the exchange interaction between the Rydberg electron and the core electrons, and the level structure displayed on the right-hand side of Figure 27 is obtained. In that limit, the spin of the ion core is coupled to its orbital angular momentum, giving rise to the $\mathrm{E}_{3/2}$ and $\mathrm{E}_{1/2}$ levels discussed in the previous paragraph. The Rydberg electron is only coupled weakly to the ion core by the exchange interaction, which scales as n^{-3}. The symmetries of the electronic states can thus be obtained by taking the direct product of the symmetry of the ionic state and the Rydberg electron. Each Rydberg levels of the ns series converging to the $^2\mathrm{E}_{3/2}$ ground state give rise to two E levels ($\mathrm{E}_{3/2} \otimes \mathrm{E}_{1/2} = \mathrm{E} \oplus \mathrm{E}$), whereas levels converging to the $^2\mathrm{E}_{1/2}$ level split into three levels ($\mathrm{E}_{1/2} \otimes \mathrm{E}_{1/2} = \mathrm{A}_1 \oplus \mathrm{A}_2 \oplus \mathrm{E}$). Figure 27 bears a close resemblance to Figure 3 representing the transition from LS to jj-coupling in atoms.

2.3.4 Vibronic structure and symmetry

The vibrational structure of polyatomic molecules is discussed in detail in hrs003 (Quack and coworkers 2010), so that only a very brief description of the vibronic structure of polyatomic molecules is presented here.

Linear and nonlinear polyatomic molecules have $3N-5$ and $3N-6$ vibrational degrees of freedom, respectively. The transformation properties of the vibrational modes can be determined in a normal coordinate analysis. The vibronic symmetry of a vibrationally excited molecule can be determined

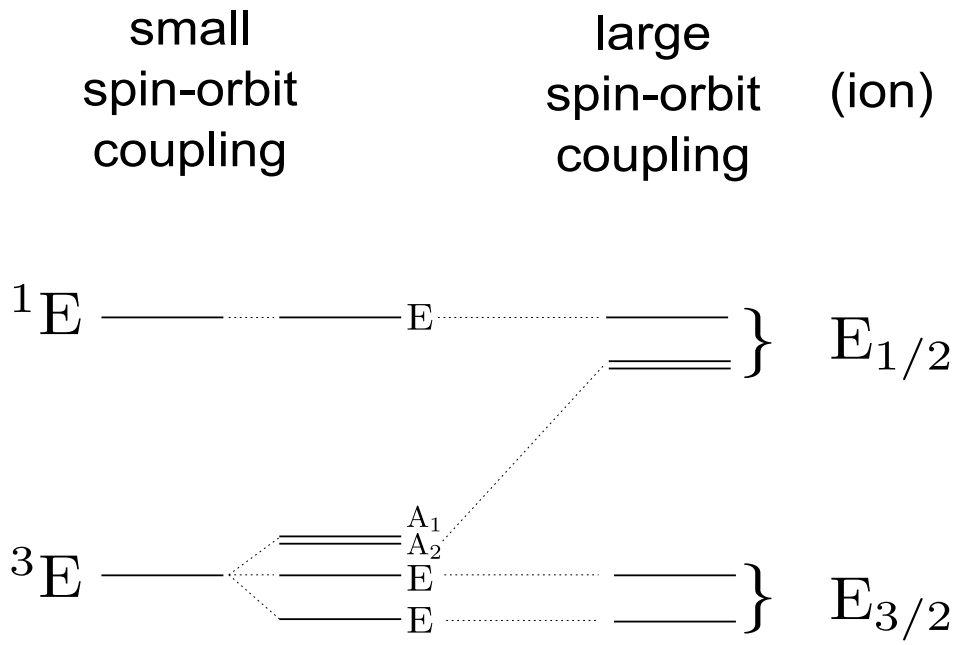

Figure 27: Energy levels of an electronic state of configuration $\ldots(\mathrm{e})^3(\mathrm{a}_1)^1$ of a $C_{3\mathrm{v}}$ molecule for small and large spin-orbit coupling constants. On the right-hand side the lower two E states correlate with the $\mathrm{E}_{3/2}$ electronic state resulting from the $\ldots(\mathrm{e})^3$ configuration of the ion, whereas the upper group of states correlates with the $\mathrm{E}_{1/2}$ ionic electronic state of the same configuration (adapted from Ref. Herzberg (1991)).

from the direct product

$$\Gamma_{\mathrm{ev}} = \Gamma_{\mathrm{e}} \otimes \Gamma_{v_1}^{n_1} \otimes \Gamma_{v_2}^{n_2} \otimes \ldots, \tag{140}$$

where the product extends over all normal vibrations, and n_i is the number of vibrational quanta in the individual vibrational modes.

Example: H_2O has three vibrational modes, two of A_1 symmetry (the symmetric stretching mode (ν_1) and the bending mode (ν_2) and one of B_2 symmetry (the asymmetric stretching mode (ν_3)). The vibronic symmetry of the (0,0,1) vibrational state of the electronic ground state of H_2O is therefore $A_1 \otimes B_2 = B_2$.

Degenerate vibrational modes create a vibrational angular momentum that can couple with the electronic angular momentum.

Example: CO_2^+ in its ground electronic state (X $^2\Pi_{ig}$) is a linear molecule with four vibrational modes: the symmetric stretching mode, the twofold-degenerate bending mode and the asymmetric stretching mode. Single excitation of the bending mode ($\Gamma_{\mathrm{v}} = \Pi_{\mathrm{u}}$) results in a vibrational angular momentum $\hbar l$ with $l = 1$ along the C_∞ axis. The interaction of this vibrational angular momentum with the electronic angular momentum (the Renner-Teller effect, see also chapter hrs060 (Köppel *et al.* 2010) and Section 2.3.6) leads, according to Equation (140) and Table 9, to four vibronic states of symmetries $^2\Sigma_{\mathrm{u}}^+$, $^2\Sigma_{\mathrm{u}}^-$, $^2\Delta_{u3/2}$ und $^2\Delta_{u5/2}$.

2.3.5 Rovibronic structure and symmetry

The rotational structure of polyatomic molecules is discussed in detail in chapter hrs002 (Bauder 2010).

Since the interactions between rotational, spin and orbital motions can often be neglected in polyatomic molecules, their rotational structure can be treated in simple terms as eigenstates of a purely rotational Hamiltonian (see chapter hrs002 (Bauder 2010)). If the electron spins play a role, the rovibronic states split into multiplets that can be classified in the appropriate spin double group, as explained in Subsections 2.3.2 and 2.3.3.

2.3.6 Vibronic coupling: The Renner-Teller and Jahn-Teller effects

The Born-Oppenheimer approximation (see Section 1) allows the separation of nuclear and electronic degrees of freedom, provided that the separation between the electronic states is significantly larger than the vibrational intervals. In many polyatomic molecules, particularly in excited electronic states, this condition is not fulfilled, which results in a coupling of electronic and nuclear motions called vibronic coupling. Vibronic coupling is ubiquitous in electronically excited states, especially in the vicinity of intersecting potential energy surfaces (conical intersections) where it is essential in understanding photochemical and photophysical processes. Special cases characterized by a high molecular symmetry, such as the "Renner-Teller" and "Jahn-Teller effects" are particularly interesting because they enable one to study the vibronic interactions in detail thanks to symmetry selection rules. Comprehensive theories of vibronic coupling have been formulated (see, e.g., hrs060 Köppel *et al.* 2010, or Bersuker 2006). Here we provide a brief overview of the Renner-Teller and Jahn-Teller effects and refer to chapter hrs060 for details.

The Renner-Teller effect occurs in degenerate electronic states ($\Pi, \Delta, \Phi, ...$) of linear molecules. These states are characterized by an electronic angular momentum $\pm\Lambda\hbar$ along the internuclear axis as shown in Figure 28. Vibrationally excited bending levels possess a vibrational angular momentum $\ell\hbar$ about the axis as shown in Figure 28. The two angular momenta couple to form a total vibronic angular momentum $\pm\hbar K$ with $K = |\pm\Lambda \pm \ell|$.

As an example, we consider C_3, with point group $D_{\infty h}$ in the linear configuration, in its $\tilde{A}\ ^1\Pi_u$ first excited singlet electronic state. If only the bending vibrational mode is excited with a single quantum ($v_{\rm bend} = 1$), $|\Lambda| = |\ell| = 1$, which leads to four vibronic levels with $K = 2, 2, 0, 0$. The symmetry of the resulting vibronic levels is easily predicted from group theory: $\Gamma_{\rm ev} = \Pi_u(e) \otimes \Pi_u(v) = \Sigma_g^+ + \Sigma_g^- + \Delta_g$. The two Σ states have $K = 0$ and the Δ state possesses two components with $K = 2$. The energetic ordering of these vibronic states is as shown in Figure 28.

In general, a vibrational level with $v_{\rm bend}$ quanta of excitation has a vibrational angular momentum quantum number $\ell = -v_{\rm bend}, -v_{\rm bend} + 2, ..., +v_{\rm bend} - 2, +v_{\rm bend}$. The vibronic levels of a Π state thus have the vibronic quantum numbers $K = -v_{\rm bend} - 1, -v_{\rm bend} + 1, ..., +v_{\rm bend} - 1, +v_{\rm bend} + 1$ with the following vibronic symmetries: $K = 0 : \Sigma$; $|K| = 1 : \Pi$; $|K| = 2 : \Delta$, ...

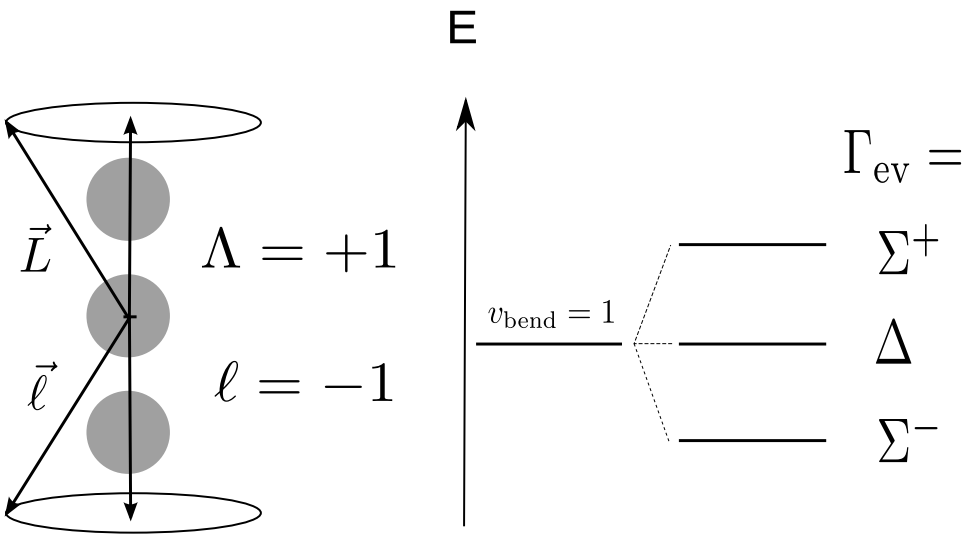

Figure 28: Electronic and vibrational angular momenta in the Renner-Teller effect of a linear molecule in a $^1\Pi$ electronic state, with its bending mode being excited with a single quantum. The left-hand side of the figure illustrates the case of electronic (vibrational) angular momentum projection quantum number $\Lambda = +1$ ($\ell = -1$). The right-hand side shows the splitting of the $v_{\rm bend} = 1$ level into three sublevels of vibronic symmetries Σ^- and Σ^+ ($\Lambda + \ell = 0$), and Δ ($|\Lambda - \ell| = 2$) arising from the Renner-Teller effect.

The Renner-Teller effect has a strong influence on the potential energy surfaces. The degeneracy of the two components of a Π electronic state in the linear configuration is lifted when the molecule bends, resulting in two potential energy surfaces V^+ and V^-. For symmetry reasons, the functional form of the potential energy surface of a Π electronic state in the absence of a Renner-Teller effect can only contain even powers of the bending coordinate Q

$$V^0 = aQ^2 + bQ^4 + ... \tag{141}$$

For the same symmetry reasons, the splitting between the V^+ and V^- surfaces can also only contain even powers of Q

$$V^+ - V^- = \alpha Q^2 + \beta Q^4 + ... \tag{142}$$

In general, three qualitatively different types of potential energy functions along the bending coordinate can be obtained, as illustrated in Figure 29. In the first case, (a), the RT effect is so weak that it preserves the linearity of the molecule and only affects the curvature of the potential energy surface along the bending mode. In the second case, (b), the lower-lying surface has a minimum at a bent geometry, whereas the higher-lying surface retains its minimum at the linear geometry. Finally, in the last case, (c), both surfaces have their minimum shifted to a bent geometry. In cases (b) and (c), the molecules are permanently distorted only if the depth of the potential minimum significantly exceeds the zero-point energy of the bending vibration. If the potential energy minimum occurs at

a nonlinear geometry but the well depth is comparable to or smaller than the zero-point energy of the bending vibration, the molecule essentially behaves like a linear molecule. This is a special case of so-called "quasilinear" molecules, however quasilinearity is also encountered in the absence of the Renner-Teller effect.

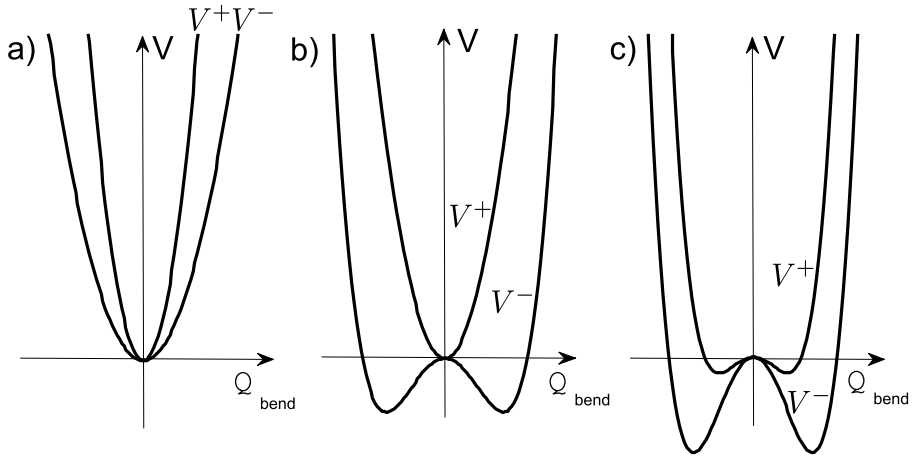

Figure 29: Adiabatic potential energy surfaces resulting from a Renner-Teller effect in a degenerate electronic state of a linear molecule induced by the bending mode.

A classical example of the Renner-Teller effect represented in Figure 29c is the $\tilde{A}\ ^2A_1 \leftarrow \tilde{X}\ ^2B_1$ transition of NH_2. The potential energy minima in the $\tilde{X}$ and $\tilde{A}$ states occur at very different bending angles (103.4° and 144°, respectively), resulting in a long progression of the bending vibration in the electronic spectrum (Johns *et al.* 1976). Examples for cases (a) and (b) are the $\tilde{A}\ ^1\Pi_u$ state of C_3 and the $\tilde{X}\ ^2A_1$ and $\tilde{A}\ ^2\Pi_u$ states of BH_2, respectively.

The Jahn-Teller (JT) effect describes the geometrical distortion of nonlinear molecules in degenerate electronic states (Jahn and Teller 1937) of symmetries E, F[a], G and H. As stated by Jahn and Teller "any nonlinear molecular system in a degenerate electronic state will be unstable and will undergo distortion to form a system of lower symmetry and lower energy thereby removing the degeneracy". The theorem of Jahn and Teller does not state how large the distortion should be or which of the distortions allowed by symmetry will be the dominant one. As in the case of the Renner-Teller effect, the driving force for the molecular distortion is the stabilization of the electronic structure that is achieved in the distorted configuration.

The JT effect profoundly modifies the potential energy surfaces. They are best described in Taylor expansions around a reference geometry $\vec{Q}_0$, most conveniently chosen as the geometry of highest symmetry. At this geometry, the electronic state has its maximal degeneracy (see, e.g., Bersuker (2006); Domcke *et al.* (2004); Köppel *et al.* (1984); Barckholtz and Miller (1998); Wörner and Merkt

[a]Historically, threefold degenerate states were designated with the letter T instead of the letter F. Both nomenclatures are in use in the literature.

(2009))

$$\hat{V}(\vec{Q}) = \sum_{k=1}^{\infty} \frac{1}{k!} \sum_{i=1}^{3N-6} \left(\frac{\partial^k \hat{V}}{\partial Q_i^k} \right)_0 Q_i^k + V(\vec{Q}_0), \tag{143}$$

where Q_i represents the vibrational coordinates. In many cases, the expansion can be truncated at $k = 1$ or 2, corresponding to linear and quadratic Jahn-Teller activity, respectively.

Group theory can be used to predict which modes are Jahn-Teller "active". The general selection rule for vibronic coupling between two electronic states of irreducible representations Γ_A and Γ_B mediated by a vibrational mode of symmetry Γ_ν is

$$\Gamma_\mathrm{A} \otimes \Gamma_\mathrm{B} \supseteq [\Gamma_\nu]^k , \tag{144}$$

where $[\Gamma_\nu]^k$ is the symmetric k^{th} power of the irreducible representation of the vibrational mode ν. When Eq. (144) is fullfilled, the vibrational mode is said to be an active mode of order k. According to Eq. (144), vibronic coupling of order k between the different components of a degenerate electronic state of irreducible representation $\Gamma_\mathrm{el,deg.}$, which is the simplest case of the Jahn-Teller effect, is allowed along mode ν if

$$[\Gamma_\mathrm{el,deg.}]^2 \supseteq [\Gamma_\nu]^k . \tag{145}$$

Vibronic coupling between a degenerate state ($\Gamma_\mathrm{el,deg.}$) and a nondegenerate state ($\Gamma_\mathrm{el,nondeg.}$), the so-called Pseudo-Jahn-Teller effect, can only occur along mode ν if

$$\Gamma_\mathrm{el,deg.} \otimes \Gamma_\mathrm{el,nondeg.} \supseteq [\Gamma_\nu]^k . \tag{146}$$

To illustrate the Jahn-Teller and Pseudo-Jahn-Teller effects, we now consider the examples of the cyclopentadienyl radical (C_5H_5) and cation ($C_5H_5^+$), which are subject to a Jahn-Teller effect and a Pseudo-Jahn-Teller effect in their ground doublet and singlet states, respectively.

In their most symmetric configuration, C_5H_5 and $C_5H_5^+$ have $D_{5\mathrm{h}}$ symmetry (see character table in Table 14). Relevant for a discussion of the low-lying electronic states of C_5H_5 is the π-system of molecular orbitals already presented in Subsection 2.3.1b. C_5H_5 has the ground electronic configuration ($(a_2'')^2(e_1'')^3$) which gives rise to a single electronic ground state of $^2E_1''$ symmetry. In the $D_{5\mathrm{h}}$ point group, $[E_1'']^2 = A_1' \oplus E_2'$ (see Table 18), so that the vibrational modes of e_2' symmetry mediate a linear Jahn-Teller coupling. Since $[e_1']^2$ and $[e_1'']^2$ both contain e_2', vibrational modes of symmetry e_1' and e_1'' are quadratically Jahn-Teller active (see Eq. (145)). In $D_{5\mathrm{h}}$(M), linear and quadratic Jahn-Teller activities are therefore mutually exclusive, which leads to cylindrically symmetric potential energy surfaces in the respective two-dimensional subspaces of degenerate vibrational coordinates. The ground-state potential energy surface of C_5H_5 is schematically represented in Figure 30.

A vibrational mode of symmetry E can be represented using two Cartesian coordinates (x, y) or two cylindrical coordinates (ρ,θ) related by

$$x = \rho\cos(\theta) \text{ and } y = \rho\sin(\theta). \tag{147}$$

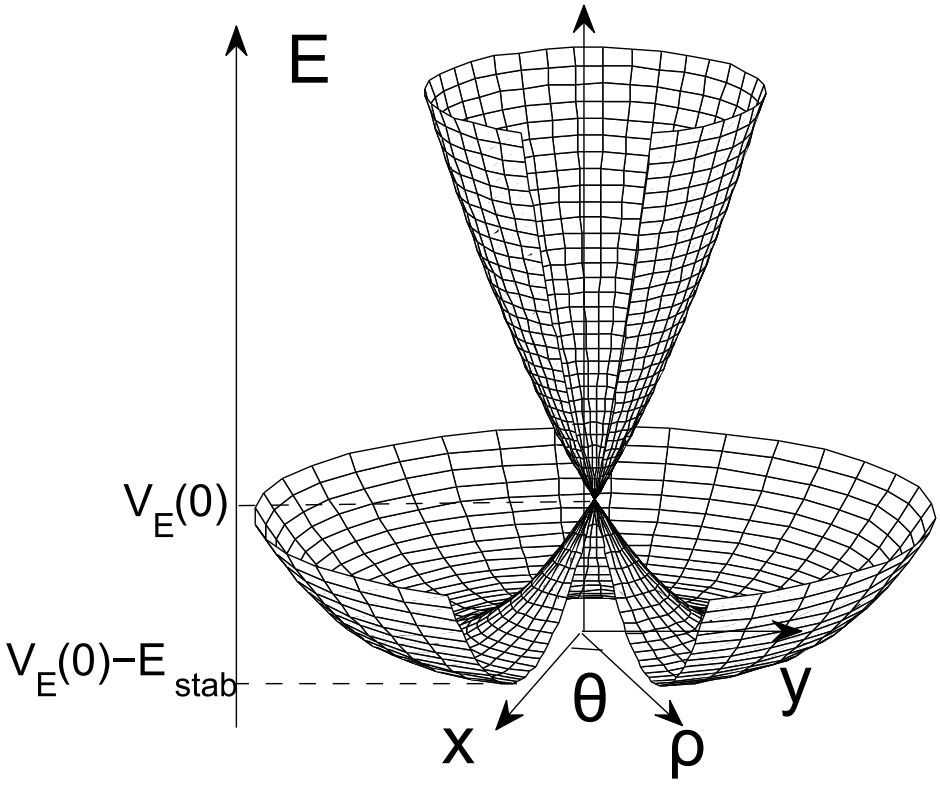

Figure 30: Adiabatic potential energy surfaces resulting from a linear Jahn-Teller effect in a doubly degenerate electronic state induced by a single doubly degenerate vibrational mode with coordinates x and y.

In the case of a single linearly JT-active mode of symmetry E, the potential energy surface of a doubly degenerate electronic state takes the form

$$V_{\mathrm{E}^\pm}(\rho,\theta) = V_{\mathrm{E}^\pm}(\rho) = V_{\mathrm{E}}(0) + \frac{\omega_{\mathrm{JT}}}{2}\rho^2 \pm g\rho, \tag{148}$$

where $V_{\mathrm{E}}(0)$ is the electronic potential energy at the reference geometry, ω_{JT} is the frequency of the vibrational mode and g is the JT coupling constant. The corresponding shape of the potential energy surfaces is illustrated in Figure 30. The linear Jahn-Teller effect thus decreases the potential energy of the lower component of the E electronic state by the stabilization energy

$$E_{\mathrm{stab}} = \frac{g^2}{2\omega_{\mathrm{JT}}}. \tag{149}$$

The Pseudo-Jahn-Teller effect occurs when a vibrational mode couples a degenerate and a non-degenerate electronic state, according to Eq. (146), and is discussed here using the cyclopentadienyl cation as an example. The three lowest electronic states of the cyclopentadienyl cation result from the configuration $((\mathrm{a}_2'')^2(\mathrm{e}_1'')^2)$ and have the electronic symmetries $^3\mathrm{A}_2'$, $^1\mathrm{E}_2'$ and $^1\mathrm{A}_1'$ (in order of increasing energy, see Subsection 2.3.1). These electronic states have been investigated by photoelectron spec-

Table 18: Irreducible representations Γ of D_{5h} and their symmetrized squares $[\Gamma]^2$.

Γ	a_1'	a_2'	e_1'	e_2'	a_1''	a_2''	e_1''	e_2''
$[\Gamma]^2$	a_1'	a_1'	$a_1'+e_2'$	$a_1'+e_1'$	a_1'	a_1'	$a_1'+e_2'$	$a_1'+e_1'$

troscopy (Wörner *et al.* 2006; Wörner and Merkt 2007, 2009). The triplet ground state is not involved in vibronic coupling and therefore has a D_{5h} equilibrium geometry. The doubly-degenerate $^1E_2'$ state undergoes both Jahn-Teller and Pseudo-Jahn-Teller effects. From Equation (145) and Table 18, one can conclude that the e_1' vibrational modes are linearly Jahn-Teller active, and that the e_2' and e_2'' vibrational modes are quadratically active in the $^1E_2'$ state. However, the Jahn-Teller effect in an electronic state having two electrons in two degenerate orbitals (configuration e^2) vanishes in the absence of configuration interaction (Watson 1999a) and will therefore be negelected. The Pseudo-Jahn-Teller coupling between the $^1E_2'$ and $^1A_1'$ states ($e_2' \otimes a_1' = e_2'$) is mediated by vibrational modes of e_2' symmetry in first order and modes of e_1' or e_1'' symmetry in second order. The potential energy surfaces of the second and third lowest electronic states of $C_5H_5^+$ are represented schematically in Figure 31. For a single doubly-degenerate PJT-active mode with Cartesian coordinates (x, y) or cylindrical coordinates (r, ϕ), two of the surfaces repel each other whereas the third remains unchanged. Assuming identical vibrational frequencies in the A and E states, the following potential surfaces are obtained

$$\begin{aligned} V_A(r,\phi) = V_A(r) &= \frac{V_E(0)+V_A(0)}{2} + \frac{\omega_{PJT}}{2}r^2 + \sqrt{\left[\frac{V_A(0)-V_E(0)}{2}\right]^2 + 2\lambda^2 r^2} \\ V_{E_y}(r,\phi) = V_{E_y}(r) &= V_E(0) + \frac{\omega_{PJT}}{2}r^2 \\ V_{E_x}(r,\phi) = V_{E_x}(r) &= \frac{V_E(0)+V_A(0)}{2} + \frac{\omega_{PJT}}{2}r^2 - \sqrt{\left[\frac{V_A(0)-V_E(0)}{2}\right]^2 + 2\lambda^2 r^2}, \end{aligned} \tag{150}$$

where $V_E(0)$ and $V_A(0)$ are the electronic potential energies at the reference geometry, ω_{PJT} is the frequency of the vibrational mode, and λ is the PJT coupling constant. The corresponding shape of the potential energy surfaces is illustrated in Figure 31.

The spectroscopic characterization of the Jahn-Teller and Pseudo-Jahn-Teller effect in C_5H_5 and $C_5H_5^+$ is discussed in Subsection 3.4.3.

3 Electronic spectra

3.1 Transition moments and selection rules

The intensity $I(\nu_{fi})$ of a transition between an initial state of an atom or a molecule with wave function Ψ_i and energy E_i and a final state with wave function Ψ_f and energy E_f is proportional to the square of the matrix element $\hat{V}_{fi}$, where the matrix $\hat{V}$ represents the operator describing the interaction between

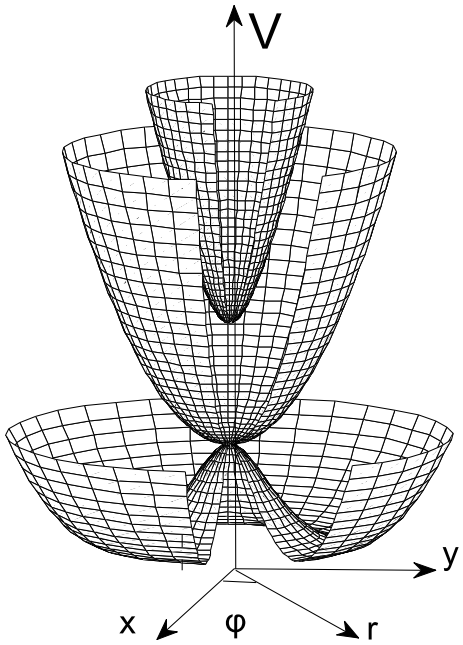

Figure 31: Adiabatic potential energy surfaces resulting from a linear Pseudo-Jahn-Teller effect between a lower-lying doubly degenerate electronic state (E) and a higher-lying nondegenerate state (A) induced by a single doubly degenerate vibrational mode

the radiation field and the atom or the molecule

$$I(\nu) \propto |\langle \Psi_\mathrm{f} | \hat{V} | \Psi_\mathrm{i} \rangle|^2 = \langle \mathrm{f} | \hat{V} | \mathrm{i} \rangle^2 = \hat{V}_\mathrm{if}^2. \tag{151}$$

The transition is observed at the frequency $\nu_{fi} = |E_f - E_i|/h$.

A selection rule enables one to predict whether a transition can be observed or not on the basis of symmetry arguments. If $\langle \Psi_\mathrm{f} | \hat{V} | \Psi_\mathrm{i} \rangle = 0$, the transition f $\leftarrow$ i is said to be "forbidden" , i.e., not observable; if $\langle \Psi_\mathrm{f} | \hat{V} | \Psi_\mathrm{i} \rangle \neq 0$, the transition f $\leftarrow$ i is said to be "allowed".

The interaction between molecules and electromagnetic radiation of a wavelength much larger than the molecular size is dominated by the interaction between the electric dipole moment and the electric field of the radiation

$$\hat{V} = -\vec{\hat{M}} \cdot \vec{E}, \tag{152}$$

and, in the following, we restrict the discussion to this interaction.

In the case of linearly polarized radiation, the electric field vector, defined in the laboratory-fixed (X, Y, Z) frame, is $(0, 0, E)$, and, therefore, $\hat{V} = -\hat{M}_Z E$. When studying the spectra of atoms, the laboratory-fixed (or space-fixed) reference frame is the only relevant frame, because it can always be chosen to coincide with an internal, "atom-fixed" reference frame. Indeed, the point-like nature of the nucleus implies that there are no rotations of the nuclear framework. For this reason, atomic spectra are simpler to treat than molecular spectra.

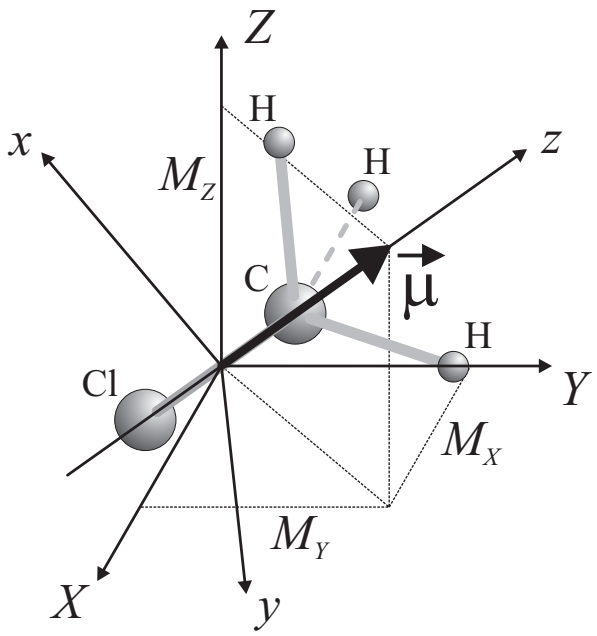

Figure 32: Relationship between the dipole moment $\vec{\mu} = (\mu_x, \mu_y, \mu_z)$, which is naturally expressed in the molecule-fixed reference frame (x, y, z), and the dipole moment $\vec{M} = (M_X, M_Y, M_Z)$ in the space-fixed (X, Y, Z) reference frame. For the molecule CH_3Cl used as illustration, the permanent dipole-moment vector $\vec{\mu}$ lies along the z axis of the molecule-fixed reference frame.

In molecules, the components $\hat{\mu}_\xi$ of the electric dipole moment have a simple expression, and can be computed or interpreted easily, in the *molecule-fixed* reference frame (x, y, z) in which they are given by

$$\hat{\mu}_\xi = \sum_j q_j \xi_j \quad \text{with} \quad \xi = x, y, \text{ oder } z, \tag{153}$$

where q_j and ξ_j are the charge and the ξ coordinate of the j^{th} particle, and the sum extends over all particles (electrons and nuclei) in the molecule. The important quantities for the interaction defined in Equation (152) are the space-fixed components $\hat{M}_X$, $\hat{M}_Y$ and $\hat{M}_Z$ of $\vec{\hat{M}}$. To evaluate Equation (151) using Equations (152) and (153) the relative orientation of the molecule-fixed and space-fixed reference frames must be considered, as illustrated by Figure 32.

Figure 33 shows how the relative orientation of the space-fixed and molecule-fixed frames can be defined using three angles known as the three Euler angles (θ, ϕ and χ) (see Zare (1988)).

The rotation matrices corresponding to the three rotations represented in Figure 33 allow one to express the space-fixed components of $\vec{\hat{M}}$ as a function of the molecule-fixed components $\hat{\mu}_\xi$. The Z component, for instance, is given by

$$\hat{M}_Z = \lambda_{xZ}\hat{\mu}_x + \lambda_{yZ}\hat{\mu}_y + \lambda_{zZ}\hat{\mu}_z = \sum_\alpha \lambda_{\alpha Z}\hat{\mu}_\alpha, \tag{154}$$

where the values of the direction cosines λ_{iJ} are easily obtained from the form of the rotation matrices

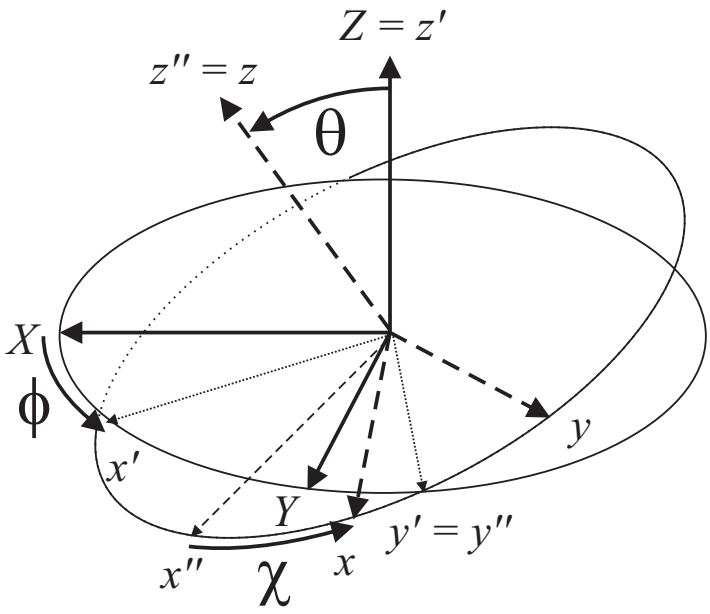

Figure 33: Euler angles θ, ϕ, χ defining the relative orientation of the space-fixed reference frame (X, Y, Z) and the molecule-fixed reference frame (x, y, z). Starting from the space-fixed reference frame, the molecule-fixed reference frame is obtained by 1) rotation by an angle ϕ around the Z axis, leading to the intermediate (x', y', z') frame; 2) rotation by an angle θ around the y' axis, leading to the second intermediate (x'', y'', z'') frame; and 3) rotation by an angle χ around the z'' axis.

(see, e.g., Zare (1988); p78-81). The selection rules can be derived from the integral

$$\langle \Psi_{\rm f} | \hat{M}_z | \Psi_{\rm i} \rangle. \tag{155}$$

We begin the discussion of electronic transitions and selection rules by considering wave functions of the form given by Equation (1). The product form of such functions is based on the assumption that the electronic, spin, vibrational and rotational motions are separable, which represents an approximation. The interactions between the various types of motion, e.g. spin-orbit interaction (see Subsection 2.1.4) or the interaction between rotational and electronic motions (see Subsection 2.2.7), or interactions between vibrational and electronic motion (see subsection 2.3.6) are often significant, in which case the selection rules derived on the basis of Equation (1) may be violated.

Using Equations (1) and (154), Equation (155) can be written as

$$\langle \Phi'_{\rm elec} \Phi'_{\rm espin} \Phi'_{\rm vib} \Phi'_{\rm rot} \Phi'_{\rm nspin} | \sum_\alpha \lambda_{\alpha Z} \hat{\mu}_\alpha | \Phi''_{\rm elec} \Phi''_{\rm espin} \Phi''_{\rm vib} \Phi''_{\rm rot} \Phi''_{\rm nspin} \rangle. \tag{156}$$

The electric-dipole-moment operator (Equation (153)) is independent of the spin variables. The integration over electron and nuclear spin coordinates in Equation (156) may thus be performed separately from the integration over spatial (rovibronic) coordinates

$$\langle \Phi'_{\rm espin} | \Phi''_{\rm espin} \rangle \langle \Phi'_{\rm nspin} | \Phi''_{\rm nspin} \rangle \langle \Phi'_{\rm elec} \Phi'_{\rm vib} \Phi'_{\rm rot} | \sum_\alpha \lambda_{\alpha Z} \hat{\mu}_\alpha | \Phi''_{\rm elec} \Phi''_{\rm vib} \Phi''_{\rm rot} \rangle. \tag{157}$$

The wave functions corresponding to different electron-spin and nuclear-spin states are orthogonal, so that the first two integrals in Equation (157) are zero, unless $|\Phi'_{\mathrm{espin}}\rangle = |\Phi''_{\mathrm{espin}}\rangle$ and $|\Phi'_{\mathrm{espin}}\rangle = |\Phi''_{\mathrm{espin}}\rangle$. The resulting selection rules imply the conservation of the total electron spin

$$\Delta S = 0, \tag{158}$$

and the total nuclear spin

$$\Delta I = 0, \tag{159}$$

and also the conservation of nuclear-spin symmetry.

In the absence of interactions between the vibronic and rotational degrees of freedom, the vibronic wave functions $\Phi_{\mathrm{elec}}\Phi_{\mathrm{vib}}$ are independent of the Euler angles, and so are the molecule-fixed components $\hat{\mu}_\alpha$ of the electric-dipole-moment operator. Morever, the direction cosine matrix elements $\lambda_{\alpha Z}$ and the rotational functions Φ_{rot} do not depend on the vibronic coordinates. Consequently, the integration over the vibronic coordinates and the Euler angles in the last factor of Equation (157) can be performed separately to a good approximation:

$$\langle \Phi'_{\mathrm{elec}}\Phi'_{\mathrm{vib}}\Phi'_{\mathrm{rot}}| \sum_\alpha \lambda_{\alpha Z}\hat{\mu}_\alpha |\Phi''_{\mathrm{elec}}\Phi''_{\mathrm{vib}}\Phi''_{\mathrm{rot}}\rangle = \sum_\alpha \langle \Phi'_{\mathrm{rot}}|\lambda_{\alpha Z}|\Phi''_{\mathrm{rot}}\rangle \langle \Phi'_{\mathrm{elec}}\Phi'_{\mathrm{vib}}|\hat{\mu}_\alpha|\Phi''_{\mathrm{elec}}\Phi''_{\mathrm{vib}}\rangle. \tag{160}$$

The first, angle-dependent factor on the right-hand side of Equation (160) implies the conservation of angular momentum. The electric-dipole moment operator $\hat{\vec{M}}$ is a vector and can therefore be represented as a spherical tensor of rank $J = 1$ (Zare 1988). Consequently, the transition moment $\langle \Psi'|\hat{\vec{M}}|\Psi''\rangle$ vanishes unless

$$\Delta J = J' - J'' = 0, \pm 1 \quad (0 \leftrightarrow 0 \text{ forbidden}). \tag{161}$$

Considering the polarization of the radiation leads to the following selection rules for the magnetic quantum number:

$$\Delta M_J = M'_J - M''_J = 0 \quad \text{(linear polarization parallel to } Z \text{ axis)} \tag{162}$$

$$\Delta M_J = M'_J - M''_J = \pm 1 \quad \text{(linear polarization perpendicular to } Z \text{ axis)} \tag{163}$$

$$\Delta M_J = M'_J - M''_J = 1 \quad \text{(circular polarization with positive helicity)} \tag{164}$$

$$\Delta M_J = M'_J - M''_J = -1 \quad \text{(circular polarization with negative helicity).} \tag{165}$$

The electric-dipole moment operator is also antisymmetric with respect to the parity operation which reverses the sign of all coordinates in the laboratory-fixed frame. Given that the parity is a conserved quantity as long as parity violation by the weak force is neglected (see Quack (2010)), transitions can only occur between rovibronic states of opposite parity, i.e.,

$$+ \leftrightarrow - \quad (+ \leftrightarrow + \text{ and } - \leftrightarrow - \text{ are forbidden}). \tag{166}$$

It is important to note that the $\pm$ signs in Equation (166) refer to the total (rovibronic) parity of the energy levels (see Equation (110)), and must be distinguished from the $\pm$ signs in the electronic term

symbol. The parity selection rule will be discussed in more detail in Subsection 3.3.4 in the treatment of the rotational structure of electronic transitions.

Equations (161)-(166) are general to all electric-dipole transitions in all systems, not only atoms. When the transitions connect hyperfine levels, J'' and (J') must be replaced by F'' and (F'), respectively. Equations (158) and (159) are also general to all electric-dipole transitions but hold less strictly because they result from the approximation of separable wave functions.

These considerations make it obvious that two-photon transitions (e.g., Raman transitions), or magnetic-dipole transitions do not obey the same set of selection rules. The treatment of such transitions can be made in an analogous manner, but by using the appropriate form of the interaction operators.

Further selection rules, specific of the symmetry properties of the atomic or molecular systems under investigation, result from the second, angle-independent term on the right-hand side of Equation (160). These selection rules can be derived from group-theoretical arguments on the basis of the following considerations:

1. electronic Φ_{elec} and vibrational Φ_{vib} wave functions transform as irreducible representations of the appropriate point group,

2. the molecule-fixed components $\hat{\mu}_\xi$ of the electric-dipole-moment operator transform as the translations T_x, T_y und T_z,

3. a product of two or more functions transforms as the product of the corresponding representations, and

4. the integral over a product of functions differs from zero only if the product of the corresponding representations contains the totally-symmetric representation, usually A_1 (or Σ^+ in diatomic molecules, and S in atoms; we use A_1 in this section to designate this representation).

An allowed transition between the states i and f with the irreducible representations Γ_{i} and Γ_{f} must therefore fullfill the condition in the electric-dipole approximation

$$\Gamma_{\mathrm{i}} \otimes \Gamma(T_\alpha) \otimes \Gamma_{\mathrm{f}} \supseteq \mathrm{A}_1, \text{ with } \alpha = x, y, z. \tag{167}$$

Considering the last, vibronic, factor in Equation (160):

$$\langle \Phi'_{\mathrm{elec}} \Phi'_{\mathrm{vib}} | \hat{\mu}_\alpha | \Phi''_{\mathrm{elec}} \Phi''_{\mathrm{vib}} \rangle = \langle \Phi'_{\mathrm{ev}} | \hat{\mu}_\alpha | \Phi''_{\mathrm{ev}} \rangle, \tag{168}$$

one concludes that a transition is vibronically allowed if

$$\Gamma''_{\mathrm{ev}} \otimes \Gamma(T_\alpha) \otimes \Gamma'_{\mathrm{ev}} \supseteq \mathrm{A}_1. \tag{169}$$

Example: In the $C_{2\mathrm{v}}$ point group, T_x, T_y and T_z transform as B_1, B_2 and A_1, respectively (see Table 12). Vibronic

wave functions of symmetry $\Gamma'_{\rm ev} = {\rm B}_1, {\rm B}_2$ or ${\rm A}_1$ can thus be excited from an initial vibronic state of symmetry $\Gamma''_{\rm ev} = {\rm A}_1$ (e.g., the ground state of H_2O), and the corresponding transition moment lies along the x, y and z axis of the molecule-fixed reference frame, respectively. Transitions to levels of vibronic symmetry $\Gamma'_{\rm ev} = A_2$ are vibronically forbidden.

Within the Born-Oppenheimer approximation, the electronic motion can be separated from the vibrational motion of the nuclear framework, and the integration over the electronic coordinates in Equation (168) can be performed for any given value of the nuclear coordinates $\vec{Q}$

$$\langle \Phi'_{\rm vib} [\langle \Phi'_{\rm elec} | \hat{\mu}_\alpha | \Phi''_{\rm elec} \rangle_{\rm e}] \Phi''_{\rm vib} \rangle = \langle \Phi'_{\rm vib} | \mu^{\rm e}_\alpha(\vec{Q}) | \Phi''_{\rm vib} \rangle. \tag{170}$$

In Equation (170)

$$\mu^{\rm e}_\alpha(\vec{Q}) = \langle \Phi'_{\rm elec} | \hat{\mu}_\alpha | \Phi''_{\rm elec} \rangle_{\rm e} \tag{171}$$

depends on the nuclear coordinates $\vec{Q}$ and thus on the $3N-6$ (or $3N-5$ for linear molecules) symmetrized normal coordinates Q_i. When this dependence is weak, $\mu^{\rm e}_\alpha(\vec{Q})$ can be expanded in a Taylor series around a reference geometry, e.g. the equilibrium geometry $\vec{Q}_{\rm eq}$ of the initial electronic state of the transition,

$$\mu^{\rm e}_\alpha(\vec{Q}) = \mu^{\rm e}_\alpha(\vec{Q}_{\rm eq}) + \sum_j \frac{\partial \mu^{\rm e}_\alpha}{\partial Q_j}|_{\rm eq} Q_j + \ldots, \tag{172}$$

where the summation extends over all normal coordinates Q_j. Retaining only the constant and linear terms of the Taylor series of $\mu^{\rm e}_\alpha(\vec{Q})$, Equation (170) can be expressed as a sum of two terms

$$\mu^{\rm e}_\alpha|_{eq} \langle \Phi'_{\rm vib} | \Phi''_{\rm vib} \rangle + \sum_j \frac{\partial \mu^{\rm e}_\alpha}{\partial Q_j}|_{\rm eq} \langle \Phi'_{\rm vib} | Q_j | \Phi''_{\rm vib} \rangle. \tag{173}$$

Equation (173) forms the basis of the classification of electronic transitions as electronically allowed transitions, on the one hand, and as electronically forbidden, but vibronically allowed transitions, on the other. These two types of electronic transitions are now described in more detail.

Electronically allowed transitions:

In the case of an electronically allowed transition, the contribution arising from the first term of Equation (173) is nonzero, which implies that

$$\Gamma'_{\rm elec} \otimes \Gamma(T_\alpha) \otimes \Gamma''_{\rm elec} \supseteq {\rm A}_1 \text{ with } \alpha = x, y, z. \tag{174}$$

Neglecting the second term in Equation (173) leads to the following two conclusions. Firstly, the intensity of an electronically allowed transition is proportional to the square of the electronic transition moment evaluated at the equilibrium geometry of the initial state, i.e., to $|\langle \Phi'_{\rm elec} | \hat{\mu}_\alpha(\vec{Q}_{\rm eq}) | \Phi''_{\rm elec} \rangle_{\rm e}|^2$. Secondly, the intensity of a transition from the vibrational level $\Phi''_{\rm vib}$ of the initial state to the vibrational level $\Phi'_{\rm vib}$ of the final state is proportional to the square of the overlap of the vibrational wave functions, i.e., to

$$|\langle \Phi'_{\rm vib} | \Phi''_{\rm vib} \rangle|^2, \tag{175}$$

a quantity known as a Franck-Condon factor. Group-theoretical arguments further lead to the conclusion that the Franck-Condon factors are nonzero only if

$$\Gamma'_{\text{vib}} \otimes \Gamma''_{\text{vib}} \supseteq \text{A}_1 \quad (\text{or } \Sigma^+). \tag{176}$$

For example, transitions from the ground vibrational level of a molecule, which must have $\Gamma''_{\text{vib}} = \text{A}_1$, are observable only to totally-symmetric vibrational levels of the final electronic state, i.e., to vibrational levels with $\Gamma'_{\text{vib}} = \text{A}_1$. This condition is fulfilled by all vibrational levels having only even numbers of vibrational quanta in non-totally-symmetric vibrational modes. More generally, Equation (176) can be expressed as

$$\Delta v_i = v'_i - v''_i = 0, \pm 2, \pm 4, \ldots \tag{177}$$

for all non-totally-symmetric vibrational modes i, and as

$$\Delta v_j = v'_j - v''_j = 0, \pm 1, \pm 2, \ldots \tag{178}$$

for all totally-symmetric vibrational modes j. When the Born-Oppenheimer potential energy hypersurface of the two electronic states connected by an electronic transition are identical, the observed transitions are characterized by $\Delta v_i = 0$ for all modes i, because of the orthogonality of the vibrational wave functions (see Figure 44 below). The observation of long vibrational progressions in electronic spectra indicates that the initial and final electronic states have different equilibrium geometries and the length of a progression in a given mode can be correlated to the change of geometry along this mode.

Electronically forbidden but vibronically allowed transitions:

The second term of Equation (173) becomes the dominant term when the transition is electronically forbidden. This term is nonzero if

$$\Gamma'_{\text{vib}} \otimes \Gamma_{Q_i} \otimes \Gamma''_{\text{vib}} \supseteq \text{A}_1 \quad (\text{or } \Sigma^+), \tag{179}$$

in which case one speaks of electronically forbidden but vibronically allowed transitions. Such transitions gain intensity by the vibronic coupling of the final electronic state to another electronic state which is connected to the initial electronic state by an electronically allowed transition. The vibronic coupling is mediated by the non-totally-symmetric normal mode with coordinate Q_i. Consequently, observable vibronic transitions are characterized by

$$\Delta v_i = v'_i - v''_i = 1, \pm 3, \pm 5, \ldots, \tag{180}$$

and would be forbidden in an electronically allowed transition. The vibronic coupling leading to the observation of electronic forbidden transition is known as Herzberg-Teller coupling, or Herzberg-Teller intensity borrowing mechanism, and results from a breakdown of the Born-Oppenheimer approximation. The observation of vibrational progressions following the selection rule (180) provides important

information on vibronic coupling in that it enables one to identify the modes responsible for the coupling.

Example: $A_1 \leftrightarrow A_1$, $B_2 \leftrightarrow A_1$ and $B_1 \leftrightarrow A_1$ transitions of C_{2v} molecules are electronically allowed, but $A_2 \leftrightarrow A_1$ transitions are electronically forbidden in the electric dipole approximation. Such transitions may become observable by vibronic coupling to electronic states of A_1, B_2, and B_1 electronic symmetry induced by vibrational modes of A_2, B_1, and B_2 symmetry, respectively.

Specific selection rules, which depend on the point-group symmetry of the molecular system under consideration, can be derived from the general results presented above. Such selection rules are now discussed in more detail, and separately, for atoms, diatomic (and linear) molecules and polyatomic molecules in the next subsections.

When discussing selection rules of the kind presented above, it is important to always keep in mind that all equations derived in this subsection are the result of approximations, approximations in the treatment of the interaction between the atomic or molecular systems with the radiation field, approximations concerning the separability of the different types of motion, and approximations resulting from the truncation of expansions. These approximations are helpful in the interpretation of electronic spectra, but, often, a fully satisfactory treatment of intensity distributions makes it necessary to go beyond them, for instance (i) by considering the interaction between the rotational, vibrational and electronic motions and the spin-orbit interaction, (ii) by accounting for the fact that the normal modes of the initial electronic state do not always coincide with the normal modes of the final electronic state, or even, in some cases, (iii) by recognizing that the initial and final electronic states belong to different point groups.

Point groups are convenient and adequate to discuss vibronic selection rules in many molecular systems. Rovibronic selection rules and selection rules in electronic transitions connecting electronic states subject to large-amplitude motions or belonging to different point-group symmetry, are more conveniently treated in symmetry groups representing the true symmetry properties of the Hamiltonian describing the molecular system, such as the complete-nuclear-inversion-permutation groups or the molecular symmetry groups (Bunker and Jensen 1998). Further information on such groups and their applications in high-resolution spectroscopy are discussed in the articles by Schnell (2010); Oka (2010); Quack (2010) in this handbook.

3.2 Electronic spectra of atoms

An immense body of data exists on the electronic spectra of atoms. Extensive tables of atomic energy levels and transition frequencies have been published (see, for instance, Moore (1949, 1952, 1958)). Data exist on almost all atoms, in almost all charge states. Rather than trying to recompile these data, the present chapter introduces elementary aspects of the electronic spectra of atoms that are

necessary to make good use of the published material. After a brief summary of electric-dipole selection rules in Subsection 3.2.1, the elementary aspects of electronic atomic spectroscopy are illustrated in Subsection 3.2.2 with the examples of hydrogen and hydrogen-like atoms, alkali-metal atoms, and rare-gas atoms. The first example was chosen because of the immense importance of the spectrum of the H atom in the development of quantum mechanics and electronic spectroscopy. It also gives an idea of the extreme precision of spectroscopic measurements and how high-resolution electronic spectroscopy can be used to reveal the finest details of the energy level structure of atoms. The second example presents the electronic spectra of the alkali-metal atoms, which were at the origin of the s, p, d, f,... nomenclature used to label atomic states. Alkali-metal atoms play a dominant role in current research in atomic physics. For instance, the knowledge of the fine and hyperfine structures of selected transitions is required to understand laser cooling. With the electronic spectra of the rare-gas atoms, we discuss atomic systems with more than one unpaired electron, which have electronic states of different spin multiplicity.

3.2.1 Selection rules

Selection rules complementing the general ones already presented in Equations (161)-(166) can be derived using the point group K_{h} (see Table 1) if the electron spin and orbital motions can be separated, in which case $\Delta S = 0$ (see Equation (158)). As mentioned in the previous subsection, the laboratory-fixed reference frame is the only relevant frame when determining selection rules for atoms. The X, Y and Z components of the electric-dipole-moment operator $\hat{\vec{M}}$ transform as the $\mathrm{P_u}$ irreducible representation of K_{h} so that the single-photon selection rules corresponding to the transition moment $\langle \Psi' | \hat{\vec{M}}_i | \Psi'' \rangle$ with $i = X, Y, Z$ can be expressed as

$$\Gamma' \otimes \Gamma'' \supseteq \mathrm{P_u}. \tag{181}$$

Using the direct-product table (Table 2), this equation leads to the selection rule known as Laporte rule

$$\Delta L = L' - L'' = 0, \pm 1 \quad (0 \leftrightarrow 0 \text{ forbidden}). \tag{182}$$

and to

$$\mathrm{g} \leftrightarrow \mathrm{u} \quad (\mathrm{g} \leftrightarrow \mathrm{g} \text{ and } \mathrm{u} \leftrightarrow \mathrm{u} \text{ forbidden}). \tag{183}$$

Whenever electron-correlation effects are negligible and the electronic wave function can be represented as a single determinant (see Equation (15)), absorption of a single photon leads to a final electronic state differing from the initial one by a single spin-orbital, say ϕ_ℓ, so that the selection rules (182) and (183) reduce to $\langle \phi_{\ell'} | \hat{\vec{M}} | \phi_{\ell''} \rangle$

$$\Delta \ell = \ell' - \ell'' = \pm 1. \tag{184}$$

The same argumentation can easily be extended to the derivation of magnetic-dipole or electric-quadrupole selection rules as well as selection rules for multiphoton processes.

3.2.2 Selected examples

Hydrogen and other one-electron atoms

The spectra of hydrogen and hydrogen-like atoms have been of immense importance for the development of quantum mechanics and for detecting and recognizing the significance of fine, hyperfine and quantum-electrodynamics effects. They are also the source of precious information on fundamental constants such as Rydberg's constant and the fine-structure constant. The desire to observe the spectrum of the H atom at ever higher spectral resolution and to determine the transition frequencies at ever higher accuracy has been one of the major driving forces in methodological and instrumental developments in high-resolution electronic spectroscopy.

If fine, hyperfine, and quantum-electrodynamics effects are neglected, the energy level structure of the hydrogen atom is given by Equation (5) and is characterized by a high-degree of degeneracy. The allowed electronic transitions can be predicted using Equation (184) and their wavenumbers determined using Equation (185)

$$\tilde{\nu} = R_M/n''^2 - R_M/n'^2 \tag{185}$$

which, for $n'' = 2$, reduces to Balmer's formula. The transitions obeying the selection rule (184) are depicted schematically in Figure 34a, in which, for simplicity, only transitions from and to the $n = 1$ and $n = 2$ levels are indicated by double-headed arrows. Because of their importance, many transitions have been given individual names. Lines involving $n = 1$, 2, 3, 4, 5, and 6 as lower levels are called Lyman, Balmer, Paschen, Brackett, Pfund, and Humphrey lines, respectively. Above $n = 6$, one uses the n value of the lower level to label the transitions. Lines with $\Delta n = n' - n'' = 1, 2, 3, 4, 5, \ldots$ are labeled $\alpha, \beta, \delta, \gamma, \phi, \ldots$, respectively. Balmer β, for instance, designates the transition from $n = 2$ to $n = 4$. The spectral positions of the allowed transitions are indicated in the schematic spectrum presented in Figure 34b.

The degeneracies implied by Equation (5) make the spectrum of the hydrogen atom and single-electron atoms simpler than the spectrum of other atoms at low resolution, but more complex at high resolution. Precision measurements have revealed the fine and hyperfine structure of many lines of hydrogen and hydrogen-like atoms, and even of energy shifts resulting from the interaction of the atoms with the zero-point radiation field, so-called Lamb shifts (Lamb and Retherford 1947). Today, the energy level structure of the hydrogen atom are known with exquisite precision (see Figure 35, in which the level positions calculated without hyperfine structure from Mohr (2008) are given and the fine and hyperfine structures are taken from Brodsky and Parsons (1967); Essen *et al.* (1971); Fischer *et al.* (2004); Lundeen and Pipkin (1986); Kolachevsky *et al.* (2009); Mohr *et al.* (2008). The splitting of ≈ 0.0475 cm^{-1} of the 1s ^{2}S$_{1/2}$ ground state results from the hyperfine interaction. This splitting scales with n^{-3} and rapidly decreases with increasing n value, and also with increasing ℓ value. The spin-orbit splittings, which are zero for s levels, are largest for p levels and also scale as n^{-3}. The two components of the ^{2}P level with $J = 1/2$ and 3/2 are separated by ≈ 0.365 cm^{-1}. Dirac's relativistic treatment predicts two components for $n = 2$, a lower, doubly degenerate spin-orbit level with $J = 1/2$

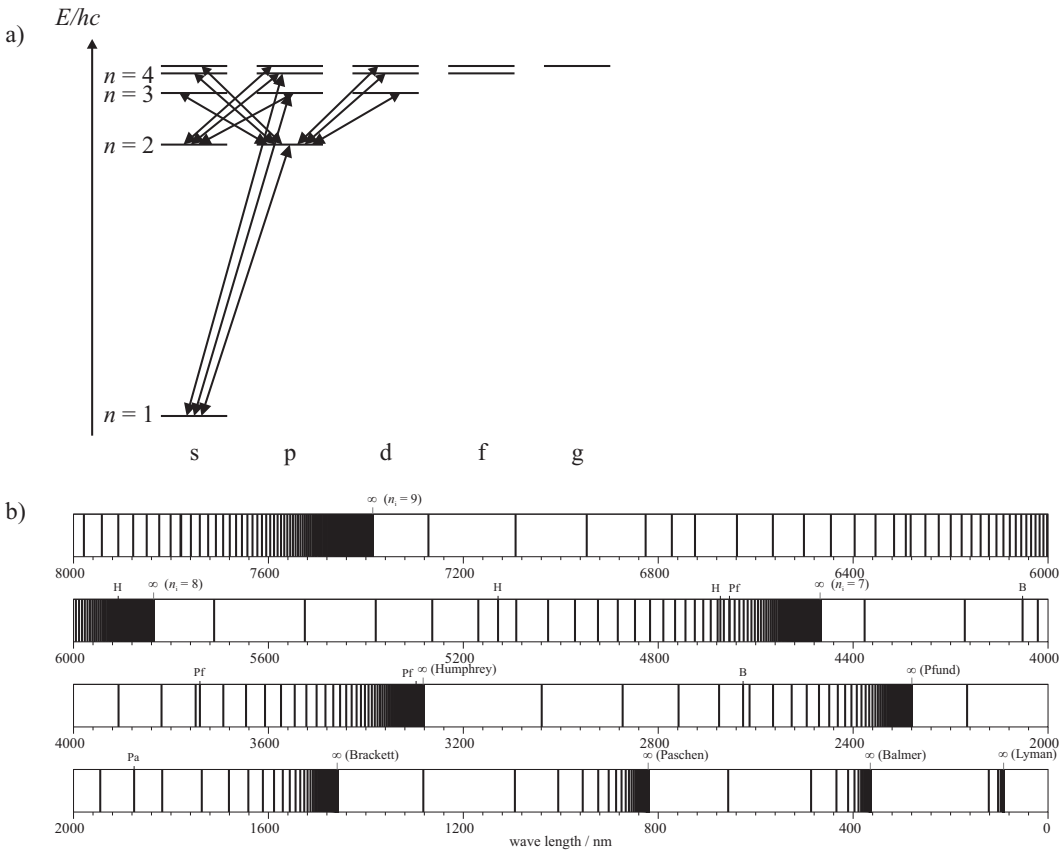

Figure 34: a) Energy level diagram of the H atom neglecting fine, hyperfine, and quantum electrodynamics effects. Possible single-photon transitions to and from the $n = 1$ and 2 levels are indicated by double-headed arrows. b) Schematic spectrum of H showing that the electronic spectrum extends from the microwave to the vacuum ultraviolet ranges of the electromagnetic spectrum.

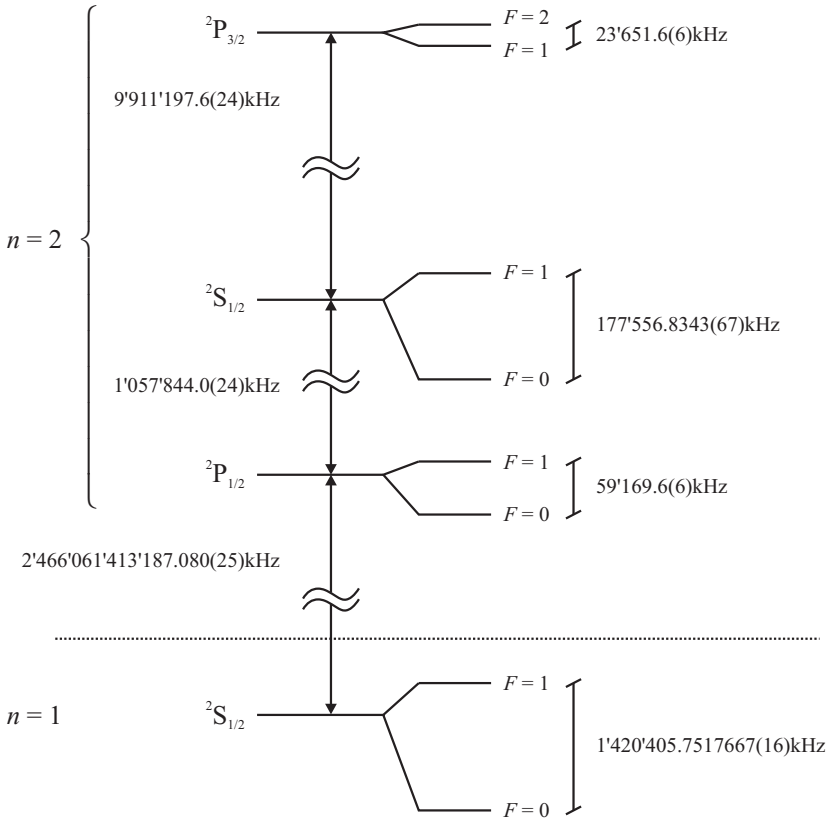

Figure 35: Fine and hyperfine structure of the (a) $n = 1$ and (b) $n = 2$ levels of the hydrogen atom. Numerical values were taken from Mohr (2008) for the positions without hyperfine structure and from Refs. Brodsky and Parsons (1967); Essen *et al.* (1971); Fischer *et al.* (2004); Lundeen and Pipkin (1986); Kolachevsky *et al.* (2009); Mohr *et al.* (2008) for other intervals.

and an upper, nondegenerate level with $J = 3/2$. The interaction with the zero-point radiation field removes the degeneracy of the lower component and induces a splitting of ≈ 0.0354 cm^{-1}.

High-resolution spectroscopy of hydrogen-like atoms such as H, He^+, Li^{2+}, Be^{3+} ... and their isotopes continues to stimulate methodological and instrumental progress in electronic spectroscopy. Measurements on "artificial" hydrogen-like atoms such as positronium (atom consisting of an electron and a positron), protonium (atom consisting of a proton and an antiproton), antihydrogen (atom consitsting of an antiproton and a positron), muonium (atom consisting of a positive muon μ^+ and an electron), antimuonium (atom consisting of a negative muon μ^- and a positron), etc., have the potential of providing new insights into fundamental physical laws and symmetries and their violations, such as those discussed in hrs076 (Quack 2010).

Alkali-metal atoms

A schematic energy level diagram showing the single-photon transitions that can be observed in the spectra of the alkali-metal atoms is presented in Figure 36. The ground-state configuration corresponds

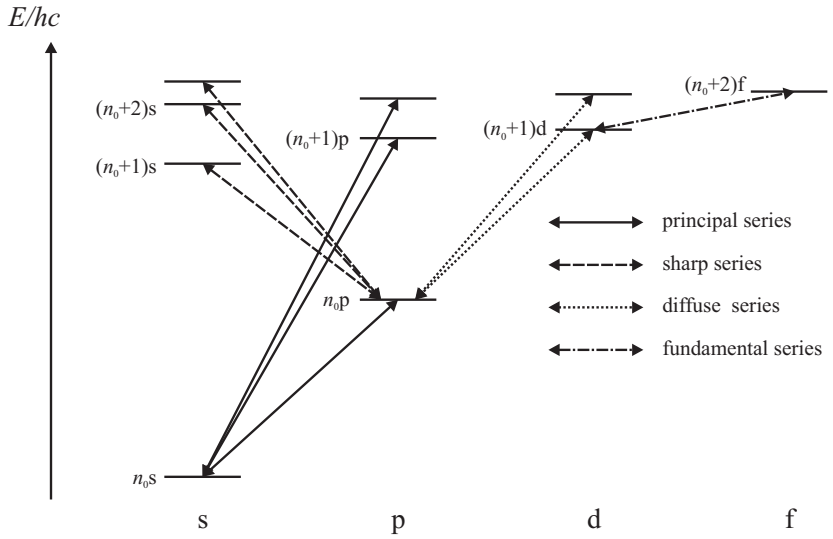

Figure 36: Schematic diagram showing the transitions that can be observed in the single-photon spectrum of the alkali-metal atoms.

to a closed-shell rare-gas-atom configuration with a single valence n_0s electron with $n_0 = 2, 3, 4, 5$ and 6 for Li, Na, K, Rb and Cs, respectively. The energetic positions of these levels can be determined accurately from Rydberg's formula (Equation (58)). The Laporte selection rule (Equation (182)) restricts the observable single-photon transitions to those drawn as double-headed arrows in Figure 36. Neglecting the fine and hyperfine structures, their wave numbers can be determined using Equation (186)

$$\tilde{\nu} = R_M/(n'' - \delta_{\ell''})^2 - R_M/(n' - \delta_{\ell'})^2. \tag{186}$$

The deviation from hydrogenic behavior is accounted for by the ℓ-dependent quantum defects. Transitions from (or to) the lowest energy levels can be grouped in Rydberg series, which have been called principal, sharp, diffuse and fundamental. Comparing Figure 36 with Figure 34, one can see that the principal series of the alkali metal atoms (called principal because it is observed in absorption and emission) corresponds to the Lyman lines of H, the diffuse and sharp series to the Balmer lines, and the fundamental series to the Paschen lines.

The quantum defects are only very weakly dependent on the energy. Neglecting this dependence, the quantum defects of the sodium atom are $\delta_\mathrm{s} \approx 1.35$, $\delta_\mathrm{p} \approx 0.86$, $\delta_\mathrm{d} \approx 0.014$, and $\delta_\mathrm{f} \approx 0$, so that the lowest-frequency line of the principal series (called the sodium D line because it is a doublet, see below) lies in the yellow range of the electromagnetic spectrum, and not in the VUV as Lyman α. The fact that the $n_0\mathrm{p} \leftarrow n_0\mathrm{s}$ lines of the alkali metal atoms lie in the visible range of the electromagnetic spectrum makes them readily accessible with commercial laser sources, and therefore extensively studied and exploited in atomic-physics experiments.

Most transitions of the alkali-metal atoms reveal fine and hyperfine structures. As in the case of H, the hyperfine-structure splittings are largest in the ground state (3s $^2\mathrm{S}_{1/2}$ in the case of Na)

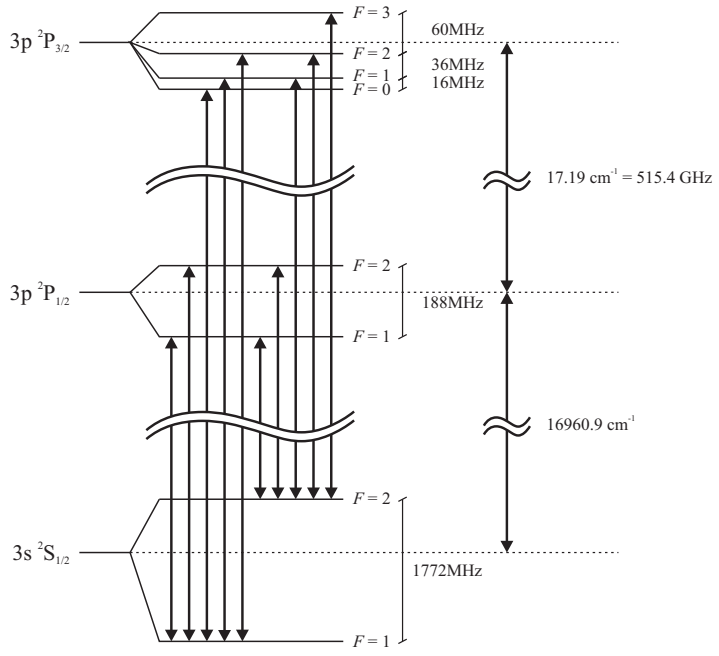

Figure 37: Schematic diagram showing the fine and hyperfine structure of the 3s and 3p levels involved in the lowest-frequency line of the principal series of ^{23}Na.

and the fine-structure splittings are largest in the lowest-lying p level (3p $^2\mathrm{P}_J$ with $J = 1/2, 3/2$ in the case of Na). The details of the structure of these two levels of Na are presented in Figure 37. At low resolution, the 3p←3s line appears as a doublet with two components at 16960.9 cm^{-1} and 16978.1 cm^{-1}, separated by an interval of 17.2 cm^{-1} corresponding to the spin-orbit splitting of the 3p state. The second largest splitting (≈ 0.06 cm^{-1}) in the spectrum arises from the hyperfine splitting of 1772 MHz of the 3s state. Finally, splittings of less than 200 MHz result from the hyperfine structure of the 3p levels.

The level structures depicted in Figure 37 are characteristic of the n_0p← n_0s transitions of all alkali-metal atoms, which are nowadays widely used in the production of cold and ultracold atoms by laser cooling. Laser-cooling experiments exploit so-called closed transitions, and achieve a reduction of velocity of the sample in the direction opposite to the laser propagation direction as a result of a large number of subsequent absorption-emission cycles. If a narrow-band laser is tuned to the low-frequency side of a spectral line, only atoms with a positive Doppler shift, i.e., atoms moving towards the laser light source can absorb radiation. By doing so, they also acquire a momentum $\hbar k$ ($k = 2\pi/\lambda$) in the direction opposite to their motion, which reduces their velocity. Spontaneous re-emission of the absorbed photons occurs with an isotropic probability distribution so that, on average, the momentum of the atoms is reduced by $\hbar k$ per absorption-emission cycle. Several thousand cycles are required to stop a sodium atom initially leaving an oven in an effusive beam.

The efficiency of the cooling process is reduced if the optical cycle is not closed, i.e., if spontaneous emission can populate other hyperfine levels of the ground state. Inspection of Figure 37 leads to the

conclusion that only two of the 10 possible hyperfine components of the 3p $^2\mathrm{P}_J \leftarrow$ 3s $^2\mathrm{S}_{1/2}$ transition correspond to closed transitions, the $F' = 3 \leftarrow F'' = 2$ and the $F' = 0 \leftarrow F'' = 1$ components. Near-resonant excitation of the $F' = 1$ and 2 hyperfine components, however, occasionally lead to emission to the $F'' = 1$ and $F'' = 2$ levels, which lie too far from the $F' = 3 \leftarrow F'' = 2$ and the $F' = 0 \leftarrow F'' = 1$ transitions, respectively, for further efficient absorption, so that the optical cycling is terminated. This problem is usually overcome by repumping the $F'' = 1$ or the $F'' = 2$ level with other lasers. The efficiency of the laser cooling process can also be increased by using circularly polarized radiation, exploiting the selection rules (164) and (165).

These considerations illustrate the importance of high-resolution spectroscopic measurements of electronic transitions in atoms, and the understanding of their structures, without which important applications would never have been developed. Indeed, to fully exploit the potential of laser cooling, a very detailed knowledge of the fine and hyperfine structure of electronic transitions is mandatory. If one desires to load the cold atoms in traps, it is also necessary to study the effects of electric and magnetic fields on the hyperfine structure levels. For further details on laser cooling, the reader is referred to the article by Metcalf and van der Straten (2003).

Rare gas atoms

The $^1\mathrm{S}_0$ ground state of the rare-gas atoms (Rg=Ne, Ar, Kr and Xe) results from the full-shell configurations $([\ldots](n_0\mathrm{p})^6$ with $n_0 = 2, 3, 4$ and 5 for Ne, Ar, Kr, and Xe, respectively. Single-photon absorption by electrons in the $(n_0\mathrm{p})^6$ orbitals leads to the excitation of $J = 1$ states of the configurations $[\ldots](n_0\mathrm{p})^5(n\mathrm{s})^1$ and $[\ldots](n_0\mathrm{p})^5(n\mathrm{d})^1$.

Compared to H and the alkali-metal atoms discussed in the previous examples, the lowest excited electronic configurations contain two, instead of only one, unpaired electrons, which leads to both $S = 0$ and $S = 1$ states. Moreover, these states form Rydberg series that converge on two closely spaced ionization limits corresponding to the two spin-orbit components ($J^+ = 1/2, 3/2$) of the $^2\mathrm{P}_{J^+}$ ground state of Rg^+, rather than on a single ionization limit, as is the case for H and the alkali-metal atoms. This situation, which is encountered in most atoms, results in spectrally more dense spectra with pronounced perturbations. Figure 38 depicts schematically the $J = 1$ Rydberg series of the rare-gas atoms located below the $^2\mathrm{P}_{J^+}$ ($J^+ = 1/2, 3/2$) ionization thresholds that are optically accessible from the $^1\mathrm{S}_0$ ground state.

Two angular momentum coupling schemes are used to label these Rydberg states. The first one corresponds to the familiar LS-coupling scheme discussed in Section 2.1.4 and tends to be realized, if at all, only for the lowest Rydberg states and the lightest atoms. Five series are optically accessible, two s series ($(n_0\mathrm{p})^5(ns)^1$ $^3\mathrm{P}_1$ and $^1\mathrm{P}_1$) and three d series ($(n_0\mathrm{p})^5(nd)^1$ $^3\mathrm{D}_1$, $^3\mathrm{P}_1$ and $^1\mathrm{P}_1$). The second one is a variant of the jj coupling scheme, and becomes an increasingly exact representation at high n values, when the spin-orbit coupling in the $^2\mathrm{P}_{J^+}$ ion core becomes stronger than the electrostatic (including exchange) interaction between the Rydberg and the core electrons. As a result, the core

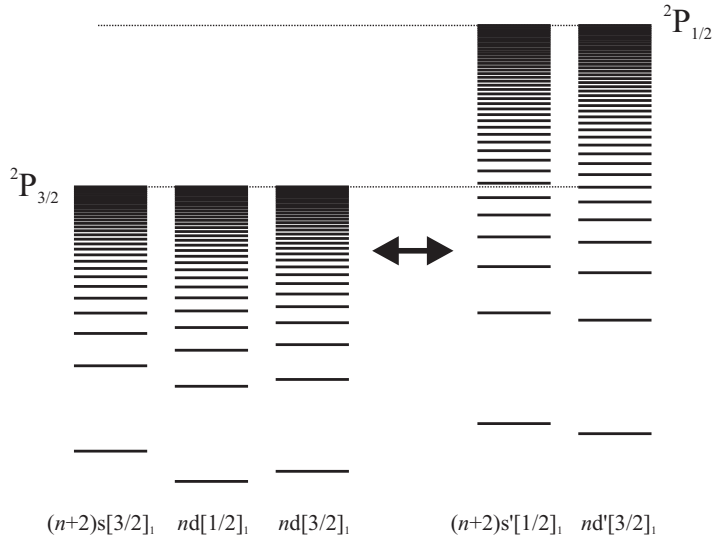

Figure 38: Schematic diagram showing Rydberg series converging to the two spin-orbit components $^2\mathrm{P}_J$ ($J = 1/2, 3/2$) of the rare gas atomic ions Rg^+. The series are designated in Racah notation as $n\ell'[k]_J$, the $'$-sign designating series converging on the upper ($^2\mathrm{P}_{1/2}$) ionization threshold. Interaction between series are represented by horizontal arrows.

and Rydberg electrons are decoupled, and J^+ becomes a good quantum number instead of S. In this labeling scheme, the states are designated $(^2\mathrm{P}_{J^+})n\ell[k]_J$, k being the quantum number resulting from the addition of $\vec{J^+}$ and $\vec{\ell}$. The five optically accessible $J = 1$ series are labeled $n\mathrm{s}[3/2]_1$, $n\mathrm{s}'[1/2]_1$, $n\mathrm{d}[1/2]_1$, $n\mathrm{d}[3/2]_1$, $n\mathrm{d}'[3/2]_1$, the "prime" being used to designate the two series converging to the $^2\mathrm{P}_{1/2}$ ionization limit (see Figure 38).

The interactions between the series converging to the different ionization limits lead to pronounced perturbations below the $^2\mathrm{P}_{3/2}$ ionization limit and to the autoionization of the $n\mathrm{s}'$ and $n\mathrm{d}'$ series in the energetic region between the $^2\mathrm{P}_{3/2}$ and $^2\mathrm{P}_{1/2}$ ionization limits. Because of the series interactions, the spectral positions are not accurately described by Rydberg's formula, but are best described by multichannel quantum defect theory (Lee and Lu 1973; see also Jungen (2010a) in this handbook).

Several sections of the single-photon VUV spectrum of Ar are presented in Figure 39. Figure 39a) corresponds to the region where Rydberg states of principal quantum number $n \geq 33$ below the $^2\mathrm{P}_{3/2}$ ionization limit can be excited from the ground state. In the region below 127060 cm^{-1}, only the $n\mathrm{d}[3/2]_1$ and $n\mathrm{s}[3/2]_1$ carry intensity. These two series are almost degenerate. The splittings can hardly be seen on the wave-number scale used to draw the spectrum, but are clearly visible on the expanded scale of the spectrum labeled B, which corresponds to the region of principal quantum number around $n = 55$. The high-n region of the spectrum is also displayed on an enlarged scale in the spectrum labeled C. The $n\mathrm{d}[1/2]_1$ series is extremely weak at n values below 50, but becomes the dominant series beyond $n = 80$. In an unperturbed Rydberg series, the intensity should decrease as n^{-3}, as explained in Subsection 2.1.6. The anomalous intensity distribution of the $n\mathrm{d}[1/2]_1$ series has

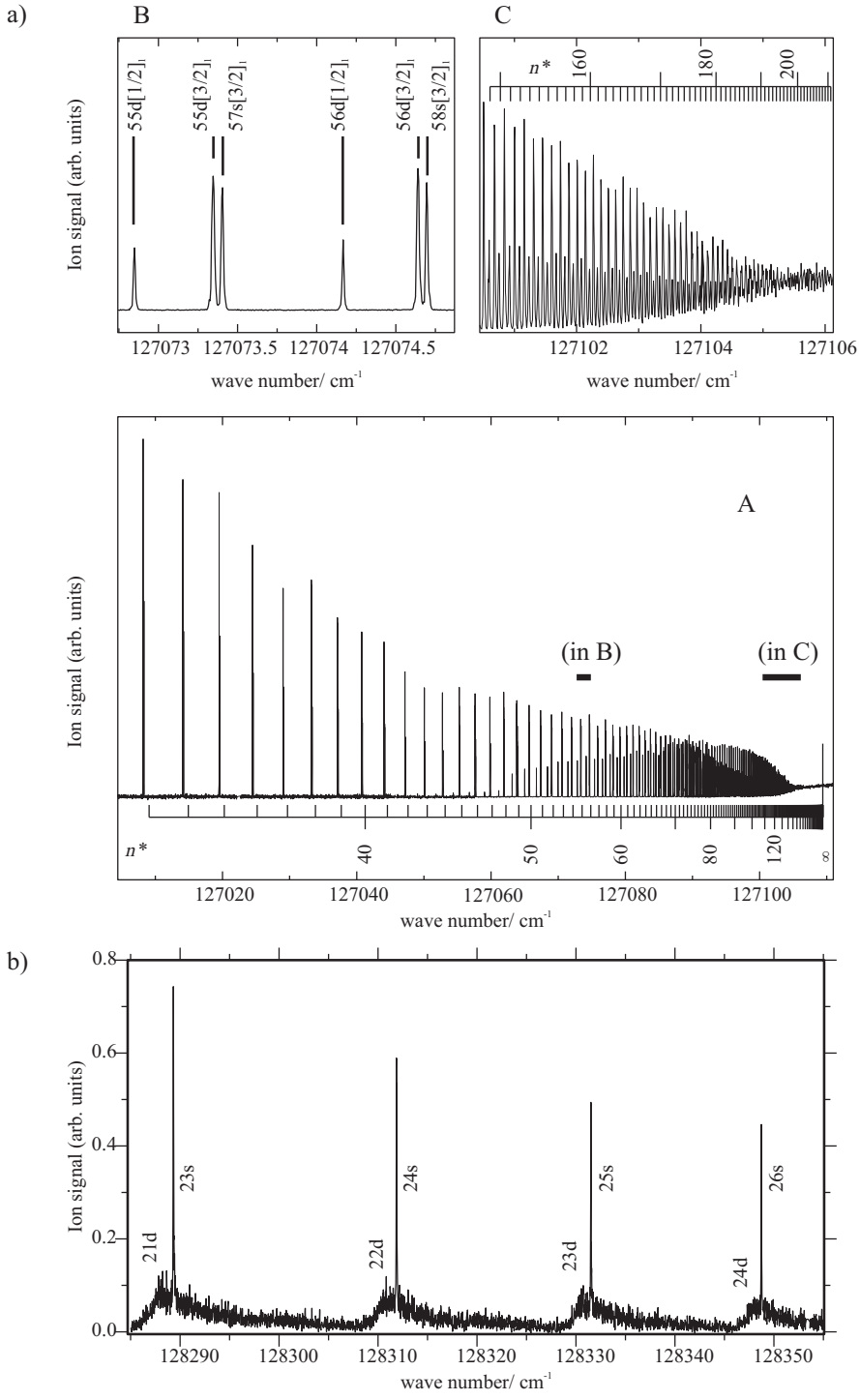

Figure 39: High-resolution VUV laser spectra of Ar recorded with a narrow-band laser. a) Region below the $^2P_{3/2}$ ionization threshold showing the perturbed ns/d$[k]_{J=1}$ series. The spectra shown labeled B and C represent sections of the spectrum labeled A presented on an enlarged scale. b) Region above the $^2P_{3/2}$ revealing the broad asymmetric nd$'[3/2]_1$, and the narrow, symmetric ns$'[1/2]_1$ resonances (adapted from Hollenstein (2003)).

its origin in the interactions with the series converging to the $^2P_{1/2}$ ion core, which are such that, in some spectral regions, it has almost pure $S = 1$ character and cannot be excited from the $S = 0$ ground state. Figure 39b displays a section of the VUV spectrum of Ar in the region between the $^2P_{3/2}$ and $^2P_{1/2}$ ionization limits. The $ns'[1/2]_1$ and $nd'[3/2]_1$ series appear as sharp, symmetric, and broad, asymmetric autoionization resonances in this region, respectively.

The VUV absorption spectra of Ne, Kr and Xe are qualitatively similar to that of Ar. Ne, Kr and Xe all have several isotopes, some of which have a nonzero nuclear spin and a hyperfine structure. The hyperfine structures in the VUV absorption spectrum of ^{83}Kr, ^{129}Xe, and ^{131}Xe appear complex at first sight but can be quantitatively described by MQDT using the same series-interaction parameters as the $I = 0$ isotopes (Wörner *et al.* 2003, 2005; Schäfer and Merkt 2006; Paul *et al.* 2009; Schäfer *et al.* 2010; see also discussion of spin-orbit and hyperfine autoionization in Subsection 3.5.1).

The fact that several low-lying levels of the rare-gas atoms have almost pure $S = 1$ character results in the metastability of these levels. The radiative decay of the lowest electronically excited $S = 1$ state with $J = 0$ and 2 to the $S = 0$ ground state is strongly forbidden by single-photon electric-dipole selection rules. Consequently, these states are very long-lived, so that, for many purposes, they can be used in experiments as if they were stable ground state atoms: their long lifetimes enable precision measurements, they give access to spectroscopic investigation of other $S = 1$ states, they can be laser cooled using closed transitions in the triplet manifold of states, they can be used in reactive scattering experiments, etc.

3.2.3 Stark and Zeeman effects in atomic spectra

When considering the effects of static electric and magnetic fields on electronic transitions, it is convenient to discuss the effects of these fields on the selection rules and on the spectral positions separately. The effects of magnetic and electric fields on the energy level structure of atoms have been described in Subsections 2.1.7 and 2.1.8, respectively. We therefore focus here on the selection rules and their manifestations in electronic spectra of atoms.

In the presence of a homogeneous electric (or magnetic) field, the symmetry of space is reduced from spherical (isotropic) to cylindrical. Consequently, the total angular momentum quantum number J (or F) ceases to be a good quantum number, the only good quantum number being the magnetic quantum number M_J (or M_F) associated with the projection of $\vec{J}$ ($\vec{F}$) along the direction of the field vector. The Z axis of the laboratory-fixed reference frame is commonly chosen to lie parallel to the static field vector, i.e., $\vec{E} = (0, 0, E)$ and $\vec{B} = (0, 0, B)$.

The electric-dipole selection rules depend on the relative orientation of the polarization vector of the radiation field and the static field vector. If the radiation is linearly polarized with polarization vector perpendicular to the static field vector, then

$$\Delta M_J = \pm 1 \quad (\text{or } \Delta M_F = \pm 1), \tag{187}$$

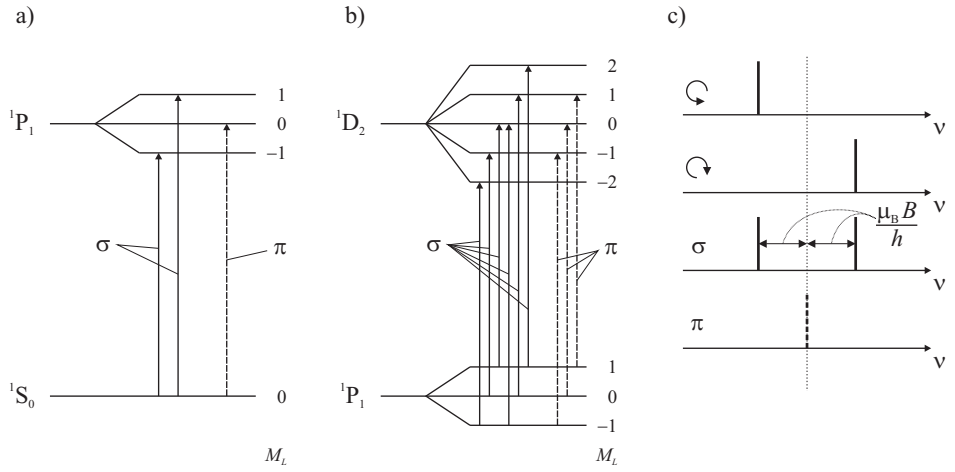

Figure 40: The normal Zeeman effect in the electronic spectrum of atoms. a) $^1S_0 \leftrightarrow ^1 P_1$ transition, b) $^1P_1 \leftrightarrow ^1 D_2$ transition, c) schematic representation of the spectra.

in which case one speaks of a σ configuration, from the German word "senkrecht" (= perpendicular), replacing the first letter by its Greek equivalent, s $\rightarrow \sigma$. If the radiation is linearly polarized with polarization vector parallel to the static field vector, then

$$\Delta M_J = \pm 0 \quad (\text{or } \Delta M_F = \pm 0), \tag{188}$$

and the configuration is referred to as π (from the German word "parallel", p $\rightarrow \pi$). The use of circularly polarized radiation leads to the most restrictive selection rule on M_J (M_F) if the radiation propagates in a direction parallel to the static field vector, in which case one has either

$$\Delta M_J = 1 \quad (\Delta M_F = 1), \tag{189}$$

or

$$\Delta M_J = -1 \quad (\Delta M_F = -1), \tag{190}$$

depending on the helicity.

Magnetic fields and Zeeman effect

Because the electron-Zeeman effect is much larger than the nuclear Zeeman effect, we consider here only the influence of the former on electronic transitions of atoms. If the states connected by the transitions are singlet states ($S = 0$), the Zeeman effect arises solely from the orbital motion and particularly simple spectral structures result (see Figure 8, and Equations (60) and (61) describing the normal Zeeman effect). Equation (61) implies that, in this case, the frequency intervals between neighboring Zeeman levels are the same ($\mu_B B/h$) in the lower and upper electronic states. The transitions allowed by the selection rules (187)-(190) are indicated in Figure 40a and b for $^1S_0 \leftrightarrow ^1 P_1$ and $^1P_1 \leftrightarrow ^1 D_2$ transitions, respectively, from which one sees that only three lines can be observed, two in σ and one in π polarization configuration, separated by a frequency interval of $\mu_B B/h$. The

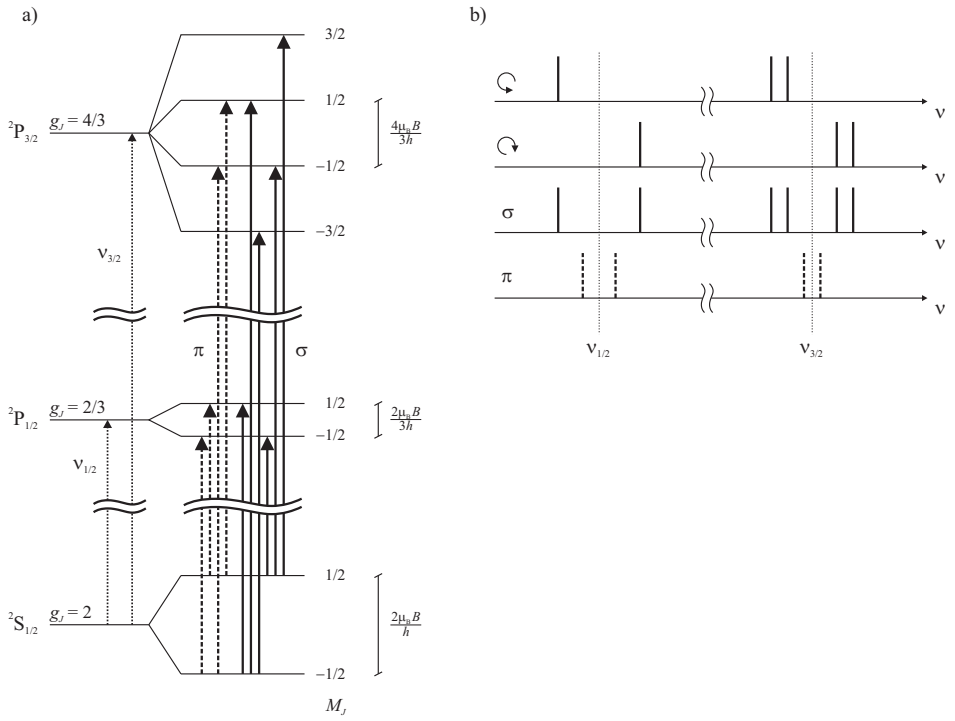

Figure 41: The anomalous Zeeman effect in a $^2S_{1/2} \leftrightarrow ^2 P_J$ ($J = 1/2, 3/2$) transition. a) energy level diagram in which the allowed transition for π and σ polarization configurations are indicted. b) Schematic representation of the spectra.

schematic spectra displayed in Figure 40c illustrate the fact that the appearance of the spectra is entirely determined by the polarization configuration and does not depend on the L value of the states involved in the transition.

The situation is more complicated in $S \geq 1/2$ states because, in this case, the Zeeman effect is anomalous and the Zeeman level shifts are given by Equation (63) and depend on the values of L, S, and J via the dependence of g_J on these quantum numbers (see Equation (52)). For example, Figure 41 illustrates the case of a $^2S_{1/2} \leftrightarrow ^2 P_J$ ($J = 1/2, 3/2$) transition, for which, according to the selection rules (187)-(190), 10 lines can be observed with the different polarization arrangements. Because the Zeeman splittings now depend on the values of L, S, and J, the spectral patterns are characteristic of the terms involved in the electronic transitions, which can be used to assign them.

Electric fields and Stark effect

To illustrate the effect of electric fields on atomic spectra, we first discuss the Stark effect in the Lyman α transition of H. The Stark effect leads to a coupling of the closely spaced $n = 2$ s and p states which are split at zero field by the Lamb shift and the spin-orbit interaction (see Figure 35). Figures 42a and b depict the calculated electric-field dependence of the $n = 2$ energy levels, and VUV spectra of the Lyman α line of H recorded in a field of 5465 V/cm, respectively, as reported by Rottke

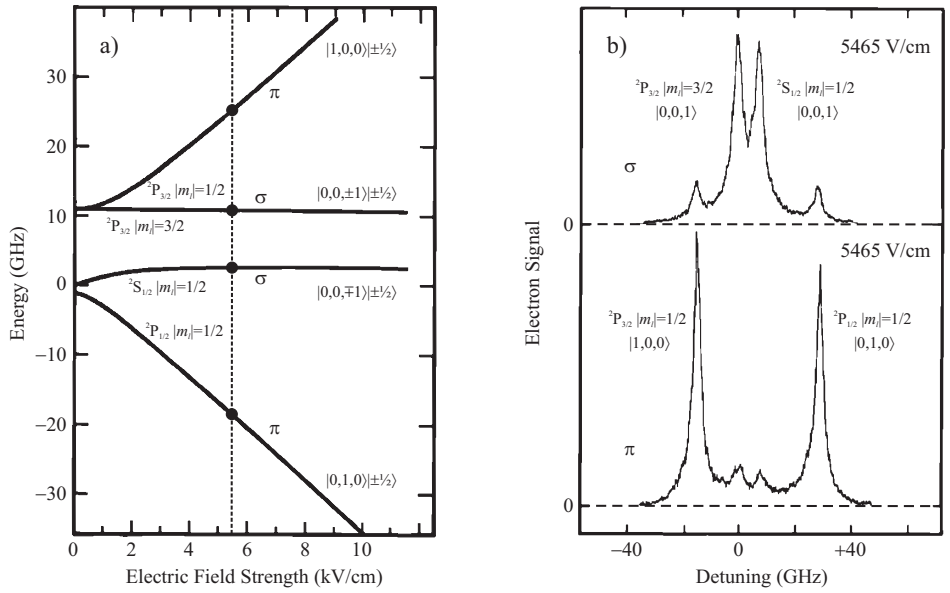

Figure 42: a) Stark effect in the $n = 2$ levels of H. At low electric fields, the levels are labeled with the usual term symbols. At high fields, the levels are labeled using the parabolic quantum numbers n_1, n_2, and m_ℓ defined in Section 2.1.8 as $|n_1, n_2, |m_\ell|\rangle|m_S\rangle$. The vertical dashed line indicates the field used for the measurements presented in panel b), and σ and π designate the levels that can be excited from the 1 $^2S_{1/2}$ level using σ and π polarization configurations, respectively. b) Experimental spectra of the Lyman α line of atomic hydrogen recorded in σ (top spectrum) and π (bottom spectrum) polarization configurations. Each line is labeled by the parabolic quantum numbers $|n_1, n_2, |m_\ell|\rangle$ and by the dominant contribution to the wave function of the $n = 2$ level. The hyperfine structure is not resolved in the experiment (Adapted from Rottke and Welge (1986)).

and Welge (1986).

Because of the near degeneracy of these levels, the Stark effect rapidly becomes linear with increasing electric field, but a fine structure remains noticeable. In the absence of fine-structure splittings,, the Stark level structure would consist of three levels (see Figure 11): Two outer components with $m_\ell = 0$ corresponding to the $|n_1, n_2, |m_\ell|\rangle = |1, 0, 0\rangle$ and $|0, 1, 0\rangle$ Stark states, i.e., to values of k of ± 1, and one central component corresponding to the $|0, 0, 1\rangle$ Stark state. With the selection rules for σ ($\Delta m_\ell = \pm 1$) and π ($\Delta m_\ell = \pm 0$) polarization configurations, one would expect to see either the central $|0, 0, 1\rangle$ component (σ configuration) or the $|1, 0, 0\rangle$ and $|0, 1, 0\rangle$ components (π configuration). This expectation corresponds to the experimental observations, which, however, also reveal fine-structure effects and weak lines corresponding to the "forbidden" Stark components. These components are observed because m_j, rather than m_ℓ, is the good quantum number when spin-orbit coupling is considered, and also because the polarization of the VUV laser radiation was not perfectly linear, as discussed by Rottke and Welge (1986).

In Rydberg states of atoms and molecules, the Stark effect leads to very characteristic spectral

structures. Figure 43 presents π-polarized VUV laser spectra of transitions from the $^1S_0$ ground state of Ar to Stark states belonging to the $n = 22\,(M_J = 0)$ manifold of states located below the $^2P_{3/2}$ ground state of Ar^+ (Vliegen *et al.* 2004). The spectra recorded at different fields have been shifted along the vertical axis, so that the origins of their intensity scale coincide with the values of the electric field (in V/cm) used to record them. At low fields (bottom spectra), the optically allowed $J = 1$ series converging to the $^2P_{3/2}$ ground state of Ar^+ ($23d[1/2]_1$, $24s[3/2]_1$ and $23d[3/2]_1$) are observed. As the field increases, transitions to the 24 and 25 $p[1/2]_0$ levels gain intensity by Stark mixing with the d levels following the Stark-mixing selection rule $\Delta\ell = \pm 1$ (see Equation (67)). Stark mixing also takes place with the f levels which are almost degenerate with the $\ell \geq 4$ levels and form with them a manifold of states subject to a linear Stark effect. This high-ℓ manifold of Stark states becomes the dominant spectral pattern at high fields.

Series of spectra such as those presented in Figure 43 are referred to as Stark maps and have been recorded for many atoms (e.g., alkali metal atoms (Zimmerman *et al.* 1979), rare gas atoms (Ernst *et al.* 1988; Brevet *et al.* 1990; Grütter *et al.* 2008)) and even molecules (e.g. H_2, (Fielding and Softley 1991; Hogan *et al.* 2009)). The strong field dependence of the outer members of the linear Stark manifolds is indicative of very large electric dipole moments, which have been recently exploited to decelerate beams of Rydberg atoms and molecules (Procter *et al.* 2003; Vliegen *et al.* 2004) and to load cold Rydberg atom and molecule samples in electric traps (Vliegen *et al.* 2007; Hogan *et al.* 2009). High-resolution electronic spectroscopy of Rydberg Stark states in cold, high-density samples has also been used to study dipole-dipole interactions between neighboring Rydberg atoms (Mourachko *et al.* 1998).

3.3 Electronic spectra of diatomic molecules

This section describes elementary aspects of the electronic spectra of diatomic molecules, with emphasis on selection rules and the overall structure of electronic transitions.

3.3.1 Selection rules

The set of selection rules presented in Equations (161)-(166) can be extended by considering those that can be derived using the point groups $D_{\infty h}$ for homonuclear diatomic molecules, and $C_{\infty v}$ for heteronuclear diatomic molecules. In diatomic molecules, the vibronic symmetry $\Gamma_{ev} = \Gamma_{elec} \otimes \Gamma_{vib}$ is always equal to the electronic symmetry Γ_{elec} because the only vibrational mode is totally symmetric

$$\Gamma_{vib} = \Sigma_g^+ \quad \text{for } D_{\infty h} \tag{191}$$

and

$$\Gamma_{vib} = \Sigma^+ \quad \text{for } C_{\infty v}. \tag{192}$$

Electronically forbidden transitions are therefore necessarily also vibronically forbidden (see Equations (174) and (179)).

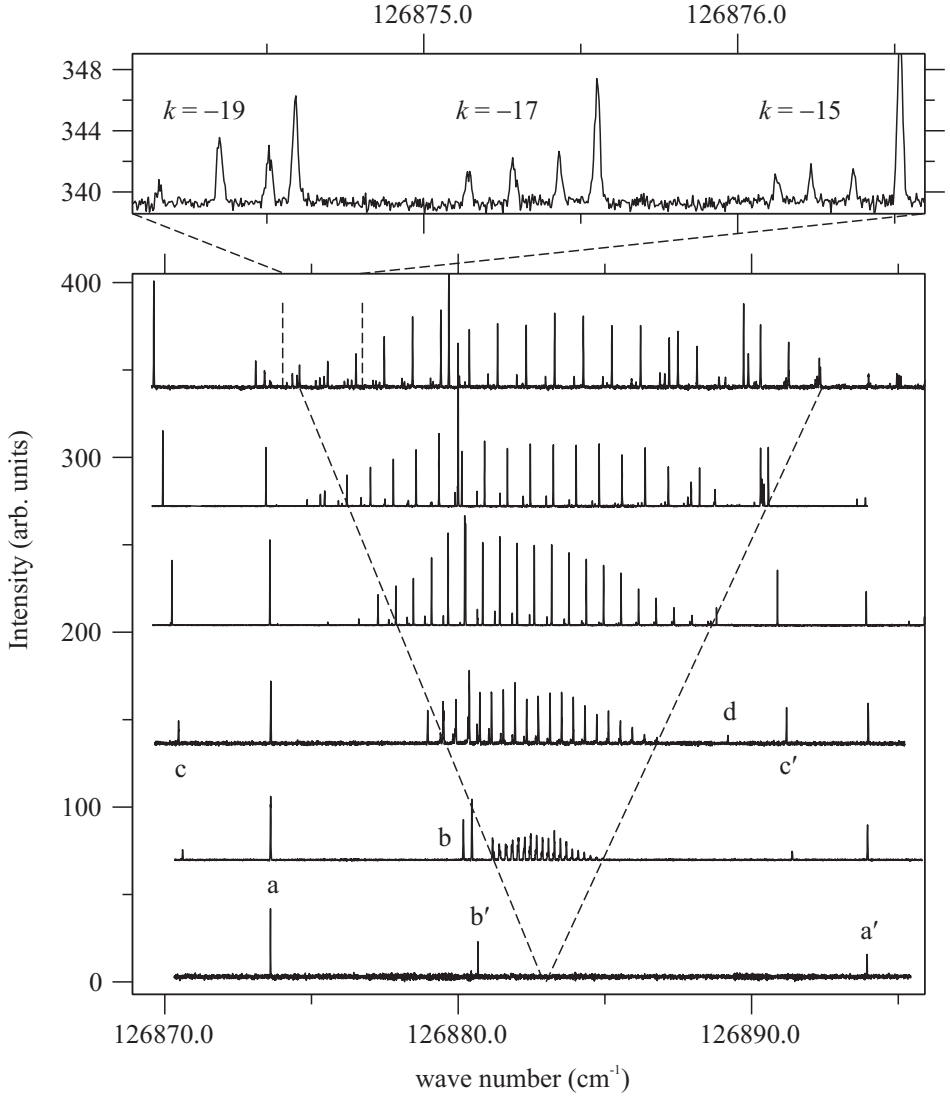

Figure 43: Stark effect in the $n = 22$, $M_J = 0$ levels of Ar located below the $^2P_{3/2}$ ground state of Ar^+. The spectra recorded at different fields have been shifted along the vertical axis so that the origins of their intensity scale coincide with the values of the electric field (in V/cm) used to record them, from bottom to top 0 V/cm, 70 V/cm, 136 V/cm, 204 V/cm, 272 V/cm, and 340 V/cm. The linear high-ℓ Stark manifold is situated between the dotted lines. The states labeled a,a',b,b',c,c' and d correspond to the $22d[1/2]_1$, $23d[1/2]_1$, $22d[3/2]_1$, $24s[3/2]_1$, $23p[1/2]_0$, $24p[1/2]_0$ and $24p[1/2]_2$ states, respectively. The top panel shows the fine structure of three Stark states with $k = -19, -17$ and -15, where k represents the difference $n_1 - n_2$ (Adapted from Vliegen *et al.* (2004)).

Electronically allowed transitions fulfill either

$$\Gamma'_{\text{elec}} \otimes \Gamma(T_z) \otimes \Gamma''_{\text{elec}} \supseteq \Sigma^+_{(\text{g})} \tag{193}$$

or

$$\Gamma'_{\text{elec}} \otimes \Gamma(T_{x,y}) \otimes \Gamma''_{\text{elec}} \supseteq \Sigma^+_{(\text{g})}, \tag{194}$$

where the (g) subscripts only applies to homonuclear diatomic molecules. Because T_x and T_y transform as the Π_u irreducible representation of the $D_{\infty\text{h}}$ point group (or as the Π representation of the $C_{\infty\text{v}}$ group), and T_z transforms as Σ^+_g (or Σ^+), Equations (193) and (194) can be written as

$$\Gamma'_{\text{elec}} \otimes \Gamma''_{\text{elec}} \supseteq \Sigma^+_{(\text{u})}, \tag{195}$$

in which case the transition moment lies parallel to the internuclear (z) axis and one speaks of a parallel transition, and

$$\Gamma'_{\text{elec}} \otimes \Gamma''_{\text{elec}} \supseteq \Pi_{(\text{u})}, \tag{196}$$

respectively, in which case the transition moment lies perpendicular to the internuclear (i.e., along the x or y) axis and one speaks of a perpendicular transition. Evaluating Equations (195) and (196) using the direct-product table (Table 9) leads to the selection rules

$$\Delta\Lambda = 0, \quad (\text{u} \leftrightarrow \text{g}) \tag{197}$$

for parallel transitions and

$$\Delta\Lambda = \pm 1, \quad (\text{u} \leftrightarrow \text{g}) \tag{198}$$

for perpendicular transitions.

Examples: In $D_{\infty\text{h}}$ molecules, $\Sigma^+_\text{g} \leftrightarrow \Sigma^+_\text{u}$, $\Pi_\text{g} \leftrightarrow \Pi_\text{u}$,... transitions are allowed parallel transitions, and $\Sigma^+_\text{g} \leftrightarrow \Pi_\text{u}$, $\Sigma^+_\text{u} \leftrightarrow \Pi_\text{g}$, $\Pi_\text{g} \leftrightarrow \Delta_\text{u}$, $\Pi_\text{u} \leftrightarrow \Delta_\text{g}$, ... are allowed perpendicular transitions.

Additional selection rules are given by Equations (158) and (159). As stated above, the ΔM_J selection rule depends on the polarization of the radiation field. When the electronic states involved in the transition are not well described by Hund's angular momentum coupling cases (a) or (b), but rather by Hund's case (c), the $\Delta S = 0$ selection rule no longer applies, and Λ must be replaced by Ω in Equations (197) and (198), i.e.,

$$\Delta\Omega = 0, \quad (\text{u} \leftrightarrow \text{g}) \tag{199}$$

for parallel transitions and

$$\Delta\Omega = \pm 1, \quad (\text{u} \leftrightarrow \text{g}) \tag{200}$$

for perpendicular transitions (see also below).

3.3.2 Forbidden electronic transitions

Electronically (and vibronically) forbidden single-photon transitions in diatomic molecules may nevertheless be observable experimentally. Such transitions can be classified in two categories.

1. **Magnetic dipole and electric quadrupole transitions**

   Absorption results from the interaction of the electromagnetic radiation field with the magnetic dipole or the electric quadrupole moment of the molecule. Since the (x, y, z) components of the magnetic dipole moment transform as the rotations R_x, R_y and R_z and the components of the quadrupole moment transform as $\Gamma(\alpha_{ij})$ (see Tables 7 and 8), the corresponding selection rules can be derived as in the case of an electric-dipole transition. The selection rule for magnetic-dipole transitions is thus

   $$\Gamma_\mathrm{i} \otimes \Gamma(R_\alpha) \otimes \Gamma_\mathrm{f} \supseteq {}^1\Sigma^+_\mathrm{(g)} \quad \text{with } \alpha = x, y, z \tag{201}$$

   and that for electric-quadrupole transitions is

   $$\Gamma_\mathrm{i} \otimes \Gamma(\alpha_{(ij)}) \otimes \Gamma_\mathrm{f} \supseteq {}^1\Sigma^+_\mathrm{(g)}. \tag{202}$$

   Example: ${}^1\Sigma^+_\mathrm{g} \leftrightarrow {}^1\Sigma^-_\mathrm{g}$ transitions are electric-dipole-forbidden, but magnetic-dipole-allowed transitions, because R_z transforms as Σ^-_g in $D_{\infty\mathrm{h}}$ molecules (see Table 8).

   ---

2. **Intercombination transitions**

   Intercombination transitions violate the $\Delta S = 0$ selection rule (Equation (158)). Such transitions mainly occur in molecules possessing a significant spin-orbit interaction. In this case, the Hund's angular momentum coupling cases (a) and (b) upon which the selection rules (197) and (198) rely, are no longer a perfect description, and neither Σ, nor Λ are good quantum numbers.

   When the spin-orbit interaction is dominant, a Hund's case (c) nomenclature is more appropriate and the selection rules (199) and (200) must be used instead of the selection rules (197) and (198). When the spin-orbit interaction is weak, so that Hund's case (a) or (b) representations remain good approximations, group theoretical arguments can still be used to predict which intercombination transitions are observable, but spin double groups are required for this task. Such groups are obtained from the corresponding point groups by including 2π rotations with negative character to take into account the fact that a half-integer spin function has a periodicity of 4π. The character table of the $\mathrm{C}^{(2)}_{\infty\mathrm{v}}$ spin double group is represented in Table 19, and Table 20 shows how the electron spin functions transform in the $\mathrm{D}^{(2)}_{\infty\mathrm{h}}$ and the $\mathrm{C}^{(2)}_{\infty\mathrm{v}}$ point groups. The symmetry Γ_es of the electronic wave functions (now including electron spin) can be determined from the product

   $$\Gamma_\mathrm{es} = \Gamma_\mathrm{elec} \otimes \Gamma_\mathrm{espin}, \tag{203}$$

Table 19: Character table of the extended $C^{(2)}_{\infty\mathrm{v}}$ point group. The character table of the extended $D^{(2)}_{\infty\mathrm{h}}$ point group can be obtained from the $D_{\infty\mathrm{h}}$ by making the corresponding changes.

$\mathrm{C}^{(2)}_{\infty\mathrm{v}}$	E	$2C^{\varphi}_{\infty}$	$2C^{2\varphi}_{\infty}$	$2C^{3\varphi}_{\infty}$	...	$\infty\sigma_v$	R	$2C^{\varphi}_{\infty}R$	...	
$\Sigma^+(=\mathrm{A}_1)$	1	1	1	1	...	1	1	1	...	z
$\Sigma^-(=\mathrm{A}_2)$	1	1	1	1	...	-1	1	1	...	R_z
$\Pi(=\mathrm{E}_1)$	2	$2\cos\varphi$	$2\cos(2\varphi)$	$2\cos(3\varphi)$	...	0	2	$2\cos\varphi$	...	$x, y; R_x, R_y$
$\Delta(=\mathrm{E}_2)$	2	$2\cos(2\varphi)$	$2\cos(4\varphi)$	$2\cos(6\varphi)$	...	0	2	$2\cos(2\varphi)$	...	
$\Phi(=\mathrm{E}_3)$	2	$2\cos(3\varphi)$	$2\cos(6\varphi)$	$2\cos(9\varphi)$	...	0	2	$2\cos(3\varphi)$	...	
...	...	...	...	...	...	...	...	...	...	
$\mathrm{E}_{1/2}$	2	$2\cos(\varphi/2)$	$2\cos\varphi$	$2\cos(3\varphi/2)$	...	0	-2	$-2\cos(\varphi/2)$	...	
$\mathrm{E}_{3/2}$	2	$2\cos(3\varphi/2)$	$2\cos(3\varphi)$	$2\cos(9\varphi/2)$	...	0	-2	$-2\cos(3\varphi/2)$	...	
$\mathrm{E}_{5/2}$	2	$2\cos(5\varphi/2)$	$2\cos(5\varphi)$	$2\cos(15\varphi/2)$	...	0	-2	$-2\cos(5\varphi/2)$	...	
...	...	...	...	...	...	...	...	...	...	

Table 20: Transformation properties of the electron spin functions in the extended point group $D^{(2)}_{\infty\mathrm{h}}$. The transformation properties in the extended point group $C^{(2)}_{\infty\mathrm{v}}$ can be obtained by disregarding the subscript g.

S	0	1/2	1	3/2	...
Γ_S	Σ^+_g	$\mathrm{E}_{1/2,\mathrm{g}}$	$\Sigma^-_\mathrm{g}+\Pi_\mathrm{g}$	$\mathrm{E}_{1/2,\mathrm{g}}+\mathrm{E}_{3/2,\mathrm{g}}$	...

which can be evaluated using the transformation properties of the electron-spin functions summarized in Table 20. An intercombination transition is only observable if Equation (204) is fulfilled instead of Equations (193) and (194)

$$\Gamma'_{\mathrm{es}} \otimes \Gamma(T_\alpha) \otimes \Gamma''_{\mathrm{es}} \supseteq^1 \Sigma^+_{(\mathrm{g})} \quad \text{with } \alpha = x, y, z. \tag{204}$$

Example: We consider the electronically forbidden $^1\Sigma^+_\mathrm{g} \rightarrow {}^3\Pi_\mathrm{u}$ transition with $\Delta S = 1$ (singlet-triplet transition). With the help of Tables 19, 20 and 9, one obtains $\Gamma''_{\mathrm{es}} = \Sigma^+_\mathrm{g}$ and $\Gamma'_{\mathrm{es}} = \Gamma'_{\mathrm{elec}} \otimes \Gamma'_{\mathrm{espin}} = \Pi_\mathrm{u} \otimes (\Sigma^-_\mathrm{g} + \Pi_\mathrm{g}) = \Pi_\mathrm{u} + \Sigma^+_\mathrm{u} + \Sigma^-_\mathrm{u} + \Delta_\mathrm{u}$. The transformation properties of $T_{x,y,z}$ in $D_{\infty\mathrm{h}}$ imply that only the Π_u and Σ^+_u components of the $^3\Pi_\mathrm{u}$ state can be accessed from an initial state of symmetry $^1\Sigma^+_\mathrm{g}$. Alternatively, one may choose to express the selection rules in Hund's coupling case (c) as $\Delta\Omega = 0, \pm 1$ which does not necessitate the specification of the total electron spin quantum number S.

3.3.3 Vibronic structure and the Franck-Condon principle

Equation (173) implies that the intensity $I_{\alpha',v',\alpha'',v''}$ of a transition between two vibronic states should be approximately proportional to the square of the overlap integral $\langle\Phi'_{\text{vib}}|\Phi''_{\text{vib}}\rangle$ of the vibrational wave functions

$$I_{\alpha',v',\alpha'',v''} \propto |\langle\Phi'_{\text{vib}}|\Phi''_{\text{vib}}\rangle|^2 = |\langle v'|v''\rangle|^2. \tag{205}$$

The square of the integral $\langle\Phi'_{\text{vib}}|\Phi''_{\text{vib}}\rangle$, which is called the Franck-Condon factor (see Subsection 3.1), thus indicates how the intensity of an electronically allowed transition between the electronic states α'' and α' is partitioned among the various vibrational bands.

Figure 44 shows two schematic illustrations of the Franck-Condon principle applied to the absorption spectrum of diatomic molecules in their ground state. In Figure 44a, the Born-Oppenheimer potential energy functions of the two electronic states are almost identical. In this case, vibrational wave functions of the same vibrational quantum number ($v' = v''$) are also almost identical in the two electronic states. The orthogonality of the vibrational wave functions implies the selection rule $\Delta v = 0$ and the electronic spectrum consists of a single dominant vibrational band corresponding to the $v' = 0 \leftarrow v'' = 0$ band (labeled 0-0 in the spectrum drawn at the bottom of the figure).

In Figure 44b, the potential energy functions of the two states differ from each other. The equilibrium internuclear separation R'_{e} of the upper potential function is larger than that of the lower state. Consequently, transitions originating from the $v'' = 0$ level of the lower electronic state can access several vibrational levels of the upper state. The Franck-Condon factors are therefore nonzero in the energetic region where the repulsive part of the upper potential energy function lies vertically above the region where the ground state vibrational function has a nonzero amplitude. The expected vibrational structure of the corresponding band is represented schematically below the potential energy diagram and extends beyond the dissociation limit of the upper electronic state where the spectrum becomes continuous. The shaded areas in Figure 44 represent the regions where the vibrational wave function of the initial state has a significant amplitude. They help to see which vibrational levels of the final state are accessible from the ground state.

Franck-Condon factors represent an approximation of the relative intensities which relies on the assumption that the electronic transition moment does not vary with internuclear separation, at least not over the range where the relevant vibrational functions have a significant amplitudes. Given that diatomic molecules have zero dipole moments both in the separated-atoms and the united-atoms limits, the dipole moment function must go through at least one maximum at intermediate distances. Neglecting its variation with R thus represents an approximation, and indeed it is often necessary to include higher terms than the first in Equation (172) to properly account for the vibrational intensity distribution of an electronic spectrum. The dependence of the electric dipole moment on the nuclear geometry has the largest consequences in the spectra of polyatomic molecules, because it can lead to the observation of electronically forbidden transitions, as explained in Subsection 3.1 and illustrated by the electronic spectrum of benzene in Subsection 3.4.2.

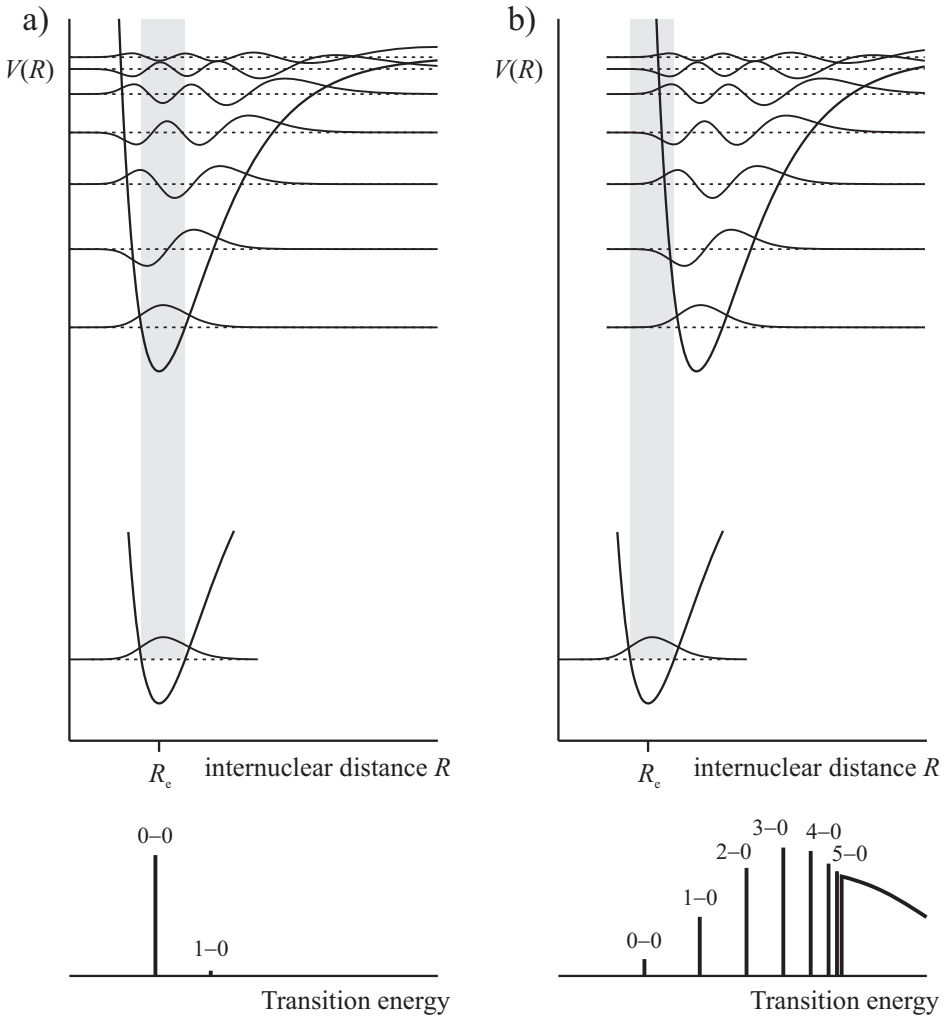

Figure 44: Illustration of the Franck-Condon principle for (a) an electronic transition between two electronic states having almost identical Born-Oppenheimer potential energy functions and (b) an electronic transition between two electronic states with $R''_e << R'_e$. The shaded areas in Figure 44 represent the regions where the vibrational wave function of the initial state has a significant amplitude. The spectra displayed below the potential energy diagrams represent schematically the expected appearance of electronic spectra recorded from the $v = 0$ level of the lower electronic state.

3.3.4 Rovibronic structure

The description of the rotational structure of electronic transitions requires the parity selection rule (Equation (166)) and also, in homonuclear diatomic molecules, consideration of the conservation of nuclear spin symmetry, in addition to the selection rules discussed in the previous subsections. The parity of a rovibronic state indicates whether its rovibronic wave function remains invariant under inversion of all space-fixed coordinates, or whether it changes sign. In the former case, one speaks of positive parity (labeled as '+') and, in the latter, of negative parity (labeled as '−'). Since

1. the dipole moment operator has negative parity,
2. wave functions in isotropic space have a well-defined parity,
3. the parity of a product of functions corresponds to the product of their parities,
4. the integral of a function of negative parity is zero,

the intensity of an electric-dipole transition of the form (155) differs from zero only if Ψ_f and Ψ_i possess opposite parities. The parities of rovibrational levels of diatomic molecules can be determined using Equation (110) and are indicated in the energy level diagrams presented in Figure 19.

Combined with the generalized Pauli principle, the conservation of nuclear-spin symmetry implied by the second factor of Equation (157) leads to a further selection rule for homonuclear diatomic molecules

$$\mathrm{s} \leftrightarrow \mathrm{s}, \quad \mathrm{a} \leftrightarrow \mathrm{a}, \quad (\mathrm{s} \leftrightarrow \mathrm{a} \text{ forbidden}), \tag{206}$$

where the "s" and "a" labels indicate whether the rovibronic wave function is symmetric or antisymmetric with respect to permutation of the coordinates of the identical nuclei, respectively. If the nuclei are bosons (fermions), rovibronic wave functions of "a" symmetry combine with nuclear-spin functions of "a" symmetry ("s" symmetry), whereas rovibronic wave functions of "s" symmetry combine with nuclear wave functions of "s" symmetry ("a" symmetry). For a given value of the nuclear spin quantum number I of the identical nuclei, the numbers N_s and N_a of symmetric and antisymmetric nuclear spin wave functions, respectively, are given by

$$N_\mathrm{s} = \frac{(2I+1)^2 + (2I+1)}{2} \quad \text{and} \quad N_\mathrm{a} = \frac{(2I+1)^2 - (2I+1)}{2}, \tag{207}$$

and are refered to as nuclear-spin statistical factors. The parity (±) and permutation (a/s) symmetry of the rovibrational levels of the most common electronic states are indicated in the energy level diagrams presented in Figure 19. ^{16}O, for instance, is a boson with $I = 0$, so that in $^{16}O_2$, $N_\mathrm{s} = 1$ and $N_\mathrm{a} = 0$. The fact that, in the X $^3\Sigma_\mathrm{g}^-$ ground state of O_2, the rotational levels of even N values have "a" symmetry (see Figure 19), implies that such states cannot be populated according to the generalized Pauli principle. Consequently, all lines originating from even N levels of the ground state of O_2 are missing in an electronic spectrum, and all observable transitions connect rovibronic levels of "s" rovibronic symmetry. In the X $^1\Sigma_\mathrm{g}^+$ ground state of H_2, rotational levels of even $J = N$

values have s symmetry. H is a fermion, with $I = 1/2$, so that $N_s = 3$ and $N_a = 1$. Because the total wave function must be of "a" symmetry with respect to permutation of the coordinates of fermions, states of rovibronic "s" ("a") symmetry only exist if their nuclear-spin symmetry is "a" ("s"). Consequently, transitions from odd-J rotational levels of the ground state of H_2, which have "a" symmetry, are three-times more intense than those from even-J rotational levels, which have "s" symmetry. The conservation of nuclear-spin symmetry implied by the second factor of Equation (157) means that rovibronic states of "a" and "s" symmetry are not connected by transitions induced by electromagnetic radiation and can therefore be considered as belonging to two distinct forms of homonuclear diatomic molecules, called para and ortho forms. One should, however, note that the product form of Equation (157) is an approximation, and that hyperfine interactions can couple the nuclear-spin motion to other motions.

The rotational states (with parity and nuclear permutation symmetry) that are involved a $^1\Sigma_u^+ \leftarrow {}^1\Sigma_g^+$ (parallel) and $^1\Pi_u \leftarrow {}^1\Sigma_g^+$ (perpendicular) transitions are drawn schematically in the upper parts of Figures 45a and b, repectively. The allowed transitions are marked by arrows and grouped in P, Q and R branches. Figures 45a and b present schematic spectra corresponding to the two type of transitions. The alternation of intensities of the lines results from the fact that the spectra have been calculated for a homonuclear diatomic molecule made of atoms with a nuclear spin $I = 1$.

Only $\Delta J = \pm 1$ transitions are allowed in a parallel transition, and the rotational structure of the vibronic transition consists of two branches, one with $\Delta J = 1$ (so-called R-branch) and one with $\Delta J = -1$ (so-called P-branch; see Figures 45a and c). In a perpendicular transition, $\Delta J = 0$ transitions are also observable which leads to a third branch (so-called Q-branch; see Figures 45b and d)).

In the case of transitions between singlet states, the rotational structure of the bands can be approximately described by Equation (3))

$$\tilde{\nu} = \tilde{\nu}_{v'v''} + B'J'(J'+1) - D'(J'(J'+1))^2 - [B''J''(J''+1) - D''(J''(J''+1))^2], \tag{208}$$

where $J' = J''$ for the Q-branch, $J' = J'' + 1$ for the R-branch, $J' = J'' - 1$ for the P-branch.

In the case of transitions between doublet or triplet states, the rotational structure is more complicated. The spectral positions $\tilde{\nu}$ of the rovibronic transitions are given by (see Equation (3))

$$\tilde{\nu} = \tilde{\nu}_{v'v''} + F'(J', \ldots) - F''(J'', \ldots), \tag{209}$$

where F' and F'' represent the rotational term value and the "..." symbolize the quantum numbers necessary to designate the rotational levels, which depend on the Hund's angular momentum coupling case used to describe the rotational structure. F' and F'' must be evaluated, for each state, using the rotational (including spin-orbit interaction) Hamiltonian presented in Equation (102). The allowed transitions can then be determined from the selection rules in the same way as used in the simple cases illustrated in Figure 45. The rotational energy level diagrams presented in Figure 19 are helpful

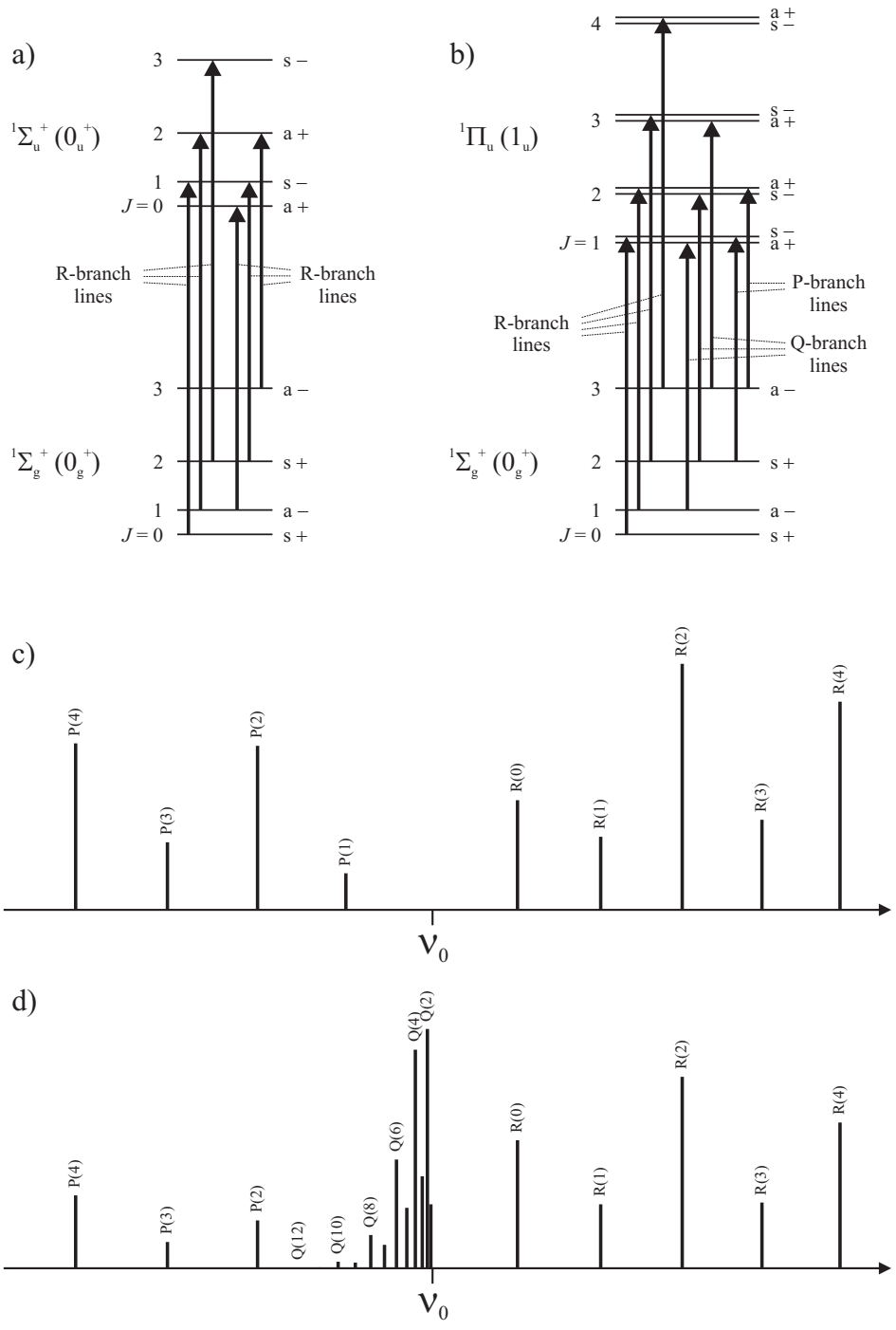

Figure 45: (a) Rotational states (with parity and nuclear permutation symmetry) that are involved in a $^1\Sigma_u^+ \leftarrow^1 \Sigma_g^+$ transition. (b) Rotational states (with parity and nuclear permutation symmetry) that are involved in a $^1\Pi_u \leftarrow^1 \Sigma_g^+$ transition. (c) and (d) Schematic structure of the rotational structure of the vibrational bands of a $^1\Sigma_u^+ \leftarrow^1 \Sigma_g^+$ and $^1\Pi_u \leftarrow^1 \Sigma_g^+$ transitions, respectively. The intensity alternation results from the fact that intensities have been calculated for a homonuclear diatomic molecules composed of atoms with a nuclear spin $I = 1$. The diagrams are also appropriate to qualitatively predict the rotational structures of $0_u^+ \leftarrow 0_g^+$, and $1_u \leftarrow 0_g^+$ transitions, respectively.

in predicting the overall rotational branch structure of electronic transitions of diatomic molecules, because they provide the parity and nuclear permutation symmetry of the rotational levels of the most common types of electronic states.

3.3.5 Selected examples

The literature on the electronic spectra of diatomic molecules is extremely rich. High-resolution spectra of electronic (allowed and forbidden) transitions connecting states of almost all possible term symbols in all Hund's cases have been reported. Rather than giving a comprehensive overview of all possible types of electronic transitions in diatomic molecules, we limit ourselves here to a few simple cases, from work in our laboratory, which illustrate the general principles in an elementary manner. Further examples of electronic spectra of diatomic molecules can be found, in this handbook, in the articles by Eikema and Ubachs (2010); Jungen (2010a); Western (2010). For a more complete and systematic overview of the broad diversity of electronic spectra of diatomic molecules, we refer to the books by Herzberg (1989); Lefebvre-Brion and Field (2004); Brown and Carrington (2003).

Figure 46 illustrates, with the example of the C $0_u^+ \leftarrow$ X 0_g^+ electronic band system of Xe_2, the Franck-Condon principle and some of the limitations in its use that result from the experimental methods chosen to record electronic transitions. The electronic states of Xe_2 are conveniently described in Hund's case (c), and the figure also gives an example of the rotational structure of a $0_u^+ \leftarrow 0_g^+$ transition, which conforms to the energy level diagram presented in Figure 45a.

Whereas the ground electronic state of Xe_2 is only weakly bound by van der Waals forces, the A, B, and C electronic states are the lowest members of Rydberg states belonging to series converging on the low-lying electronic states of Xe_2^+ (see Figure 17) that are more strongly bound and thus have equilibrium internuclear distances shorter than the ground state. This geometry change results in a long progression of vibrational bands corresponding to excitation of vibrational levels of the C state with $v' = 14$-26 (see Figure 46b). The rotational structure of the bands with the lower v' values are strongly degraded to the high wave number side of the spectrum (see Figure 46c), which also indicates a shortening of the interatomic distance ($B'_{v'} > B''_{v''}$).

Because the rotational constant of the $v' = 20$ level of the C state is significantly larger than that of the ground $v'' = 0$ level, the P-branch of the of the C 0_u^+ ($v' = 20$) $\leftarrow$ X 0_g^+ ($v'' = 0$) band displayed in Figure 46c possesses a band head at low J'' values ($J'' = 3$). The rotational structure does not show the intensity alternations between lines originating from even- and odd-J'' ground state levels that are characteristic of the spectra of homonuclear diatomic molecules (see Figure 45c). The reason is that the spectrum has been recorded by measuring the ionization signal corresponding to the $^{131}Xe^{136}Xe$ isotopomer. One should note that one retains the g/u labels in this case because isotopic substitution does not affect the electronic structure within the Born-Oppenheimer approximation.

The intensity distribution of the spectrum only partially reflects the Franck-Condon factors. Indeed, the intensity of the ion signal can be significantly reduced by predissociation of the C level.

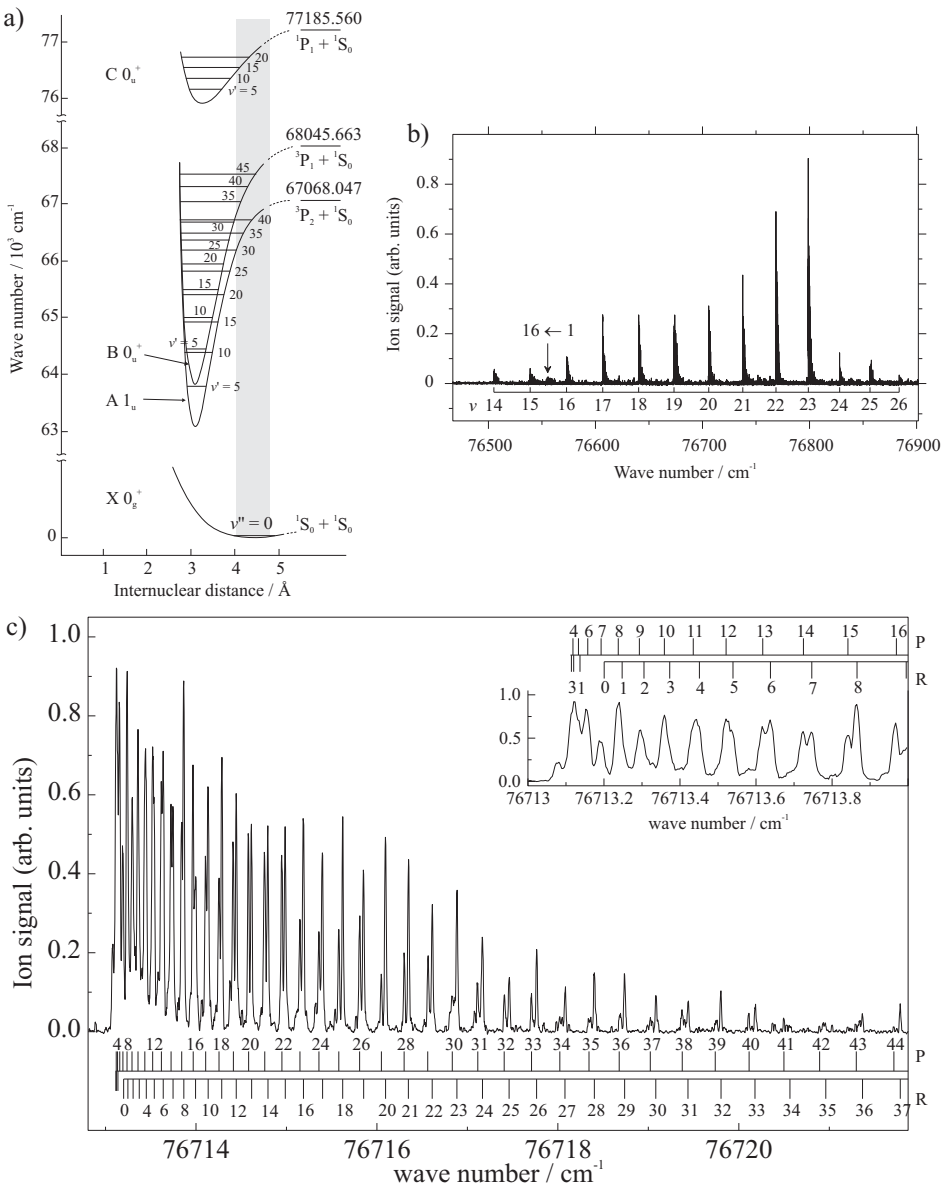

Figure 46: (a) Potential energy functions of the X 0_g^+, A 1_u, B 0_u^+ , and C 0_u^+ electronic states of Xe_2. The Franck-Condon region for excitation from the ground vibrational level of the X state is indicated by the gray area. (b) Spectrum of the C 0_u^+ ← X 0_g^+ ($v'' = 0$) transition recorded with a narrow-band pulsed VUV laser. The transitions are detected by ionizing the levels of the C state with a pulsed UV laser and monitoring the current of $^{131}Xe^{136}Xe^+$ ions as a function of the wave number of the VUV laser. The Xe_2 molecules were formed in a supersonic expansion and the population of the rotational levels corresponds to a temperature of 4 K. The vibrational bands are labeled by the vibrational quantum number of the C state. (c) Rotational structure of the C 0_u^+ ($v' = 20$) ← X 0_g^+ ($v'' = 0$) band. The numbers along the assignment bars corresponding to the P and R branches designate the rotational quantum number J'' of the ground state (Adapted from Hollenstein (2003)).

Moreover, the overall intensity distribution can be affected if the predissociation rate depends on the degree of vibrational excitation of the C state.

Next to information on the internuclear distances of the states involved in the transitions by means of the rotational constants, the spectrum also contains information on the potential energy functions and the electronic symmetry of the electronic states involved in the transition. The same transition can also be recorded by monitoring the electronically excited Xe atom fragment that result from the predissociation of the C state (not shown), so that the electronic spectrum also contains information on the dynamics of the excited state.

A more reliable way to measure intensities of electronic transitions is by recording the absorption signal. Examples of VUV absorption spectra of CO and N_2 are presented in panels a) and b) of Figure 47. In these spectra, the normalized transmission signal I/I_0 of the VUV radiation is displayed as a function of the VUV wave number. The CO and N_2 gas samples are cold ($T \approx 12$ K), skimmed supersonic expansions of CO and N_2, which are crossed at right angles by the VUV laser beam to avoid Doppler broadening. Normalization is achieved by dividing the intensity of the VUV radiation transmitted through the sample by the intensity of a reference VUV laser beam (see Sommavilla *et al.* (2002)).

The rotational structure of the bands represents an essential element of the assignment procedure. Bands recorded from a lower level of $^1\Sigma^+$ symmetry which have P, Q and R branches must have a $^1\Pi$ state as upper level, whereas those which do not have a Q branch are likely to have a $^1\Sigma$ state as upper level. Consequently, the bands centered around 109562 cm^{-1} in the spectrum of N_2 (Figure 47b), and the band centered around 109564 cm^{-1} in the spectrum of CO (Figure 47a) must have a $^1\Pi$ state as upper level, because they have a Q-branch. However, the absence of a Q-branch does not automatically imply that the upper level is $^1\Sigma$ state, because P and R lines access the components of the rotational doublets with Π^+ electronic character, and Q lines the components with a Π^- electronic character. The absence of the Q branch in a $^1\Pi \leftarrow ^1\Sigma$ transition may therefore occasionally also result from a perturbation of the Π^- state, for instance by a neighboring Σ^- state. Consequently, Σ^+ states can only be unambiguously assigned by the observation of a P(1) transition. Indeed, $J = 0$ rotational levels do not exist in $^1\Pi$ states. The two bands centered around 109449 cm^{-1} and 109481 cm^{-1} in the spectrum of CO and the band centered around 109542 cm^{-1} in the spectrum of N_2 must therefore have a $^1\Sigma$ state as upper level.

The rotational constant of the upper vibronic state provides a further important indication for the assignment, particularly when a spectrum consists of overlapping transitions to Rydberg states belonging to series converging on different ionic states. Because the rotational constants of Rydberg states are almost identical to the rotational constants of the ionic states to which the Rydberg series converge, the determination of the rotational constant of the upper level of an electronic transition can often either enable one to confirm, or rule out possible assignments by comparison with the rotational constants of the vibronic levels of the ion, if these are known. Such comparison, in addition

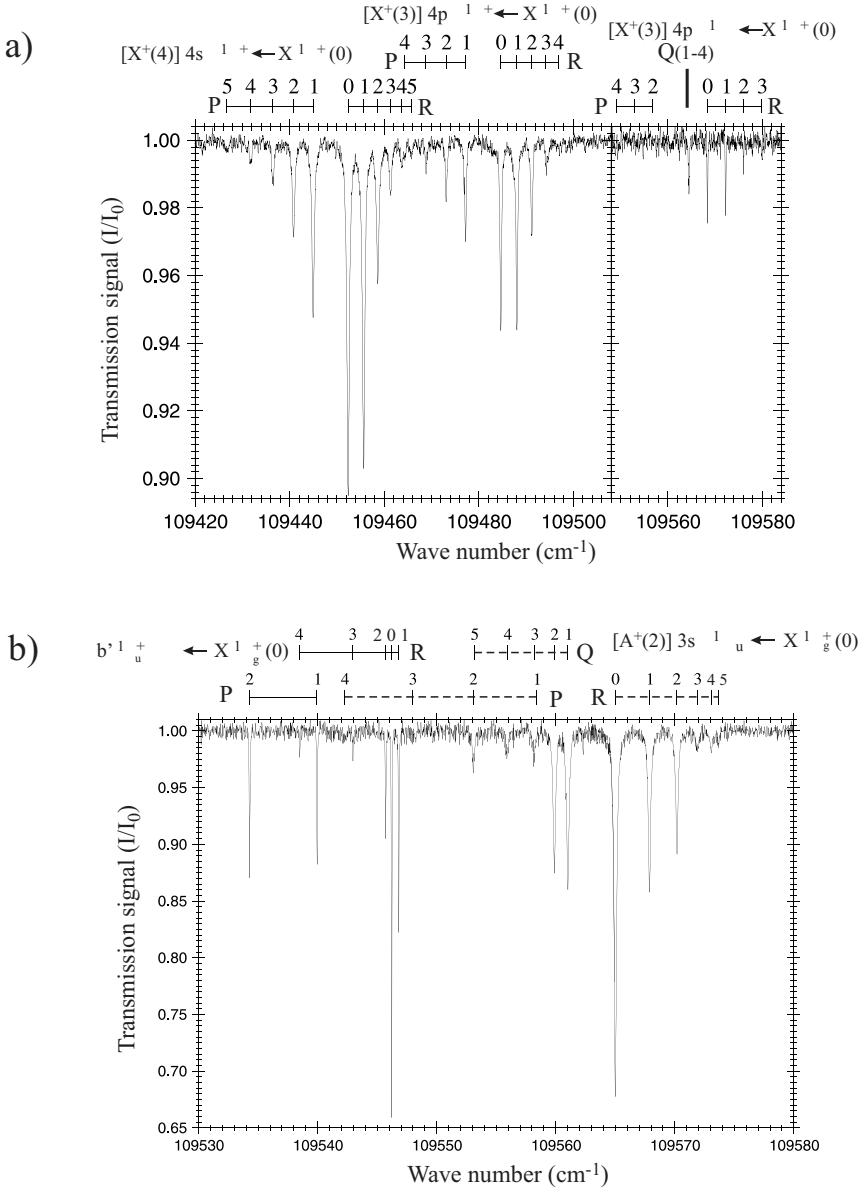

Figure 47: (a) VUV absorption spectrum of CO in the region between 109420 cm^{-1} and 109580 cm^{-1} displaying transitions from the $^1\Sigma^+$ ($v'' = 0$) ground state to the 4pπ $^1\Pi$ and 4pσ $^1\Sigma^+$ Rydberg states belonging to series converging to the $v^+ = 3$ level of the X $^+$ $^2\Sigma^+$ ground electronic state of CO^+ and to the 3sσ $^1\Sigma^+$ Rydberg state belonging to series converging to the $v^+ = 4$ level of the X^+ $^2\Sigma^+$ ground electronic state of CO^+. (b) VUV absorption spectrum of N_2 in the region between 109530 cm^{-1} and 109580 cm^{-1} displaying transitions from the $^1\Sigma_g^+$ ($v'' = 0$) ground state to the 4sσ $^1\Pi_u$ Rydberg state belonging to series converging to the $v^+ = 2$ level of the A^+ $^2\Pi_u$ first excited electronic state of N_2^+, and to the $v' = 8$ level of the b$'$ $^1\Sigma_u^+$ valence state of N_2 (Adapted from Sommavilla (2004)).

to information on the quantum defects, can be used to assign two bands of the spectrum of CO to transitions to Rydberg states with a $X^+\ ^2\Sigma^+$ ($v^+ = 3$) CO^+ ion core, and one to a Rydberg state with a $X^+\ ^2\Sigma^+$ ($v^+ = 4$) CO^+ ion core. Similarly, the band centered around 109564 cm^{-1} in the spectrum of N_2 can be assigned to a transition to a Rydberg state with an $A^+\ ^2\Pi_u$ ($v^+ = 2$) N_2^+ ion core. The much smaller rotational constant of the upper level of the transition centered around 109542 cm^{-1} in the spectrum of N_2, which results in an R-branch band head at $J'' = 1$, is incompatible with an assignment of the upper level to a Rydberg state, and must be assigned to the b′ valence state.

The bands observed in the VUV absorption spectra of CO and N_2 have different linewidths and, therefore, different predissociation rates. A measurement of the same transitions by resonance-enhanced two-photon ionization spectroscopy would therefore have led to different relative intensities: the bands with broad lines would have appeared less intense in these spectra compared to those with narrow lines than in the case of the absorption spectra displayed in Figure 47.

Finally, one could note that the transitions from $J'' = 0$ and 2 levels are more intense compared to the $J'' = 1$ and 3 lines in the spectrum of N_2 than they are in the spectrum of CO. This difference is the manifestation of the nuclear spin statistical factors of 2(1) of rotational levels of even-(odd-) J'' levels of N_2 (see Equation (207)).

3.4 Electronic spectra of polyatomic molecules

The general principles needed to rationalize or predict the structure of electronic spectra of polyatomic molecules have been presented in Subsection 3.1, and only differ from those needed in studies of diatomic molecules as a result of the larger number of vibrational degrees of freedom and the different point-group symmetries. The transitions are classified as electronically allowed if Equation (174) is fulfilled, in which case the vibrational intensity distribution can approximately be described by Franck-Condon factors (Equation (176)) and the selection rules (177) and (178). If Equation (174) is not fulfilled, electronic transitions may nevertheless be observed, in which case they fall into three categories, two of which have already been discussed for diatomic molecules in Subsection 3.3.2:

1. **Magnetic dipole transitions and electric quadrupole transitions**

   This case can be treated in analogy to the discussion, in Subsection 3.3.2, of magnetic dipole and electric quadrupole transitions in diatomic molecules

   Example: The $\tilde{A}\ ^1A_2 \leftarrow \tilde{X}\ ^1A_1$ transition in H_2CO is electronically forbidden (see Table 8). However, the transition is observed as a magnetic dipole transition ($\Gamma(R_z) = A_2$ in this C_{2v} molecule).

2. **Intercombination transitions**

   Intercombination transitions in polyatomic molecules can also be treated following the same procedure as that introduced in Subsection 3.3.2 to treat such transitions in diatomic molecules.

   Example: We consider the $\tilde{A}\ ^3F_2 \leftarrow \tilde{X}\ ^1A_1$ transition in a tetrahedral molecule. The character table of the spin double group of a tetrahedral molecule is given in Table 21. $\Gamma(T_{x,y,z}) = F_2$ in this group.

Table 21: Character table of the spin double group of tetrahedral molecules $T_d^{(2)}$.

T_d	I	$8C_3$	$6\sigma_d$	$6S_4$	$3S_4^2$	R	$8C_3^2$	$6S_4^3$	
A_1	1	1	1	1	1	1	1	1	
A_2	1	1	−1	−1	1	1	1	−1	
E	2	−1	0	0	2	2	−1	0	
F_1	3	0	−1	1	−1	3	0	1	R_x, R_y, R_z
F_2	3	0	1	−1	−1	3	0	−1	x, y, z
$E_{1/2}$	2	1	0	$\sqrt{2}$	0	−2	−1	$-\sqrt{2}$	
$E_{5/2}$	2	1	0	$-\sqrt{2}$	0	−2	−1	$\sqrt{2}$	
$G_{3/2}$	4	−1	0	0	0	−4	1	0	

Table 22: Transformation properties of electron spin functions in the $T_d^{(2)}$ spin double group.

S	0	1/2	1	3/2	2	5/2
Γ_S	A_1	$E_{1/2}$	F_1	$G_{3/2}$	$E + F_2$	$E_{5/2} + G_{3/2}$

According to Table 22, the $S = 0$ and $S = 1$ electron spin functions transform as the A_1 and F_1 irreducible representations, respectively. We therefore obtain $\Gamma''_{es} = A_1$ and $\Gamma'_{es} = \Gamma'_{elec} \otimes \Gamma'_{espin} = F_2 \otimes F_1 = A_2 + E + F_1 + F_2$. Consequently, only the F_2 component corresponds to an observable intercombination transition.

3. **Electronically forbidden but vibronically allowed transitions**

The mechanism by which such transitions are observed is the Herzberg-Teller intensity borrowing mechanism mentioned in Subsection 3.1 in the context of electronically forbidden but vibronically allowed transitions. In this case, the selection rule (179) applies and requires an odd change in the number of vibrational quanta in non-totally-symmetric modes (see Equation (180)). Electronically forbidden, but vibronically allowed transitions are not possible in diatomic molecules, because the only vibrational mode is totally symmetric.

Example: Consider the electronically forbidden transition between the $\tilde{X}\ ^1A_1$ vibrationless ground state and the $\tilde{Y}\ ^1A_2$ electronic state of a C_{2v} molecule. Excitation of a B_1 vibration in the upper electronic state results in an excited state of vibronic symmetry $\Gamma_{ev} = A_2 \otimes B_1 = B_2$. A transition to this state originating in the A_1 state is vibronically allowed. However, the transition only carries significant intensity if the B_2 vibronic state interacts with a close-lying electronic state $\tilde{Z}$ of electronic symmetry B_2. The intensity of the transition is 'borrowed' from the $\tilde{Z} \leftarrow \tilde{X}$ by the Herzberg-Teller effect.

Table 23: Character table of the D_{3h} point group.

D_{3h}	I	$2C_3$	$3C_2$	σ_h	$2S_3$	$3\sigma_v$	
A_1'	1	1	1	1	1	1	
A_2'	1	1	−1	1	1	−1	R_z
E'	2	−1	0	2	−1	0	x, y
A_1''	1	1	1	−1	−1	−1	
A_2''	1	1	−1	−1	−1	1	z
E''	2	−1	0	−2	1	0	R_x, R_y

3.4.1 Electronically allowed transitions - an example

The general symmetry selection rules governing electronic transitions in polyatomic molecules have been formulated in Equations (158), (159), (161)-(166), (174), and (176)-(178). In polyatomic molecules, an electronic transition can be induced by any of the three Cartesian components of the transition dipole moment. When an electronic transition is allowed, the relative intensities of the transitions to different vibrational levels of the electronically excited state approximately correspond to Franck-Condon factors (see Equation (175)), and the vibrational structure of an electronically allowed transition contains information on the relative equilibrium geometries of the two electronic states connected through the transition.

An illustrative example of an electronically allowed transition is the absorption spectrum of ammonia, which is displayed in Figure 48. The electronic ground state of ammonia has an equilibrium structure of pyramidal C_{3v} point-group symmetry. However, two pyramidal configurations are separated by a low barrier along the symmetric bending (umbrella) mode, which leads to inversion of the molecule through tunneling on the picosecond time scale and to a tunneling splitting of 0.8 cm^{-1}. When this tunneling splitting is resolved, the appropriate point group to treat the energy level structure is D_{3h}, the character table of which is given in Table 23. The vibrational wave functions are nevertheless mainly localized at the minima of the potential energy surfaces corresponding to a C_{3v} geometry. In the C_{3v} point group, the electronic configuration of ammonia in the $\tilde{X}$ ground electronic state is $(1a_1)^2(2a_1)^2(1e)^4(3a_1)^2$. The lowest-lying electronically allowed transition corresponds to the excitation of an electron from the $3a_1$ orbital, which is a nonbonding orbital (lone pair) of the nitrogen atom, into the diffuse 3s Rydberg orbital with a NH_3^+ planar ion core. In the electronically excited state, the molecule has a planar structure with D_{3h} point-group symmetry. In this point group, the excited electronic configuration and the electronic state are labeled $(1a_1')^2(2a_1')^2(1e')^4(1a_2'')^1(3sa_1')^1$ $\tilde{A}\ ^1A_2''$.

The absorption spectrum of the $\tilde{A} \leftarrow \tilde{X}$ transition recorded using a room-temperature sample in which only the ground vibrational level of the $\tilde{X}$ state is significantly populated is displayed in Figure 48. The spectrum consists of a single progression in the out-of-plane bending (umbrella) mode

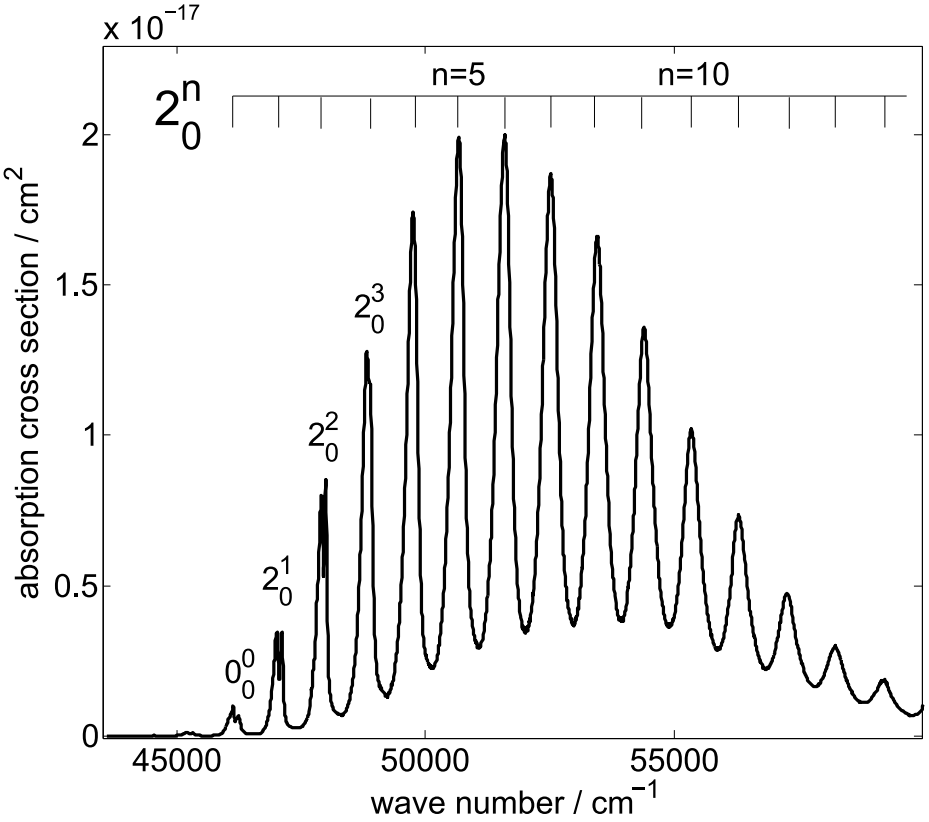

Figure 48: Absorption spectrum of the $\tilde{\mathrm{A}} \leftarrow \tilde{\mathrm{X}}$ transition of ammonia (data from Cheng *et al.* (2006)). The origin of the electronic transition is labeled as 0_0^0 and the dominant progression in the out-of-plane bending mode ν_2 is labeled 2_0^n. The members of this progression originate in the vibrational ground state of the $\tilde{\mathrm{X}}$ state and end in the $v_2 = n$ level of the $\tilde{\mathrm{A}}$ excited state.

ν_2 of the $\tilde{\mathrm{A}}$ state. The origin band is labeled as 0_0^0 and the members of the progression as 2_0^n, indicating that the electronic transition originates in the vibrational ground state of the $\tilde{\mathrm{X}}$ state of ammonia and ends in the $v_2 = n$ vibrationally excited level of the $\tilde{\mathrm{A}}$ state. The weak band observed at lower wave numbers than the origin band is the hot band 2_1^0. The very long progression, extending beyond $n = 15$, is characteristic of a large change in equilibrium geometry between the two electronic states involved in the transition.

The simplest way to understand the fact that transitions to both even and odd vibrational levels are observed without noticeable intensity alternations between even and odd levels is to evaluate the selection rules in the $C_{3\mathrm{v}}$ point group (see top left part of Table 16). In this group, the electronic transition is allowed, and the umbrella mode is totally symmetric, so that the vibrational selection rule and intensity distribution can be described by the vibrational selection rule (178) and the Franck-Condon factors given by Equation (175), respectively.

The vibrational intensity distribution can also be explained in the $D_{3\mathrm{h}}$ point group. However,

in this group, the umbrella mode ν_2 is not totally symmetric, but of a_2'' symmetry. Consequently, one would predict on the basis of Equation (177) that the vibrational bands corresponding to odd values of the vibrational quantum number v_2 of the umbrella mode should be missing in an absorption spectrum from the ground vibrational level. The reason why transitions to vibrational levels with odd values of v_2 are observed is that they originate from the upper tunneling component of the ground state which has A_2'' vibronic symmetry (and thus may be regarded as the first excited vibrational level of the ground state). Transitions to vibrational levels with even values of v_2 originate from the lower tunneling component of the ground state, which has A_1' symmetry. The two tunneling components are almost equally populated under the experimental conditions used to record the spectrum displayed in Fig. 48, so that no intensity alternations in the ν_2 progression are observed.

This example also served the purpose of illustrating some of the difficulties one encounters in interpreting electronic states with equilibrium structures corresponding to different point groups.

3.4.2 Electronically forbidden but vibronically allowed transitions - an example

Electronically forbidden transitions may gain intensity from an allowed transition through vibronic coupling mediated by a non-totally-symmetric mode (the Herzberg-Teller effect), as discussed above.

A prototypical example of this situation is the electronically forbidden $\tilde{A}\ ^1B_{2u} \leftarrow \tilde{X}\ ^1A_{1g}$ transition of benzene (C_6H_6). This transition is also referred to as the $S_1 \leftarrow S_0$ transition, according to the nomenclature introduced in Section 2.3.1. The excited electronic state arises from the electronic configuration $(a_{2u})^2(e_{1g})^3(e_{2u})^1$ (showing the π molecular orbitals only). The direct product of the irreducible representations of the partially occupied orbitals is $e_{1g} \otimes e_{2u} = b_{1u} \oplus b_{2u} \oplus e_{1u}$, giving rise to the electronic states $^3B_{1u}$, $^1B_{1u}$, $^3B_{2u}$, $^1B_{2u}$, $^3E_{1u}$, and $^1E_{1u}$. In both the $\tilde{A}\ ^1B_{2u}$ and the $\tilde{X}\ ^1A_{1g}$ state, the benzene molecule has D_{6h} point-group symmetry. The dipole moment operator transforms as $A_{2u} \oplus E_{1u}$ and thus the only allowed electronic transitions originating from the ground electronic state end in states of electronic symmetry A_{2u} or E_{1u}. The $\tilde{A}\ ^1B_{2u} \leftarrow \tilde{X}\ ^1A_{1g}$ transition in benzene is thus forbidden, while the $\tilde{C}\ ^1E_{1u} \leftarrow \tilde{X}\ ^1A_{1g}$ transition is allowed (see Table 13). However, vibrational modes of symmetry $b_{2u} \otimes e_{1u} = e_{2g}$ induce vibronic coupling between the $\tilde{A}$ and $\tilde{C}$ electronic states.

Figure 49 shows a low-resolution overview spectrum of benzene in the region of 37000-42000 cm^{-1}, which was first analyzed by Callomon *et al.* (1966). The spectrum is dominated by a strong regular progression of absorption bands connecting the ground vibrational level of the $\tilde{X}$ state to vibrationally excited levels of the $\tilde{A}$ state. The nomenclature $1_0^n 6_0^1$ indicates that the lower level of the transition has the quantum numbers $v_1 = v_6 = 0$, i.e. both ν_1 and ν_6 are unexcited, whereas the upper level of the transition has $v_1 = n$ and $v_6 = 1$. The origin of the band system, designated as 0_0^0, does not carry intensity, as expected for an electronically forbidden transition. The ν_1 and ν_6 vibrational modes have A_{1g} and E_{2g} symmetry, respectively, in both electronic states. The vibronic symmetry of the upper levels of the observed transition is thus $\Gamma_e \otimes \Gamma_v = b_{2u} \otimes [a_{1g}]^n \otimes e_{2g} = e_{1u}$ which can be accessed from the ground vibronic state through the E_{1u} component of the electric-dipole-moment operator

(see Table 13).

All strong transitions in this band system end in $v_6 = 1$ levels, which indicates that, among all vibrational modes of benzene, ν_6 is the mode primarily involved in mediating the vibronic interaction. Below the origin of the band, the weak transition labeled as 6^0_1 originates from the thermally populated $v_6 = 1$ vibrationally excited level of the ground electronic state and ends in the vibrational ground state of the $\tilde{A}\ ^1B_{2u}$ state. Such a transition is a hot band and is not observed when the vibrational temperature of the molecule is sufficiently low. One should note that the 6^1_0 band is vibronically allowed, which explains why it is observed, whereas transitions from other thermally populated excited vibrational levels of the ground state are not detected.

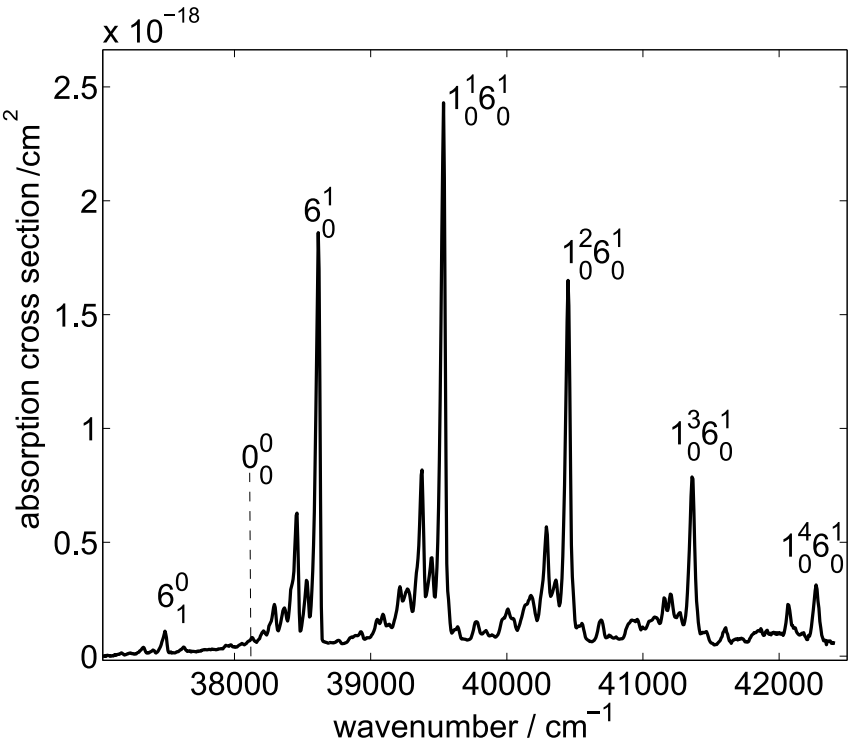

Figure 49: Low-resolution absorption spectrum of benzene in the 38000-42000 cm^{-1}region (data from Etzkorn *et al.* (1999)). The transitions labeled $1^n_0 6^1_0$ originate from the vibrational ground state of the $\tilde{X}\ ^1A_{1g}$ state and end in the ($v_1 = n$,$v_6 = 1$) vibrational states of the $\tilde{A}\ ^1B_{2u}$ electronically excited state. The origin of the band (marked as 0^0_0) does not carry intensity. The vibronically allowed hot band 6^0_1 is observed below the origin band.

3.4.3 Electronic transitions and the Jahn-Teller effect

The distortions of molecular structures which result from the Jahn-Teller effect have a profound impact on the vibrational structure and intensity distribution of electronic spectra. The reduction of

molecular symmetry which follows from Jahn-Teller distortions leads to the observation of dense manifolds of vibronic transitions, and the observation of vibrational progressions in certain modes usually indicates that these modes are Jahn-Teller active. In cases where the Jahn-Teller effect is accompanied by large-amplitude motions, such as pseudorotations along the potential troughs in Figures 30 and 31, progressions in low-frequency modes with irregular spacings are observed, the interpretation of which often requires extensive modeling. Rather than providing an exhaustive treatment of the possible cases, we only present here two examples, involving C_5H_5 and $C_5H_5^+$, without providing any detailed and comprehensive treatment, with the primary goal to draw the attention to the fact that electronic spectra of molecules subject to the Jahn-Teller effect are very complex, and thus particularly interesting. We refer to Subsection 2.3.6, and mostly also to the bibliography, for more comprehensive and exhaustive treatments of the Jahn-Teller effect.

The Jahn-Teller effect in the $\tilde{X}\ ^2E_1''$ state of C_5H_5 has been discussed in section 2.3.6. The $\tilde{X}\ ^2E_1''$ of C_5H_5 has been characterized experimentally through the measurement of the laser-induced dispersed fluorescence from the first excited electronic state $\tilde{A}\ ^2A_2''$ back to the ground state (Applegate *et al.* 2001b,a). The emission spectrum from the $\tilde{A}\ 11^1$ state is shown in Figure 50. The vibrational mode ν_{11} is of e_2' symmetry and linearly Jahn-Teller active. The emission spectrum is dominated by two progressions that are labeled by the axes on top of the figure. The quantum number j represents the total vibronic angular momentum and n_j represents the harmonic oscillator quantum number. In the electronically nondegenerate $\tilde{A}$ state, the vibronic and vibrational angular momentum quantum numbers are identical ($j = \ell$), and, consequently, integer numbers. In the doubly degenerate $\tilde{X}$ state, ℓ is no longer a good quantum number and each vibronic level with $\ell \geq 1$ splits into two levels with $j = |\ell| \pm 1/2$. Since the mode ν_{11} is degenerate, it possesses a vibrational angular momentum $|\ell| = 1$, and thus the $\tilde{A}\ 11^1$ state can fluoresce back to both $j = 1/2$ and $j = 3/2$ states. The complexity of the spectrum in Figure 50 is typical of electronic transitions in molecules subject to the Jahn-Teller effect. The irregular spacings of vibronic levels in the ground electronic state of C_5H_5 and the high density of vibronic levels at low energies are characteristic of a strong multimode JT effect. The assignment of the spectra often require extensive theoretical modeling and many measurements exploiting the excitation of selected vibronic levels. The reader is referred to Applegate *et al.* (2001b,a) and to the reading list at the end of the chapter for further information.

The PJT effect in the $\tilde{a}^+\ ^1E_2'$ state of $C_5H_5^+$ has been discussed in section 2.3.6. The $\tilde{a}^+\ ^1E_2'$ state of $C_5H_5^+$ has been characterized by pulsed-field-ionization zero-kinetic-energy (PFI-ZEKE) spectroscopy following resonance-enhanced two-photon excitation through selected vibrational levels of the $\tilde{A}$ state of C_5H_5 Wörner and Merkt (2006, 2007, 2009). The PJT effect in the $\tilde{a}^+\ ^2E_1'$ is very strong, leading to a stabilization by about 4000 cm^{-1}. Moreover, the absence of significant quadratic coupling results in a vibronic structure that is close to the limit of a pseudorotational motion. This limit corresponds to an unhindered large-amplitude motion along the minimum of the trough of the lowest potential energy surface displayed in Figure 31. The corresponding vibronic progressions are labeled along the

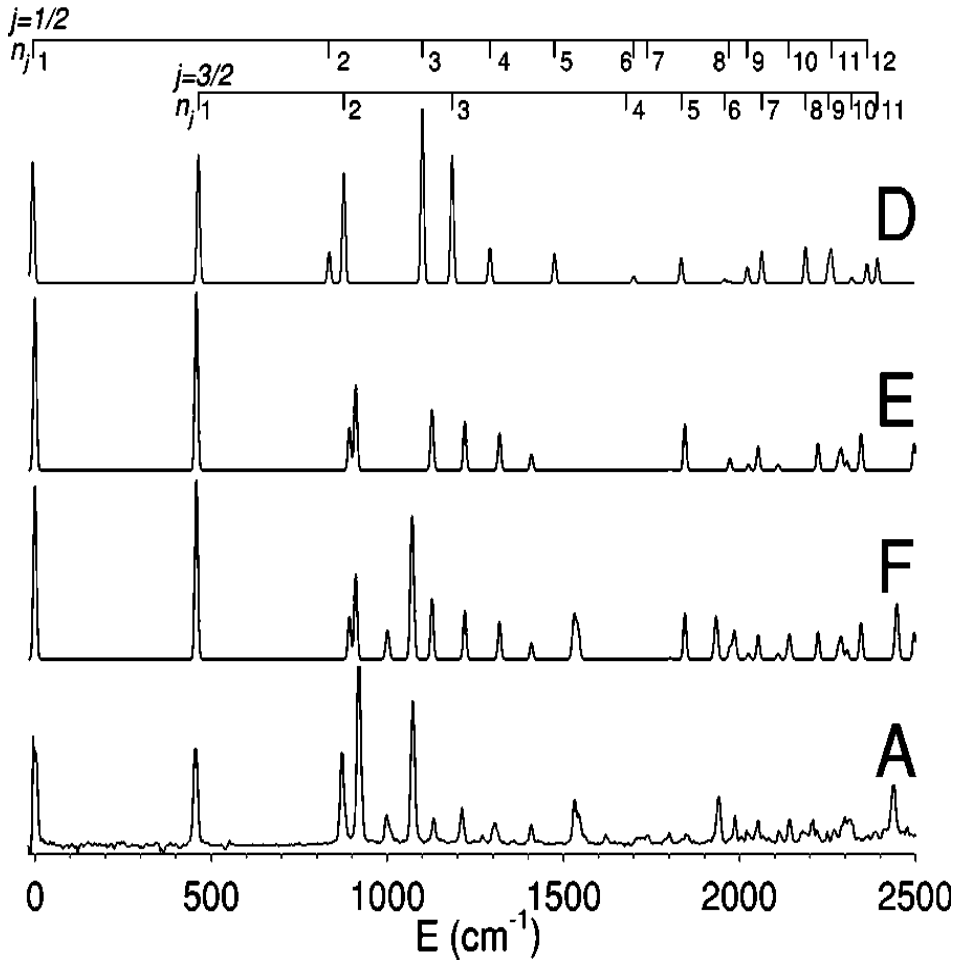

Figure 50: (A) Experimental emission spectrum of the $\tilde{\mathrm{A}}\ ^2\mathrm{A}_2'', 11^1 \rightarrow \tilde{\mathrm{X}}\ ^2\mathrm{E}_1''$ transition of C_5H_5. (D) Calulated spectrum of Jahn-Teller active modes using the Jahn-Teller parameters derived from ab initio calculations. The assignment bars above the spectrum indicate the $|j, n_j\rangle$ assignment of each feature in the spectrum. (E) Simulated spectrum of Jahn-Teller active modes using the Jahn-Teller parameters as determined from fitting the experimental spectrum. (F) Simulated emission spectrum. (From Ref. Applegate *et al.* (2001a)), with permission of the authors).

assignment bars at the top of Figure 51. By contrast to the JT effect in C_5H_5, which is characterized by half-integer vibronic angular momentum quantum numbers j (see Figure 50), the PJT effect in $C_5H_5^+$ is associated with integer quantum numbers. The lowest progression ($u = 0$) shows the simple appearance expected for the case of free pseudorotation, i.e. vibronic level positions following a quadratic dependence on their vibronic quantum number, i.e., $E \propto j^2$. At higher energies, the vibronic structure becomes very complicated because three vibrational modes of e_2' symmetry are involved in the PJT effect. The alternation in the intensities of the three lowest vibronic levels observed following excitation through different intermediate states is reproduced by a simple vibronic coupling calculation (shown as stick spectra in Figure 51) assuming that the intensity of the forbidden

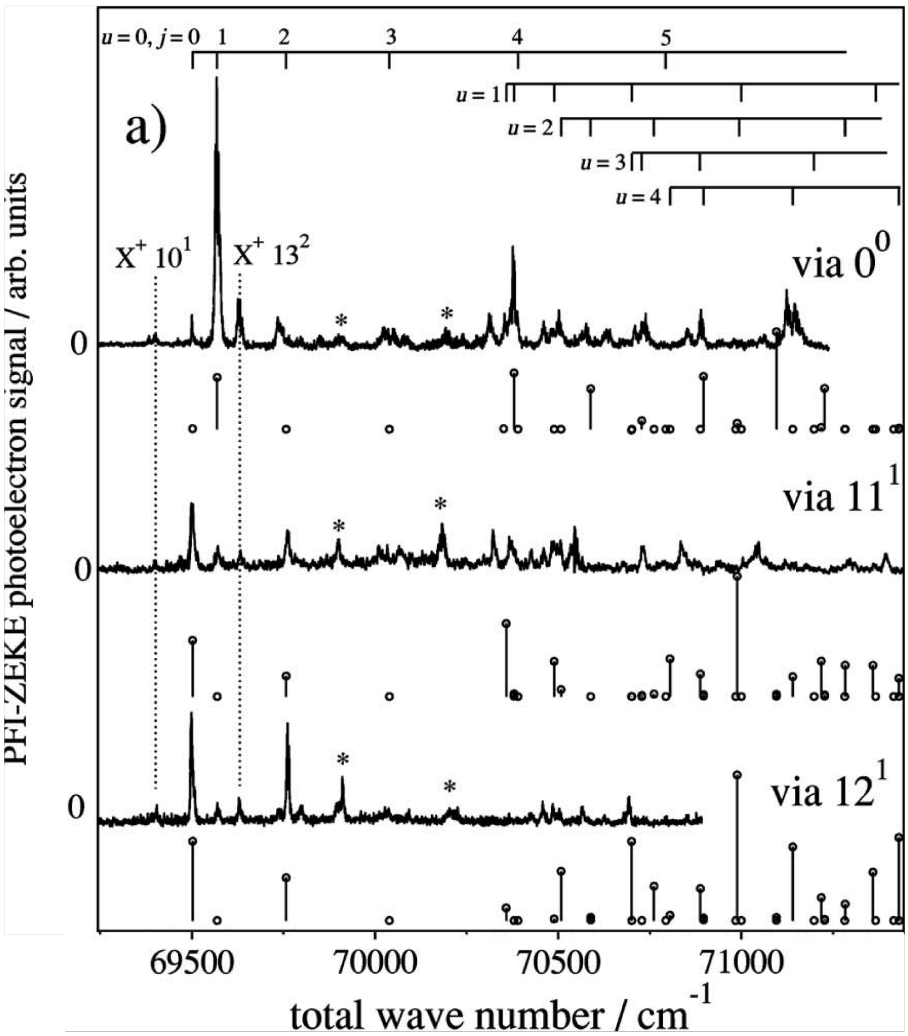

Figure 51: PFI-ZEKE photoelectron spectra of C_5H_5 recorded following two-photon resonant excitation to the lower component of the $\tilde{a}^+\ ^1E_2'$ state via selected vibrational levels of the $\tilde{A}\ ^2A_2''$ state. The intermediate level is indicated on the right-hand side above the spectra. The spectra are compared to calculations (vertical stick spectra) of the vibronic structure including the modes ν_{10}, ν_{11}, and ν_{12} in $C_5H_5^+$. The bands marked with an asterisk coincide with lines of the precursor C_5H_6 (adapted from Ref. Wörner and Merkt (2007)).

$\tilde{a}^+ \leftarrow \tilde{A}$ photoionization transition is borrowed from the allowed $((a_2'')^1(e_1'')^3)\ ^1E_1' \leftarrow \tilde{A}$ state through a Herzberg-Teller effect (see Wörner *et al.* (2007); Wörner and Merkt (2009) for more details).

3.4.4 Electronic excitations in complex molecules: the exciton model

Large polyatomic molecules typically have a low point-group symmetry and, therefore, selection rules provide much less qualitative understanding of their electronic spectra than is the case for highly

symmetric molecules. In large polyatomic molecules, electronic transitions are often localized to certain groups of atoms, also called "chromophores". This property is widely used in analytical chemistry to identify functional groups of molecules through their ultraviolet absorption spectrum (see, for instance, Skoog *et al.* (2000)). The corresponding transitions are labeled according to the type of orbitals involved in the transitions, as discussed in Section 2.3.1. The aldehyde group -CHO is an example of a chromophore that possesses a weak absorption around 280 nm, corresponding to a $\pi^* \rightarrow n$ promotion. Benzene rings show weak absorptions close to 260 nm corresponding to $\pi \rightarrow \pi^*$ excitations, as discussed in the previous subection. C=C double bonds show intense absorption feartures in the region around 180 nm, just as ethylene itself.

In larger molecules possessing several chromophores, electronic excitations rarely occur independently but the chromophores are often coupled to each other. In the case of several identical chromophores, the coupling can lead to the splitting of otherwise degenerate electronic transitions. In general, the coupling can also lead to energy transfer between different chromophores. In all these cases, the electronic spectrum can be qualitatively understood from the interaction of several localized excitations which are referred to as "excitons" (Coffman and McClure 1958).

Diphenylmethane, depicted in Figure 52 is a prototyipcal molecule with two nearly degenerate interacting aromatic chromophores (Stearns *et al.* 2008). The $\pi - \pi^*$ excitations occur in the phenyl rings and interact with each other. Diphenylmethane has a C_2 equilibrium structure with the phenyl rings at dihedral angles of approximatley 60° with respect to the plane bisecting the methylene C-H bonds. Labeling the two chromophores A and B, one can define zero-order states $|A^*B\rangle$, $E^0_{A^*B}$ and $|AB^*\rangle$, $E^0_{AB^*}$ corresponding to excited states with electronic excitation localized on a single chromophore. The inclusion of the coupling V between the two states leads to the exciton states with spectral positions

$$E_\pm = \frac{E^0_{A^*B} + E^0_{AB^*}}{2} \pm \frac{\sqrt{(E^0_{A^*B} + E^0_{AB^*})^2 - 4E^0_{A^*B}E^0_{AB^*} + 4V^2}}{2}. \tag{210}$$

and wave functions:

$$\Psi_+ = c_1|A^*B\rangle + c_2|AB^*\rangle \quad \text{and} \quad \Psi_- = c_2|A^*B\rangle - c_1|AB^*\rangle. \tag{211}$$

In the limiting case of degenerate zero-order states ($E^0_{A^*B} = E^0_{AB^*} = E^0$), Equations (210) and (211) become

$$\Psi_\pm = \frac{1}{\sqrt{2}}\left(|A^*B\rangle \pm |AB^*\rangle\right), \quad E_\pm = E^0 \pm V. \tag{212}$$

The magnitude and sign of the interaction between the two states depends on the distance between the chromophores and the relative orientation of their transition dipole moments. The dominant interactions are electrostatic. When the separation between the chromophores is large compared to the extension of the orbitals, only the long-range dipole-dipole electrostatic interaction usually needs to be considered. The electronic excitation of one of the chromophores induces a polarization of the orbitals of the other that can be described by a local transition dipole moment on either of the

chromophores. The interaction of the two dipole moments is then described by the dipole-dipole interaction

$$V(\theta_{\rm a}, \theta_{\rm b}, \phi) = \frac{\mu_{\rm a}\mu_{\rm b}}{4\pi\epsilon_0 R^3}(2\cos\theta_{\rm a}\cos\theta_{\rm b} + \sin\theta_{\rm a}\sin\theta_{\rm b}\cos\phi), \tag{213}$$

where $\theta_{a,b}$ are the angles between the transition dipoles of the two chromophore and the axis connecting them, ϕ is the dihedral angle between them, and $\mu_{a,b}$ are the magnitudes of the two transition dipole moments. Figure 52 shows three different geometric configurations of diphenylmethane with point-group symmetries C_2 (a), $C_{\rm s}$ (b) and $C_{2\rm v}$ (c). On the potential energy surface of the ground electronic state, structure (a) corresponds to the global minimum which possesses two energetically equivalent enantiomeric forms, whereas (b) and (c) are saddle points. To anticipate the manifestations of electronic excitation in this molecule, we apply Equation (213) to these structures. In the $C_{2\rm v}$-symmetric structure (c), the interaction between the transition dipole moments is maximized and the electronic excitation delocalized over the two rings. In the $C_{\rm s}$-symmetric structure, the transition dipole moments are perpendicular to each other and $V = 0$, leading to localized electronic excitations.

The analysis of the electronic spectra of a diphenylmethane crystal at low temperatures (Coffman and McClure 1958; McClure 1958) revealed a weak absorption band 145 $\rm cm^{-1}$above the origin of the first absorption band which was attributed to the upper member of the exciton pair. An excited state geometry of C_2 symmetry was inferred with a very similar geometry to that of the ground electronic state. In a delocalized excited system with C_2 symmetry, one exciton state has a transition dipole parallel to the C_2 axis and therefore has A symmetry, whereas the other has a transition dipole perpendicular to the C_2 axis and B symmetry. McClure (1958) thus concluded from Equation (213) that the sequence of excitons was A below B in diphenylmethane crystals, where A and B refer to the symmetry of the transition dipole in the C_2 point group.

The electronic transitions to these two electronic states, also labeled S_1 and S_2, were recently investigated by rotationally resolved laser-induced fluorescence spectroscopy in the unperturbed environment of a molecular jet (Stearns *et al.* 2008). The origins of the $S_1 \leftarrow S_0$ and $S_2 \leftarrow S_0$ transitions in (doubly deuterated) diphenylmethane-$d_{1,2}$ are shown in Figure 53(a) and Figure53(b), respectively. The rotational analysis of the $S_1 \leftarrow S_0$ transition of diphenylmethane and diphenylmethane-$d_{1,2}$ shows that *a*-type and *c*-type Q-branch transitions dominate the spectrum, which establishes the S_1 state as the delocalized antisymmetric combination of the two chromophore excitations (the principal axes *a*, *b* and *c* are defined in the caption of the figure). The origin of the $S_2 \leftarrow S_0$ transition, which appears shifted toward higher wave numbers by +123 $\rm cm^{-1}$ in diphenylmethane and +116 $\rm cm^{-1}$ in diphenylmethane-$d_{1,2}$, displays *b*-type Q-branch transitions and lacks the *a*-type Q-branch features present in the $S_1 \leftarrow S_0$ transition. This observation demonstrates that the transition dipole moment giving rise to the upper excitonic state is parallel to the C_2 axis, which further implies that the S_2 state corresponds to the symmetric combination of the two excitations. However, a complete rotational analysis of the $S_2 \leftarrow S_0$ transition was not possible because the vibronic coupling between the S_2 and S_1 states strongly perturbs the spectra. This example shows that rotationally resolved electronic

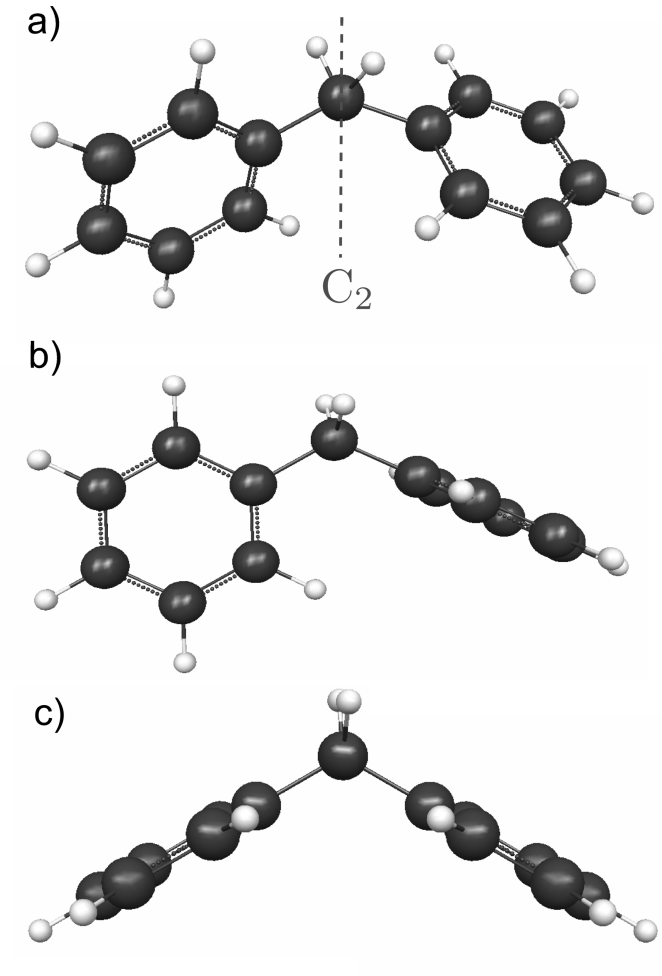

Figure 52: Geometric structures of diphenylmethane possessing C_2 (a), C_s and C_{2v} point-group symmetries, respectively. Structure (a) corresponds to the geometry of the global minimum of the ground electronic state potential energy surface. Structures (b) and (c) correspond to saddle points of this surface (Stearns *et al.* 2008). The principal axis system of structure c) has the b axis along the C_2 symmetry axis, the c axis pointing out of the plane of the page, and the a axis parallel to the line connecting the centers of mass of the two chromophores.

spectroscopy is possible in large molecules, and that it can provide insight into electronic excitations of complex systems. Further examples of rotationally resolved electronic spectra of large molecules are discussed in hrs054 (Pratt 2010a; Schmitt and Meerts 2010)

3.5 Nonradiative transitions

Electronically excited states of molecules can decay by fluorescence to lower-lying states. This process is governed by the same selection rules as photoexcitation. The excited states can also undergo nonradiative transitions which can have profound effects on the intensity distribution of electronic

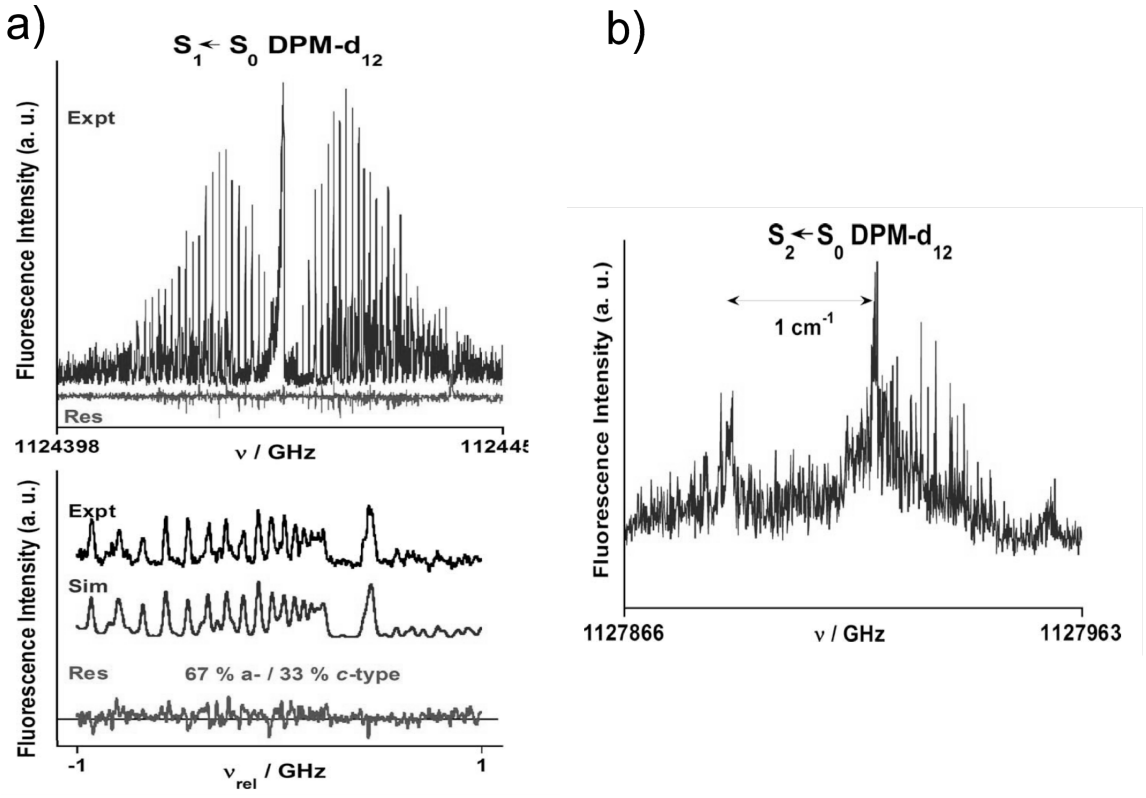

Figure 53: Rotationally resolved fluorescence excitation spectra of the $S_1 \leftarrow S_0$ (panel a) and $S_2 \leftarrow S_0$ (panel b) origin bands of diphenylmethane-$d_{1,2}$. The top panel in (a) shows the observed spectrum (blue line) and the residuals from a fit of the rotational structure (red line). The lower panel in (a) shows the central part of the spectrum and the residuals from a fit to *a*- and *c*-type transitions on an increased scale. (adapted from Stearns *et al.* (2008))

spectra. Nonradiative decay of an electronic state of an atom can only be observed above the lowest ionization threshold and leads to the emission of an electron. This process is termed autoionization (or preionization (Herzberg 1991)) and is illustrated schematically in Figure 54. Molecules can also decay through predissociation, if the electronic state lies above at least one dissociation threshold. Autoionization and predissociation are usually much faster than radiative decay and contribute to broaden absorption lines in electronic spectra by reducing the lifetime of the electronically excited state. In most molecular systems, several effects are in competition. Considering an isolated level (or, more correctly, an isolated resonance) of an electronic state that can decay through a nonradiative process, its linewidth Γ is proportional to its inverse lifetime τ^{-1} and, if further sources of decay (such as internal conversion, intersystem crossings, intramolecular energy redistribution, see below) are ignored, can be expressed as the sum of the autoionization Γ_a, predissociation Γ_p and radiative

Γ_r decay widths:

$$\Gamma = \Gamma_a + \Gamma_p + \Gamma_r. \tag{214}$$

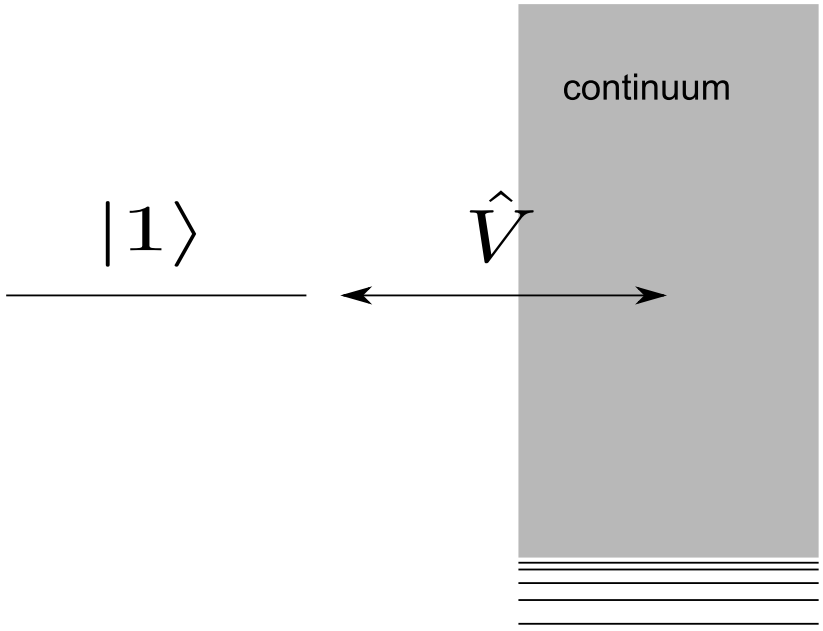

Figure 54: Generic illustration of the occurence of a resonance in autoionization or predissociation: an electronic level $|1\rangle$ is coupled to an (electronic or dissociative) continuum. The coupling is described by an interaction operator $\hat{V}$.

3.5.1 Autoionization

When an atom or a molecule is excited above its lowest ionization threshold, it can ionize either directly if excitation takes place to an ionization continuum or it can reach an excited state that decays subsequently by autoionization (i.e., an autoionization resonance). In this case, the electron is ejected by exchanging energy with the ionic core. Autoionization is classified according to the type of energy that is exchanged between the core and the electron as electronic, rotational, vibrational, spin-orbit and hyperfine autoionization. The process of autoionization is discussed in detail by Pratt (2010b) and its treatment by multichannel quantum defect theory by Jungen Jungen (2010a).

Autoionization occurs because the resonance that is populated is not an eigenstate of the molecular system. Usually, a resonance can decay to different final states of the molecular cation. Whereas the linewidth only provides information on the total decay rate, a measurement of the photoelectron kinetic energy distribution can provide information on the product states of the ion. It is useful to define a "partial linewidth" for the decay of an initial state characterized by the electronic, vibrational and rotational quantum numbers α, J, v to a final state of the molecular cation with the quantum

numbers α^+, J^+, v^+ and a photoelectron of energy ϵ. Defining the interaction matrix element between the discrete level $|1\rangle$ and the continuum to which it is coupled as $H_{1,\alpha,J,v;2,\epsilon,\alpha^+,J^+,v^+}$, the partial autoionization width can be estimated with Fermi's Golden Rule formula (Lefebvre-Brion and Field 2004)

$$\Gamma_{1,\alpha,J,v;2,\epsilon,J^+,v^+} = 2\pi \left| H_{1,\alpha,J,v;2,\epsilon,J^+,v^+} \right|^2 \tag{215}$$

In the case of an autoionizing Rydberg state with effective principal quantum number n^*, the electronic part I of the matrix element $H_{1;2}$ between the bound state and the continuum varies slowly with energy and the partial autoionization width becomes

$$\Gamma_{n,v;\epsilon,v^+} = 2\pi \frac{2R_M}{(n^*)^3} I^2 \langle v|v^+\rangle^2, \tag{216}$$

where R_M is the Rydberg constant. Autoionization proceeds through an exchange of energy between the Rydberg electron and the ionic core and, therefore, its probability is proportional to the Rydberg electron density in the region of the ionic core ($\propto n^{-3}$, see Section 2.1.6). The conceptually simplest case is that of purely electronic autoionization. Rydberg levels converging to an electronically excited level of the cation decay into the continuum of a lower-lying electronic state. The total electronic symmetry of the ion core - electron system must be the same for the discrete level and the continuum. An example is given by the $ns\sigma_g$ $^1\Pi_u$ Rydberg series converging to the A $^2\Pi_u$ state of N_2^+ which lies $\sim$ 9000 cm^{-1} above the X $^2\Sigma_g^+$ ground state of N_2^+. The levels with $n \geq 5$ are located above the ionization threshold and can decay into the $\epsilon p\pi_u$ $^1\Pi_u$ continuum associated with the ground electronic state. In general, this type of electronic autoionization is allowed when the two states (quasibound and continuum) are derived from configurations that differ by at most two orbitals because the interaction is mediated by electrostatic interactions between electron pairs, and is proportional to $1/r_{ij}$. Electronic autoionization is thus an example of processes that cannot be explained within the Hartree-Fock approximation.

Rotational autoionization has been studied in greatest details in the H_2 molecule (Herzberg and Jungen 1972; Jungen and Dill 1980). As an example, we consider the np-Rydberg states converging to the $N^+ = 0$ and $N^+ = 2$ thresholds of the vibronic ground state of H_2^+. The lowest-lying members of these Rydberg series ($n \leq 9$) are best described in Hund's case (b) and have either $^1\Sigma_u^+$ or $^1\Pi_u$ symmetry. Their energetic positions are given by Equation (58), where the quantum defect is μ_σ for $^1\Sigma_u^+$ levels and μ_π for $^1\Pi_u$ levels. Higher-lying Rydberg states are better described in Hund's case (d) (see Subsection 2.1.6). The autoionization width for the decay of a high Rydberg state of principal quantum number n converging to the threshold $N^+ = 2$ into the continuum of $N^+ = 0$ is given by

$$\Gamma_{n,J} = 2\pi \frac{2R_M}{(n^*)^3} \frac{J(J+1)}{(2J+1)^2} \left(\mu_\pi - \mu_\sigma\right)^2, \tag{217}$$

where μ_π and μ_σ are the quantum defects and J is the total angular momentum quantum number of the autoionizing level (Herzberg and Jungen 1972; Jungen and Dill 1980). The rate of rotational autoionization is thus seen to be related to the energy splitting between Σ and Π states that originates

from the nonspherical nature of the ionic core, or, equivalently, from the interaction between the Rydberg electron and the electric quadrupole of the ionic core.

Vibrational autoionization occurs when a Rydberg state converging to a vibrationally excited level of the cation decays into the continuum of a lower-lying vibrational state. The interaction is mediated by the nuclear kinetic energy operator. The potential energy curve of a Rydberg state with electronic angular momentum projection quantum number Λ, $V_{n,\Lambda}(R)$ is not strictly parallel to that of the molecular cation $V^+(R)$, which leads to a weak R-dependence of the quantum defect $\mu_\lambda(R)$ according to

$$U_{n\Lambda}(R) = U^+(R) - \frac{R_M}{(n-\mu_\lambda(R))^2}. \tag{218}$$

Defining $n^* = n - \mu_{\lambda,(R=R_e^+)}$ and keeping only the linear term of a Taylor expansion of $\mu_\lambda(R)$, one can express the linewidth for vibrational autoionization of the level n, v^+ into the continuum $v^+ - 1$ as (Herzberg and Jungen 1972)

$$\Gamma_{n,v^+-1} = 2\pi \frac{2R_M}{(n^*)^3} \left[\frac{d\mu_\lambda}{dR}\right]^2 \langle \phi^{v^+} | \hat{R} - R_e^+ | \phi^{v^+-1} \rangle. \tag{219}$$

In the harmonic approximation, the only nonzero matrix elements of the $(\hat{R} - R_e^+)$ operator are $\Delta v = \pm 1$, which gives rise to a strong propensity rule in vibrational autoionization (Berry 1966; Herzberg and Jungen 1972). In H_2, the width for $\Delta v = -2$ autoionization is typically two orders of magnitude smaller than for $\Delta v = -1$ (Lefebvre-Brion and Field 2004).

Spin-orbit autoionization affects Rydberg levels lying between different multiplet components of the cation. The best known example are the rare gas atoms Rg= Ne, Ar, Kr and Xe (see e.g. Beutler (1935); Lu (1971); Wörner *et al.* (2005), and also Figures 38 and 39). Rydberg levels converging to the $^2P_{1/2}$ level of the Rg^+ ion can decay into the continuum associated with the $^2P_{3/2}$ level. Spin-orbit autoionization also occurs in molecules, for example in O_2. Rydberg states converging to the $^2\Pi_{3/2}$ upper spin-orbit component of the X^+ ground state of O_2^+ can decay into the continuum associated with the $^2\Pi_{1/2}$ lower spin-orbit component. As an example, we consider the $(p\pi)(ns\sigma)$ $^3\Pi_1$ and $^1\Pi_1$ Rydberg series converging to the X^+ $^2\Pi$ state of O_2^+. The lowest members of these series are best described in Hund's case (a) because the exchange interaction is much larger than the spin-orbit interaction in the cation (see analogous discussion for the rare gas atoms in Subsection 3.2.2). Therefore, their energetic position follows the Rydberg formula (Eq. (58)) with quantum defects μ_3 and μ_1 for the $^3\Pi_1$ and $^1\Pi_1$ levels, respectively. The autoionization linewidth of the Rydberg levels converging to the X^+ $^2\Pi_{3/2}$ substate into the continuum of the X^+ $^2\Pi_{1/2}$ substate is given by (Lefebvre-Brion and Field 2004)

$$\Gamma_n = 2\pi \frac{2R}{(n^*)^3} \left(\frac{\mu_3 - \mu_1}{2}\right)^2. \tag{220}$$

Consequently, spin-orbit autoionization can be considered to be a consequence of the nondegeneracy of singlet and triplet levels that is caused by the exchange interaction.

Hyperfine autoionization has been discussed only very recently (Wörner *et al.* 2005) because it can only be observed at very high spectral resolution and in very high Rydberg states. It occurs when Rydberg levels converging to an excited hyperfine structure component of an ionic fine-structure level decay into the continuum associated with a lower-lying hyperfine component of the same fine-structure level. The simplest case is the decay of np Rydberg levels converging to the $F^+ = 0$ level of the $^2S_{1/2}$ ground state of $^3He^+$ (with nuclear spin $I = 1/2$) into the continuum of the lower-lying $F^+ = 1$ level. The hyperfine autoionization linewidth can also be estimated with Eq. (220) where μ_3 and μ_1 are the quantum defects in LS coupling of the $^3P_1$ and $^1P_1$ Rydberg series of He, respectively. The hyperfine interval of the $^2S_{1/2}$ state of $^3He^+$ amounts to only 0.2888 cm^{-1} (Fortson *et al.* 19660, setting a lower limit of $n \approx 620$ for the lowest level that can decay by hyperfine autoionization. In the heavier rare gas atoms, e.g. ^{83}Kr, ^{129}Xe, and ^{131}Xe, hyperfine autoionization rates have been predicted by calculations (Wörner *et al.* 2005; Paul *et al.* 2009).

The discussion so far on was based on the implict assumption of Lorentzian line shapes, which are observed when photoexcitation populates exclusively the resonance and direct ionization is forbidden (see Figure 5b of Merkt *et al.* (2010)). In most atomic and molecular systems, the selection rules allow both the excitation of the quasibound state and the continuum. Two pathways to the same final state exist, which results in interference phenomena and in deviations of the observed line shapes from Lorentzian profiles (Fano 1961). In the case of an isolated resonance interacting with one continuum, the line shape is described by the Beutler-Fano formula Fano (1961)

$$\sigma_a = \sigma_d + \sigma_i \frac{(q+\epsilon)^2}{1+\epsilon^2}, \tag{221}$$

where σ_d represents the cross-section for direct excitation of the continuum and σ_i that for the excitation of the quasibound state. The lineshape is characterized by the parameters $\epsilon = (E - E_r)/(\Gamma/2)$, where E_r and Γ are the energy and full width of the resonance state, and q characterizes the interaction between the bound state and the continuum (see Fano (1961)). The limit $q \to \pm\infty$ corresponds to a Lorentzian line shape, whereas for $q = 0$, the resonance appears as a local minimum in the cross-section also called a "window resonance" (see Figure 5 of Merkt *et al.* (2010)).

The Beutler-Fano formula has been generalized to the case overlapping resonances by Mies (1968) and to the case of two interacting continua by Beswick and Lefebvre (1975). In most systems, multiple overlapping resonances interact with multiple continua. In such cases, multichannel quantum defect theory (see Jungen (2010a)) is required to achieve a quantitative understanding of the spectral structures.

3.5.2 Predissociation

Predissociation is a process by which a nominally bound vibrational level decays into atomic or molecular fragments through coupling to a dissociation continuum. Two different types of predissociation have been characterized: predissociation by rotation and electronic predissociation.

Predissociation by rotation occurs for levels with $J > 0$ when the centrifugal energy $\hbar^2 J(J+1)/2\mu R^2$ added to the potential energy curve is large enough to lead to the appearance of quasibound levels. Such levels lie above the dissociation threshold of their electronic state but are trapped behind a centrifugal barrier (see also hrs093Schinke (2010)).

Electronic predissociation occurs when a bound vibrational level of an electronically excited state decays by coupling to the dissociation continuum of another electronic state. The potential energy curves of the two electronic states do not necessarily have to cross.

The mixing of a bound state $\Psi_{1,\alpha,v,J}$ with a state in a dissociation continuum $\Psi_{2,\alpha,E,J}$ is described by the matrix element

$$H_{v,J;E,J} = \langle \Psi_{1,\alpha,v,J} | V | \Psi_{2,\alpha,E,J} \rangle = \langle \phi_1(\vec{r},\vec{R}) \chi_{v,J}(\vec{R}) | H | \phi_2(\vec{r},\vec{R}) \chi_{E,J}(\vec{R}) \rangle, \tag{222}$$

where $\vec{r}$ and ϕ are the electronic coordinates and wave functions, respectively, $\vec{R}$ and χ are the vibrational coordinates and wave functions, respectively, and E is the kinetic energy of the free nuclei in the continuum. The continuum states are taken to be energy normalized. Fano's theory of resonances shows how the discrete state amplitude is mixed into the continuum eigenfunctions (Fano 1961). When $H_{v,J;E,J}$ varies slowly with energy, the admixture of the bound level into the continuum is a Lorentzian function, with predissociation linewidth $\Gamma_{E,\alpha,v,J}$ given by

$$\Gamma_{E,\alpha,v,J} = 2\pi \left| V_{v,J;E,J} \right|^2 . \tag{223}$$

In diatomic molecules, if the electronic matrix element $H_{v,J;E,J}$ varies slowly with the internuclear separation R, the matrix element can be factorized into an electronic and a vibrational part

$$H_{v,J;E,J} = \langle \phi_1(r,R) | V | \phi_2(r,R) \rangle \langle \chi_{v,J}(R) \chi_{E,J}(R) \rangle, \tag{224}$$

in which case the predissociation linewidth can be expressed as a product of an electronic and a vibrational factor

$$\Gamma_{E,J} = 2\pi \left| V_{\mathrm{e}} \right|^2 \langle \chi_{v,J}(R) | \chi_{E,J}(R) \rangle^2 . \tag{225}$$

3.5.3 Dynamics in large polyatomic molecules

In addition to the decay mechanisms of predissociation and autoionization discussed above, and which are the dominant decay mechanisms in small molecules, large polyatomic molecules can be subject to additional types of nonradiative transitions. The different kinds of dynamics are often described in terms of so-called "bright" and "dark" states, which can be regarded as "fictive" zero-order levels in the absence of interactions between the levels. The bright state can be populated by the absorption of a photon as illustrated in Figure 55 while the excitation to the dark states is forbidden. When the interaction between bright and dark states is considered, the dark state becomes optically accessible. The Herzberg-Teller coupling mechanism discussed in Subsection 3.4.2 may be described in this language, the dark state being the electronically forbidden but vibronically allowed state.

Different types of couplings can be distinguished, associated with the phenomena known as intersystem crossing (ISC), internal conversion (IC) and internal vibrational redistribution (IVR). In a time-dependent picture, the molecule can be thought of as being first excited to a bright state and subsequently evolving according to the couplings to isoenergetic dark states. When only few states are coupled, for instance because the molecule is small or it possesses a high symmetry, periodic motions occur, leading to distinct structures in the absorption spectrum and recurrence phenomena in time-domain experiments. If the bright state is coupled to a dense manifold of dark states, the long-time behavior mimics an irreversible decay following Fermi's Golden Rule. This usually results in structureless absorption spectra.

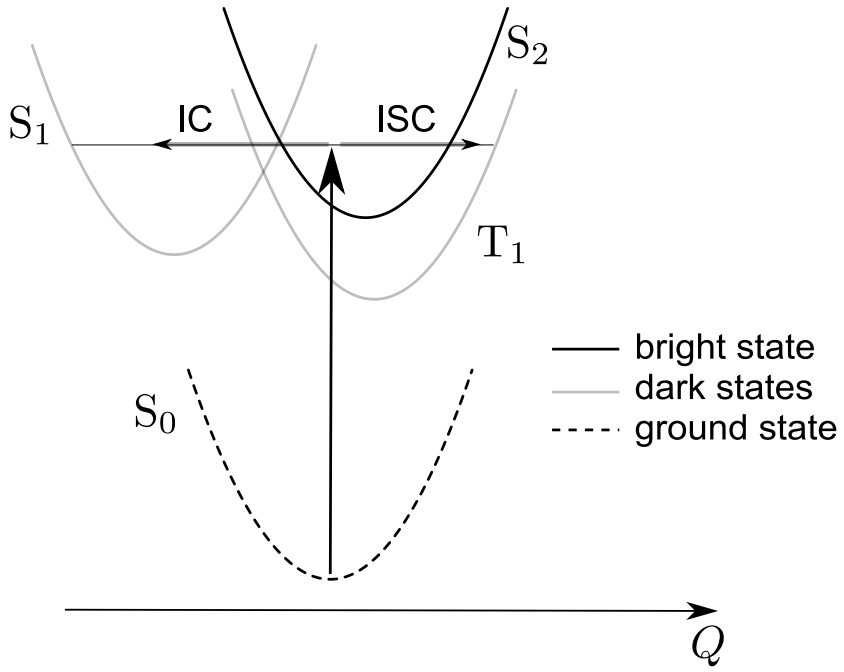

Figure 55: Schematic representation of the potential energy surfaces of a polyatomic molecule as a function of a vibrational coordinate Q of the molecule. The absorption of a photon excites the molecule from the singlet electronic ground state S_0 into a bright state S_2, which subsequently decays into a set of dark states through internal conversion (to another singlet state, S_1) or through intersystem crossing into a triplet state (T_1).

Intersystem crossing (ISC) arises from the spin-orbit coupling between electronic states of different multiplicities. Typically, it occurs between the vibrational levels of an excited singlet state that are mixed with the dense manifold of vibronic levels of a lower-lying triplet state. In diatomic molecules, the singlet-triplet (spin-orbit) interaction matrix element is easily decomposed into an electronic and a vibrational overlap factor. The situation is more complex in polyatomic molecules. The interaction between two electronic states of similarly shaped potential energy surfaces decreases continuously with increasing energy separation (an effect often refered to as the "energy-gap rule"). If the potential

energy surfaces differ significantly in shape, a small number of "active" vibrational modes usually mediate the coupling and the corresponding vibrational levels are called "doorway states". In this case, ISC becomes mode specific.

Internal conversion (IC) is a dynamical process that conserves the total spin of the molecule ($\Delta S = 0$). In diatomic molecules, potential energy functions of the same symmetry cannot cross (a fact refered to as the "noncrossing rule"). In polyatomic molecules, this rule no longer applies because certain vibrational modes distort the molecule and change its point-group symmetry. Two electronic states may thus have different quantum numbers in a high-symmetry region but the same quantum numbers in a region of lower symmetry, leading to conical intersections. A special case of conical intersections arises from the Jahn-Teller effect and has been discussed in Section 2.3.6 (see 30).

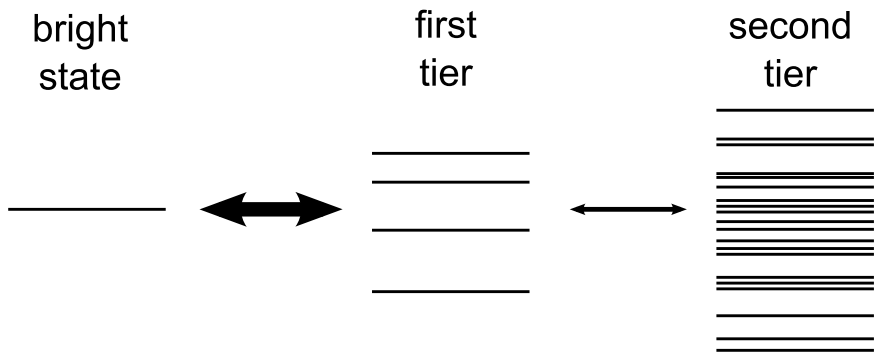

Figure 56: Schematic representation of the mechanism of internal vibrational redistribution. The level initially populated by photoabsorption decays into a set of "first tier" states that are usually strongly coupled to the bright state. The molecule subsequently decays into a denser "second tier" of states that are more weakly coupled to the first tier.

Intramolecular vibrational redistribution (IVR) differs from ISC and IC in that it does not result from the coupling of different electronic states. It occurs between near-resonant vibrational levels of the same electronic state by rovibrational interaction (Coriolis interaction, Fermi interaction and high-order anharmonic interaction, see Quack and coworkers (2010)) and is also highly specific to the molecule. A bright state is typically only strongly coupled to a relatively sparse group of dark levels, known as the "first tier" of states as represented in Figure 56. These levels are also called "doorway states" because they are usually more weakly coupled to a second denser set of states, known as "second tier". The molecule is prepared in the bright state through the absorption of a photon and subsequently decays through the first tier into the second tier of levels. IVR thus leads to a rapid redistribution of the energy of the absorbed photon into vibrational degrees of freedom of the molecule.

Acknowledgements

We thank Dr. Urs Hollenstein (ETH Zurich) for his help in the preparation of the figures and Drs. Martin Schäfer and Julie Michaud (both ETH Zurich) for their useful comments on the manuscript. F. M. also thanks Dr. Pierre Pillet and the Laboratoire Aimé Cotton du CNRS (Orsay, France) for their hospitality during the summer 2009 when part of this article was written.

Further reading list

General spectroscopy:

- G. Herzberg, *Molecular Spectra and Molecular Structure*, Vol. I: Spectra of Diatomic Molecules, Krieger Publishing Company, Malabar, 1989
- G. Herzberg, *Molecular Spectra and Molecular Structure*, Vol. II: Infrared and Raman Spectra of Polyatomic Molecules, Krieger Publishing Company, Malabar, 1991
- G. Herzberg, *Molecular Spectra and Molecular Structure*, Vol. III: Electronic Spectra and Electronic Structure of Polyatomic Molecules, Krieger Publishing Company, Malabar, 1991
- E.U. Condon and G.H. Shortley, *The Theory of Atomic Spectra*, Cambridge University Press, Cambridge, 1935
- H.W. Kroto, *Molecular Rotation Spectra*, John Wiley & Sons, London, 1975 [republication: Dover Publications, New York, 1992]
- C.H. Townes and A.L. Schawlow, *Microwave Spectroscopy*, McGraw-Hill, New York, 1955 [republication: Dover Publications, New York, 1975]
- J.M. Hollas, *High Resolution Spectroscopy*, 2nd edition, John Wiley & Sons, 1998
- W. Demtröder, *Laser Spectroscopy*, 3rd edition, Springer-Verlag, Berlin, 2003

General and molecular Quantum mechanics

- L. D. Landau and E. M. Lifshitz, *Quantum mechanics: non-relativistic theory*, Course of Theoretical Physics, Vol. 3, 3rd edition (reprinted) Pergamon Press, Oxford, 1985
- A. Messiah, *Quantum Mechanics*, Vols. 1 & 2, North Holland, Amsterdam, 1961
- P.W. Atkins and R.S. Friedman, *Molecular Quantum Mechanics*, 4th edition, Oxford University Press, Oxford, 2004

Rydberg states

- T.F. Gallagher, *Rydberg Atoms*, Cambridge University Press, Cambridge, 1994

Multichannel quantum defect theory

- Ch. Jungen (Ed.), *Molecular Applications of Quantum Defect Theory*, Institute of Physics Publishing, Bristol and Philadelphia, 2003

Diatomic molecules

- H. Lefebvre-Brion and R.W. Field, *The Spectra and Dynamics of Diatomic Molecules*, 2nd edition (of *Perturbations in the Spectra of Diatomic Molecules*), Elsevier Academic Press, Amsterdam, 2004
- J.M. Brown and A. Carrington, *Rotational Spectroscopy of Diatomic Molecules*, Cambridge University Press, Cambridge, 2003

Hyperfine Structure

- T. M. Dunn, in *Nuclear Hyperfine Structure in the Electronic Spectra of Diatomic Molecules*, in *Molecular Spectroscopy: Modern Research*, K.N. Rao and C. W. Mathews (eds.), Academic Press, 1972, p. 231-257

Angular momentum

- R.N. Zare, *Angular Momentum*, John Wiley & Sons, New York, 1988

Group theory

- M. Tinkham, *Group Theory and Quantum Mechanics*, McGraw-Hill, New York, 1964
- P.R. Bunker and P. Jensen, *Molecular Symmetry and Spectroscopy*, 2nd edition, NRC Research Press, Ottawa, 1998
- A. Vincent, *Molecular Symmetry and Group Theory*, 2nd edition, John Wiley & Sons, Chichester, 2001

Vibronic Coupling and Dynamics of Polyatomic Molecules

- I. B. Bersuker, *The Jahn-Teller effect*, Cambridge University Press, 2006
- W. Domcke, D.R. Yarkony and H. Köppel (ed.), *Conical intersections: Electronic structure, dynamics and spectroscopy*, *Advanced Series in Physical Chemistry* **15**, 2004
- W. Domcke, G. Stock, Theory of ultrafast nonadiabatic excited-state processes and their spectroscopic detection in real time, *Advances in Chemical Physics*, 1997, Wiley, New York
- M. Quack, Molecular quantum dynamics from high resolution spectroscopy and laser chemistry, J. Mol. Struct. **292**, pp. 171-196 (1993)

- D. J. Nesbitt and R. W. Field, Vibrational Energy Flow in Highly Excited Molecules: Role of Intramolecular Vibrational Redistribution, J. Phys. Chem. **100**, pp. 12735-12756 (1996)

Constants

- K.P. Huber and G. Herzberg, *Molecular Spectra and Molecular Structure*, Vol. IV: Constants of diatomic molecules, Van Nostrand Reinhold, New York, 1979
- P.F. Bernath, Diatomic database: http://diref.uwaterloo.ca/
- C.E. Moore, *Atomic Energy Levels*, Natl. Bur. Stand. (U.S.) Circular 467 Vol. I (1949) (H through V); Vol. II (1952) (Cr through Nb); and Vol. III (1958) (Mo through La, Hf through Ac). (U.S. Gov. Printing Office, Washington, D.C).
  NIST Atomic Spectra Database: http://physics.nist.gov/PhysRefData/

References

Applegate, B. E., Bezant, A. J., and Miller, T. A. (2001a) The Jahn-Teller and related effects in the cyclopentadienyl radical. II. Vibrational analysis of the $\tilde{A}\ ^2A_2''$ - $\tilde{X}\ ^2E_1''$ electronic transition. *J. Chem. Phys.*, **114** (11), 4869–4882.

Applegate, B. E., Miller, T. A., and Barckholtz, T. A. (2001b) The Jahn-Teller and related effects in the cyclopentadienyl radical. I. The *ab initio* calculation of spectroscopically observable parameters. *J. Chem. Phys.*, **114** (11), 4855–4868.

Ashfold, M. N. R., King, G. A., Nix, M. G. D., and Oliver, T. A. A. (2010) High-resolution Photofragment Translational Spectroscopy using Rydberg Tagging Methods, *in* Quack, M. and Merkt, F., (eds.) *Handbook of High Resolution Spectroscopy*, Wiley, Chichester, New York.

Barckholtz, T. A. and Miller, T. A. (1998) Quantitative insights about molecules exhibiting Jahn–Teller and related effects. *Int. Rev. Phys. Chem.*, **17** (4), 435–524.

Bauder, A. (2010) Fundamentals of Molecular Rotational Spectra, *in* Quack, M. and Merkt, F., (eds.) *Handbook of High Resolution Spectroscopy*, Wiley, Chichester, New York.

Berry, R. S. (1966) Ionization of Molecules at Low Energies. *J. Chem. Phys.*, **45**, 1228.

Bersuker, I. B. (2006) *The Jahn-Teller effect*, Cambridge University Press, Cambridge UK.

Beswick, J. A. and Lefebvre, R. (1975) On a level shift occurring in the treatment of a discrete state coupled to two interacting continua. *Mol. Phys.*, **29**, 1611–1614.

Bethe, H. A. and Salpeter, E. E. (1957) *Quantum Mechanics of One- and Two-Electron Atoms*, Springer, Berlin.

Beutler, H. (1935) Über Absorptionsserien von Argon, Krypton und Xenon zu Termen zwischen den beiden Ionisierungsgrenzen $^2P^o_{3/2}$ und $^2P^o_{1/2}$. *Z. Phys.*, **93** (3–4), 177–196.

Bohr, N. (1914) The spectra of helium and hydrogen. *Philosophical Magazine*, **26**, 857–875.

Borden, W. T. (1982) *Diradicals*, John Wiley and Sons, New York.

Breidung, J. and Thiel, W. (2010) Predictions of Vibrational Spectra from Ab Initio Theory, *in* Quack, M. and Merkt, F., (eds.) *Handbook of High Resolution Spectroscopy*, Wiley, Chichester, New York.

Brevet, P. F., Pellarin, M., and Vialle, J. L. (1990) Stark effect in argon Rydberg states. *Phys. Rev. A*, **42** (3), 1460–1466.

Brodsky, S. J. and Parsons, R. G. (1967) Precise theory of the Zeeman spectrum for atomic hydrogen and deuterium and the Lamb shift. *Phys. Rev.*, **163**, 134–146.

Brown, J. M. and Carrington, A. (2003) *Rotational Spectroscopy of Diatomic Molecules*, Cambridge University Press, Cambridge.

Bunker, P. R. and Jensen, P. (1998) *Molecular Symmetry and Spectroscopy*, NRC Research Press, Ottawa, 2nd ed.

Callegari, C. and Ernst, W. E. (2010) Helium Droplets as Nanocryostats for Molecular Spectroscopy - from the Vacuum Ultraviolet to the Microwave Regime, *in* Quack, M. and Merkt, F., (eds.) *Handbook of High Resolution Spectroscopy*, Wiley, Chichester, New York.

Callomon, J. H., Dunn, T. M., and Mills, I. M. (1966) Rotational Analysis of the 2600 angstrom Absorption System of Benzene. *Phil. Trans. Roy. Soc. A*, **259**, 499–532.

Carrington, A., Gammie, D. I., Page, J. C., Shaw, A. M., and Taylor, S. M. (1999) Microwave electronic spectrum of the $Ne\cdots Ne^+$ long-range complex. *Phys. Chem. Chem. Phys.*, **1** (1), 29–36.

Carrington, A., Pyne, C. H., Shaw, A. M., Taylor, S. M., Hutson, J. M., and Law, M. M. (1996) Microwave spectroscopy and interaction potential of the long-range He-Kr^+ ion: An example of Hund's case (e). *J. Chem. Phys.*, **105** (19), 8602–8614.

Carrington, T. (2010) Using Iterative Methods to Compute Vibrational Spectra, *in* Quack, M. and Merkt, F., (eds.) *Handbook of High Resolution Spectroscopy*, Wiley, Chichester, New York.

Cheng, B.-M., Lu, H.-C., Chen, H.-K., Bahou, M., Lee, Y.-P., Mebel, A. M., Lee, L. C., Liang, M.-C., and Yung, Y. L. (2006) Absorption Cross Sections of NH_3, NH_2D, NHD_2, and ND_3 in the Spectral Range 140-220 nm and Implications for Planetary Isotopic Fractionation. *Astrophys. J.*, **647**, 1535.

Coffman, R. and McClure, D. S. (1958) The electronic spectra of crystalline toluene, dibenzyl, diphenylmethane, and biphenyl in the near ultraviolet. *Can. J. Chem.*, **36**, 48–58.

Cohen, J. S. and Schneider, B. (1974) Ground and excited states of Ne_2 and Ne_2^+. I. Potential curves with and without spin-orbit coupling. *J. Chem. Phys.*, **61** (8), 3230–3239.

Domcke, W., Yarkony, D. R., and Köppel, H., (eds.) (2004) *Conical intersections: Electronic structure, dynamics and spectroscopy*, vol. 15 of *Adv. Ser. in Phys. Chem.*

Dunn, T. M. (1972) Nuclear hyperfine structure in the electronic spectra of diatomic molecules, *in* Rao, K. N. and Mathews, C. W., (eds.) *Molecular Spectroscopy: Modern Research*, Academic Press, New York, vol. 1, p. Chapter 4.4.

Eikema, K. S. E. and Ubachs, W. (2010) Precision Laser Spectroscopy in the Extreme Ultraviolet, *in* Quack, M. and Merkt, F., (eds.) *Handbook of High Resolution Spectroscopy*, Wiley, Chichester, New York.

Enz, C. P. (2002) *No time to be brief - A scientific biography of Wofgang Pauli*, Oxford University Press, Oxford and New York.

Ernst, W. E., Softley, T. P., and Zare, R. N. (1988) Stark-effect studies in xenon autoionizing Rydberg states using a tunable extreme-ultraviolet laser source. *Phys. Rev. A*, **37** (11), 4172–4183.

Essen, L., Donaldson, R. W., Bangham, M. J., and Hope, E. G. (1971) Frequency of the hydrogen maser. *Nature*, **229**, 110–111.

Etzkorn, T., Klotz, B., S/orensen, S., Patroescu, I. V., Barnes, I., Becker, K. H., and Platt, U. (1999) Gas-phase absorption cross sections of 24 monocyclic aromatic hydrocarbons in the UV and IR spectral ranges. *Atmos. Environ.*, **33**, 525–540.

Fano, U. (1961) Effects of Configuration Interaction on Intensities and Phase Shifts. *Phys. Rev.*, **124** (6), 1866–1878.

Field, R. W., Baraban, J. H., Lipoff, S. H., and Beck, A. R. (2010) Effective Hamiltonians for Electronic Fine Structure and Polyatomic Vibrations, *in* Quack, M. and Merkt, F., (eds.) *Handbook of High Resolution Spectroscopy*, Wiley, Chichester, New York.

Fielding, H. H. and Softley, T. P. (1991) Observation of the Stark effekt in autoionising Rydberg states of molecular hydrogen. *Chem. Phys. Lett.*, **185** (3–4), 199–205.

Fischer, M., Kolachevsky, N., Zimmermann, M., Holzwarth, R., Undem, T., Hänsch, T. W., Abgrall, M., Grünert, J., Maksimovic, I., Bize, S., Marion, H., Santos, F. P. D., Lemonde, P., Santarelli, G., Laurent, P., Clairon, A., Salomon, C., Haas, M., Jentschura, U. D., and Keitel, C. H. (2004) New limits on the drift of fundamental constants from laboratory measurements. *Phys. Rev. Lett.*, **92**, 230802.

Fortson, E. N., Major, F. G., and Dehmelt, H. G. (1966) Ultrahigh Resolution $\Delta F = 0, \pm 1$ $(He^3)^+$ Hfs Spectra by an Ion-Storage Collision Technique. *Phys. Rev. Lett.*, **16** (6), 221–225.

Frosch, R. A. and Foley, H. M. (1952) Magnetic Hyperfine Structure in Diatomic Molecules. *Phys. Rev.*, **88** (6), 1337–1349.

Gallagher, T. F. (1988) Rydberg Atoms. *Rep. Prog. Phys.*, **51** (2), 143–188.

Gallagher, T. F. (1994) *Rydberg Atoms*, Cambridge University Press, Cambridge.

Grütter, M., Zehnder, O., Softley, T. P., and Merkt, F. (2008) Spectroscopic study and multichannel quantum defect theory analysis of the Stark effect in Rydberg states of neon. *J. Phys. B: At. Mol. Opt. Phys.*, **41** (11), 115001.

Guennoun, Z. and Maier, J. P. (2010) Electronic Spectroscopy of Transient Molecules, *in* Quack, M. and Merkt, F., (eds.) *Handbook of High Resolution Spectroscopy*, Wiley, Chichester, New York.

Herzberg, G. (1989) *Molecular Spectra and Molecular Structure, Volume I, Spectra of Diatomic Molecules*, Krieger Publishing Company, Malabar, 2nd ed.

Herzberg, G. (1991) *Molecular Spectra and Molecular Structure, Volume III, Electronic Spectra and Electronic Structure of Polyatomic Molecules*, Krieger Publishing Company, Malabar, 2nd ed.

Herzberg, G. and Jungen, Ch. (1972) Rydberg series and ionization potential of the H_2 molecule. *J. Mol. Spectrosc.*, **41** (3), 425–486.

Hogan, S. D., Seiler, Ch., and Merkt, F. (2009) Rydberg-state-enabled deceleration and trapping of cold molecules. *Phys. Rev. Lett.*, **103** (12), 123001.

Hollenstein, U. (2003) *Erzeugung und spektroskopische Anwendungen von schmalbandiger, kohärenter, vakuum-ultravioletter Strahlung*, PhD thesis, Eidgenössische Technische Hochschule Zürich, ETH Zürich, CH-8093 Zürich, Switzerland, Diss. ETH Nr. 15237.

Hougen, J. T., Bunker, P. R., and Johns, J. W. C. (1970) The vibration-rotation problem in triatomic molecules allowing for a large-amplitude bending vibration. *J. Mol. Spectrosc.*, **34** (1), 136–172.

Huber, K. P. and Herzberg, G. (1979) *Molecular Spectra and Molecular Structure, Volume IV, Constants of Diatomic Molecules*, Van Nostrand Reinhold Company, New York.

Hund, F. (1926a) Zur Deutung der Molekelspektren. I. *Z. Phys.*, **40** (10), 742–764.

Hund, F. (1926b) Zur Deutung einiger Erscheinungen in den Molekelspektren. *Z. Phys.*, **36** (9–10), 657–674.

Hund, F. (1927a) *Linienspektren und Periodisches System der Elemente*, Springer, Berlin.

Hund, F. (1927b) Symmetriecharaktere von Termen bei Systemen mit gleichen Partikeln in der Quantenmechanik. *Z. Phys.*, **43** (11–12), 788–804.

Hund, F. (1927c) Zur Deutung der Molekelspektren. II. *Z. Phys.*, **42** (2–3), 93–120.

Hund, F. (1927d) Zur Deutung der Molekelspektren. III. *Z. Phys.*, **43** (11–12), 805–826.

Hund, F. (1928) Zur Deutung der Molekelspektren. IV. *Z. Phys.*, **51** (11–12), 759–795.

Hund, F. (1930) Zur Deutung der Molekelspektren. V. Die angeregten Elektronenterme von Molekeln mit zwei gleichen Kernen (H_2, He_2, Li_2, N_2^+, N_2 ...). *Z. Phys.*, **63** (11–12), 719–751.

Hund, F. (1933) *Allgemeine Quantenmechanik des Atom- und Molekelbaues*, Springer, Berlin, pp. 561–694.

Jahn, H. A. and Teller, E. (1937) Stability of Polyatomic Molecules in Degenerate Electronic States. I. Orbital Degeneracy. *Proc. R. Soc. London Ser. A*, **161** (905), 220–235.

Johns, J. W. C., Ramsay, D. A., and Ross, S. C. (1976) The $\tilde{A}\ ^2A_1$ - $\tilde{x}\ ^2b_1$ absorption spectrum of NH_2 between 6250 and 9500 Å. *Can. J. Phys.*, **54**, 1804 –1814.

Jungen, Ch.. (2010a) Elements of Quantum Defect Theory, *in* Quack, M. and Merkt, F., (eds.) *Handbook of High Resolution Spectroscopy*, Wiley, Chichester, New York.

Jungen, Ch. and Dill, D. (1980) Calculation of rotational–vibrational preionization in H_2 by multichannel quantum defect theory. *J. Chem. Phys.*, **73** (7), 3338–3345.

Jungen, M. (2010b) Ab Initio Calculations for Rydberg States, *in* Quack, M. and Merkt, F., (eds.) *Handbook of High Resolution Spectroscopy*, Wiley, Chichester, New York.

Kim, N. J., Jeong, G., Kim, Y. S., Sung, J., Kim, S. K., and Park, Y. D. (2000) Resonant two-photon ionization and laser induced fluorescence spectroscopy of jet-cooled adenine. *J. Chem. Phys.*, **113** (22), 10051–10055.
URL: *http://link.aip.org/link/?JCP/113/10051/1*

Kolachevsky, N., Matveev, A., Alnis, J., Parthey, C. G., Karshenboim, S. G., and Hänsch, T. W. (2009) Measurement of the 2S hyperfine interval in atomic hydrogen. *Phys. Rev. Lett.*, **102**, 213002.

Kopfermann, H. (1958) *Nuclear Moments*, Academic Press, New York.

Köppel, H., Cederbaum, L. S., and Domcke, W. (1984) Strong non-adiabatic effects in $C_2D_4^+$. *Chem. Phys. Lett.*, **110** (5), 469–473.

Köppel, H., Cederbaum, L. S., and Mahapatra, S. (2010) Theory of the Jahn-Teller Effect, *in* Quack, M. and Merkt, F., (eds.) *Handbook of High Resolution Spectroscopy*, Wiley, Chichester, New York.

Lamb, W. E. and Retherford, R. C. (1947) Fine Structure of the Hydrogen Atom by a Microwave Method. *Phys. Rev.*, **72**, 241–243.

Lee, C.-M. and Lu, K. T. (1973) Spectroscopy and Collision Theory. II. The Ar Absorption Spectrum. *Phys. Rev. A*, **8** (3), 1241–1257.

Lefebvre-Brion, H. and Field, R. W. (2004) *The Spectra and Dynamics of Diatomic Molecules*, Elsevier, Amsterdam.

Lindgård, A. and Nielsen, S. E. (1977) Transition probabilities for the alkali isoelectronic sequences Li I, Na I, K I, Rb I, Cs I, Fr I. *At. Data Nucl. Data Tables*, **19** (6), 533–633.

Lu, K. T. (1971) Spectroscopy and Collision Theory. The Xe Absorption Spectrum. *Phys. Rev. A*, **4** (2), 579–596.

Lundeen, S. R. and Pipkin, F. M. (1986) Separated oscillatory field measurement of the Lamb shift in H, $n = 2$. *Metrologia*, **22**, 9–54.

Marquardt, R. and Quack, M. (2010) Global Potential Hypersurfaces for Molecular Spectroscopy, *in* Quack, M. and Merkt, F., (eds.) *Handbook of High Resolution Spectroscopy*, Wiley, Chichester, New York.

Mastalerz, R. and Reiher, M. (2010) Relativistic Electronic Structure Theory for Molecular Spectroscopy, *in* Quack, M. and Merkt, F., (eds.) *Handbook of High Resolution Spectroscopy*, Wiley, Chichester, New York.

McClure, D. S. (1958) Energy transfer in molecular crystals and in double molecules. *Can. J. Chem.*, **36**, 59–71.

Merkt, F. (1997) Molecules in High Rydberg States. *Ann. Rev. Phys. Chem.*, **48**, 675–709.

Merkt, F., Willitsch, S., and Hollenstein, U. (2010) High-resolution Photoelectron Spectroscopy, *in* Quack, M. and Merkt, F., (eds.) *Handbook of High Resolution Spectroscopy*, Wiley, Chichester, New York.

Metcalf, H. J. and van der Straten, P. (2003) Laser cooling and trapping of atoms. *Journal of the Optical Society of America. B, Optical physics*, **20** (5), 887–908.

Mies, F. H. (1968) Configuration Interaction Theory. Effects of Overlapping Resonances. *Phys. Rev.*, **175**, 164–175.

Miron, C. and Morin, P. (2010) High-resolution Inner-shell Photoionization, Photoelectron and Coincidence Spectroscopy, *in* Quack, M. and Merkt, F., (eds.) *Handbook of High Resolution Spectroscopy*, Wiley, Chichester, New York.

Mohr, P. (2008) Energy levels of hydrogen and deuterium. *NIST standard reference database*, **142**, http://physics.nist.gov/hdel.

Mohr, P. J., Taylor, B. N., and Newell, D. B. (2008) CODATA recommended values of the fundamental physical constants: 2006. *Rev. Mod. Phys.*, **80** (2), 633–730.

Moore, C. E. (1949) *Atomic Energy Levels*, NBS Circular 467/1, National Bureau of Standards, Washington, D. C.

Moore, C. E. (1952) *Atomic Energy Levels*, NBS Circular 467/2, National Bureau of Standards, Washington, D. C.

Moore, C. E. (1958) *Atomic Energy Levels*, NBS Circular 467/3, National Bureau of Standards, Washington, D.C.

Mourachko, I., Comparat, D., de Tomasi, F., Fioretti, A., Nosbaum, P., Akulin, V. M., and Pillet, P. (1998) Many-Body Effects in a Frozen Rydberg Gas. *Phys. Rev. Lett.*, **80** (2), 253–256.

Mulliken, R. S. (1930a) Correlation of Atomic J Values and Molecular Quantum Numbers, with Applications to Halogen, Alkaline Earth Hydride, and Alkali Molecules. *Phys. Rev.*, **36** (9), 1440–1450.

Mulliken, R. S. (1930b) The Interpretation of Band Spectra. Parts I, IIa, IIb. *Rev. Mod. Phys.*, **2** (1), 60–115.

Mulliken, R. S. (1930c) The Interpretation of Band Spectra, Parts I, IIa, IIb. Additions and Corrections. *Rev. Mod. Phys.*, **2** (4), 506–508.

Mulliken, R. S. (1931) The Interpretation of Band Spectra. Part IIc. Empirical Band types. *Rev. Mod. Phys.*, **3** (1), 89–155.

Mulliken, R. S. (1970) Potential Curves of Diatomic Rare-Gas Molecules and Their Ions, with Particular Reference to Xe_2. *J. Chem. Phys.*, **52** (10), 5170–5180.

Mulliken, R. S. and Christy, A. (1931) Λ-Type Doubling and Electron Configurations in Diatomic Molecules. *Phys. Rev.*, **38** (1), 87–119.

Oka, T. (2010) Orders of Magnitude and Symmetry in Molecular Spectroscopy, *in* Quack, M. and Merkt, F., (eds.) *Handbook of High Resolution Spectroscopy*, Wiley, Chichester, New York.

Paul, Th. A., Liu, J., and Merkt, F. (2009) Nuclear spin effects in the photoionization of krypton. *Phys. Rev. A*, **79** (2), 022505.

Pratt, D. W. (2010a) Electronic Spectroscopy in the Gas Phase, *in* Quack, M. and Merkt, F., (eds.) *Handbook of High Resolution Spectroscopy*, Wiley, Chichester, New York.

Pratt, S. T. (2010b) High-resolution Valence-shell Photoionization, *in* Quack, M. and Merkt, F., (eds.) *Handbook of High Resolution Spectroscopy*, Wiley, Chichester, New York.

Procter, S. R., Yamakita, Y., Merkt, F., and Softley, T. P. (2003) Controlling the motion of hydrogen molecules. *Chem. Phys. Lett.*, **374** (5–6), 667–675.

Quack, M. (2010) Fundamental symmetries and symmetry violations in high resolution spectroscopy, *in* Quack, M. and Merkt, F., (eds.) *Handbook of High Resolution Spectroscopy*, Wiley, Chichester, New York.

Quack, M. and coworkers (2010) Molecular Vibrational-Rotational Spectra, *in* Quack, M. and Merkt, F., (eds.) *Handbook of High Resolution Spectroscopy*, Wiley, Chichester, New York.

Rottke, H. and Welge, K. H. (1986) Photoionization of the hydrogen atom near the ionization limit in strong electric fields. *Phys. Rev. A*, **33** (1), 301–311.

Rupper, P. and Merkt, F. (2002) Assignment of the first five electronic states of Ar_2^+ from the rotational fine structure of PFI-ZEKE photoelectron spectra. *J. Chem. Phys.*, **117** (9), 4264–4281.

Schäfer, M. and Merkt, F. (2006) Millimeter wave spectroscopy and multichannel quantum-defect-theory analysis of high Rydberg states of krypton: The hyperfine structure of $^{83}Kr^+$. *Phys. Rev. A*, **74** (6), 062506.

Schäfer, M., Raunhardt, M., and Merkt, F. (2010) Millimeter-wave spectroscopy and multichannel quantum-defect-theory analysis of high Rydberg states of xenon: The hyperfine structure of $^{129}Xe^+$ and $^{131}Xe^+$. *Phys. Rev. A*, accepted.

Schinke, R. (2010) Photodissociation Dynamics of Polyatomic Molecules: Diffuse Structures and Nonadiabatic Coupling, *in* Quack, M. and Merkt, F., (eds.) *Handbook of High Resolution Spectroscopy*, Wiley, Chichester, New York.

Schmitt, M. and Meerts, W. L. (2010) Rotationally Resolved Electronic Spectroscopy and Automatic Assignment Techniques Using Evolutionary Algorithms, *in* Quack, M. and Merkt, F., (eds.) *Handbook of High Resolution Spectroscopy*, Wiley, Chichester, New York.

Schnell, M. (2010) Group Theory for High-resolution Spectroscopy of Nonrigid Molecules, *in* Quack, M. and Merkt, F., (eds.) *Handbook of High Resolution Spectroscopy*, Wiley, Chichester, New York.

Sharp, T. E. (1971) Potential-energy curves for molecular hydrogen and its ions. *Atomic Data*, **2**, 119–169.

Skoog, D. A., West, D. M., and Holler, F. J. (2000) *Analytical chemistry: an introduction*, Saunders College Pub.

Sobolewski, A. L. and Domcke, W. (2002) On the mechanism of nonradiative decay of DNA bases: ab initio and TDDFT results for the excited states of 9H-adenine. *Eur. Phys. J. D*, **20**, 369–374.

Sommavilla, M. (2004) *Photoabsorption-, Photoionisations- und Photoelektronenspektroskopie von Atomen und kleinen Molekülen im VUV-Bereich*, PhD thesis, Eidgenössische Technische Hochschule Zürich, ETH Zürich, CH-8093 Zürich, Switzerland, Diss. ETH Nr. 15688.

Sommavilla, M., Hollenstein, U., Greetham, G. M., and Merkt, F. (2002) High-Resolution Laser Absorption Spectroscopy in the Extreme Ultraviolet. *J. Phys. B: At. Mol. Opt. Phys.*, **35** (18), 3901–3921.

Stearns, J. A., Pillsbury, N. R., Douglass, K. O., Müller, C. W., Zwier, T. S., and Plusquellic, D. F. (2008) Rotationally resolved studies of S_0 and the exciton coupled S_1/S_2 origin regions of diphenylmethane and the d_{12} isotopologue. *J. Chem. Phys.*, **129** (224305).

Tennyson, J. (2010) High Accuracy Rotation - Vibration Calculations on Small Molecules, *in* Quack, M. and Merkt, F., (eds.) *Handbook of High Resolution Spectroscopy*, Wiley, Chichester, New York.

Tew, D. P., Klopper, W., Bachorz, R. A., and Hättig, Ch.. (2010) Ab Initio Theory for Accurate Spectroscopic Constants and Molecular Properties, *in* Quack, M. and Merkt, F., (eds.) *Handbook of High Resolution Spectroscopy*, Wiley, Chichester, New York.

Veseth, L. (1973) Hund's coupling case (c) in diatomic molecules. I. Theory. *J. Phys. B: At. Mol. Phys.*, **6** (8), 1473–1483.

Vliegen, E., Hogan, S. D., Schmutz, H., and Merkt, F. (2007) Stark deceleration and trapping of hydrogen Rydberg atoms. *Phys. Rev. A*, **76** (2), 023405.

Vliegen, E., Wörner, H. J., Softley, T. P., and Merkt, F. (2004) Nonhydrogenic Effects in the Deceleration of Rydberg Atoms in Inhomogeneous Electric Fields. *Phys. Rev. Lett.*, **92** (3), 033005.

Watson, J. K. G. (1999a) Multiple groups in the symmetry classification of adiabatic electronic wavefunctions. *Mol. Phys.*, **96** (12), 1721–1733.

Watson, J. K. G. (1999b) Rotation-Electronic Coupling in Diatomic Rydberg States, *in* Sándorfy, C., (ed.) *The Role of Rydberg States in Spectroscopy and Photochemistry*, Kluwer Academic Publishers, New York, pp. 293–327.

Western, C. M. (2010) Introduction to Modeling High-resolution Spectra, *in* Quack, M. and Merkt, F., (eds.) *Handbook of High Resolution Spectroscopy*, Wiley, Chichester, New York.

Wörner, H. J. and Corkum, P. B. (2010) Attosecond Spectroscopy, *in* Quack, M. and Merkt, F., (eds.) *Handbook of High Resolution Spectroscopy*, Wiley, Chichester, New York.

Wörner, H. J., Grütter, M., Vliegen, E., and Merkt, F. (2005) Role of nuclear spin in photoionization: Hyperfine-resolved photoionization of Xe and multichannel quantum defect theory analysis. *Phys. Rev. A*, **71** (5), 052504, see erratum in Phys. Rev. A 73, 059904(E) (2006).

Wörner, H. J., Hollenstein, U., and Merkt, F. (2003) Multichannel quantum defect theory of the hyperfine structure of high Rydberg states of ^{83}Kr. *Phys. Rev. A*, **68** (3), 032510.

Wörner, H. J. and Merkt, F. (2006) Photoelectron Spectroscopic Study of the First Singlet and Triplet States of the Cyclopentadienyl Cation. *Angew. Chem. (int. ed. engl.)*, **45** (2), 293–296.

Wörner, H. J. and Merkt, F. (2007) Diradicals, antiaromaticity, and the pseudo-Jahn-Teller effect: Electronic and rovibronic structures of the cyclopentadienyl cation. *J. Chem. Phys.*, **127** (3), 034303.

Wörner, H. J. and Merkt, F. (2009) Jahn–Teller effects in molecular cations studied by photoelectron spectroscopy and group theory. *Angew. Chem. (int. ed. engl.)*, **48** (35), 6404–6424.

Wörner, H. J., Mollet, S., Jungen, Ch., and Merkt, F. (2007) Role of spins in molecular photoionization: Spectroscopy and dynamics of autoionizing Rydberg states of ortho-H_2. *Phys. Rev. A*, **75** (6), 062511.

Wörner, H. J., van der Veen, R., and Merkt, F. (2006) The Jahn-Teller Effect in the Methane Cation: Rovibronic Structure and the Geometric Phase. *Phys. Rev. Lett.*, **97** (17), 173003.

Yamaguchi, Y. and Schäfer, H. F. (2010) Analytical Derivative Methods in Molecular Electronic Structure Theory: A New Dimension to Quantum Chemistry and its Applications to Spectroscopy, *in* Quack, M. and Merkt, F., (eds.) *Handbook of High Resolution Spectroscopy*, Wiley, Chichester, New York.

Zare, R. N. (1988) *Angular Momentum*, John Wiley & Sons, New York.

Zehnder, O. and Merkt, F. (2008) The low-lying electronic states of $ArXe^+$ and their potential energy functions. *J. Chem. Phys.*, **128** (1), 014306.

Zimmerman, M. L., Littman, M. G., Kash, M. M., and Kleppner, D. (1979) Stark structure of the Rydberg states of alkali-metal atoms. *Phys. Rev. A*, **20** (6), 2251–2275.